EFFECT OF URBANIZATION ON EXTREME CLIMATE INDICES AND COMPOUND EVENTS IN KERALA

Thesis

Submitted in partial fulfilment of the requirements for the degree of

DOCTOR OF PHILOSOPHY

by

ANJALI VIJAY

Reg. No: **165109AM16F02**

DEPARTMENT OF WATER RESOURCES AND OCEAN ENGINEERING

NATIONAL INSTITUTE OF TECHNOLOGY KARNATAKA,

SURATHKAL,

MANGALORE - 575 025

April – 2024

DECLARATION

by the Ph.D. Research Scholar

I hereby *declare* that the Research Thesis entitled "**Effect of Urbanization on Extreme Climate Indices and Compound Events in Kerala**" which is being submitted to the National Institute of Technology Karnataka, Surathkal in partial fulfilment of the requirements for the award of the Degree of Doctor of Philosophy in **Department of Water Resources and Ocean Engineering** is a *bonafide report of the research work carried out by me*. The material contained in this Research Thesis has not been submitted to any University or Institution for the award of any degree.

Place: NITK-Surathkal

Date: 04/04/2024

ANJALI VIJAY

165109AM16F02

Department of Water Resources and Ocean Engineering

CERTIFICATE

This is to *certify* that the Research Thesis entitled "**Effect of Urbanization on Extreme Climate Indices and Compound Events in Kerala**" submitted by **Anjali Vijay** (Register Number: 165109AM16F02) as the record of the research work carried out by her, is *accepted as the Research Thesis submission* in partial fulfilment of the requirements for the award of degree of Doctor of Philosophy.

Varija K
5/4/24

Dr. K. Varija

Professor and HOD

Research Supervisor & Chairman-DRPC

WR&OE

ACKNOWLEDGMENTS

Thanks to Almighty!

I am forever grateful to my research guide, Dr. K Varija, for her supervision, valuable input, and patience during my Ph.D. study. Madam, You have always been calm and supportive during the difficult times of my Ph.D. journey.

Let me express my gratitude to my RPAC members, Prof. Ammai Mahesha and Dr. B Manu for their valuable input and suggestions.

Let me express my thanks to Prof. G. S. Dwarakish, Prof. Amai Mahesha, Prof. Amba Shetty, Prof. B. M. Dodamani, the former Heads of the Department, and Dr. Varija K, the present Head of the Department, for granting me use the departmental facilities required for my Ph.D. work.

I sincerely acknowledge the help and support from all the faculties, staff, and the research scholars of the Department of Water Resources and Ocean Engineering.

To my family, Achan, amma, and Eatan, for always believing in me and supporting me throughout my Ph.D. journey. My sister, Chinju, for building my confidence during the tough times. To my ammamma for the blessings and love. I also express my heartfelt thanks to my Gurus for their support and love.

To my pillar of strength, my best friend – Dr. Vishnu M, for his endless support that helped me conquer my fears and insecurities. ThankYou!

To all my friends who have extended their support and love, dear CHY, Dr. Nithya, Mr.Parthasarathy, Mrs. Ashwitha, Dr. Tom, Dr. Dinu, Dr. Athul, Dr. Amogh bro, Dr.Dineshkumar M., Dr. Sinan, Dr. Rishikesh, Mr. Rony, Dr. Dinu, Dr. Diwan, and all other research scholars.

Anjali Vijay

ABSTRACT

Studies on historical patterns of climate variables and climate indices have attained significant importance because of the increasing frequency and severity of extreme events worldwide. While the recent events in the tropical state of Kerala (India) have drawn attention to the catastrophic impacts of extreme rainfall events leading to landslides and loss of human lives, a comprehensive and long-term spatiotemporal assessment of climate variables is still lacking. This study investigates the long-term trend analysis (119 years) of climate variables at 5% significance level over the state using gridded datasets of daily rainfall (0.25° x 0.25° spatial resolution), temperature (1° x 1° spatial resolution) at annual and seasonal scales (south-west monsoon, north-east monsoon, winter, and summer). Five trend analysis techniques, including the Mann-Kendall test (MK), three modified Mann-Kendall tests, and innovative trend analysis (ITA) test, were performed in the study. It is evident from the trend analysis results that more than 83% of grid points were showing negative trends in annual and south-west monsoon season rainfall series (at a mean rate of 39.70 mm and 28.30 mm per decade, respectively). All the trend analysis tests identified statistically significant increasing trends in mean and maximum temperature at annual and seasonal scales (0.10 to 0.20 °C/decade) for all grids. The K-means clustering algorithm delineated 59 grid points into five clusters for annual rainfall, illustrating a clear geographical pattern over the study area. There is a clear gradient in rainfall distribution and concentration inside the state at annual and seasonal scales. The majority of annual rainfall is concentrated in a few months of the year. That may lead the state vulnerable to water scarcity in non-rainy seasons.

Land Use and Land Cover (LULC) analysis gives essential information on how the region has evolved over time. Due to adverse environmental effects, the significant and widespread changes in the LULC resulting from human activities have become a pressing issue for decision planners and the Government. Kerala, an ecologically diverse state in India characterized by complex topography, has experienced substantial LULC transformations due to rapid urbanization. These changes were assessed by analyzing Landsat images from 1990 to 2020, utilizing two distinct machine learning classification techniques, namely Random Forest (RF) and Classification And Regression Trees (CART), within the Google Earth Engine (GEE) platform.

Normalized Difference Vegetation Index (NDVI), Normalized Differences Built-up Index (NDBI), Modified Normalized Difference Water Index (MNDWI), and bare soil index (BSI) are the indices used in addition to aid the accurate LULC classification. Results showed that the performance of RF is better than CART in all the years. Thus, RF algorithm outputs are used to infer the change in the LULC for three decades. The changes in the NDVI values indicate the loss of vegetation for the urban area expansion during the study period. The increasing value of NDBI and BSI in the state indicates growth in high-density built-up areas and barren plains. The slight reduction in the value of MNDWI indicates the shrinking water bodies in the state. The results of LULC showed the urban expansion (158.2%) and loss of agricultural area (15.52%) in the region during the study period. It was noted that the area of the barren class and the water class decreased steadily from 1990 to 2020.

The study adopted a dynamic classification method using time-varying land cover data to classify the urban and rural grids. This approach provided a more comprehensive understanding of the urbanization process in Kerala over the past three decades. The study incorporated 24 extreme climate indices, including 12 temperature extremes and 12 precipitation extremes, tailored to the unique climatic features of Kerala state. Various statistical methods were applied to investigate changes in long-term trends and spatial variation of heat wave characteristics. Additionally, the research aimed to examine the spatio-temporal variation of heat wave-drought compound events in Kerala from 1951 to 2020. A comparative analysis was conducted to assess the intensity and duration of heat waves within compound events compared to individual heat wave events, providing insights into their distinct characteristics and patterns. By comparing the trends between urban and nearby rural grids, the study employed a method to estimate the impact of urbanization on climate extremes. This approach yielded valuable insights into the changes occurring in extreme weather events in Kerala and their connection to urbanization, enhancing our understanding of this relationship. Long-term trend analysis of extreme climate indices showed that more than 60% of the grids in the region had experienced a decrease in indices such as CWD, R10, R20, R25, RX5 day, PRCPTOT, and SDII, whereas 80% of grid points showed an increasing trend in indices like R95p, R99p, RX1 day, and R50. The rising incidence of CDD, coupled

with a declining number of CWD occurrences in the state, signifies an extended period of drought conditions in Kerala. An increasing trend is observed in the extreme hot temperature indices. In contrast, all extreme cold indices demonstrate decreasing trends, indicating a concerning rate of decline in cold extremes alongside the rise in warm extremes. Results pointed out that urbanization has decreased light rain and increased extreme precipitation in urban areas. It is seen that urbanization has a statically significant positive effect on heat waves and compound events, with more substantial impacts observed for HWD, HWF, and HWL compared to HWA.

Keywords: Compound events, Extreme climate indices, Heat wave, Kerala, , LULC, Rainfall, Temperature

TABLE OF CONTENTS

LIST OF FIGURES

LIST OF TABLES

LIST OF ABBREVIATIONS

Abbreviation	Description
API	Application Programming Interface
BSI	Bare soil index
CART	Classification And Regression Trees
CV	Coefficient of variation
CDD	Consecutive Dry Days
CDF	Cumulative distribution function
CL	Confidence Limit
CWD	Consecutive Wet Days
DTR	Diurnal temperature range
ECDF	Empirical cumulative density function
ENSO	El Niño-Southern Oscillation
ESS	Effective Sample Size
ETCCDI	Expert Team on Climate Change Detection and Indices
GDP	Gross Domestic Product
GEE	Google Earth Engine
GHGs	Greenhouse gases
HW	Heat Wave
HWA	Heat wave amplitude
HWD	Heat wave duration
HWE	End date of Heat wave event
HWF	Heat wave frequency
HWL	Heat wave length
HWM	Heat wave magnitude
HWN	Heat wave number
HWO	Onset of Heat wave event
IDE	Integrated Development Environment
IMD	India Meteorological Department
ITA	Innovative trend analysis
KS test	Kolmogorov-Smirnoff test

LULC	Land Use and Land Cover
MIR	Middle infrared band
MK	Mann-Kendall test
MK-CF1	Modified Mann-Kendall test 1
MK-CF2	Modified Mann-Kendall test 2
MK-PW	Pre-whitening Mann-Kendall test
ML	Machine Learning
MMK	Modified Mann-Kendall test
MNDWI	Modified Normalized Difference Water Index
NDBI	Normalized Differences Built-up Index
NDVI	Normalised Difference Vegetation Index
NE	North-East Monsoon
NIR	Near-infrared band
PCA	Principal component analysis
PCI	Precipitation concentration index
PRCPTOT	Total precipitation on wet day
R	Precipitation
RD	Rainy Days
ROIs	Regions of interest
RCPs	Representative Concentration Pathways
RF	Random Forest Classifier
RX1 day	Maximum 1-day precipitation value
RX5 day	Maximum 5-day precipitation value
SD	Standard deviation
SI	Seasonality Index
SPI	Standard Precipitation Index
SSPs	Shared Socioeconomic Pathways
SU	Summer days
SVM	Support Vector Machine
SW	South-West Monsoon
SQ-MK	Sequential Mann-Kendall Test
TR	Tropical Nights

TX	Maximum Temperature
TN	Minimum Temperature
Uc	Contribution of urbanization
UHI	Urban heat islands
WDSI	Warm spell duration indicator
WMO	World Meteorological Organization

CHAPTER 1

INTRODUCTION

1.1 GENERAL

Urbanization is a dynamic progression fuelled by industrialization and economic advancement, culminating in the expansion of cities and ultimately giving rise to distinct alterations in environmental patterns and human behaviours specific to urban areas. A supportive ecological environment plays a vital role in facilitating sustainable growth. It serves as a fundamental foundation for promoting a friendly atmosphere. A conducive environment is crucial in promoting urbanization, while sustainable urbanization offers vital technical and financial assistance in effectively preventing and managing natural hazards. Even though urban development can improve the quality of human lives, improper planning and excessive growth can also lead to ecological degradation and extreme climate events. Projections indicate that by 2050, over 60% of the global population will reside in urban areas, with India experiencing a substantial rise of 416 million urban residents (United Nations Publications 2019). The uncontrolled population increase frequently stimulates urban expansion and alters LULC dynamics. In the future, cities with large concrete buildings and a tendency to accumulate anthropogenic heat will be at a higher risk. This is due to the growing agreement that urban areas can expose a larger population to extreme hazards such as flooding, heat waves, and compound events. Urbanization is a vital indicator reflecting a country's development level while simultaneously intensifying the interplay between human society and the environment. Rapid and unsustainable urbanization has resulted in significant environmental degradation, posing numerous challenges such as habitat destruction, deteriorating water quality, air pollution, and deforestation. In recent decades, the frequency of natural hazards has increased, and there is ongoing investigation into the role of urbanization in their occurrence.

The urbanization process heightens the vulnerability to flooding by amplifying both the peak discharge and volume of water while concurrently reducing the time available to reach the peak flow (Nirupama and Simonovic 2007). Impervious surface changes the

land surface properties and the dynamic structure of the boundary layer and hence modifies the energy budget, which leads to changes in the climate parameters in urban areas compared to surrounding rural areas (Ren et al. 2008; Ren and Yaqing 2014). In highly urbanized areas, over half of the rainfall becomes surface runoff, and deep infiltration is only a tiny fraction of the natural situation (Yang and Zhang 2011). Given the expanding global human population and the escalating trend of rural-to-urban migration, urbanization is expected to persist for several more decades. The persistent urbanization trend will amplify the consumption of land and resources, aggravating preexisting environmental problems that pose substantial threats to our planet. Additionally, these environmental challenges have already incurred significant economic costs, amounting to billions of dollars. To effectively address the critical problems brought on by urbanization, it is imperative that governments and planning agencies immediately acknowledge and effectively include an environmental perspective in land-use planning and decision-making processes.

1.2 EFFECT OF URBANIZATION ON THE ENVIRONMENT

Land use refers to the human activities and purposes associated with these features, whereas the land cover of a place pertains to the physical features of the earth's surface. Urbanization and industrialization have recently become the main driving forces behind the worldwide demographic, social, economic, and environmental changes (Liu et al. 2018; Patra et al. 2018; Devkota et al. 2023). The process involves rapidly transforming agricultural fields, bodies of water, and vegetation into artificial surfaces. Urbanization and industrialization have caused significant changes in a region's Land Use and Land Cover (LULC), which have led to the depletion of natural resources, the development of urban heat islands (UHI), the destruction of habitat, greenhouse gas emissions, and the loss of water resources (Chu and Ren 2005; Govind and Ramesh 2019; Raj et al. 2020). For the efficient and effective utilization of natural resources, it is essential to understand the LULC in a specific location. Reducing natural ecosystems in favor of built-up areas diminishes the availability of ecosystem services (Xiao et al. 2022). When natural ecosystems and agricultural lands are converted into built-up areas, it will lead to alteration in the runoff pattern (Liu et al. 2019; Dixit et al. 2022), lowering of the groundwater table (Patra et al. 2018), and a rise in the occurrence of natural disasters

(Arowolo et al. 2018). Surface energy fluxes, cloud dynamics, and surface rainfall can all be affected by the LULC changing from the rural to the urban class (Shepherd et al. 2002). The changes in moisture and energy budgets resulting from the LULC transformations impact the local climate (Mahmood et al. 2014). Therefore, urban development is a significant factor that induces environmental and ecological modifications in terrestrial ecosystems. Due to their high energy consumption and contribution to environmental degradation through air, water, and land pollution, urban-induced LULC alterations are a vital source of global environmental challenges (Yan et al. 2016).

Despite occupying a relatively small portion of the earth's land surface, urban areas provide shelter for over half of the global population. Most of the anthropogenic gas emissions are contributed by urban areas, and it has replaced more than 80% of the natural habitat loss (Chen et al. 2020). The drawbacks of urbanization stem from the rise in urban population, uncontrolled expansion of urban areas, and insufficient infrastructure. The rapid growth, fueled by both natural increase and migration, has significantly strained public services like residences, health care, schooling, and more. Urban growth is frequently defined as a drastic shift in land-use classes and alterations to land surface characteristics such as albedo, soil moisture, and heat storage. Several researchers have pointed out that urbanization-induced heat islands play a vital role in the warming trends. Various studies have shown that the effects of UHI are more prominent in dry climates than in cold climatic conditions (Liao et al. 2018). The phenomenon of UHI measures the heat accumulation induced by urban structures' thermal, radiative, and aerodynamic aspects. It is distinguished by temperature variations between nearby urban and rural regions, increasing upward sensible heat flux during the daytime and warming the boundary layer (Voogt and Oke 2003). The expansion of urban areas can intensify the UHI effect by altering the surface energy balance, affecting local thermal circulation and precipitation patterns.

Places with growing population density, urbanization, deforestation, and agricultural diversification are those where the influence of LULC changes is most noticeable (Gogoi et al. 2019). Human-induced land cover changes have a noticeable impact on

the local and regional environment. These alterations modify the surface energy balance and can subsequently impact surface temperature, altering the region's climate. The occurrence of extreme climate events such as heat waves, flash floods, and droughts are also affected by alterations in the LULC (Boyaj et al. 2020; Dixit et al. 2022; Gogoi et al. 2019; Halder et al. 2016; Skariah and Suriyakala 2022; Zhu and Li 2014). The hydrological cycle, including surface runoff, subsurface runoff, and groundwater recharge, is significantly influenced by the dynamics of LULC, which can potentially contribute to flooding (Miller et al. 2014; Zhu and Li 2014; Xu and Zhao 2016; Dixit et al. 2022). It is essential to analyze the dynamics of LULC change to cope with environmental changes and promote sustainability. Several studies (Halder et al. 2016; Kumar et al. 2017) have discovered a connection between variations in LULC and aerosol levels, which can, directly and indirectly, affect temperature. This temperature modulation can also impact rainfall patterns, leading to droughts or floods due to changes in the frequency of extreme climate events (Gogoi et al. 2019; Mohan and Kandya 2015). So cumulatively, urbanization, industrialization, and deforestation contribute to land-use impacts on the climate, eventually resulting in unpredictable heavy rainfall and increasing temperatures.

1.3 EFFECT OF URBANIZATION ON EXTREME CLIMATE EVENTS

Urbanization can transform multiple components of the hydrological cycle due to the expansion of impervious surfaces. The rise in the artificial surfaces reduces the infiltration, increases the surface runoff and stream flow, and decreases the base flow and groundwater recharge. The rainfall-runoff process is related to complex factors in the urban catchment, such as LULC, river network morphology, construction of drainage systems, and water transfer. The complexity of the underlying surface, the uncertainty of anthropogenic disturbance, and the lack of high-quality datasets for calibration and validation may limit our research on the rainfall-runoff processes in an urban catchment. One of the significant causes of rapidly changing climate is the combined effect of global warming and urbanization, leading to problems like extreme climate events, flash floods, droughts, vegetation loss, etc. The combined impact of global warming and climate change has jeopardized the environment and human lives. According to various researchers, the local climates in urban areas are significantly

distinct from those in the neighbouring suburbs. The massive alteration of the land surface and atmospheric boundary layers in urban areas impacts the near-surface climate by altering the energy and water balance. According to the studies, climate extremes showed increasing frequency characterized by longer duration and high intensity during recent decades as the global temperature increased and is expected to be severe in coming years (Wang et al. 2021b). The combined effects of climate change and urban warming have increased the frequency, duration, and intensity of extreme climate events across the globe (Lin et al. 2020; Mukherjee et al. 2018). The changes in extreme temperature and rainfall events are directly associated with the anthropogenic influence of greenhouse gases (Yang et al. 2017c). Subsequent infrastructure development is essential to sustain the growing urban population. The downside of this development is the conversion of vegetated areas and water bodies in the peri-urban areas to urbanized regions with impervious surfaces. The increase in the impervious surfaces can increase the runoff, leading to a significant decline in the infiltration rate and changes in evapotranspiration (McGrane 2016). Hence the growth of impervious areas can adversely affect groundwater recharge and storage.

Extreme precipitation poses significant risks to natural ecosystems and human society, potentially causing flash flooding, crop failure, landslides, and runoff contamination. Projections of extreme climate indices and effective disaster risk reduction strategies in a changing climate require a clear understanding of the historical alterations in extreme precipitation characteristics, such as frequency, intensity, and duration changes. To effectively address the emerging climate risks, it is vital to identify differences in the characteristics of extreme precipitation and comprehend the underlying causes, to facilitate adaptation strategies. Despite a significant amount of attention being directed towards studying urban-induced changes in surface air temperature, precisely the UHI effect, investigating urban-induced changes in rainfall has proven to be a more challenging task. This is due to the heterogeneous nature of spatial and temporal rainfall distributions, as opposed to the homogeneous distributions that surface air temperatures display. Studying the influence of urbanization on the characteristics of extreme precipitation presents a formidable and unresolved challenge. Over time, urbanization has experienced an intensification that has resulted in elevated urban temperatures and an amplified UHI effect (Luo et al. 2021). The transformations occurring in urban areas

lead to modifications in their river systems, necessitating further investigation to evaluate their impacts on diverse environmental aspects. These include vegetation restoration, atmospheric visibility, agricultural production, and the livelihoods of the residents inhabiting these areas. Given that the influence of urbanization on different extreme events can vary depending on the climatic context and terrain conditions, it is crucial to analyze these changes to enhance disaster risk management strategies.

1.4 URBANIZATION IN INDIA

Urbanization is considered the most prevailing LULC change in developing countries like India. Changes in the land surface led to variations in the moisture content of the soil, heat retention capacity, and surface emissivity. India has witnessed the rapid growth of urbanization since its independence, and various economic liberalization strategies put forward by the government have further encouraged immigration from rural areas. As per Census 2011 , 31.8% of the population in India is living in urban areas, and it is expected to contribute 416 million urban dwellers by 2050. The rapid growth of urbanization in India over the past 40 years has been accompanied by unprecedented growth in the urban population and UHI. Over the past few centuries, India has been grappling with several challenges, including population growth, depletion of resources, and environmental degradation (Chakrabarti 2001; Das et al. 2022; Ray and Ray 2011). The unsustainable use of resources and its negative environmental impact has happened concurrently with uneven population expansion and development across the country. The LULC changes in India following independence have been marked by tremendous agricultural growth, frequently destroying forests and other natural habitats (Roy et al. 2015; Mondal and Zhang 2018). This pattern lasted till the 1960s when the Green Revolution was implemented as a means of increasing agricultural output through the adoption of efficient crop varieties, the building of irrigation systems, and the use of chemical compounds for productivity. Even though the Green Revolution boosted agricultural outputs and reduced the pressure on forests, it also had unanticipated consequences such as soil degradation, water pollution, and biodiversity loss (Singh 2000; John and Babu 2021). Moreover, modern economic development plans and their implementation since the 1960s have significantly impacted LULC changes in India, leading to increased industrialization,

urbanization, and infrastructure development. The agricultural fields, grasslands, and water bodies were changed to built-up areas after 1960 (Roy et al. 2015).

It is seen that India's rapid industrialization, rising economy, and population growth have resulted in significant increases in urbanization and pollution levels (Das et al. 2022; Kaur and Pandey 2021; Ray and Ray 2011). The changes in LULC, such as agriculture and urbanization, have been attributed to the notable spatial variability observed in the characteristics of extreme rainfall in the country (Singh et al. 2016). India is experiencing exceptional dynamism in land transformation, as the urban population is anticipated to grow by 416 million from 2014 to 2050 (UN 2015). The downside of this development is the transformation of water bodies and vegetated areas in the semi-urban regions into urbanized areas with artificial surfaces. Due to the increase in population and urbanization, the conversion of large areas of forest and vegetation into other land uses in India has resulted in significant changes to the local climate (Roy et al. 2015; Tian et al. 2014). Various researchers have pointed out the significant correlation between the increase in urbanization in India and the spatial distribution of heavy rainfall amounts (Kishtawal et al. 2010; Shastri et al. 2015). Urbanization and climate conditions are the leading causes of the increase in extreme rainfall events in a large portion of India during the post-urbanization phase compared to the previous time (Bisht et al. 2018).

Developing countries like India must prioritize addressing the impacts of LULC changes, including water scarcity, air and water quality degradation, and biodiversity loss, to promote sustainable development and protect society's and the environment's well-being. With over half of India's population residing in urban areas, the local climate, including climate extremes, is greatly influenced by the escalating urbanization and human activities in these regions. Although urbanization has experienced rapid growth over the past five decades, there remains a significant gap in our understanding of the extent to which it contributes to extreme climate events and heat waves in India. Mukherjee et al. 2018 conducted a study that projected a rise in the frequency of extreme precipitation events in India's central and southern regions. The study linked this intensification to anthropogenic climate change, which encompasses the impact of human activities on the climate system. So, urbanization has emerged as a significant

local factor strongly linked to the changes in trends and patterns of extreme precipitation over the country. India ranks among the nations experiencing a substantial number of natural calamities annually, and the impact of anthropogenic activities on the environment is progressively strengthening, resulting in a higher frequency of natural hazards such as flash floods, droughts, landslides, and heat waves in the country (Das et al. 2022; Mukherjee et al. 2018). While it is evident that anthropogenic warming has led to different temperature extremes and precipitation extremes contributing to both drought and extreme flood events in India, studies exploring the association between temperature and precipitation are relatively limited in number.

Kerala has witnessed rapid urbanization during the past three decades, with an increase of 83.20% over the last decade as per the 2011 census (Census 2011). Moreover, the state is very vulnerable to climate extremes due to the complicated topography and fragile environment. Therefore, a proper knowledge of the quantification of urbanization's contribution to Kerala's changing climate is essential to alleviate the environmental issues in Kerala that challenge sustainable regional planning. According to the Census 2011, the population of Kerala is 33,387,677, an increase from 31,838,619 in 2001. The number of towns in the State has tripled, resulting in significant growth in the urban population over the past decade (Cyriac 2022; Lal and Nair 2017). Kerala experienced a substantial increase in urbanization from 2001 to 2011, with a steep rise of 92.27%. As a result, it has become one of the most urbanized states in India (Firoz et al. 2014). In 2011, Kerala surpassed Maharashtra (45.2%) in the percentage of urban population to the total population. Nonetheless, due to its larger size as a state, Maharashtra still maintains its lead in terms of the absolute number of individuals, with 50.8 million people (Census 2011). Even though Kerala's urban population is considerably smaller than that of larger states like Maharashtra, the increase of 92.8% during 2001-2011 has presented many challenges for policymakers in Kerala. The share of the urban population in the State has risen sharply from 25.96% in 2001 to 47.72% in 2011, compared to 25.52% in 2001 and 31.16% in 2011 for India as a whole.

Regarding urbanization, Kerala ranked 19th among the States of India in 2001 but rose to 9th in 2011. The growth in the urban population in Kerala can be attributed to two

main factors: the rise in the number of urban areas and the urbanization of peripheral regions surrounding major urban centers. Kerala's settlement pattern is also distinctive, with habitation continuously spread throughout most parts of the State, with few open lands or fields separating them (Firoz C, Mohammed and Banerji, Haimanti and Sen 2014). This pattern alone creates an impression of urbanization. Additionally, access to education and healthcare facilities is similar for both rural and urban populations in Kerala, resulting in similar infrastructural facilities for the general population (https://spb.kerala.gov.in/economic-review/ER2016/chapter01_02.php).

1.5 ORGANISATION OF THE THESIS

The thesis report consists of the following seven chapters:

Chapter 1 (Introduction) provides a comprehensive overview of the study

Chapter 2 (Literature Review) summarizes previous research on climate change data analysis, LULC classification, extreme climate events, and the impact of urbanization on changes in extreme climate events. The chapter also presents key conclusions from these studies, identifies existing literature gaps, and outlines the research objectives.

Chapter 3 (Study Area) provides detailed information about the study area.

Chapter 4 (Methodology) outlines the data products and methodology employed to achieve each study objective.

Chapter 5. (Results and Discussions) presents the study's findings and a detailed discussion.

Chapter 6 (Conclusions) summarizes the key findings from the current research. Following this chapter, the references used for the study are provided.

CHAPTER 2

LITERATURE REVIEW

2.1 GENERAL

The literature review was categorized into five major sections: trend analysis of climate variables, LULC mapping, extreme rainfall events, heat waves, compound events, and the impact of urbanization on extreme events. The first part of the session gives an overview of various trend analysis techniques and extreme indices for assessing change in the climatic parameters. Trend analysis is one of the most prominent methodologies scholars have used to analyze the changes in hydro-meteorological variables over the last decades. Many approaches for studying the trend of hydro-meteorological variables have been developed and utilized, each with its own set of limits and advantages. In general, trend analysis methodologies are classified as parametric or non-parametric. Experts have chosen non-parametric methods for trend analysis in recent years because they are less sensitive to outliers and can be used with non-normally distributed series with gaps in data series.

The second part of the literature review describes different approaches for mapping LULC explored, including utilizing and applying models such as the Random Forest (RF) algorithm and Classification and Regression Trees (CART). With the continuous advancements in machine learning techniques used for LULC mapping, it has emerged as a ground breaking and exceptionally potent tool for addressing unprecedented, extensive, and significant challenges in remote sensing data analysis. Investigating the causes, mechanisms, and effects of LULC changes on climate and climate variables is a key research area in environmental studies. LULC changes represent one of the most noticeable ways humans alter the global ecosystem. By understanding how LULC impacts climate, researchers can gain insights into the factors driving these changes and their far-reaching consequences. Later, the impact of urbanization on extreme indices for assessing anthropogenic influence on the environment is discussed in later sessions. The changes in the pattern of extreme climate events, heat waves, and compound events profoundly impact the environment and society. The rapid changes in LULC due to

urbanization led to an increase in the variations in surface temperature anomalies, and various researchers have pointed out the fluctuations of extreme events over urban areas. Under a warming climate with more extreme rainfall and flash flood events, it is crucial to know the anthropogenic influence of these extremes for better urban planning.

2.2 TREND ANALYSIS

Studies around the world have reported the spatial and temporal variation of climatic variables (Burn and Elnur 2002; Caloiero et al. 2011; Martinez et al. 2012; Alexander 2016; Yang et al. 2017). The studies executed on climatic variables in India pointed out the reduction in monsoon rainfall (Parthasarathy and Dhar 1974; Rao 1993; Krishnamurthy and Shukla 2000; Goswami et al. 2006; Guhathakurta and Rajeevan 2008; Pal and Al-Tabbaa 2009; Ghosh et al. 2009; Kumar et al. 2010; Jain and Kumar 2012; Jain et al. 2013; Guhathakurta et al. 2015; Mondal et al. 2015) whereas an increasing trend in temperature (Hingane et al. 1985; Bhutiyani et al. 2007; Shafiq et al. 2019; Machiwal et al. 2019)**.** Guhathakurta et al. 2015 conducted a study on the trend of south-west monsoon using 111 years of monthly rainfall data over India and revealed that decreasing trend in monsoon rainfall post-1950 period due to multi-decadal epochal variability. The study also revealed the decreasing trend of frequencies of wet and rainy days over most parts of the country. Dey and Mujumdar 2019 used relative entropy to examine the spatial variability and change in uniformity of rainfall distribution over India and observed a significant relationship between rainfall uniformity and low rainfall intensity. Variations in the onset and quantity of annual rainfall received can negatively impact the hydrological cycle and agricultural productivity. The characteristics of high-intensity rainfall events are affected by rising temperatures, thus altering the uniformity in rainfall distribution (Dey and Mujumdar 2019).

Temperature is considered as a crucial climate variable closely related to other significant climate variables like atmospheric humidity and precipitation. The fifth assessment report of the Intergovernmental Panel on Climate Change reported the increase in surface air temperature by 0.87°C during 1880-2012 (Myhre et al. 2013; Guo et al.

2020). Given the above, many studies have attempted to analyze the pattern of temperature on the global scale (Kruger and Shongwe 2004; Tabari and Talaee 2011; Saboohi et al. 2012; Ahmadi et al. 2018) as well as national scale (Kothawale et al. 2010; Pal and Al-Tabbaa 2010; Jhajharia and Singh 2011). Pal and Al-Tabbaa 2010 analyzed the long-term pattern of monthly and seasonal extreme temperatures over India from 1901 to 2003 and found that minimum temperature changes were more variable, spatially and temporally, than the corresponding maximum temperature changes with results of lesser significance. The western Himalaya region is India's most vulnerable area to climate change, with the highest variation and temperature increase, probably leading to melting glaciers (Pal and Al-Tabbaa 2010). Abrupt changes in climatic parameters, like precipitation, temperature, etc., can negatively impact human health and comfort.

Analysis of rainfall trend in Kerala indicated a decreasing trend in annual as well as south-west monsoon rainfall (Soman et al. 1988; Singh et al. 1989; Guhathakurta and Rajeevan 2008; Nikhil Raj and Azeez 2012; Nair et al. 2014) and an increasing trend in post-monsoon and winter rainfall (Krishnakumar et al. 2009; Adarsh and Janga Reddy 2015; Thomas and Prasannakumar 2016). Kerala receives more of the south-west monsoon in the northern parts of the state while the southern parts get more of the north-east monsoon (Nair et al. 2014). During the active spell of the south-west monsoon, north Kerala comes under the cyclonic shear area of the low-level jet, while south Kerala falls in the anti-cyclonic shear zone, which is the main reason for this asymmetry (Simon and Mohankumar 2004). The increasing frequency of dry days and a decreasing trend in extreme rainfall events during monsoons in Kerala indicates the increasing probability of water scarcity during the non-monsoon season (Pal and Al-Tabbaa 2009). The decreasing trend of the south-west monsoon rainfall leads to short-term meteorological droughts, which will directly affect the agricultural sector as well as the water resources of the state (Thomas and Prasannakumar 2016). The reduction of rainy days in central Kerala during the south-west monsoon is the main reason for higher intensities of rainfall over a shorter period, which contributed to the faster filling up of reservoirs and major landslides in Kerala over the recent years (Vijay et al. 2021). Even though few studies are available showing the variability of rainfall over Kerala,

there exists a lack of detailed research focusing on regional temperature trend patterns in the state.

2.3 RAINFALL CONCENTRATION

Changes in rainfall concentration, as well as its seasonality, have been the subject of numerous studies during the past years across the world (Kanellopoulou 2002; Zhang et al. 2009; De Luis et al. 2011; Feng et al. 2013; Thomas and Prasannakumar 2016; Zamani et al. 2018; Tolika 2019; Zhang et al. 2019). Since rainfall and temperature are the significant influence characterizing the local climate in India, it is highly essential to determine whether the pattern and concentration of climatic variables are also changing in the context of climate change and urbanization. Various researchers have used PCI (Precipitation concentration index) and seasonality (SI) to identify temporal heterogeneity of rainfall distribution in many regions of the world. However, there has been no detailed study of the influence of geographical parameters like latitude and longitude on these indices in India.

2.4 LAND USE AND LAND COVER MAPPING (LULC)

Remote sensing has been extensively used in the field of urbanization with its advancement in spatial technology and large-scale data management. With the advantages of rapid and large-scale data monitoring, remote sensing technology has proven to be an effective way to map LULC dynamics at multiple spatiotemporal scales (Dong et al. 2016; Huang et al. 2017; Patel et al. 2015; Wagle et al. 2020; Zhao et al. 2020). Despite atmospheric disturbances posing complications, multi-temporal satellite data can be utilized through remote sensing to monitor the changes in land cover. Many researchers have successfully adopted the Landsat imageries for urban growth monitoring at various timescales (Huang et al. 2017; Liu et al. 2018; Meng et al. 2021; Patel et al. 2015). These satellite-derived outputs are pivotal in understanding the timely growth of urbanization and its dynamics (Liu et al. 2018, 2020; Zhao et al. 2020). It is often employed in research because of its wide availability and large spatial coverage. In growing urbanization, detailed land cover mapping at various time scales can give important information for preserving the environment, climate studies, and sustainable

social development. Urbanization is one of the crucial factors for LULC changes that shape the current development pattern(Bharath et al. 2018). Despite the many benefits of growing urbanization, it has resulted in the alteration of land cover and the loss of agricultural and green spaces. The increasing urbanization rates have led to variations in land surface temperature mainly due to the changes in the land cover since each land class type has unique energy absorption and radiation (Ahmed et al. 2013; Rana and Sarkar 2021). Therefore, mapping urban dynamics is essential in supporting sustainable policy-making and addressing environmental problems like global climate change and environmental management.

The spatial and temporal phases of urban dynamics can be captured by satellite remote sensing observations at various spatial and temporal resolutions. It is proven helpful for mapping compared with other survey methods. Recently multiple researchers have attempted to give an insight into the complex urban dynamics using various satellite images at finer spatial resolutions. Most studies have used long-term Landsat data for monitoring urban growth because of the availability and spatial resolutions. There are vast possibilities for remote sensing in urban dynamics mapping at global (Gong et al. 2020; Liu et al. 2018, 2020), and regional (Bharath et al. 2018; Cao et al. 2021; Yang et al. 2019) and local scales (Dhanaraj and Angadi 2021; Dutta et al. 2021). This extensive research shows the significant urban expansion in developing countries like India and China. Many researchers have reported complex LULC pattern changes, indicating climate shift (Goldblatt et al. 2016; Choudhury et al. 2019; Dutta et al. 2021). Rana and Sarkar 2021 examined the increase in the built-up area in Bangladesh during the study period of twenty years. In contrast, vegetation has reduced significantly and played an essential role in urban expansion. Cao et al. 2021 examined that urban growth in China has increased nearly fourfold from 1986 to 2017 at the cost of agricultural land, water bodies, and forests. Dhanaraj and Angadi 2021 documented the urban growth of Mangalore city with the help of Landsat images and found that the built-up area has increased by 400% during 1972-2018. In Kenya, Kogo et al. 2021 employed maximum likelihood algorithm for land use and land cover classification for various years using Landsat datasets and detected the urban area growth by 225% from 1995 to 2017.

The Google Earth Engine (GEE) is an open-access and free platform for research and non-profit activities which is widely used as a computing platform for earth system studies in the rise of achievements in cloud computing technologies(Gorelick et al. 2017; Meng et al. 2021; Parastatidis et al. 2017; Xiong et al. 2021). The emergence of the GEE platform enabled users to process large datasets directly and rapidly compared to conventional image processing methods(Gorelick et al. 2017). Platforms such as these come as a boon in terms of lowering the cost and difficulty of handling large datasets, which helps manage societal issues, including climate monitoring, flood and drought management, resource protection, and management. The availability of a multi-petabyte collection of geospatial data on open-source archives with very high cloud-computing resources has wholly changed the remote sensing field, enabling the rapid visualization and easy accessibility of large data sets. The advantage is reduced computation time by pre-processing the raw data, removing the cloud, and mosaicking it in the GEE (Kulithalai Shiyam Sundar and Deka 2022).

GEE computes the resources like satellite imagery and geospatial datasets directly on the platform, making it suitable for various earth system studies, including LULC change detection, trend mapping, and prediction of climate variables at any scale. It has been extensively utilized in urban studies because of its cloud-based geospatial processing power and access to a broad collection of geospatial datasets. The data catalog of GEE contains large publicly available datasets, including Landsat archives, Sentinel series, and weather and climate forecasts which are pre-processed for fast and efficient access. The data management and analysis in GEE are managed through JavaScript API and Python API (Kulithalai Shiyam Sundar and Deka 2022). GEE presents images as raster data comprising one or more bands, whereas vector data appears in GEE as a feature type (Gomes et al. 2020). One of the primary benefits of GEE is that users may view the images in the platform through a web-based Integrated Development Environment (IDE) without downloading the data. The recent advancements in the field of machine learning have significantly improved the accuracy of LULC classification (Dong et al. 2016; Acharya et al. 2019; Wagle et al. 2020). Many researchers have employed ML algorithms over conventional methods due to their efficient computing performance and ease of use (Dong et al. 2016; Patel et al.

2015; Acharya et al. 2019). GEE is handled and accessed via the internet by employing an Application Programming Interface (API) and a related web-based Interactive Development Environment (IDE), which enables rapid visualization (Gorelick et al. 2017). For the betterment of education and research, the remote sensing and climate data catalog of GEE keeps being updated with 6000 scenes per day from active missions (Gorelick et al. 2017; Venkatappa et al. 2021).

GEE has been widely employed in various fields of earth observation studies that include LULC mapping (Huang et al. 2017; Pan et al. 2021), urban growth monitoring (Patel et al. 2015; Goldblatt et al. 2016), and resource management (Shelestov et al. 2017; Venkatappa et al. 2021), to list a few. Goldblatt et al. (2016) used three different classifiers on GEE for detecting the urban areas in India from Landsat 7 and Landsat 8 imageries. Huang et al. 2017 documented the changes in the LULC classes in Beijing over three decades with the help of GEE. Framework was proposed on GEE for mapping annual urban dynamics in China by (Cao et al. 2021). Kulithalai Shiyam Sundar and Deka 2022 utilized three different machine learning techniques, namely support vector machine (SVM), Random Forest (RF), and CART for LULC mapping of the Vembanad Lake system, Kerala on the GEE platform. Abraham and Kundapura 2022 employed a random forest classifier for LULC mapping of the Meenachil and Manimala basins in Kerala, India, for five different periods and projected the LULC map up to 2050. An efficient framework was proposed in this study for mapping the urban dynamics of Kerala at an annual scale using classification methods and time series analysis. Two supervised machine learning classifiers were used to classify the LULC using the GEE platform; Random Forest (RF) method and the Classification And Regression Tree (CART) for 3 decades. The areal change in the study for each class is further analysed.

2.5 EXTREME CLIMATE INDICES

Previous studies on climate variables have revealed that climate change is an undisputed fact, causing a series of problems like the frequent occurrence of extreme climate events such as heat waves, extreme precipitation, and flash floods, etc. (Field et al. 2012; Mukherjee et al. 2018; Wang et al. 2021a; Zhao et al. 2019). The sharp rise

in extreme climate indices is one of the primary indicators of global climate change, which imposes immense environmental and societal challenges worldwide. Therefore, research on climate extremes has received considerable interest across the globe for disaster management and sustainable development. World economic forum 2020 has ranked climate extremes as first among the top ten risks in impact over the next ten years (McLennan 2021). The frequency and intensity of extreme events have increased in recent years and are likely to escalate due to human-induced climate change (Chapman et al. 2017; Lau and Nath 2014). Due to the substantial damage caused by heavy rainfall in cities, an increasing amount of research has been directed toward examining the impact of urbanization on extreme rainfall events. Climate extreme studies based on various indicators have marked an overall rise in duration, frequency, and intensity in the past few decades (Alexander 2016; Asfaw et al. 2018; Chu et al. 2010; Kumar et al. 2020). Many researchers have pointed out the influence of anthropogenic factors in increasing the frequency and duration of these events. Prior studies suggested that UHI is linked to increased extreme temperature events (Lin et al. 2020; Luber and McGeehin 2008) and extreme precipitation events (Lin et al. 2020; Yang et al. 2017c). Numerous efforts have been made to assess the impact of urbanization on different climate events through the comparison of meteorological data collected from urban and rural stations (Ren et al. 2008; Ren and Yaqing 2014; Gu et al. 2019b; Zhao et al. 2019; Lin et al. 2020; Zhang et al. 2021; Oh et al. 2021; Pimonsree et al. 2021; Wang et al. 2021b; Liao et al. 2021; Kang et al. 2021; Manalo et al. 2022).

Ren et al. 2008 analyzed the urbanization effect on surface temperature in various stations of north China from 1961 to 2000 and estimated the contribution of urban warming to annual mean temperature. Ren and Yaqing 2014 did a similar study on extreme temperature indices in Mainland China during 1961-2008 and found that urbanization negatively impacted annual cold nights and led to an increase in annual warm nights. A study by Zhao et al. 2019 examined the effects of urbanization on extreme temperature and precipitation in Beijing-Tianjin-Hebei during 1980-2015 and found that negative urbanization affects cool indices in medium-sized cities. In contrast, it positively affects warm indices in large cities. The study pointed out the insignificant urbanization effect on extreme precipitation. Various studies pointed out the regional

discrepancies in urbanization effect on extreme precipitation indices than temperature extremes (Zhao et al. 201; Lin et al. 2020). The warming impact on urban areas could intensify daily rainfall extremes more than in nearby rural areas (Huang et al. 2022, 2023; Lei et al. 2023). The intensifying daily rainfall extremes with short duration periods can trigger flash floods in urban areas (Miller and Hutchins 2017). Increased built-up areas, UHI, aerosol concentration, and enhanced sensible heat are the major causes of intensifying urban rainfall (Shepherd 2006; Yang et al. 2017a; Lin et al. 2020). Pimonsree et al. 2021 also highlighted statistically significant urbanization effects on extreme temperature indices in Thailand based on 1970-2019 daily observed data. In Thailand, urbanization has led to an augmentation of rainfall extremes, resulting in alterations in the quantity, frequency, intensity, and magnitude of precipitation (Pimonsree et al. 2021). Hence, it is imperative to examine the profound effects that extreme climate events exert globally and at regional levels, considering their significant repercussions on society and the environment.

Developing countries with high populations, like India and China, are more prone to climate change. In a changing climate, India faces susceptibility to a broad spectrum of climate extremes (Bisht et al. 2019; Sharma and Mujumdar 2017). Studies suggested that urbanization highly influences rainfall amount and spatial pattern (Kishtawal et al. 2010). Shastri et al. 2015 showed that urbanization had intensified extreme rainfall in cities which is not visible in rural areas. The study highlighted the effect of urbanization on the relationship between large-scale atmospheric circulations and extreme rainfall events resulting the extreme rainfall in the post-urbanization period. Kishtawal et al. 2010 studied the relationship between Indian monsoon rainfall and urbanization using population datasets and long-term rainfall datasets. During the monsoon season, there has been a notable upward trend in the frequency of heavy rainfall observed in urban areas of India (Kishtawal et al. 2010). The intensification in UHI magnitude caused by rising buildings and increasing artificial surfaces significantly altered the frequency, intensity, and rainfall pattern in Indian cities (Shastri et al. 2015). The study by Mondal and Mujumdar 2015 revealed that non-stationarity in rainfall extremes in India is primarily attributed to local changes rather than factors like global warming or large-scale natural variability like the El-Nino–Southern Oscillation index.

This current study aims to connect the changes in extreme climate events with the level of urbanization in India, driven by the conclusions of previous research and the requirement for sustainable development in the region. This study holds great significance in planning and policy formulation, particularly regarding the effects of urbanization and global warming in urban and rural areas in the Indian subcontinent.

2.6 HEAT WAVES AND COMPOUND EVENTS

Due to their significant impact on human health, extreme weather events such as heat waves have garnered widespread attention. Heat waves generally refer to consecutive hot days and are considered the silent meteorological killer (Mora et al. 2017). It has the potential to endanger various aspects of society and ecosystems, such as health care, agriculture production, and ecosystem sustainability, and much research is being conducted on the magnitude, intensity, and frequency of HW events at global and regional scales, particularly in developing countries such as China and India (Das and Umamahesh 2022; Liao et al. 2018; Lin et al. 2018; Luo and Lau 2017; Mishra et al. 2017; Singh et al. 2021; Wu et al. 2021b). Due to global warming, heat wave activity in many parts of the world has intensified over the past few decades and is projected to increase further, posing increasingly severe threats to society (Luo and Lau 2017; Lin et al. 2018). The primary objective of the Paris Agreement is to limit global emissions to ensure that the temperature increase remains below 2 degrees Celsius compared to pre-industrial levels, which can be accomplished by adhering to RCP 2.5 scenarios. Unfortunately, since 2005, the world has been more aligned with RCP 8.5, and if current policies persist, it is projected that the temperature will rise by over 3 degrees Celsius by the end of the century (Schleussner et al. 2016; Wang et al. 2020a).

Over the past decades, numerous deaths and diseases have resulted from extreme heat events. The 2003 European Heat wave resulted in more than 70,000 fatalities and a substantial decline in primary productivity (Robine et al. 2008). During the summer of 2010, the exceptionally high temperatures in Russia resulted in an estimated 55,000 fatalities and caused a financial loss of billions of dollars (Barriopedro et al. 2011). Likewise, over the years, India has witnessed death due to heat waves. In various regions of India, 2248 individuals lost their lives due to the heat wave in 2015.

Persisting anomalous atmospheric conditions due to the delayed onset of the south-west monsoon was the leading cause of this unprecedented event (Rohini et al. 2016). Several studies show that the prevalence of multi-day occurrences with unusually high surface air temperatures has increased across the Indian subcontinent over the last fifty years (Mishra et al. 2017; Murari et al. 2016; Rohini et al. 2016, 2019; Singh et al. 2021; Das and Umamahesh 2022). Due to the rapid global economic and social development trend characterized by urbanization, developing countries face many challenging issues. The urbanization process in developing countries exacerbates the UHI effects, further contributing to the intensification of heat wave characteristics in the urban environment. Heat waves significantly influence the population since they cause heat-related deaths and increase the risk of exhaustion and numerous breathing issues and cardiovascular disorders, among other things (IPCC 2012.).

The number of deaths caused by heat waves has considerably increased in recent years. Every year, more than 30% of the world's population is exposed to potentially deadly combinations of heat and humidity for at least 20 days (Mora et al. 2017). Urban areas experience more intense heat wave threats than rural regions, as the UHI exacerbates the effects of heat waves on people. Most prior studies on extreme temperatures have found a shift in the frequency distribution of mean and maximum temperature, indicating that heat waves will become more common and robust in the future (Lau and Nath 2014; Luo and Lau 2017). Heat wave events induce discernible alterations in the ambient atmospheric circulation, precipitation patterns, and the land-ocean surfaces in their vicinity (Lau and Nath 2014). According to research, a slight rise in the mean temperature can alter the intensity and frequency of extreme temperature events such as heat waves (Das et al. 2022; Trenberth et al. 2007). Heat waves in Europe and Asia may be modified by the mega-ENSO and the Atlantic Multi-decadal Oscillation (Zhou and Wu 2016). In China, it was found that climate warming and anthropogenic activities were responsible for 75% of heat waves, while urbanization was located to potentially accelerate the onset of HW events (Luo and Lau 2017; Wu et al. 2021b).

Many studies have investigated the spatio-temporal characteristics and associated mechanisms of the heat wave (Liao et al. 2018; Singh et al. 2021). Recent research

conducted in India has indicated that under future climate scenarios, there is a likelihood of increased occurrence of extreme events such as heat waves in the country (Das and Umamahesh 2022; Ghatak et al. 2017; Mishra et al. 2017; Murari et al. 2016; Singh et al. 2021). The concerns for human health and the environment make examining historical and future exposure to heat waves in India essential. In recent years, there has been a concerning rise in the number of deaths caused by heat waves in India. From 1978 to 1999, a cumulative total of 5,330 deaths were reported. However, in 2003, reported deaths decreased significantly to 3,054 (Ratnam et al. 2016). Lethal heat waves that affected large stretches of the eastern coast and central India in 2015 may have been made worse by human-induced climate change (Kishore et al. 2022). The circulation pattern is modified during El Niño, weakening the south-westerlies in the Arabian Sea. These atmospheric changes are associated with more severe and prolonged heat waves during El Niño years (Murari et al. 2016). India has experienced a rise in its average temperature exceeding 0.5 °C, and it is anticipated that by the end of the twenty-first century, various regions across the country will undergo a range of regional warming between 2.2 and 5.5 °C (Das and Umamahesh 2022). The increase in simultaneous occurrences of hot days and nights in India can be attributed to anthropogenic emissions. Furthermore, these hot extremes are projected to escalate significantly faster under global warming scenarios (Mukherjee and Mishra 2018). Despite the enormous environmental impact, no systematic approach has been made to understand the characteristics of the heat wave in India at the regional level. With India currently experiencing rapid urbanization and an expected increase in urban population, it is reasonable to anticipate that heat waves in India will become more frequent and intense, resulting in significant damages, economic losses, and even loss of human lives.

Compound climate extreme events can cause more threats to society and the environment compared to individual events (Zscheischler et al. 2018). Extensive efforts have been devoted to climate risk assessment studies considering individual climate events (Gao et al. 2016; Kumar et al. 2020; Mishra et al. 2017; Singh et al. 2021; Wang et al. 2020b). Rising global temperatures significantly raise the likelihood of concurrent occurrences of multiple extremes, such as droughts and heat waves (Perkins et al.

2012). Although climate change may not directly cause droughts, it is anticipated to amplify the severity of droughts (Trenberth et al. 2014). Between 1902 and 2019, there has been a widespread increase in the occurrence probability of compound meteorological and hydrological hot-dry extremes on a global scale (Min et al. 2023). Previous studies have pointed out that compound events could result in severe natural disasters and have a prominent effect on agriculture and the ecosystem (Sharma and Mujumdar 2017; Shi et al. 2021). Many mortalities and socioeconomic losses were experienced in numerous regions worldwide due to compound event disasters in 2003, 2010, and 2018 (Bian et al. 2022). Through non-linear effects, compound events can potentially exacerbate the impacts of heat waves and stagnation on ozone (Gao et al. 2020). Various researchers have pointed out that the increase in compound events globally was mainly attributable to anthropogenic activities (Luo and Lau 2021; Wang et al. 2021a). Prior studies revealed that a rise in compound occurrences is directly linked to declining agricultural yields (Feng et al. 2019; Mishra et al. 2020), more wildfire events, and worsening human health (Poumadere et al. 2005). The changes in rainfall intensity and frequency have led to increased occurrences of severe droughts and devastating floods, adversely impacting water resources management and agriculture worldwide, including in India(Pal et al. 2021; Trenberth et al. 2014; Vijay et al. 2021). Recently, India has experienced severe droughts, while heat waves have become increasingly common across various regions of the country (Mukherjee et al. 2020; Mukherjee and Mishra 2021). It is highly likely that the escalation of dry summer conditions will significantly contribute to the occurrence of widespread and prolonged severe heat waves throughout India (Kishore et al. 2022).

By the end of the twenty-first century, a substantial rise in the affected land areas experiencing high-magnitude heat waves compared to lower magnitudes is reported by Kishore et al. 2022. India's susceptibility to diverse climate extremes, including floods, droughts, heat waves, and related events, is widely acknowledged. However, the precise extent of their co-occurrence remains uncertain. Compound climate extremes have witnessed a notable rise, primarily attributed to the combined influence of internal climatic variability and external anthropogenic forcings. This increase is expected to persist consistently into the future across different Representative Concentration

Pathways (RCPs) and Shared Socioeconomic Pathways (SSPs) (Yu et al. 2023). The increasing threat of compound events in developing countries calls for an improved understanding of the contribution of urbanization to extreme events. Nevertheless, despite initial glimpses into the role of urbanization in exacerbating compound events, there is a dearth of research investigating the specific influence of urbanization on compound events within the context of India.

2.7 ESTIMATION OF URBANIZATION CONTRIBUTION

Anthropogenic activities like greenhouse gases emission and LULC changes such as urbanization and agriculture highly influence the climate of a region. Understanding the influence of various factors on climate is crucial since it is directly linked to global warming. Prior studies pointed out the significant role of urbanization on the environment and energy flow (Kalnay and Cai 2003; Kennedy et al. 2015; Pimonsree et al. 2021; Yao et al. 2019). Urban land cover is anticipated to expand by over 1.2 million km^2 by 2030, almost three times the urban land extent in 2000 (Seto et al. 2012). This points out that the near future may witness a more substantial impact on the climate due to urbanization. It is crucial to evaluate the long-term and widespread effects of urbanization on the environment, considering its significant impact on the climate and the expected increase of this impact in the future. Both climate change and urbanization are altering the components of the hydrological cycle.

Urbanization has led to a widespread replacement of natural surfaces with artificial ones, expanding impervious areas characterized by high heat storage capacity. However, these artificial surfaces often lack water permeability, negatively impacting the natural water cycle(Lu et al. 2019). Urbanization decreases infiltration and increases peak stream flow and surface runoff. Additionally, it reduces base flow and groundwater recharge (Miller et al. 2014). Urban areas are projected to face more frequent and severe flooding due to the combined effects of climate change and urbanization (Berggren et al. 2012; Miller and Hutchins 2017). Therefore, it is imperative to prioritize the development of robust urban drainage systems capable of effectively managing and mitigating these challenges. Through their observations and modelling outputs, previous studies have confirmed that the frequency and severity of

flood events are significantly increased by urbanization, amplifying the threats in major cities (Lei et al. 2023; Marelle et al. 2020). Urban areas have a risk of experiencing dangerous events like flash floods from high-intensity, short-duration storms, which are areas that contribute to environmental change on various scales (Li et al. 2020; Yu et al. 2022).

Many studies have investigated the impact of urbanization on changes in precipitation. Most researchers agree that urbanization has played a role in elevating the quantity and frequency of rainfall in urban areas. They have examined various aspects, including the total amount of precipitation (Liu and Niyogi 2019), seasonal rainfall, precipitation frequency, and extreme precipitation events. A thorough investigation is required to investigate the impact of urban areas on several factors, such as climate impacts such as extreme climate events and heat waves. Understanding how these influences affect the urban population's environment, vegetation, atmosphere, and livelihoods is critical. Various studies show a major distinction in climate conditions between urban and rural stations (Kalnay and Cai 2003; Liao et al. 2016; Yang et al. 2011; Zhao et al. 2019). Burian and Shepherd 2005 discovered that the urban area had almost 80% more rainfall occurrences than the surrounding areas. The intersection of urban development and climate change results in a compounding effect, leading to an amplified escalation in temperatures (Manalo et al. 2022; Oh et al. 2021; Ren et al. 2008; Sajjad et al. 2021; Sussman et al. 2019). The urbanization effect can be quantified using observations in urban areas with those surrounding rural areas, and results can be different based on the criteria with which stations are chosen. The classification of urban and rural grids is done dynamically, which is suggested by various researchers (Lin et al. 2018; Wang et al. 2022, 2021b; Wu et al. 2020b, 2021b; Zhao et al. 2019).

2.8 RESEARCH GAP

Urbanization is the expansion of urban areas, which results in population growth, a rise in built-up area and population density, and modifies how people live in cities. Uncontrolled urbanization and land use land cover change result in challenges with beneficial and harmful consequences, such as unauthorized urban sprawl, agricultural land loss, high land values, and other associated issues. Monitoring urbanization is

critical for planners, management bodies, and governmental and non-governmental organizations in implementing policies to optimize natural resource use and accommodate development while minimizing environmental effects. The rapid expansion of urban areas due to population increase and economic growth is increasing the demand for natural resources, generating land-use changes, particularly in metropolitan regions. As a result, serious problems associated with rapid growth, such as expanding settlements, environmental deterioration, harm to ecological structures, and a lack of natural resources, need to be carefully examined.

Monsoon rainfall is critical to the Indian economy and people's livelihoods. An accurate understanding of climate variables is critical because rain-fed agriculture accounts for over half of the country's GDP. However, global warming and urbanization have caused regional and global climate changes, directly impacting the country's agricultural economy. An accurate study of climatic variables is crucial for regions such as India, one of the world's most drought-prone nations, despite receiving 1190 mm of rain each year. As a result, a better understanding of the trends and variability of climate variables is critical for measuring climate-induced changes and resolving water management challenges more effectively. According to the Census 2011, India's urban population increased by 2.76% per year between 2001 and 2011, reaching 377 million. The overall urbanization rate in the country increased from 27.7% in 2001 to 31.1% in 2011. Between 1992 and 2000, the GDP growth was limited to 6%, and the growth trajectory started to noticeably accelerate in the early 2000s, marking a significant change. This significant improvement is sometimes linked to the late consequences of the changes carried out in the 1990s (Erumban et al. 2019). Economic growth was one of the primary drivers for faster urbanization between 2001 and 2011.

Rapid urbanization is one of the critical causes of global warming, resulting in the degradation of ecological balance and human health. Over the past decade, the urban population of Kerala has witnessed a rapid increase, leading to significant growth. This growth is attributed to a threefold rise in the number of towns in the state. As indicated by the proportion of the state's population residing in urban areas, urbanization has experienced a substantial surge from 25.96 % in 2001 to 47.72% in 2011. In comparison, the corresponding figures for India were 25.52% in 2001 and 31.16% in

2011. According to the 2001 Census, Kerala was ranked 19th among Indian states in urbanization levels but climbed to 9th in 2011(Census 2001, 2011). Between 2001 and 2011, Kerala had the highest urbanization since the state's inception (Cyriac 2022; Lal and Nair 2017).

2.9 SCOPE OF THE STUDY

The study has explored the impact of urbanization in altering extreme climate events in Kerala using the dynamic classification method. The study has employed the K-means algorithm and PCA to delineate 59 rainfall grid points to 5 homogeneous clusters inside Kerala. Each cluster's rainfall and rainy days characteristics were analyzed, and a box-whisker plot of 5 clusters was constructed. The trend analysis of long-term rainfall, rainy days, and temperature (mean, minimum, and maximum) was done using five trend analysis techniques, and the magnitude of the trend is estimated by Sen's slope method. The seasonality index (SI) and precipitation concentration index (PCI) have examined rainfall concentration and seasonality. The extreme climate indices proposed by ETCCDI have been used to investigate climate extremes over Kerala comprehensively. A total of 24 climate extreme indices were taken for the current study based on the climatic characteristics of the Kerala state, in which 12 temperature extremes and 12 precipitation extremes were included. The changes in the long-term trends and spatial variation of various heat wave characteristics were investigated using various statistical methods.

Further, an attempt has been made to analyse the spatio-temporal variation of heat wave-drought compound events in Kerala from 1951-2020 and compare heat wave intensity and duration in compound events with that in individual heat wave events. The trend analysis of extreme climate indices, heat waves, and compound events was done using the modified Mann-Kendall technique proposed by Hamed, K. H., & Rao 1998. Sen's slope method estimated the magnitude of the trend. The study employed Landsat images taken from 1990 to 2020 using two different machine learning classifications, Random Forest (RF) and Classification And Regression Trees (CART), on Google Earth Engine (GEE) platform. Normalized Difference Vegetation Index (NDVI), Normalized Differences Built-up Index (NDBI), Modified Normalized Difference Water Index (MNDWI), and bare soil index (BSI) are the indices used in

addition to aid the accurate LULC classification. The study has employed the dynamic classification method for urban and rural grid classification with the help of time-varying land cover data, which provided better insights into the urbanization process in Kerala over the past 30 years. The approach employed to assess the impact of urbanization on climate extremes involves comparing trends between urban and adjacent rural areas. This study offers valuable insights into comprehending the alterations in extreme weather events occurring in Kerala and their association with urbanization.

2.10 RESEARCH OBJECTIVES

Based on the literature gaps identified in the related studies, the following objectives were termed

1. To perform the long-term trends test to verify climate variables over the Kerala state
   - To delineate rainfall clusters and identify the influence of geographical and statistical parameters of grids
   - To detect and quantify trends in annual and seasonal time series of rainfall, rainy days, and temperature over Kerala using five trend analysis techniques
   - To analyse the concentration and seasonality of rain in various clusters.
2. To compute various land use indices and the historical land use and land cover of Kerala
   - To classify the urban and rural grids using time-varying LULC maps
3. To quantify the contribution of urbanization to the changes in extreme climate events, heat waves, and compound events.
   - To investigate the changes in the long-term extreme climate indices, heat waves, and compound events.
   - To assess the impact of urbanization on changes in extreme events through dynamic classification methods.

CHAPTER 3

STUDY AREA

3.1 OVERVIEW OF THE STUDY AREA

The focus of the present study was Kerala, a state that is situated on India's southernmost point within latitudes 8° 15’ to 12° 50’ N and longitudes 74° 50’ to 77° 30’ (Figure 3.1). Kerala's geographical boundaries are formed by Karnataka to the north and northeast, Tamil Nadu to the east and southeast, and the Lakshadweep Sea to the west. This geographic arrangement defines Kerala's geopolitical environment within the Indian subcontinent, including its territorial boundaries and neighboring states. Such delineation is critical for administrative, political, and socioeconomic assessments, allowing for a better understanding of Kerala's regional dynamics and interstate ties. The state's topography and ecology combine the coastal regions, wetlands, plains to the west, rolling hills, and the Western Ghats Mountain range to the east.

3.2 GEOGRAPHY OF THE STATE

The area of the state is 38,863 km^2 which accounts for about 1.20 % of the total geographical area of India. Kerala's land surface and LULC are tropically diverse, with varying terrain across three distinct zones based on altitude: lowland (west side), midland (between lowland and highland), and highland (east side). The Highlands descend from the Western Ghats and lead into the Midlands, which are notable for their hills and valleys. Kerala's coastline stretches 580 kilometres and is known for its backwaters, which are linked by canals and rivers. While the Highlands and Midlands are densely forested, other parts are used for agriculture, including tea, coffee plantations and commercial crops. Overall, the state is primarily green, creating a relaxing and serene atmosphere. The midland of the Kerala serves as a hub for the key cultivation activities of the state. This region, tucked between the Western Ghats and the coastal region, produces a wide variety of crops due to its favourable climatic conditions and good soil. Rice is a staple crop grown in Kerala's midland plains, as are rubber, spices, fruits, and vegetables. The region's moderate elevation and abundant

rainfall provide an excellent environment for producing various commodities, making midland Kerala an essential contributor to the state's agricultural economy.

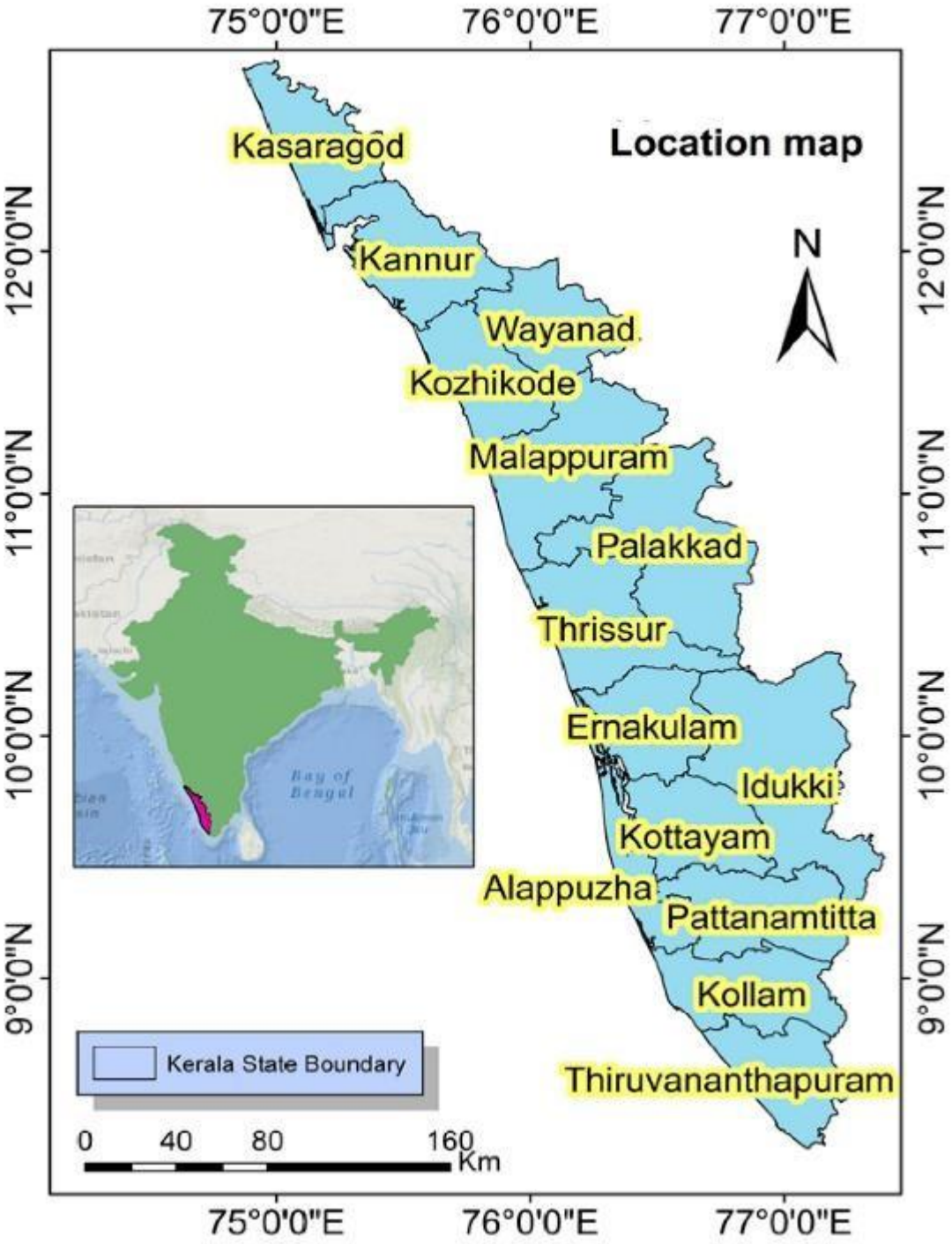

Figure 3.1. Location map of the study area -Kerala

The state's coastline is a significant economic driver, generating income through fishing, tourism, and agriculture. The fishing sector thrives on the abundant marine biodiversity, while tourism benefits from the beaches and backwaters, attracting tourists worldwide. Coastal populations rely on marine resources for food and revenue, which benefits the state's economy. In addition, the region's tropical temperature and sandy soils support agriculture, particularly coconut farming. Overall, Kerala's coastline is critical to the survival of local economies and the growth of various industries. The state is renowned for its intricate network of forty-four rivers, forty-one of which originate from the Western Ghats in Eastern Kerala. The Western Ghats, towering at an average elevation of 1500 meters above sea level, boast peaks reaching around 2500 meters, contributing to Kerala's diverse geographical profile. To the west of these mountains lies the midland plains, extending across central Kerala. Expansive paddy fields characterize the lower regions of these plains, while the elevated slopes are adorned with rubber and fruit trees and crops like black pepper and tapioca. Along the coastal belt of Kerala, the landscape transforms into flat expanses dotted with paddy fields and coconut trees, crisscrossed by a network of interconnected canals and rivers.

3.3 CLIMATE

The state's climate is humid and tropical, greatly influenced by heavy seasonal rains from the south-west and north-east monsoons and winter and summer seasons. The Palakkad gap separates the Western Ghats into two parts, which stretch about 24 kilometers. Most of Kerala's annual rainfall occurs during the monsoon period, which spans only a few months. The high-intensity storms that characterize this season lead to significant river discharges, leaving the state susceptible to water scarcity during non-rainy periods (Vijay and Varija 2022). Kerala state, recognized as the entry point for the summer monsoon in the Indian subcontinent, experiences an average annual rainfall of approximately 2666 mm (Vijay and Varija 2022). Kerala experiences four distinct seasons for rainfall: the south-west monsoon (June to September), the north-east monsoon (October to November), winter (December to February), and summer (March to May). The south-west monsoon current is responsible for most of the annual rainfall in Kerala. It undergoes a forced ascent at the Western Ghats, resulting in the windward slopes receiving significant rainfall compared to the leeward side. The

coastal region of Kerala gets abundant rainfall, while the western windward slopes of the hills and mountains experience substantial rainfall during the monsoon period. These slopes serve as watersheds for many rivers. Kerala's high humidity is caused mainly by its proximity to the Arabian Sea in the west, which serves as a moisture supply. This coastal closeness keeps the state damp, promoting lush flora and regulating temperature variations.

Rainfall in Kerala decreases towards the southern parts of the state as the height of the Western Ghats drops. The southern-most district of Thiruvananthapuram, where the Ghats are closest to the coast and at their lowest elevation, receives the least rain. Local thunderstorm showers in April and May and monsoon rains are known as 'Edavapathi,' while rainfall during the north-east monsoon is known as 'Thulavarsham.' The south-west monsoon typically comes in southern Kerala about June 1st. It covers the entire state by June 5th, with June and July being the rainiest months, accounting for approximately 23% of total annual rainfall. Despite its small size, the State exhibits diverse topographical and climatic conditions that result in a wide range of land use and cropping patterns(http://kerenvis.nic.in/Database/CLIMATE_829.aspx). Agriculture utilizes more than 50% of the land area, while approximately 30% of the State is covered by forests. Given its heavy reliance on agriculture and tourism, accurate rainfall forecasting is crucial for the state. Several studies have linked the rising occurrence of severe rainfall events to a changing climate over the past two decades and anthropogenic activities like urbanization that may affect atmospheric circulation(Krishnakumar et al. 2009; Kishtawal et al. 2010; Shastri et al. 2015; Zhang 2020)**.**

3.4 MAJOR CROPS

Kerala's agriculture revolves around rice, with numerous types grown in its paddy fields, particularly in the Kuttanad district. Tapioca is another important crop, especially in drier regions, where it is a staple food. The state is well-known for its spice production, mainly pepper, which contributes significantly to the national output. Kerala's agricultural industry relies heavily on cash crops such as tea, coffee, cashew, and coconut, with coconut playing a critical part in the state's economy. Kerala's forests are predominantly found in the Western Ghats, widely recognised as a biodiversity hotspot. These forests support a diverse range of rare and endangered plant and animal

species, adding to the region's unique biodiversity. Kerala's forests, with their lush and diverse ecosystems, are vital for conservation efforts and scientific study aimed at maintaining our planet's natural heritage. The state's natural vegetation is diverse, comprising 3,872 flowering plants, including 900 with medicinal properties. The state's forested areas cover 9,400 km², including tropical, wet evergreen, deciduous, and subtropical forests. Agriculture is central to Kerala's economy, with main crops like paddy, coconut, pepper, and cashew, alongside cash crops such as tea, coffee, spices, and cashew nuts\

3.5 URBANIZATION

The state has witnessed rapid urbanization during the past three decades, with an increase of 83.20% over the last decade, as per the 2011 census. Moreover, Kerala is very vulnerable to climate extremes due to the complicated topography and fragile eco-environment. Urban areas in Kerala predominantly line the coastal regions, with a noticeable rural-urban continuum along this narrow coastal strip (Lal and Nair 2017). According to the 2011 Census, the population of Kerala is 33,387,677, and the share of the urban population in the State has risen sharply from 25.96% in 2001 to 47.72% in 2011. Over the last decade, the State of Kerala has witnessed a remarkable three-fold increase in the number of towns, consequently driving substantial growth in its urban population. In fact, between 2001 and 2011, Kerala boasted the highest urban growth rate among all Indian states. Despite having a comparatively smaller urban population when compared to larger states, Kerala's remarkable surge of 92.8% during the 2001-2011 period. The rapid urbanization has put tremendous strain on groundwater resources throughout Kerala (Devi and Nair 2021). Urbanization in Kerala is characterized by a lack of distinct rural-urban boundaries, with a continuous transition between urban and rural areas. However, there was a significant surge in the urban population proportion during 2001-2011, the largest for any Indian state (Census 2011; Firoz C, Mohammed and Banerji, Haimanti and Sen 2014; Lal and Nair 2017).

The increase in Kerala's urban population is mainly driven by significant growth in Malappuram, Thrissur, Kollam, and Kasaragod districts. Despite this, Kannur district has continuously ranked as the most urbanised, closely followed by Ernakulam in the

1991 and 2001 census periods. However ,Ernakulam district stands out having the highest urban population among all districts. Between 1991 and 2001, urbanization in Kerala slowed, but then increased significantly to 83.73% between 2001 and 2011. Malappuram district witnessed the most significant urbanization growth among all districts, followed by Kollam, Thrissur, and Kozhikode. Between 2001 and 2011, Kerala witnessed a 17.5% decrease in urban population density, which can be attributed to the expansion or spread of urban areas throughout the state. Urbanization is currently advancing faster in the state's midlands and highlands than in its coastal regions. The state's agricultural and forestry areas are largely located in the midlands and highlands(Thaickavil 2020). The primary catalyst for development in these regions is the conversion of forest and agricultural lands into built-up structures, spurred by factors such as tourist development and highway expansion. The concept of urban agglomerations was introduced by the Census of India in 1981. In Kerala, the number of identified urban agglomerations increased from 9 during the 1981 census to 19 by the 2011 census (The government of Kerala 2012). In Kerala, urban population growth primarily arises from the expansion of urban areas and the urbanization of outlying regions surrounding major urban centres, rather than from the concentration of population into existing urban areas.

CHAPTER 4

METHODOLOGY

The datasets and the methodologies utilized in this study are discussed in this chapter. Comprehensive information regarding the data employed for each objective can be found under the respective section headings outlined below. The methodology for the proposed study is summarized in Figure 4.1, encompassing three primary components: a) Preparation and analysis of climate data, b) Land use land cover mapping, and c) Assessing the influence of urbanization on alterations in extreme climate events, including heat waves and compound events.

4.1 DATA

For this study, various trend analysis tests of climate variables were conducted using long-term gridded rainfall data with a spatial resolution of 0.25° x 0.25° (covering 59 grid points) from 1901 to 2019 (Pai et al. 2014). Additionally, gridded temperature data with a spatial resolution of 1° x 1° (from 1951 to 2019) were obtained from five grid points within the study area, sourced from the India Meteorological Department (IMD) in Pune (Srivastava et al. 2009). To create the precipitation data series, a conversion process was employed to transform 6995 station-based observations into gridded datasets using Shepard's interpolation technique, allowing for generating a spatially continuous representation of the data (Pai et al. 2014). The temperature data set was created using a modified version of Shepard's angular distance weighting algorithm based on the temperature data of 395 quality-controlled stations (Srivastava et al. 2009). The study utilized five non-parametric trend tests such as the Mann-Kendall test (MK), modified Mann-Kendall (MK-CF1), modified Mann-Kendall test (MK-CF2), Pre-whitening Mann-Kendall test (PWMK) and innovative trend analysis (ITA). For the study's second objective, Landsat images for various years were collected. The datasets used in this study are readily available in the GEE repository, which includes atmospherically corrected, tier 1 surface reflectance imagery, and many other datasets. For the LULC change mapping, Landsat 5, Landsat 7 and Landsat 8 image series with less than 20 % cloud cover are mainly utilised. Figure 4.1 illustrates the methodology chart followed for the current study. For the third objective, the long-term gridded

rainfall data of 0.25° x 0.25° spatial resolution (59 grid points) for the period from 1951 to 2020 and temperature gridded data of 0.25° x 0.25° spatial resolution were utilized. The bilinear interpolation is used to resample the temperature dataset to ensure spatial similarity in both datasets. The study utilised the modified Mann-Kendall test (MK-CF1) for assessing the significance of trends in climate indices. Sen's slope was employed to examine the temporal trends of indices, HW measures and compound events.

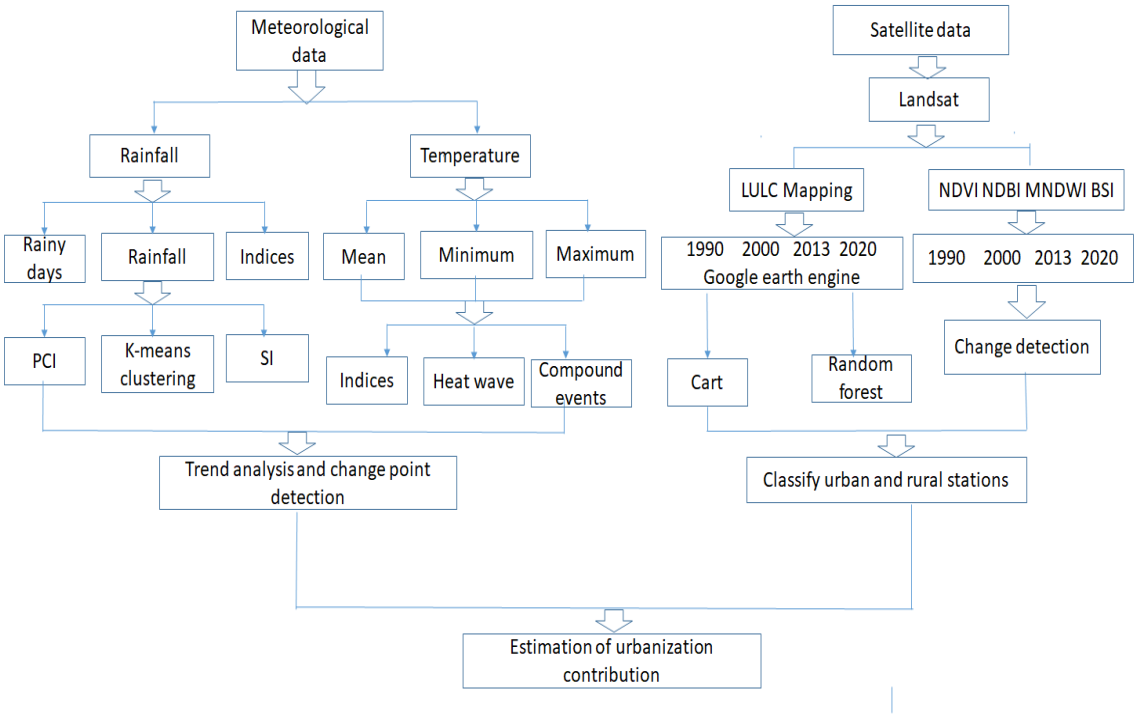

Figure 4.1. Methodology of the study

4.2 TREND ANALYSIS

The study employed five non-parametric trend tests to analyze the rainfall, rainy days, and temperature data series from 1901 to 2019. These tests included the Mann-Kendall test (MK), modified Mann-Kendall (MK-CF1), modified Mann-Kendall test (MK-CF2), Pre-whitening Mann-Kendall test (PWMK), and innovative trend analysis (ITA). These trend analysis techniques were able to assess and analyze the trends in the data comprehensively, accounting for various factors and characteristics within the dataset.

To analyze the statistical significance and direction of historical trends in rainfall, rainy days, and temperature, a significance level of 5% was used in this study.

4.2.1 Mann-Kendall Test (MK Test)

The Mann-Kendall trend test is a distribution-free, non-parametric statistical test specifically developed to detect trends in a series, even when a seasonal component may be present (Kendall 1975; Mann 1945). Researchers widely employ this test to identify and evaluate monotonic trends in different data types, such as environmental, climate, and hydrological data. Its rank-based approach allows for effective trend analysis in time series data, ensuring robustness even in seasonal variations. By utilizing the Mann-Kendall trend test, researchers can gain valuable insights into the presence and significance of trends in their datasets. In this test, the null hypothesis (H_o) assumes that the data are independently and identically distributed within a population. Conversely, the alternative hypothesis (H_1) posits the presence of a monotonic trend in the data. The Mann-Kendall test statistic is calculated according to:

$$S = \sum_{k=1}^{n-1} \sum_{j=k+1}^{n} \operatorname{sgn}(x_i - x_j) \tag{4.1}$$

With

$$sign\,(x_i - x_j) = \begin{cases} 1, \ if\ (x_i - x_j) > 0 \\ 0, \ if\ (x_i - x_j) = 0 \\ -1, \ if\ (x_i - x_j) < 0 \end{cases} \tag{4.2}$$

where x_i and x_j are the ranked values of the series and n is the length of the series. When the n is greater than 10, the statistic is said to have a normal distribution. In such cases, the mean (E(S)) and variance (Var (S)) for the statistic S can be determined using the following values;

$$E(S) = 0 \tag{4.3}$$

$$\text{Var}\,(S) = \frac{n(n-1)(2n+5) - \sum_{j=1}^{j} t_j(t_j-1)(2t_j+5)}{18} \tag{4.4}$$

where t_j signifies the duration between compared values (with zero difference), the summation over all ties is denoted. The test statistic Z is employed as an indicator of the statistical significance of the observed trend. The standardized test statistic Z is given by:

$$Z = \begin{cases} \frac{S-1}{\sqrt{\mathrm{Var}\,(S)}}, & if\ S > 0 \\ 0, & if\ S = 0 \\ \frac{S+1}{\sqrt{\mathrm{Var}\,(S)}}, & if\ S < 0 \end{cases} \quad (4.5)$$

The null hypothesis is rejected if the absolute value of the Z statistic is greater than the corresponding theoretical value of $Z_{\alpha/2}$. In such circumstances, at a present significance level (α), the alternative hypothesis indicating the presence of a trend is accepted. Rejecting the null hypothesis indicates that the trend in the time series is statistically significant. Furthermore, the sign of the Z value can determine the direction of the observed trend, indicating whether it is increasing or decreasing.

4.2.2 Modified Mann-Kendall test (MK-CF1)

To ensure accurate trend detection using the Mann-Kendall test, verifying that the data series does not exhibit significant autocorrelation is crucial. Autocorrelation has a notable impact on detecting trends by the MK test. However, it is common for hydro-climatological time series to possess significant autocorrelation. Such autocorrelation within a time series can result in the identification of false significant trends, even when the null hypothesis of no trend in the time series should not be rejected. Therefore, it is essential to address and account for the potential autocorrelation in hydro-climatological time series to ensure the reliability and accuracy of trend analysis utilizing the MK test. The modified variance of the MK test statistic is given by

$$Var(S)^* = CF_1 * Var(S) \quad (4.6)$$

CF1 is correction factor proposed by Hamed, K. H., & Rao 1998.

$$CF_1 = 1 + \frac{2}{n(n-1)(n-2)} \sum_{K=1}^{n-1} (n-k)(n-k-1)(n-k-2) r_k^R \quad (4.7)$$

Where k and r_k^R are the observation and the autocorrelation function of the ranks of the observations respectively, and n is the total length of the series. MK test with the CF1 is referred to as MK-CF1.

4.2.3 Modified Mann-Kendall test (MK-CF2)

To evaluate the significance of trends in a serially correlated data series, this study adopted another approach proposed by Yue and Wang 2004. The procedure involved mitigating the influence of significant autocorrelation coefficients presents in the time series before conducting the test. In this modified approach, known as the Modified Mann-Kendall (MMK) test, the calculation of the modified variance V(S)* is performed according to the following formula:

$$Var(S)^* = \frac{n}{n^*} Var(S) = CF\ Var(S) \qquad (4.8)$$

where n* is the effective sample size (ESS) and CF is the correction faction for serial correlation. The ESS (n*) is computed as:

$$n^* = \frac{n}{1+\frac{2}{n}\sum_{k=1}^{n-1}(n-1)\rho_k} \qquad (4.9)$$

Where ρ_k is the lag-k serial correlation coefficient of the data series, the correction factor is, hence, estimated as:

$$CF = \begin{cases} 1 + \frac{2}{n}\sum_{k=1}^{n-1}(n-k)\rho_k & for\ k > 1 \\ 1 + 2\frac{\rho_1^{n+1} - n\rho_1^2 + (n-1)\rho_1}{n(\rho_1 - 1)^2} & for\ k = 1 \end{cases} \qquad (4.10)$$

The modified standard MK statistic can then be defined as:

$$Z^* = \frac{Z}{\sqrt{CF}} \qquad (4.11)$$

where r_i is the delayed autocorrelation co-efficient, and *Var* (*S*) is calculated using Equation (4.4). Var (S) is changed to Var (S)* to calculate the Z statistic in the MMK test in Equation (4.11). At the α significance level, the value of the Z statistic derived from the above equation is contrasted with the normal standard Z.

4.2.4 Mann-Kendall Pre-whiting Test (MK-PW)

Von Storch 1995 presented an approach for addressing the issue of serial correlation and its impact on the Mann-Kendall test. This method proposes creating a new series to counteract the effects of serial correlation and is as follows:

$$X_t = X_t - r_1 X_{t-1} \qquad (4.12)$$

In the equation, r_1 represents the lag-1 serial correlation coefficient of the data series. The estimation of the r_1 can be obtained by calculating the autocorrelation function for the series (Machiwal et al. 2019).

4.2.5 Innovative Trend Analysis (ITA)

In Innovative Trend Analysis (ITA), the time series is divided into two equal parts and sorted in ascending order. The first sub-series (xi) is plotted on the horizontal axis (x-axis) in a two-dimensional Cartesian coordinate system. In contrast, the second sub-series (yi) is plotted on the vertical axis (y-axis). When the two sub-series are equal, showing no trend, the scatter plot points will align along the 1:1 line (a 45° angle line). If the scatter plot points are above the 1:1 line, the time series has an increasing trend.

Conversely, accumulating points below the 1:1 line implies a diminishing tendency in the time series (Şen 2012). Based on the distribution of the points in the scatter plot, it provides a simple approach to determining the presence and direction of the trend. The following expression is used to calculate the slope (s) of the trend in this test (Şen 2017)**.**

$$s = \frac{(\bar{y}_2 - \bar{y}_1)}{n} \qquad (4.13)$$

where $\bar{y}_1$ and $\bar{y}_2$ represent the arithmetic mean of the first and second half of the time series, respectively, and n denotes the number of data points. The confidence limits (CL) for the trend slope can be computed at α the significance level (Şen 2017). The confidence limits (s_{Cri}) calculated from a standard normal probability density function with a mean of zero and a standard deviation are used to calculate these confidence limits. The confidence bounds for the trend slope are estimated using the expression below:

The confidence limits (CL)

$$CL_{(1-\alpha)} = 0 \pm s_{Cri}\sigma_S \qquad (4.14)$$

Where σ_S is the slope's standard deviation, it can be expressed as follows.

$$\sigma_S = \frac{2\sqrt{2}}{n\sqrt{n}}\,\sigma\sqrt{1-\rho_{\bar{y}_1\,\bar{y}_2}} \qquad (4.15)$$

Where $\rho_{\bar{y}_1\,\bar{y}_2}$ Implies the cross-correlation coefficient between the two mean values in stochastic processes. The null hypothesis of no significant trend is rejected at the α significance level when the slope value (s) of each point is outside the range provided by the lower and upper confidence limit (CL) values.

4.2.6 K-Means clustering method

K-means clustering is one of the most common unsupervised techniques used for segregation (MacQueen 1967). The algorithm divides the dataset into user-defined groups that show similar patterns. This is also known as exclusive clustering since it groups data into pre-defined, non-overlapping clusters, where each point belongs only to the cluster. First, the algorithm identifies k number of centroids in the data series and assigns each point to the nearest cluster. The elbow curve obtains the value of k. The algorithm calculates the euclidean distance between each data point and the centroid of each cluster. Later, it allocates the data point to the cluster with minimum distance. Then, clusters with new centroid values are reassigned based on the average value of the coordinates of data points. Repeat the previous two steps iteratively until the centroid of clusters stops changing their position. This step was carried out using scikit-learn, which efficiently implements many machine learning algorithms with the Python interface.

4.2.7 Principal component analysis (PCA)

The principal component analysis (PCA) is a data pre-processing method mainly used to minimize the dimensionality of the data sets without losing much information. This helps to identify the relevant patterns in a data set and highlight their similarities and differences. PCA is one of the most widely used machine learning techniques for predictive models.

4.3 RAINFALL CONCENTRATION AND SEASONALITY

The precipitation concentration (PCI; Oliver 1980) is a tool for calculating rainfall concentration (De Luis et al. 2000, 2011) on annual and seasonal scales and is estimated using the following equation.

$$PCI_{annual} = \frac{\sum_{i=1}^{12} P_i^2}{(\sum_{i=1}^{12} P_i)^2} \times 100 \qquad (4.16)$$

where p_i is the rainfall for month i. The PCI at seasonal scales (i.e., South-west monsoon, north-east monsoon, winter, and summer) was also calculated (De Luis et al. 2011). The PCI value below 10 refers to uniform monthly rainfall distribution throughout the year (same amount of rainfall in each month) as described by Oliver 1980 and Zamani et al. 2018. The values from 10 to 15 imply a moderate concentration of rainfall, while the values between 16 and 20 indicate an irregular distribution; PCI values above 20 indicate strong irregularity in rainfall concentration. The PCI values above 15 show that total rainfall is concentrated in half of the year, and values above 25 indicate that total rainfall is reduced to one-third of the year (De Luis et al. 2011; Thomas and Prasannakumar 2016).

The seasonality index (SI) is a powerful indicator for measuring the degree of variability of monthly rainfall (Walsh and Lawler 1981; Guhathakurta and Saji 2013; Nair et al. 2014). This index identifies the rainfall regime based on the monthly distribution of rainfall. Therefore, SI is computed by monthly and annual mean rainfall as the following equation.

$$\mathrm{SI} = \frac{1}{\bar{R}} \sum_{i=1}^{12} \left| X_n - \frac{\bar{R}}{12} \right| \qquad (4.17)$$

X_n is the mean rainfall of month n, and $\bar{R}$ is the mean annual rainfall. The classification of SI values according to Kanellopoulou 2002 is shown in Table 4.1.

Table 4.1. Classification of Seasonality Index (SI) (after Kanellopoulou 2002)

SI	**Rainfall behaviour**
<0.19	Uniform rainfall throughout the year
0.20–0.39	Uniform rainfall but a definite wetter season
0.40–0.59	Somewhat seasonal with a short drier season

SI	Rainfall behaviour
0.60–0.79	Seasonal
0.80–0.99	Markedly seasonal with a long, drier season
1.00–1.19	Most rain in 3 months or less
>1.20	Extreme, almost all rain in 1–2 months

4.4 EXTREME CLIMATE INDICES

The climate change of a particular place can be easily accessed by investigating climate indices. In this study, the Expert Team on Climate Change Detection and Indices (ETCCDI), established by the World Meteorological Organization (WMO), was utilized to examine these indices. Notably, the index employed in this research was initially created by Zhang and Yang 2004 at the Climate Research Branch of the Meteorological Service of Canada. Table 4.2 presents the extreme climate indices used for the current study. These extreme climate indices were derived from daily maximum temperature, minimum temperature, and daily precipitation data using RClimDex (1.0) application, which is available in the R language platform. These climate indices have been widely used in analyzing the extreme climate at the regional and global scales (Alexander et al. 2006) as it can easily identify the extreme climate features of a location.

A total number of 24 climate extreme indices were taken for the current study based on the climatic characteristics of the Kerala state, in which 12 temperature extremes and 12 precipitation extremes were included. The annual occurrence of summer days (SU35) was defined using locally established thresholds of 35°C. This definition was deemed more suitable for tropical regions where temperatures during the day and night tend to be higher than at higher latitudes (Pimonsree et al. 2021). This research focused on two categories of extreme climate events percentile-based indices and threshold indices with a base period of 1970 to 2000. These indices were derived for 59 grid points from 1951 to 2020 using RClimDex. The trend analysis of the aforementioned

extreme climate indices was done using the modified Mann-Kendall Test (MK-CF1) at 5% significance level (95% confidence level) and Sen's slope estimator.

Table 4.2: Definitions of extreme climate indices used in this study

Type	Index	Definition	Unit
Temperature	TR 20	Number of days with TN≥ 20 °C (tropical night)	day
	TXx	The monthly maximum value of TX	°C
	TNx	The monthly maximum value of TN	°C
	TXn	The monthly minimum value of TX	°C
	TNn	The monthly minimum value of TN	°C
	TX90p	Number of days when TX is greater than the 90th percentile	day
	TX10p	Number of days when TX is less than the 10^{th} percentile	day
	TN90p	Number of days when TN is greater than the 90^{th} percentile	day
	TN10p	Number of days when TN is less than the 10^{th} percentile	day
	DTR	Diurnal temperature range: Monthly mean difference between T_{max} and T_{min}	°C
	WSDI	Warm spell duration indicator Annual count of days with at least six consecutive days when Tmax>90th percentile	day
	SU35	Summer days: Annual count when daily Tmax >35 ºC	day
Precipitation	R10	Number of days with Pr ≥ 10 mm day	day
	R20	Number of days with Pr ≥ 20 mm	day
	R25	Number of days with Pr ≥ 25 mm	day
	R50	Number of days with Pr ≥ 50 mm	day
	RX1day	Maximum 1-day precipitation value	mm
	RX5day	Maximum 5-day precipitation value	mm
	R95p	annual total precipitation due to events with precipitation higher than the 95^{th} percentile of the reference period	mm
	R99p	annual total precipitation due to events with precipitation higher than the 99^{th} percentile of the reference period	mm

Type	Index	Definition	Unit
	PRCPTOT	Annual total precipitation in wet days with Pr≥ 1 mm	Mm
	SDII	Mean precipitation intensity of days with Pr ≥1	mm/day
	CDD	The largest number of consecutive days with Pr≤1 mm	day
	CWD	The largest number of consecutive days with Pr≥1 mm	day

4.5 HEAT WAVES

Heat wave events are defined as three or more consecutive days with temperatures above the 95th percentile of daily maximum temperature during the base period (Deng et al. 2019). In this study, eight HW characteristics were chosen to examine the long-term variation in HW: Highest temperature of the event (HWA), Length of the longest event (HWD), the yearly sum of HW days (HWF), the average length of all annual events (HWL), the average magnitude of all yearly events (HWM), the annual number of HW events (HWN), the onset date of the first event of the year (HWO) and ending date of the last event of the year (HWE). Many researchers have employed these indicators to study heat wave characteristics (Das and Umamahesh 2022; Lin et al. 2018; Luo and Lau 2017; Wu et al. 2020b). Table 4.3 presents various heat wave characteristics used for the current study.

Table 4.3 The heat wave characteristics used for the current study.

Type	Indices	Name	Definition	Units
Intensity	HWA	Heat wave amplitude	The highest temperature of the hottest HW event	℃
	HWM	Heat wave magnitude	The average magnitude of the yearly HW events	℃
Frequency	HWN	Heat wave number	Total number of the yearly HW events	events
	HWF	Heat wave frequency	The yearly sum of all participating HW days	days
Duration	HWD	Heat wave duration	Length of the longest yearly HW event	days
	HWL	Heat wave length	The average length of all yearly events	days

4.6 HEAT WAVE-DROUGHT COMPOUND EVENTS

A heat wave that occurs concurrently with a drought is a heat wave-drought compound event. In contrast, a heat wave that occurs independently without accompanying drought is known as heat wave alone. The start date of a heat wave is extracted for each grid, followed by checking the SPI value during the corresponding month of the heat wave. When the SPI reaches the drought level, this heat wave is categorized as a heat wave-drought compound event. Otherwise, it is classified as a heat wave alone. If multiple heat waves occur during a single drought period in a month, it is counted as one heat wave-drought compound event, and both the number of droughts and the number of heat waves are equal to or greater than the number of heat wave-drought compound events. The duration and severity of heat waves in heat wave-drought compound events were computed and compared to heat waves alone. The mean value of heat wave intensity and duration in the heat wave-drought compound events was obtained by considering multiple heat waves during a monthly drought period. The climatological mean fraction of these compounds was calculated at each grid to identify regions with a high frequency of heat wave-drought compound events. This fraction represents the ratio of the number of heat wave-drought compound events to the total number of heat waves observed in that particular grid.

4.6.1 Kolmogorov-Smirnoff test (KS test)

The two-sample Kolmogorov-Smirnov test is a non-parametric statistical test to assess whether two samples adhere to the same distribution. It offers a key advantage by not assuming any specific distribution for the compared samples. The KS test is a frequently employed method in climate studies that relies on the empirical ranking of time series data. It evaluates whether two samples originate from populations with identical distributions (null hypothesis, H_o) or if they stem from distinct distributions (alternative hypothesis, Ha). This test is typically conducted at 95% confidence level.

This approach involves determining the changes in the empirical cumulative distribution function (CDF) by comparing two samples. The samples are defined as follows:

$$\widetilde{F_s}(x) = \frac{1}{\tau}\sum_{i=1}^{\tau} I(X_i \leq x) \qquad (4.18)$$

$$\widetilde{F_T}(x) = \frac{1}{n-\tau}\sum_{i=1+\tau}^{T} I(X_i \leq x) \qquad (4.19)$$

Where $\widetilde{F_s}(x)$ and $\widetilde{F_T}(x)$ are the empirical CDF of the two subsamples, and n is the sample size. The indicator function I is used, and the adjustment factors 1/τ and 1/ (n-τ) are denoted for each sample. The KS test statistic is defined as follows.

$$D_{\tau,n} = Sup_x\left|\widetilde{F_s}(x) - \widetilde{F_T}(x)\right| \qquad (4.20)$$

The equation above calculates the maximum difference between two cumulative distribution functions as a divergence measure. A larger value indicates greater changes in the cumulative distributions, reflecting increased divergence between the two samples.

4.6.2 Sequential Mann-Kendall Test (SQ-MK)

In this study, the sequential Mann-Kendall Test proposed by Sneyers 1991 was utilized to identify potential change points in long-term time series data. Researchers have widely adopted this test to detect abrupt shifts in hydro-climatic variables and assess their significance. This method generates a progressive series u(t) and a retrograde series u'(t). These series are plotted against the corresponding years, and the intersection point of the two series is identified as the starting point of the trend change. The statistic (t_i) is defined as follows:

$$t_i = \sum_{j=1}^{i} n_i \qquad (4.21)$$

The mean and variance of test statistic t_i are given by

$$E(t_i) = \frac{i(i-1)}{4} \qquad (4.22)$$

$$Var(t_i) = \frac{i(i-1)(2i-5)}{72} \qquad (4.23)$$

The sequential values of test statistics u(t_i) are estimated using the original time series (x_1,x_2…..x_n) and are denoted as follows

$$u(t_i) = \frac{t_i - E(t_i)}{\sqrt{Var(t_i)}} \quad (4.24)$$

The same equation is used to compute the values of the backward sequential statistic u'(t), starting from the end of the series. The starting point of a developing trend can be identified by combining the forward and backward sequential statistics. This approach utilizes both ends of the series to capture potential trend changes effectively.

4.7 LAND USE LAND COVER CHANGE –GOOGLE EARTH ENGINE (GEE)

Remote sensing has been extensively used in the field of urbanization with its advancement in spatial technology and large-scale data management. With the advantages of rapid and large-scale data monitoring, remote sensing technology has proven to map urban dynamics at multiple spatiotemporal scales effectively. Many researches have successfully adopted the Landsat imageries for urban growth monitoring at various timescales. These satellite-derived outputs have a pivotal role in understanding the timely growth of urbanization and its dynamics. It is often used in these studies due to its wide availability and extensive spatial coverage. Even though many studies have been done on global urban expansion monitoring, most have been done at coarser spatio-temporal scales.

GEE computes resources like satellite imagery and geospatial datasets directly on the platform, making it suitable for various earth system studies, including LULC change detection, trend mapping, and prediction of climate variables at any scale. Due to its cloud-based geospatial processing capability and accessibility to an extensive collection of geospatial datasets, GEE has been widely used in urban studies. The data catalog of GEE contains large publicly available datasets, including Landsat archives, Sentinel series, weather and climate forecasts, which are pre-processed for fast and efficient access. The data management and analysis in GEE are managed through JavaScript API and Python API (Kulithalai Shiyam Sundar and Deka 2022). GEE represents images through raster data consisting of one or more bands, whereas vector data in GEE is represented through feature type (Gomes et al. 2020). One of the significant advantages of GEE is that users can access all the images in the platform

using a web-based Integrated Development Environment (IDE) without downloading the data.

The Google Earth Engine (GEE) is an open-access and free platform for research and non-profit activities which is widely used as a computing platform for earth system research in the rise of achievements in cloud computing technologies (Gorelick et al. 2017; Meng et al. 2021; Parastatidis et al. 2017; Xiong et al. 2021). The emergence of the GEE platform enabled users to process large datasets directly and rapidly compared to conventional image processing methods (Gorelick et al. 2017). Platforms such as these come as a boon in terms of minimizing the cost and complexity of handling large datasets, which helps address societal issues, including climate monitoring, flood and drought management, resource protection, and management. The availability of a multi-petabyte collection of geospatial data on open-source archives with very high cloud-computing resources has wholly changed the remote sensing field, enabling the rapid visualization and easy accessibility of large data sets. The advantage is reduced computation time by pre-processing the raw data, removing the cloud, and mosaicking it in the GEE (Kulithalai Shiyam Sundar and Deka 2022).

The recent advancements in the field of machine learning have significantly improved the accuracy of LULC classification (Dong et al. 2016; Acharya et al. 2019; Wagle et al. 2020). Many researchers have employed ML algorithms over conventional methods due to its efficient computing performance and ease of use (Dong et al. 2016; Patel et al. 2015; Acharya et al. 2019). GEE is controlled and accessible via the internet using an application programming interface (API) and an associated web-based interactive development environment (IDE) that enables rapid visualization (Gorelick et al. 2017). For the principal objective of education and research, the GEE remote sensing and climate data catalog is regularly updated with 6000 scenes per day from active missions (Gorelick et al. 2017; Venkatappa et al. 2021). GEE has been largely employed in various fields of earth observation studies that include LULC mapping (Huang et al. 2017; Pan et al. 2021), urban growth monitoring (Patel et al. 2015; Goldblatt et al. 2016), and resource management (Shelestov et al. 2017; Venkatappa et al. 2021), to list a few. Goldblatt et al. (2016) used three different classifiers on GEE for detecting the

urban areas in India from Landsat 7 and Landsat 8 imageries. Huang et al. 2017 documented the changes in the LULC classes in Beijing over three decades with the help of GEE. A frame work was proposed on GEE for mapping annual urban dynamics in China by (Cao et al. 2021). Kulithalai Shiyam Sundar and Deka 2022 utilized three different machine learning techniques, namely support vector machine (SVM), Random Forest (RF), and classification and regression trees (CART) for LULC mapping of the Vembanad Lake system, Kerala, on the GEE platform. Abraham and Kundapura 2022 employed random forest classifier for the LULC mapping of the Meenachil and Manimala basins in Kerala, India, for five different periods and projected the LULC map up to 2050. An efficient framework was proposed for mapping the urban dynamics of Kerala at an annual scale using classification methods and time series analysis. Two supervised classifiers were used to classify the LULC-based GEE platform; Random Forest (RF) method and the Classification and regression tree (CART) for 5 decades. The best-performing algorithm is chosen for further analysis.

4.7.1 CART

The CART algorithm is a popular decision tree classification algorithm that finds widespread use in land use classification. Breiman et al. 1984b developed the algorithm and can perform classification and regression tasks using decision trees. The CART algorithm builds a binary tree by selecting a random sample of remote sensing data and subsequently prunes the tree using a testing sample. The CART algorithm is a decision tree generation method that splits a sample into two sub-samples at each non-leaf node, resulting in a binary tree structure. Gini is utilized as a split node to evaluate impurity during the splitting process. Gini coefficients vary from 0 to 1, with higher values suggesting more unevenness in the sample set (Sang et al. 2019). Gini's impurity index measures how often an element from the dataset would be incorrectly labelled if it were randomly labelled according to the distribution of labels in the dataset. The CART algorithm aims to recursively split the dataset into smaller and more homogeneous subsets using the input feature values until all subsets contain only one class of labels (Kulithalai Shiyam Sundar and Deka 2022; Raj and Sharma 2022).

4.7.2 Random Forest Algorithm

Random Forests (RF) is one of the most used supervised machine learning algorithms for classification and regression. The algorithm combines the output from various decision tree sequences to achieve new input through majority voting for classification. It is proposed by Breiman 2001. User-defined parameters and trees are the major input factors for the algorithm. The optimum number of trees to be counted ranges from 100 to 500. This algorithm usually gives accurate results even without hyper parameter tuning. The RF algorithm combines massive ensemble regression and classification trees with a decision tree to form an ensemble learning method. RF identifies the best feature among a random subset of features while splitting the node instead of going for the most significant component, resulting in a better model. The number of variables required to break a tree node is the square of the set of variables.

Based on the testing, the input variables obtained from bootstrapping are divided into subgroups (Kulithalai Shiyam Sundar and Deka 2022). The trees are trained and cross-validated using various training samples to assess the effectiveness of categorization. The decision trees in the ensemble are created independently, which sets them apart from the usual approach of classification with a single decision tree. Additionally, these trees are not pruned. Various environmental problems, such as water resource management and natural hazard management, have been successfully addressed through the widespread application of the RF algorithm. This algorithm can process diverse data types, including satellite imagery and numerical data. Recent studies have demonstrated that using RF in remote sensing applications for LULC classification results in satisfactory performance.

4.7.3 Accuracy Assessment

Image classification requires an essential and crucial step known as accuracy assessment. This step is necessary as it helps to determine the degree of correspondence between the classification results and what is present on the ground. The classified map alone may not provide a completely accurate representation of the land-use pattern. Therefore, it is necessary to assess the map's accuracy. Randomly split validation datasets were utilized to generate confusion matrices and evaluate consumer's,

producer's, and overall accuracies for accuracy assessment. The accuracy assessment is often performed using a confusion matrix. This matrix is a valuable tool for examining the relationship between classification results and reference data regarding the land class. Many classification accuracy measures can be calculated from a confusion matrix, but overall classification accuracy is the most common. This measure is determined by dividing the total number of correctly classified samples by the total number of ground reference samples. The consumer's accuracy is a metric used to evaluate errors of omission in classification results. By dividing the total number of accurately classified samples for each land cover class by the total number of reference samples for that class, the accuracy of the consumer is determined. The producer's accuracy is used to assess errors of commission (overestimation) in classification results. It is calculated by dividing the total number of samples from reference data by the number of correct samples in one class. This metric measures the accuracy of classification in determining the presence of a specific land cover class in a given area. It is crucial to evaluate the overall accuracies of the classified images for further analysis. The kappa coefficient (κ) is a statistical tool used to assess the performance of a classification model by calculating the agreement between actual and predicted labels**.** A kappa coefficient of 85% above indicates strong agreement (Abraham and Kundapura 2022a). The change detection analysis aims to find discrepancies between images of the same region taken at various intervals. This study used land cover classification images from different dates to determine the extent of various land cover classes and monitor any changes occurring during the designated period.

4.7.4 Land Cover Indices

Land cover indices have been developed to explore the characteristics of various land cover classes. The NDVI (normalized difference vegetation index) is an extensively used graphical indicator for vegetation mapping. Researchers use the NDVI index to monitor drought, agricultural production, and vegetation density. The NDVI index calculation primarily relies on two bands: the near-infrared (NIR) band, which is reflected by vegetation, and the red band, which is absorbed by vegetation. The NDVI ranges from -1 to 1, where higher positive values indicate areas with denser vegetation,

while more negative values indicate larger non-vegetated areas. Essentially, a higher NDVI value indicates a higher density of green vegetation.

$$NDVI = \frac{NIR-RED}{NIR+RED} \qquad (4.25)$$

The Built-up area of a place can be calculated using NDBI (Normalized Difference Built-up Index). NDBI values range from - 1 to +1, where values between 0 and positive 1 indicate built-up areas, with values closer to 1 representing a higher density of built-up land.

$$NDBI = \frac{MIR-NIR}{MIR+NIR} \qquad (4.26)$$

Where MIR stands for the middle infrared band.

Due to its ability to accurately differentiate water and other features, MNDWI (Modified Normalized Difference Water Index) is an efficient tool for distinguishing between water and urban areas, and thus it is well-suited for extracting water body information in both vegetated and built-up areas of towns and cities.

$$MNDWI = \frac{Green-MIR}{Green+MIR} \qquad (4.27)$$

The bare soil index (BSI) is primarily utilized to differentiate bare soil and other land cover types by combining the NDVI and NDBI. However, it can also be employed for mapping and monitoring bare soil areas.

$$BSI = \frac{(RED+MIR)-(NIR+BLUE)}{(RED+MIR)+(NIR+BLUE)} \qquad (4.28)$$

All of the indices mentioned above were calculated in the GEE platform.

4.8 DYNAMIC CLASSIFICATION OF URBAN AND RURAL GRIDS

The study used time-varying LULC maps spanning three decades (1990, 2000, 2013, and 2020) to dynamically classify urban and rural grids. Assessing the impact of urbanization on extreme climate events involves comparing climate data from urban

grids with nearby rural grids to understand differences in intensity and frequency. In studies examining the impact of urbanization on extreme climate events, grids are commonly classified as urban or rural using population data, satellite measurements of night-time light, or land use and land cover data. Despite conducting studies over extensive periods, most previous research has utilized static classification, a single time of classification data, to define urban and rural grids. Previous studies have indicated that selecting reference grids based on a static classification throughout the entire analysis period underestimates the impact of urbanization on climate events(Liao et al. 2016, 2018).

In this study, the classification process adopted the methodology detailed by Liao et al. 2018 and Han et al. 2021, which involved categorizing grids according to the evolving patterns of land use and land cover over time. The classification of urban or rural grids over the last three decades involved analysing land use and land cover data alongside NDBI maps, where an area is considered urban if either the built-up area within a 7.5 km buffer zone exceeds 33% or if it's already identified as urban on NDBI maps, with the presence of either criterion designating a grid as urban. The method is based on the assumption that significant climate-influencing elements including large-scale synoptic systems, topography, and land-sea interactions have similar impacts on climate variability at both the local and regional levels. To fulfil this hypothesis and reduce orographic differences in grid-scale analyses, only grids with elevation variations of less than 500 metres were used.

To determine the extent of built-up areas in the study region, four LULC maps covering the three-decade period were used for computation. The methodology for generating LULC maps for three decades using the Random Forest classifier is clearly described in section 4.7. The generated maps, along with NDBI for three decades, were used to determine urbanization growth over the years. To assess the urbanization level in the region, a circular buffer zone was created around each grid, with a radius of 7.5 km. Within these buffer zones, the proportion of built-up area was calculated, serving as an indicator of urbanization. A higher ratio of built-up area signifies greater urban development, while a lower proportion indicates less urbanization. Estimating the built-

up area for each grid was conducted dynamically by utilizing the time-varying LULC images starting from 1990. To classify the grids into urban and rural types, a threshold of 33% was applied to the built-up area ratio. Grids with a built-up area ratio exceeding this threshold were classified as urban, while those below were categorized as rural. It is worth noting that most studies investigating the impact of urbanization often overlook the dynamic nature of the conversion process from rural to urban over time. This oversight can result in a misinterpretation of the effects and contributions of urbanization, as many regions currently designated as urban were once rural. Hence, considering the historical rural-to-urban transformations becomes crucial for accurately assessing the urbanization process's effects.

By employing the dynamic classification scheme through the utilization of time-varying LULC data, a more precise estimation of the urbanization process's contribution to climate change can be achieved. This approach allows for a thorough understanding of the changes occurring over time. In particular, the effects of urbanization on extreme climate events were assessed by calculating the differences in trends between annual anomalies of each extreme climate index in urban and rural environments. This method enables the identification and evaluation of urbanization's specific impacts on extreme climate events, providing valuable insights into the relationship between urban development and climate change. It is acknowledged that comparing the time series difference helps to identify real trend differences between the two series by reducing noise from common variability in individual trends. The effect of urbanization (X_{ue}) on extreme climate indices for nearby urban and rural grids can be found as follows;

$$X_{ue} = X_u - X_r \qquad (4.29)$$

Where X_u and X_r are the anomalies of extreme climate indices at urban and rural grids. The trend differences (ΔX_{tre}) of extreme climate indices is similarly defined as;

$$\Delta X_{tre} = X_u^{tre} - X_r^{tre} \qquad (4.30)$$

$X_u{}^{tre}$and $X_r{}^{tre}$ and are the linear trend of anomalies of extreme climate indices at urban and rural grids, respectively. The linear trends of the annual time series of extreme climate indices were computed using Sen's slope estimator (Sen 1968), which is extensively used in time series analysis. A widely utilized non-parametric statistical test, the modified Mann-Kendall test (MK-CF1), commonly applied in detecting trends in hydrological and meteorological time series, was employed for analyzing linear trends in annual series of extreme climate events. If the ΔX_{tre} =0, it means there is no urbanization influence on the extreme event; If the ΔX_{tre} <0 or >0, it indicates that urbanization decreases or increases the extreme climate events respectively. The ratio of the effects of urbanization to the rate at which urban grids are changing is known as the relative contribution of urbanization (U_c) (Chu and Ren 2005; Pimonsree et al. 2022).

$$U_C = \left[\frac{\Delta X^{tre}}{X_u{}^{tre}}\right] \times 100 \qquad (4.31)$$

Generally, the value of U_c is less than 1. If the absolute value of U_c =100%, It demonstrates that urbanization is the only factor changing the frequency of extreme incidents. If the U_c exceeds 100%, it indicates the presence of unidentified local factors that caused the extra trend, which is considered 100% in this work. Only when the urbanization effect is statistically significant is the contribution of urbanization considered. The procedure mentioned above, which estimates the impact of urbanization on extreme events by comparing the differences in the trends between urban and rural stations, was widely used by various researchers (Liao et al. 2018; Wang et al. 2021a; Wu et al. 2020a; Zhao et al. 2019).

CHAPTER 5

RESULT AND DISCUSSION

As discussed in Chapter 4, various analyses have been performed, and the results and discussions are included in this chapter. The results and discussion for every objective are listed under the respective section headings. Firstly, the results and discussion of trend analysis of climate variables such as rainfall, rainy days, and temperature are given. The following sections cover the LULC changes in Kerala and the dynamic classification of urban and rural grids. Later the results of long-term variability of extreme climate indices, heat waves, and compound events were investigated. The final section of this chapter discusses how urbanization has altered the frequency and intensity of extreme climate occurrences in Kerala.

5.1 RAINFALL CHARACTERISTICS

The mean annual rainfall of Kerala during the study period is 2666 mm, with a standard deviation of 413.96 mm. The rainfall during the south-west monsoon accounts for 67.9% of the annual rainfall budget of Kerala, followed by the north-east monsoon (16.66%) and summer rainfall (12.43%). The coefficient of variation of annual rainfall (15.53%) shows the stability of rainfall over Kerala. The maximum and minimum recorded rainfall was 3913.23 mm in 1961 and 1522.70 mm in 2005. Winter rainfall contributes only 3% of annual rainfall with a high coefficient of variation (54.83%), which implies more rainfall variability during this time. The statistics of annual, seasonal, and monthly rainfall from 1901 to 2019 over Kerala are estimated and depicted in Table 5.1

Table 5.1. Monthly and seasonal distribution of rainfall for Kerala (1901-2019)

Season	**Rainfall**	**% contribution**	**SD**	**CV**	**50% probability**	**75% probability**	**90% probability**
January	15.75	0.60	19.18	121.7	7.86	2.81	0
February	16.69	0.62	17.34	103.9	9.17	5.12	1.09

Season	Rainfall	% contribution	SD	CV	50% probability	75% probability	90% probability
March	38.38	1.44	31.50	82.05	29.66	18.69	12.22
April	102.76	3.85	41.18	40.07	99.90	71.78	52
May	190.08	7.13	117.06	61.58	154.31	112.00	83.21
June	538.44	20.2	162.52	30.18	507.6	431.37	334.41
July	632.9	23.74	210.05	33.18	637.12	500.17	353.97
August	409.23	15.35	157.26	38.42	375.22	303.21	249.08
September	229.7	8.62	106.88	46.53	210.72	143.09	90.584
October	277.6	10.42	80.72	29.07	267.86	220.30	175.09
November	166.65	6.25	85.24	51.15	153.42	96.00	68.00
December	47.31	1.78	39.97	84.48	35.99	14.83	7.20
Annual	2666.00	100.00	413.96	15.53	2681.70	2391.70	2208.8
South-west monsoon	1810.30	67.90	370.66	20.47	1783.20	1596.20	1434.61
North-east monsoon	444.24	16.66	118.04	26.57	441.86	441.86	296.13
Winter	79.76	3.00	43.73	54.83	75.07	45.40	29.03
Summer	331.24	12.43	121.69	36.73	666.8	246.07	265.52

As depicted in Table 5.1, the south-west monsoon is the primary rainy season in the state of which about 60% of the total rainfall contributed during June (20.20%), July (23.74%), and August (15.35%), which brings out the presence of a high concentration of rainfall. Figure 5.1 shows the spatial variation of annual rainfall from 1901 to 2019

over the state. The study is performed on 59 grid points inside the state, showing the spatial variability (800 to 4900 mm) and characteristic heterogeneity of rainfall.

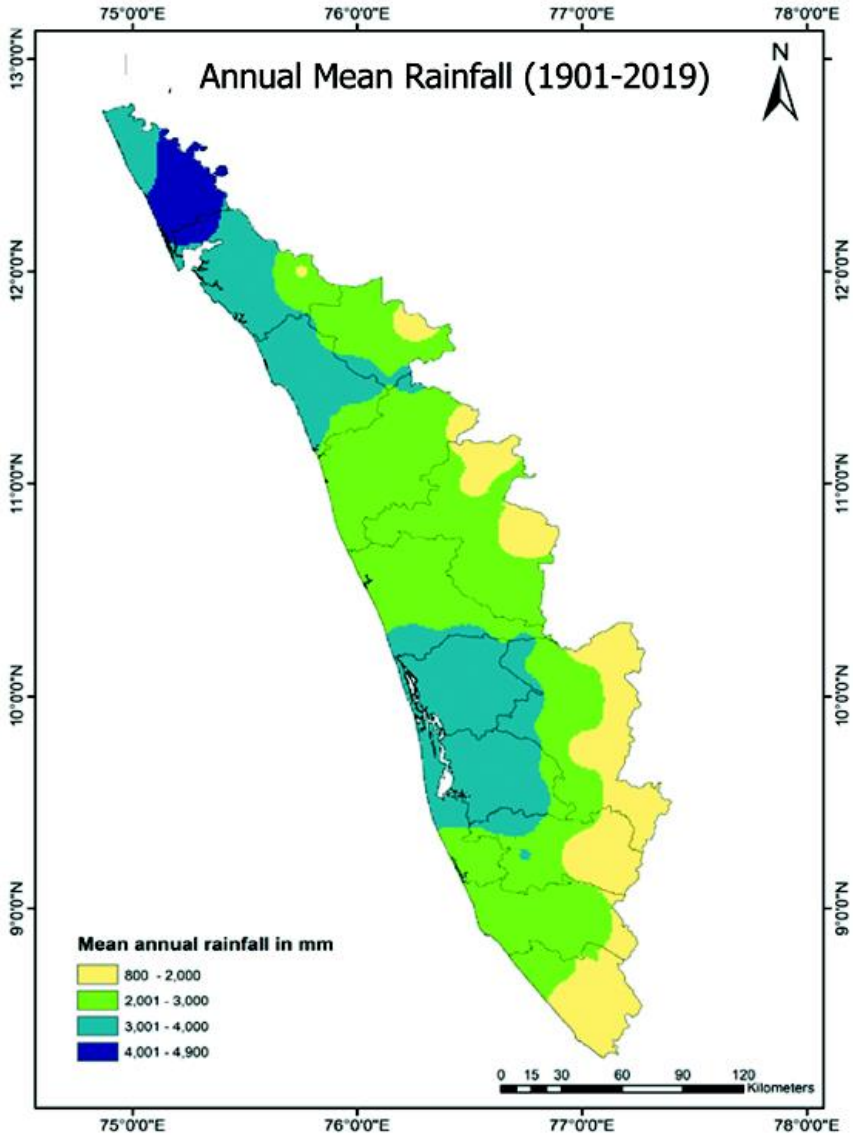

Figure 5.1. Spatial variation of mean annual rainfall

Rainfall during January and February is very negligible (0.6 and 0.62% of total rainfall, respectively), and the coefficient of variation is also high during these months (CV>100%), which clearly shows it is undependable. The dependable annual rainfall at 50 %, 75%, and 90% probabilities over Kerala is 2681.7 mm, 2391.8 mm, and 2208.8 mm, respectively. The dependable seasonal rainfall at 75% for the south-west monsoon,

north-east monsoon, winter, and summer seasons are 1596.2 mm, 441.8 mm, 45.4 mm, and 246 mm, respectively. It is noticed that compared to other months and seasons, months and seasons with high mean rainfall exhibit high standard deviation and low CV values. The coefficient of variation of seasonal rainfall was highest in winter, followed by summer rainfall, north-east monsoon, and south-west monsoon.

5.2 CLUSTERING

The K-Means algorithm has established five homogeneous rainfall clusters of 59 grid points for the annual series, shown in Figure 5.2. The relative influence of geographical factors (latitude, longitude, and altitude) and statistical parameters (mean, maximum and minimum rainfall, standard deviation (SD), and coefficient of variation (CV)) on mean rainfall was analysed using principal component analysis (PCA). These clusters show a clear geographical pattern, and the K-Means have delineated nearby grids into different clusters because of the complexity of the terrain of the study area. It is clear from Figure 5.2 that cluster 1 and cluster 3 are characterized by the highest annual mean rainfall and are located in low-altitude areas. In contrast, the CV of annual rainfall is moderate and low in the clusters mentioned above, respectively. However, the lowest annual rainfall was observed in cluster 5, with a high coefficient of variation. An in-depth examination revealed that grids of cluster 5 are mainly situated towards western parts of the state with high altitudes. Likewise, grids in cluster 2 are seen towards the northern side of Kerala with high rainfall. In contrast, cluster 4 is characterized by moderate annual mean rainfall and is located in the region with low altitude.

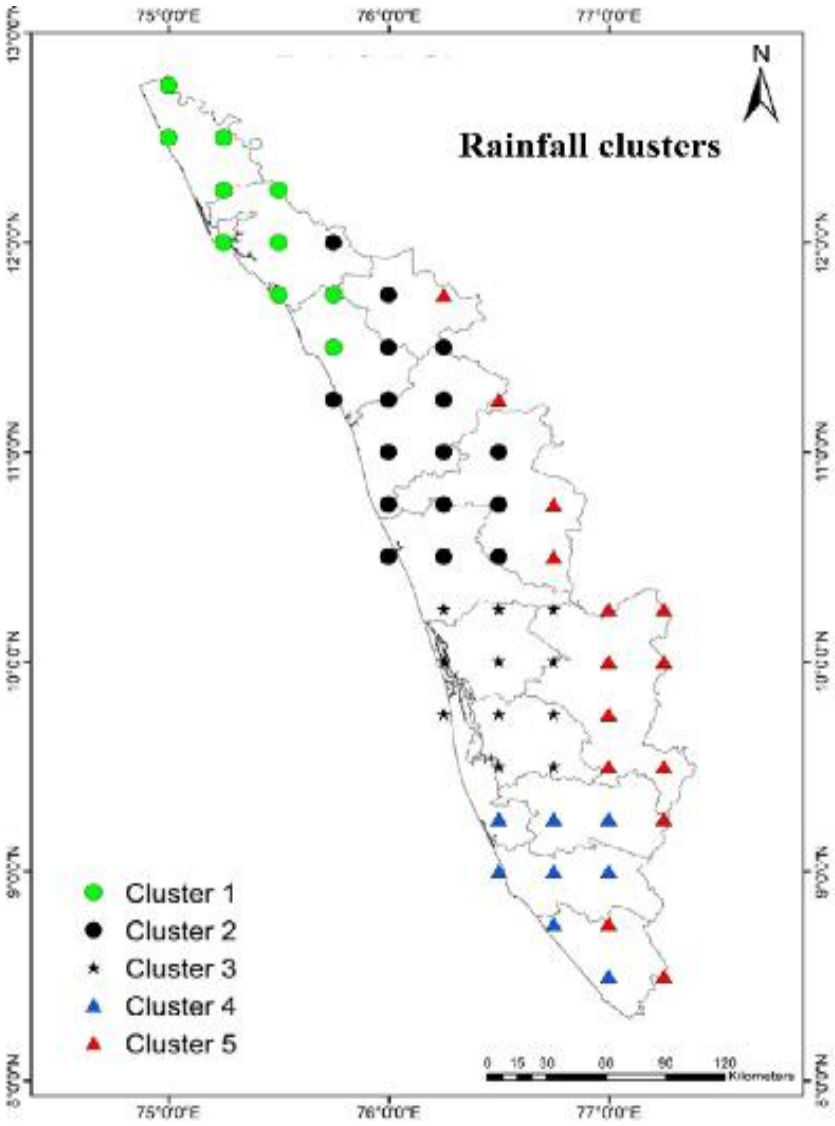

Figure 5.2. Location of rainfall clusters

Box-whisker plots are used as a better representation to compare different time-series data. Figure 5.3 depicts the temporal variation of the annual rainfall for 5 clusters. This gave a summary of five key statistics of the data distribution along with the outliers. The median of rainfall was highest in cluster 1 and lowest in cluster 5. Among all clusters, rainfall distribution is more uniform in cluster 3 as there are few outliers. It is observed from Figure 5.3 that there is a clear spatial variation in the patterns of annual rainfall. Overall, an increase in annual rainfall is observed when moving away from the high altitude of the study area to the coastal region. Since the median of the

annual rainfall data is above the middle of the box for the majority of the grids, it is evident from Figure 5.3 that annual rainfall is concentrated across a relatively narrow range. The presence of outliers near the upper part of the box in all clusters is due to extreme events occured in the study area. The annual rainfall significantly increased from the state's southern to the northern side. More than 70% of annual rainfall is contributed by the south-west monsoon in cluster 1 and cluster 2, whereas the south-west monsoon only accounts for 40 to 50 % of annual rainfall in cluster 4 and 5. The observation revealed that grids in cluster 3 receive a significant portion, exceeding 65%, of their annual rainfall during the south-west monsoon. Additionally, the north-east monsoon contributes more than 15% of these areas' overall annual rainfall budget. On the contrary, the contribution of north-east monsoon (24 to 28%), winter (5 to 8%), and summer (16 to 18%) rainfall more in cluster 4 and 5. This is because clusters 4 and 5 may experience minimal impact from the north-east monsoon due to the absence of the Western Ghats in the southern end. The grids in cluster 1, 2, and 3 receive more than 85% of annual rainfall from June to November (south-west and north-east monsoon), which shows a substantial irregularity in annual rainfall distribution in these clusters. It is noted that less than 10% of annual rainfall is contributed by the winter and summer season together in cluster 1 and 2, which leads to short-term drought in these areas.

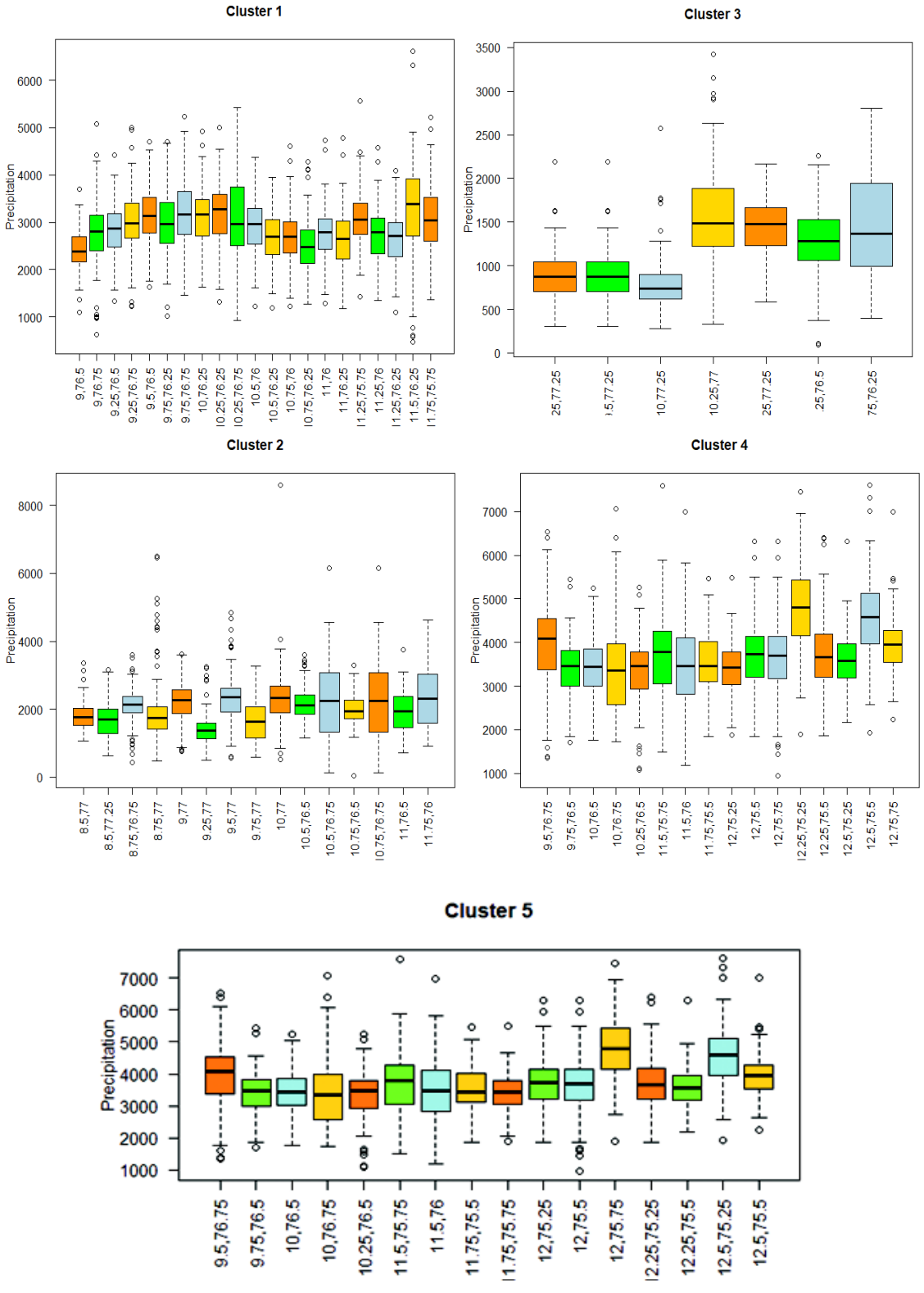

Figure 5.3. Box-whisker plots of annual rainfall for 5 clusters

The temporal variation of annual and other seasonal rainfall in 5 clusters indicated (Figure 5.4) that the magnitude of the trend is not uniform throughout the state. It is seen that annual, south-west monsoon, north-east monsoon, and winter rainfall decrease in all clusters, whereas summer rainfall increases in clusters 4 and 5. The rate of decrease of annual as well as south-west monsoon rainfall is more in cluster 1 and cluster 2, and these grids are situated in the northern parts of the state. It is worth mentioning that the contribution of south-west monsoon and summer rainfall to the annual rainfall budget is increasing. In contrast, the share of winter rainfall decreases considerably in all clusters.

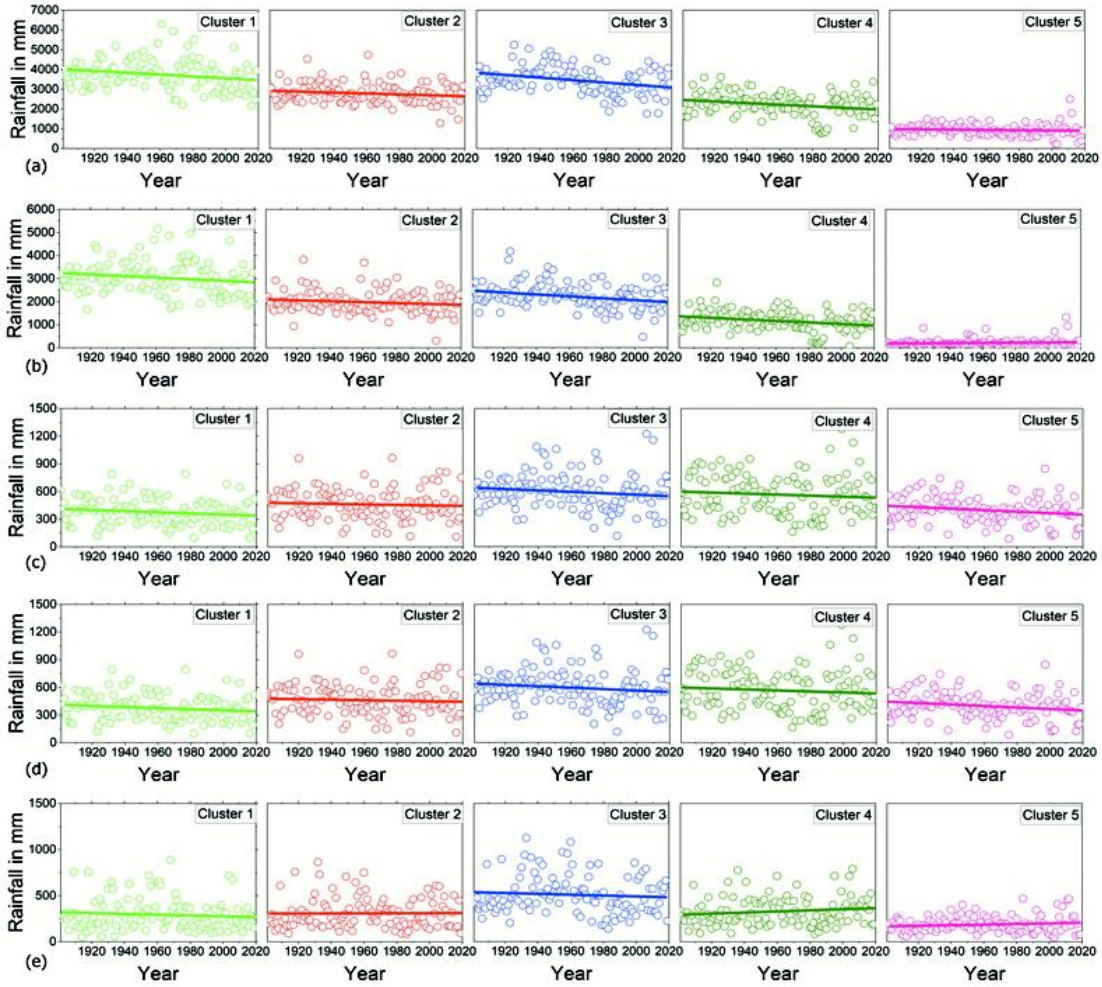

Figure 5.4. Scatter plots of long-term rainfall for (a) annual, (b) south-west monsoon, (c) north-east monsoon, (d) winter rainfall, (e) summer rainfall

The significant reduction in the contribution of the north-east monsoon in cluster 1 and 2 is also evident. On the contrary, the influence of the north-east monsoon in cluster 4 and 5 is stable because of the absence of the Western Ghats barrier against the north-easterly winds. The average rate of decrease of annual as well as south-west monsoon rainfall in cluster 1 (-4.26 and -3.49 mm/year) and cluster 2 (-5.55 and -4.73 mm/year) is more compared to other clusters. The mean rate of decrease of annual as well as south-west monsoon rainfall in cluster 3, cluster 4, and cluster 5 are -4.78 and -2.80 mm/year, -4.27 and -3.01 mm/year, -1.15 and -0.10 mm/year respectively. It is worth mentioning that rate of decrease of annual and seasonal rainfall in cluster 5 is less compared to other clusters.

Like the rainfall series, the rainy days (rainfall ≥2.5 mm/day) also decreased in all clusters **(**Figure 5.5). The rainy days are significant in runoff generation and other hydrological cycle components. The annual average rainy days in Kerala varies from 56 to 180, showing the heterogeneity and irregularity in rainy days distribution**.** The highest number of rainy days are experienced by cluster 1 and 3 (131 to 180), followed by cluster 2 and 4 (101 to 130). The rate of decrease of annual rainy days and south-west monsoon rainy days are more in cluster 3 (-3.2 and 1.3 days/decade) and cluster 4 (-2.22 and 1.2 days/decade) than in other clusters even though annual rainfall does not show a noticeable reduction. This will lead to high-intensity rainfall for a short duration in the regions mentioned above. Interestingly, summer rainy days are increasing in cluster 3 and 4. The mean rate of decrease of annual as well as south-west monsoon rainy days in cluster 1, cluster 2, and cluster 5 are -0.43 and -0.15 days/decade, -1.2 and -0.81 days/decade, -1.1 and -0.30 days/decade respectively.

It is observed that all clusters experience the maximum reduction in rainy days during the south-west monsoon, whereas minimum reduction is obtained during the winter season. Consequently, despite a decrease in rainy days, high-intensity rainfall occurrences are expected during the south-west monsoon. This pattern is evident in the state of Kerala, where significant flood events occurred during August 2018, 2019, and 2020. Remarkably, the state experienced considerably fewer rainy days during the south-west monsoon of those years compared to long-term historical records. These successive extreme events led to substantial surface runoff, ultimately contributing to increased natural disasters.

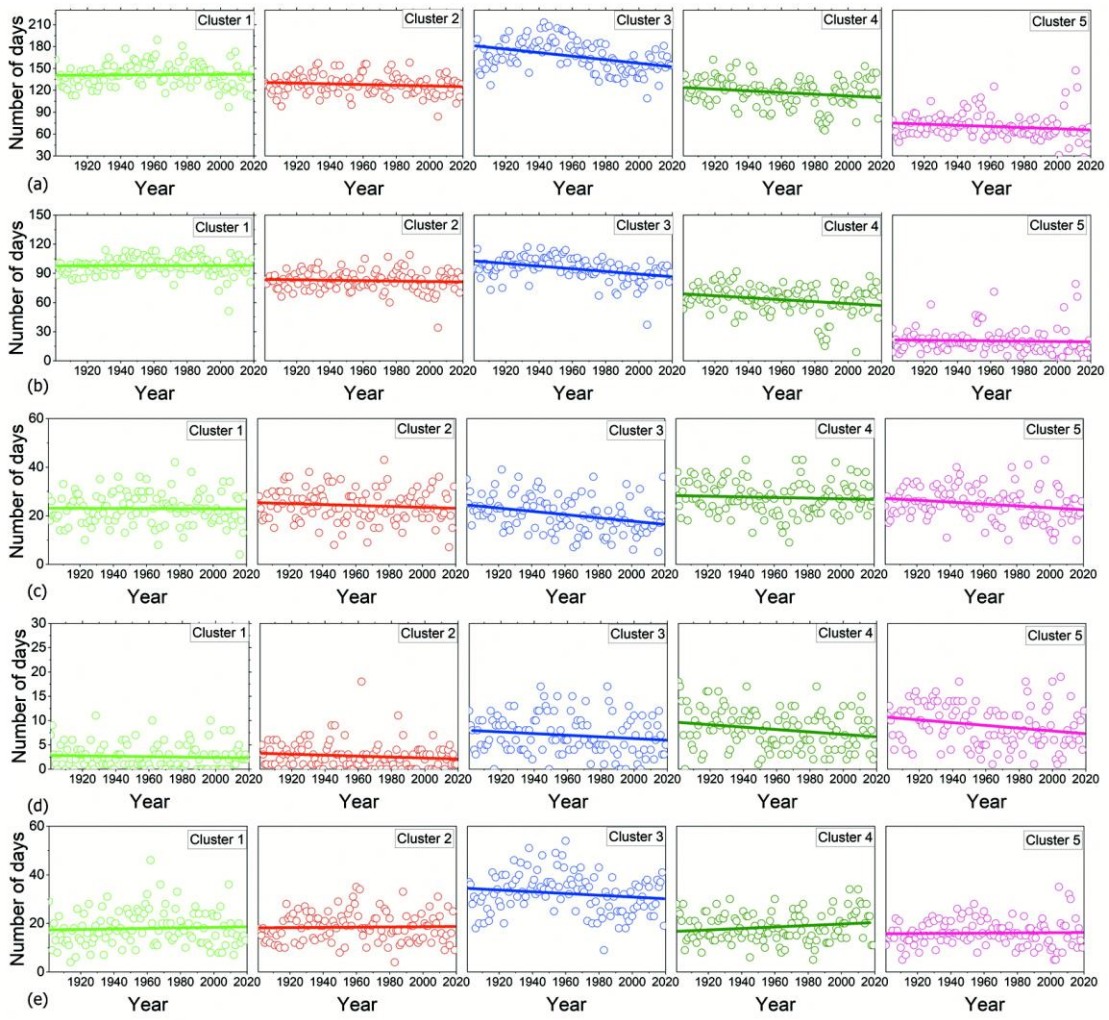

Figure 5.5 Scatter plots of rainy days for (a) annual, (b) south-west monsoon, (c) north-east monsoon, (d) winter, (e) summer

5.3 LONG-TERM TREND OF ANNUAL AND SEASONAL RAINFALL

The results of five trend analysis tests for annual rainfall are shown in Figure 5.6 and Figure 5.7. It can be observed that trends discovered by the Mann-Kendall test showed some resemblance with the findings of the MK-CF1 and MK-PW tests for all grid points and seasons. The MK-CF2 and ITA tests show similar results in all the time series.

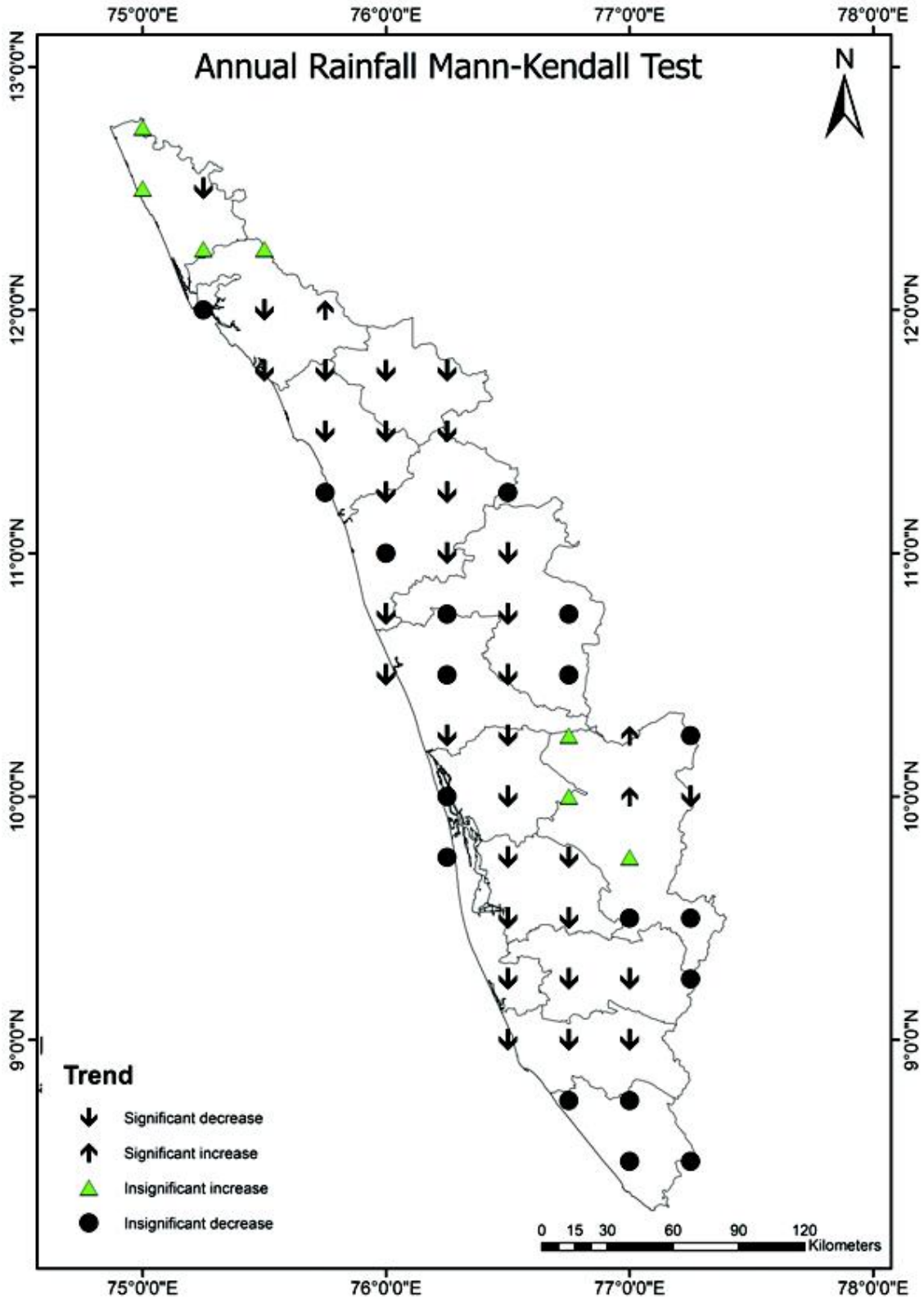

Figure 5.6 Mann-Kendall test results of annual rainfall

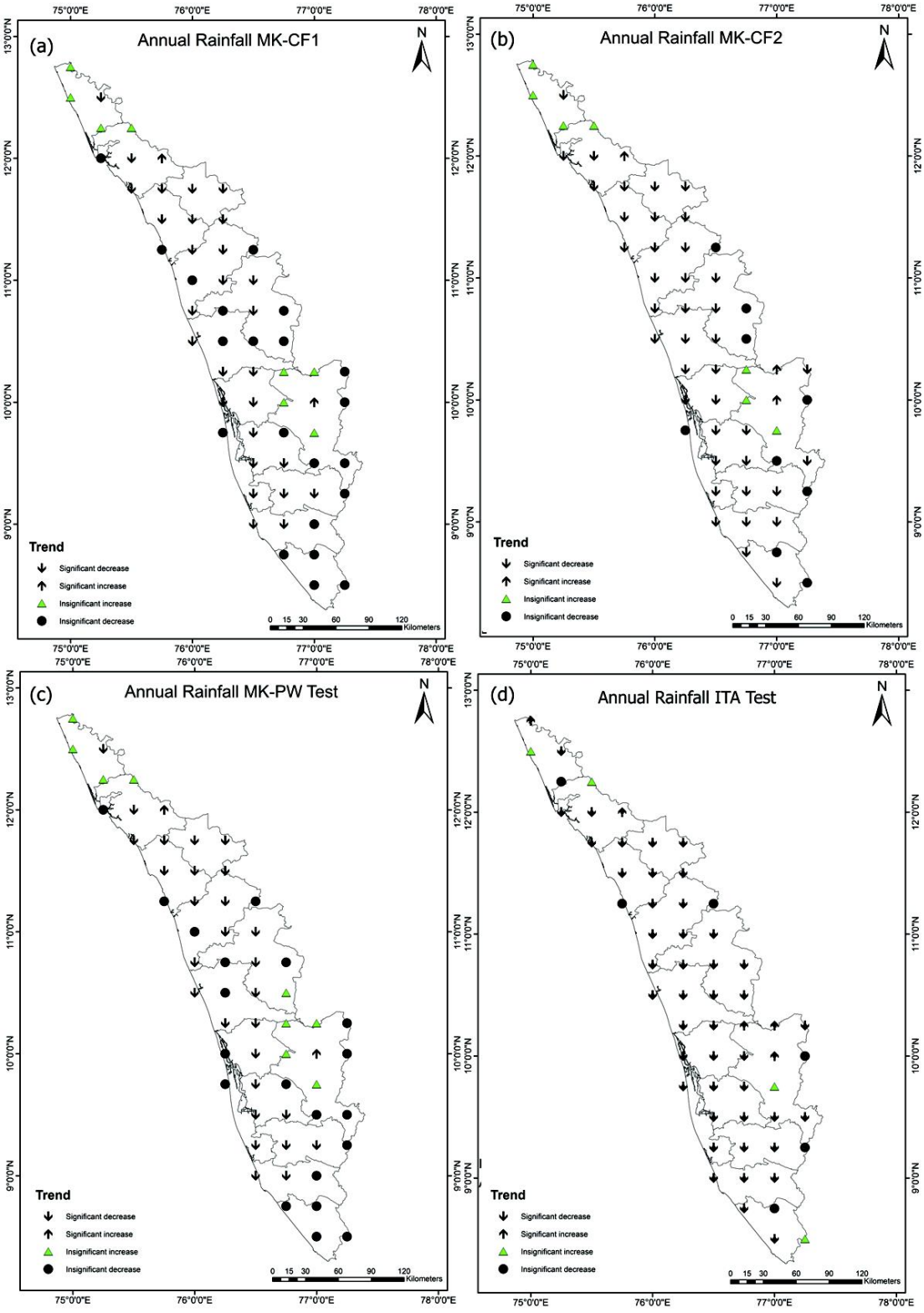

Figure 5.7. Results of (a) MK-CF1 (b) MK-CF2 (c) MK-PW (d) ITA tests of annual rainfall

Most of the grid points show negative trends, whether significant or non-significant, in all the time series. It is seen from Figure 5.6 and Figure 5.7 that the Mann-Kendall test found a significant decreasing trend of annual rainfall at 31 grid points (53%) of the total 59 grids, whereas MK-CF1 and MK-PW revealed 28 (47%) Statistically significant decreasing grid points. However, the MK-CF2 and the ITA test detected a statistically decreasing annual rainfall trend at 40 (68%) and 44 (75%) grid points. However, the annual rainfall has statistically significant increasing trends at 3(5%) grids as revealed by the Mann-Kendall test and MK-CF2. MK-CF1 and PWMK tests identified a statistically significant increasing trend at 2(3%) grids, whereas the ITA test suggested a significant increasing trend for five grids.

In the south-west monsoon rainfall series (Figure 5.8 and Figure 5.9), MK-CF2 and ITA test found statistically significant decreasing trends for 37 (63%) and 43 (73%) grids. In contrast, the Mann-Kendall test, MK-CF1, and PW-MK tests revealed a significant trend only at 32 (54%), 30 (51%), and 27 (46%) grid points, respectively. Likewise, the statistically increasing trends at 5 % significance level in the south-west monsoon rainfall are unveiled for 7 (12%), 6 (10%), 4 (7%), 3 (5%), 3 (5%) grids from the results of the ITA, MK-CF2., Mann-Kendall test, MK-CF1 and PW-MK respectively. The statistical decreasing trends at 5 % significance level in the north-east monsoon rainfall (Figure 5.10 and Figure 5.11) are unveiled for 43(73%), 40(68%), 23(39%), 17 (29%), 14 (24%) grids from the results of the ITA, MK-CF2, MK-CF1, Mann-Kendall, and PW-MK respectively. In the winter rainfall (Figure 5.12 and Figure 5.13) time series, the significant decreasing trends at 5% significance level are evident for 50 (85%), 47 (80%), 30(51%), 28(47%), 26(44%) grids from the results of the MK-CF2, ITA, MK-CF1, Mann-Kendall, and PW-MK respectively. Mann-Kendall test, MK-CF1, and PW-MK could not find any statistically significant increasing trend during the north-east monsoon and winter season. However, the ITA test and MK-CF2 detected a statistically significant increasing trend for 2(3%) and 1(2%) grids during the north-east monsoon. In the winter season, increasing trends for 4 (7%) and 2(3%) grids were statistically significant, as revealed by the ITA test and MK-CF2, respectively. In the summer rainfall (Figure 5.14 and Figure 5.15) series, the Mann-Kendall test, MK-CF1, and PWMK found statistically significant decreasing trends for

9, 8, and 7 grids, respectively. On the contrary, the ITA and MK-CF2 resulted in statistically significant decreasing trends for 39 and 17 grid points. However, the Mann-Kendall test and PWMK found statistically significant upward trends for one grid in the summer rainfall dataset. On the other hand, while MK-CF1 only showed a significant trend for one grid, the ITA and MK-CF2 found statistically significant increasing trends for four grid points.

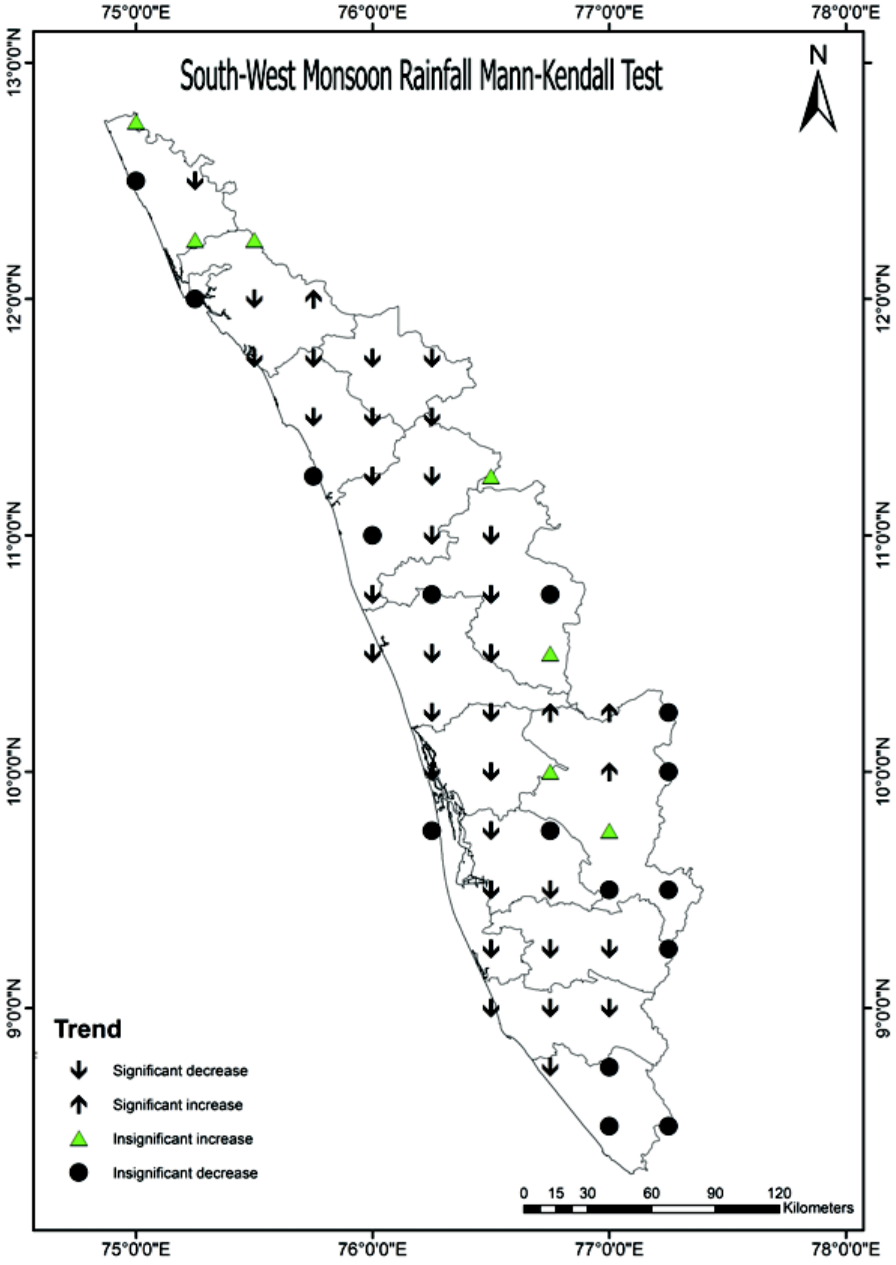

Figure 5.8. Mann-Kendall test results of south-west monsoon rainfall

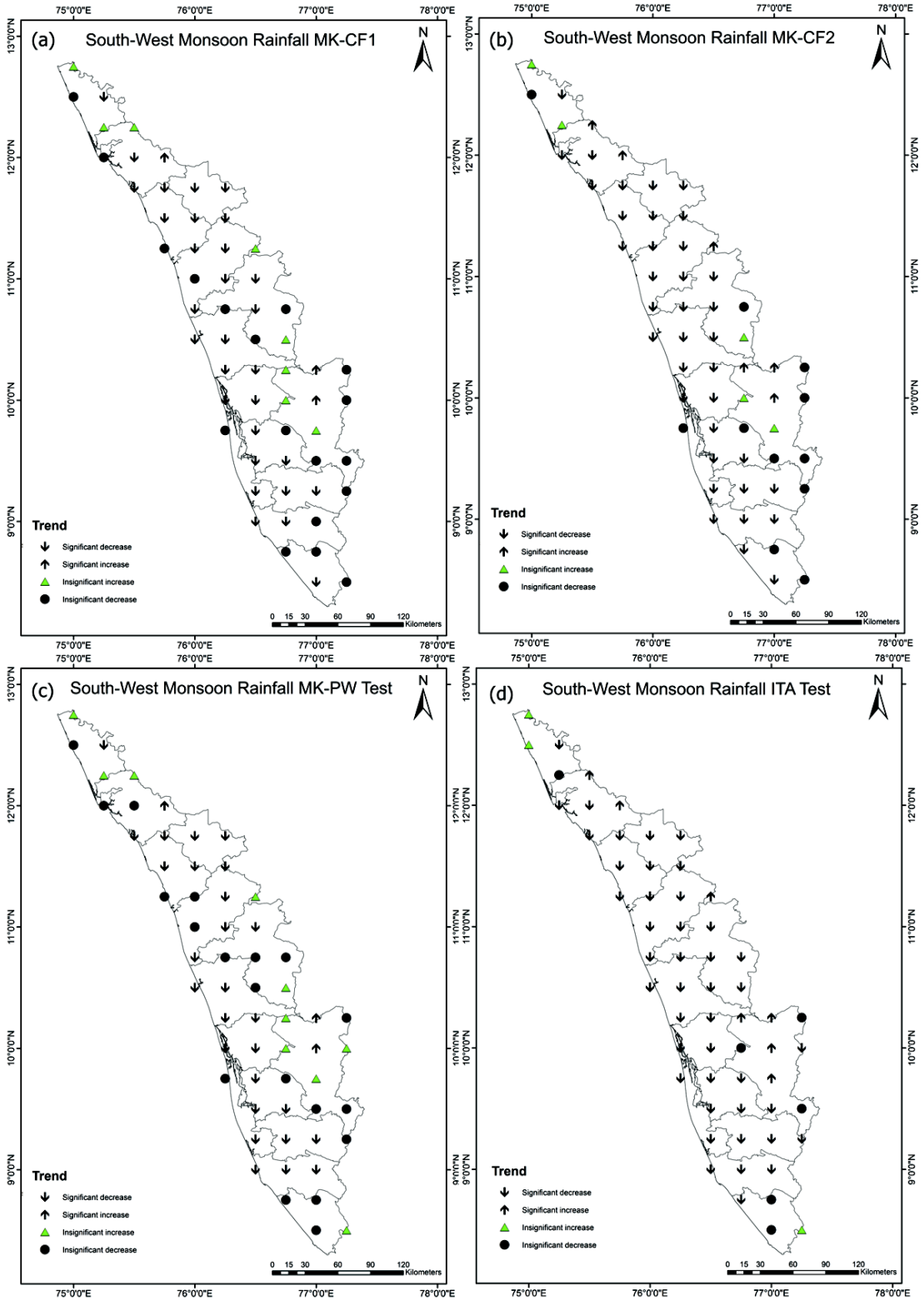

Figure 5.9. Results of (a) MK-CF1 (b) MK-CF2 (c) MK-PW (d) ITA tests of south-west monsoon rainfall

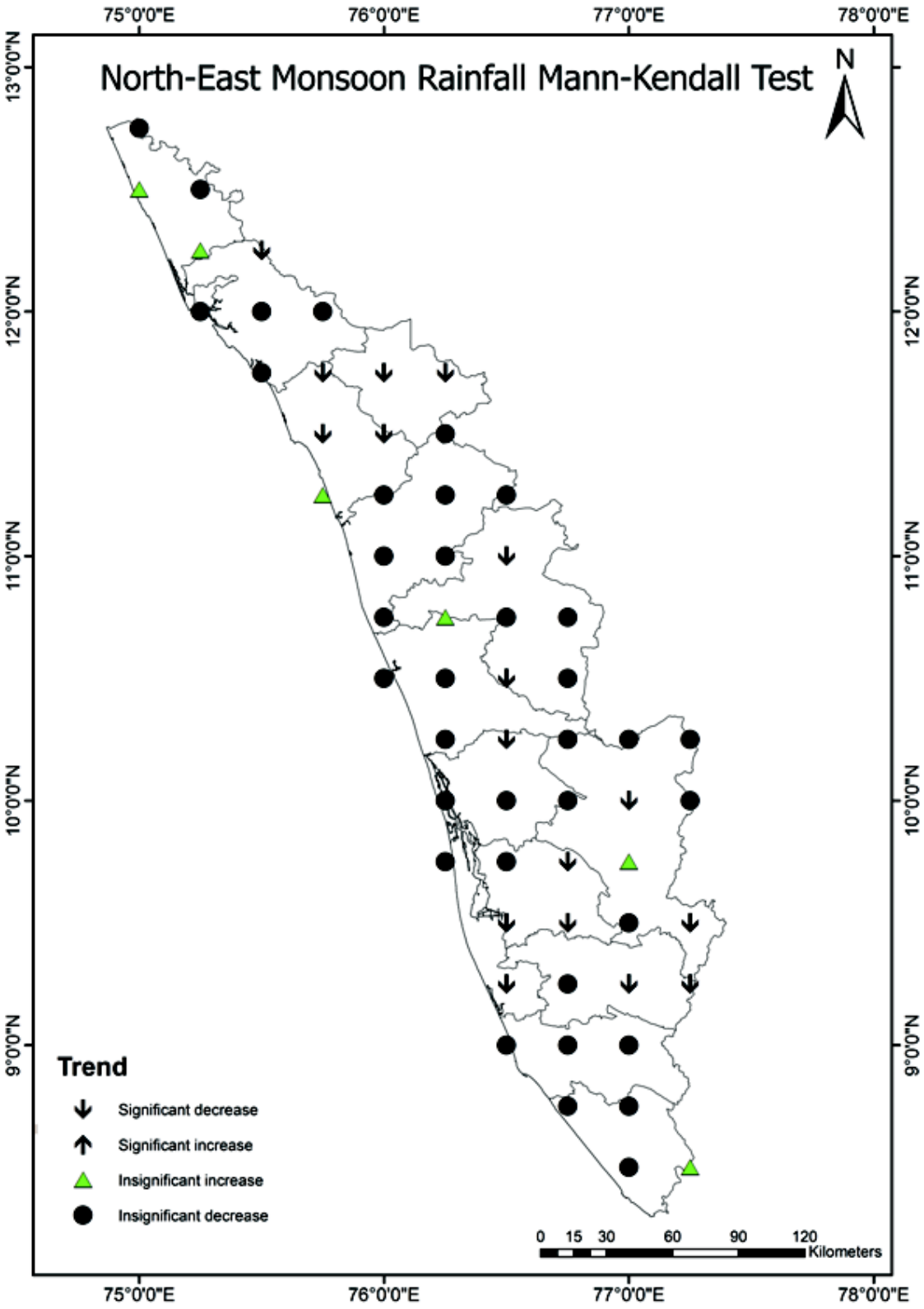

Figure 5.10. Mann-Kendall test results of north-east monsoon rainfall

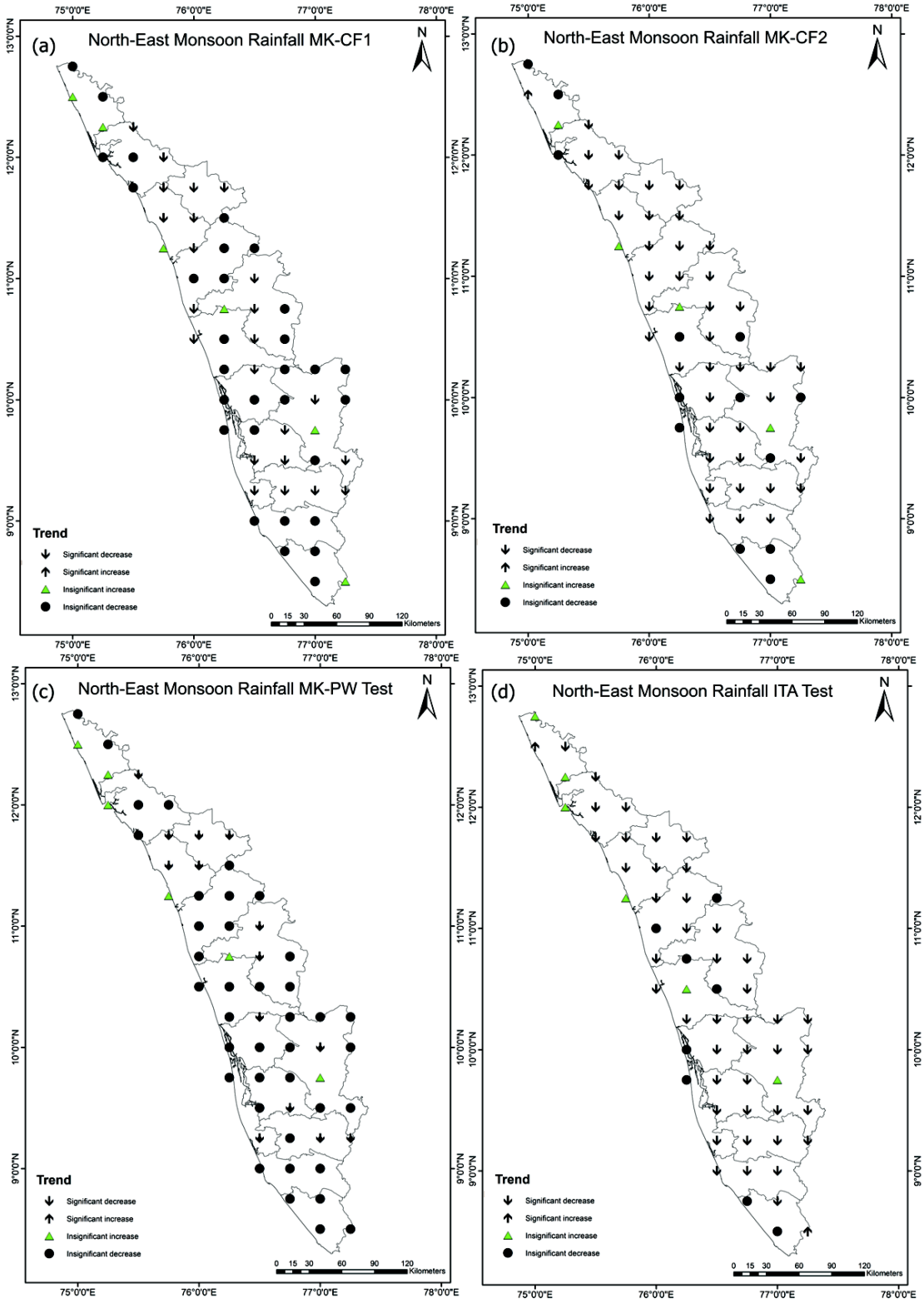

Figure 5.11. Results of (a) MK-CF1 (b) MK-CF2 (c) MK-PW (d) ITA tests of north-east monsoon rainfall

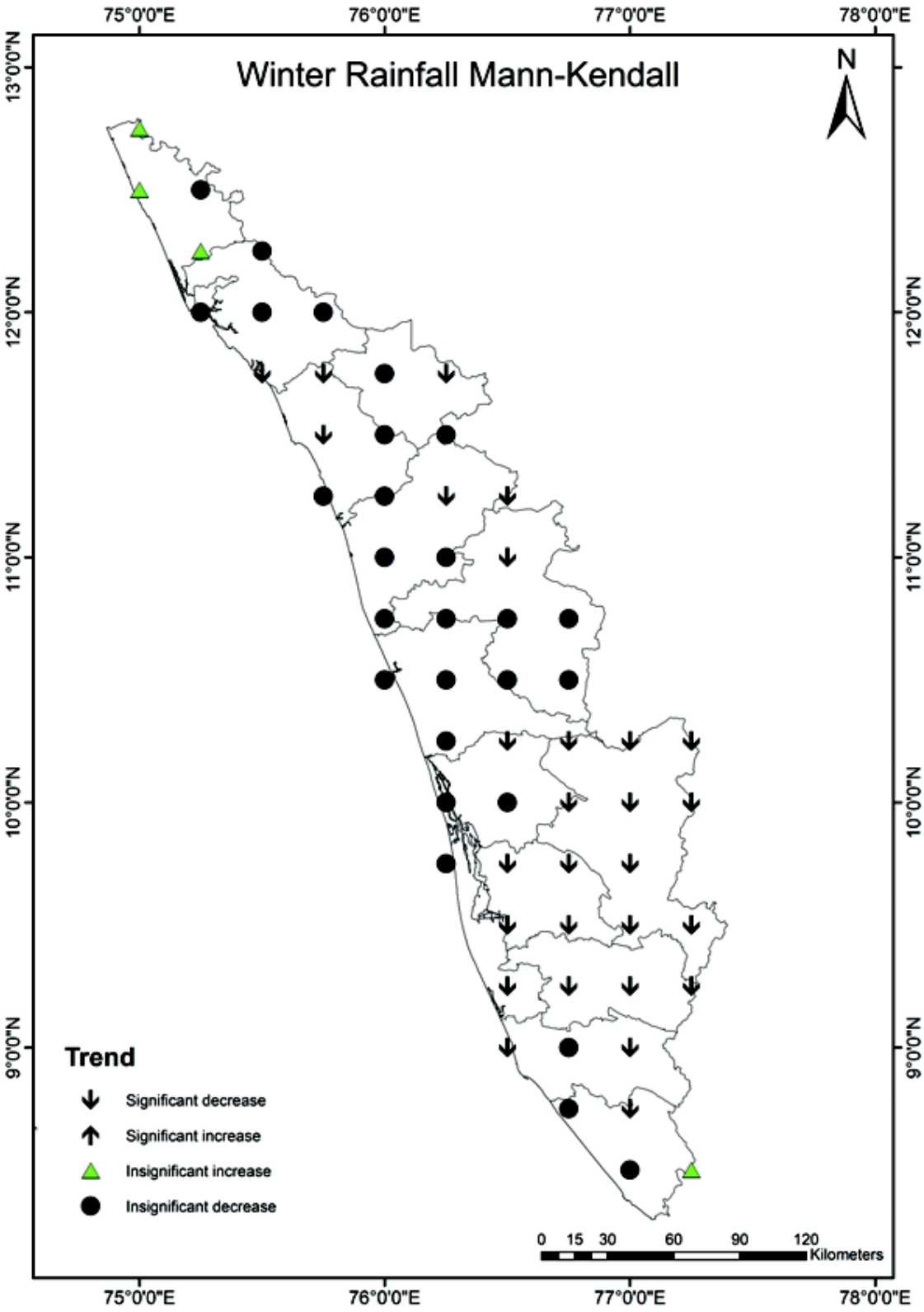

Figure 5.12. Mann-Kendall test results of winter rainfall

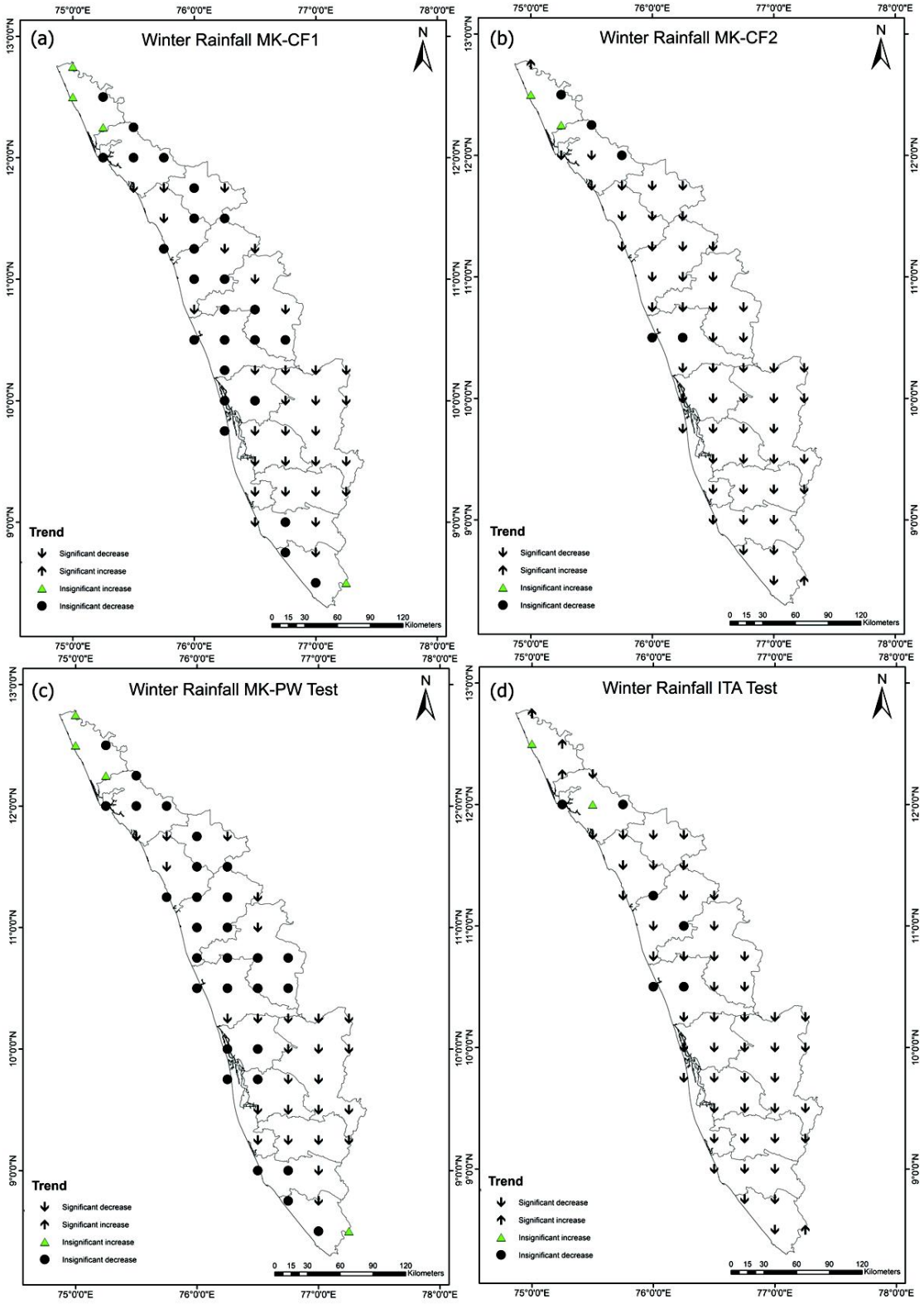

Figure 5.13. Results of (a) MK-CF1 (b) MK-CF2 (c) MK-PW (d) ITA tests of winter rainfall

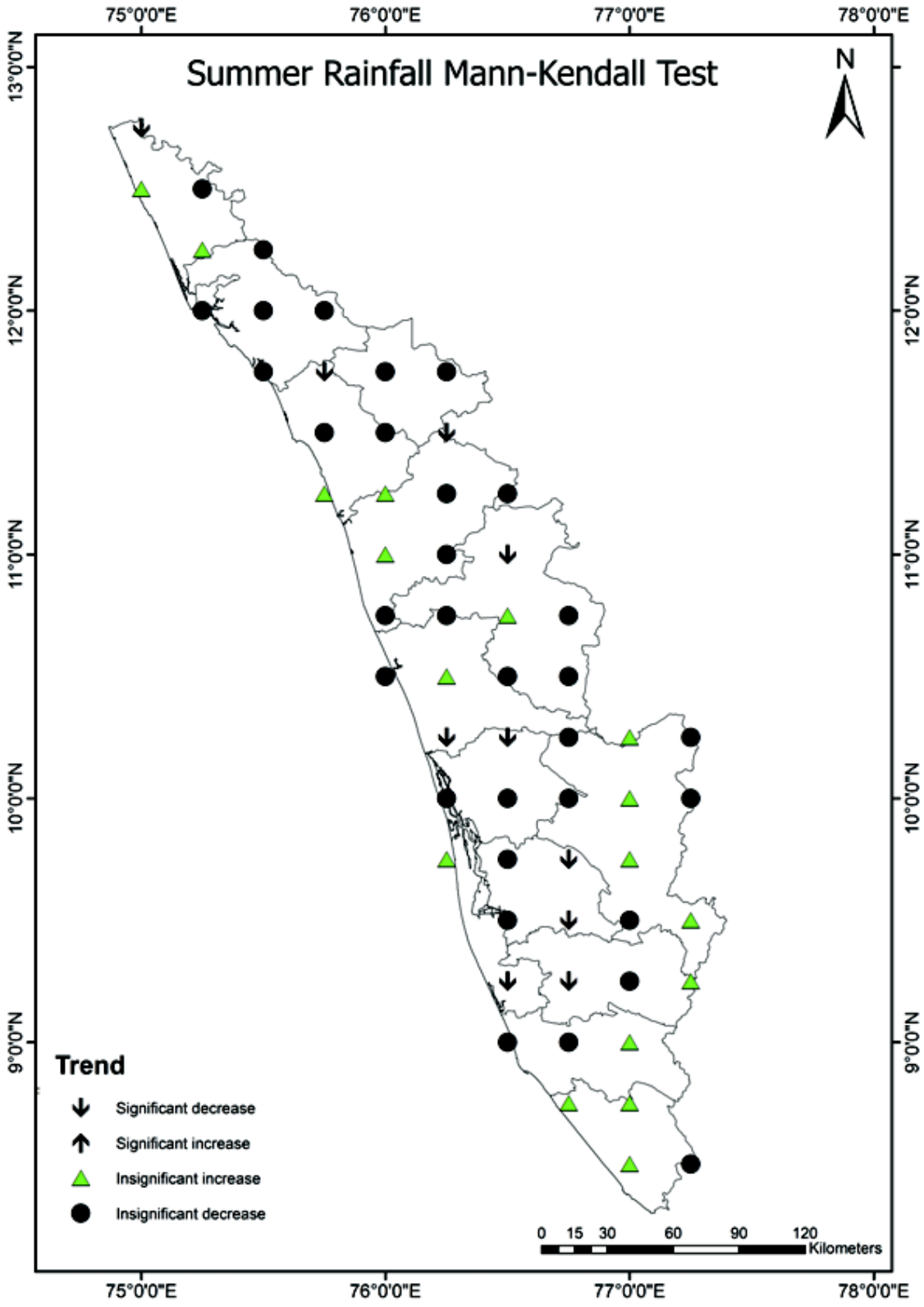

Figure 5.14. Mann-Kendall test results of summer rainfall

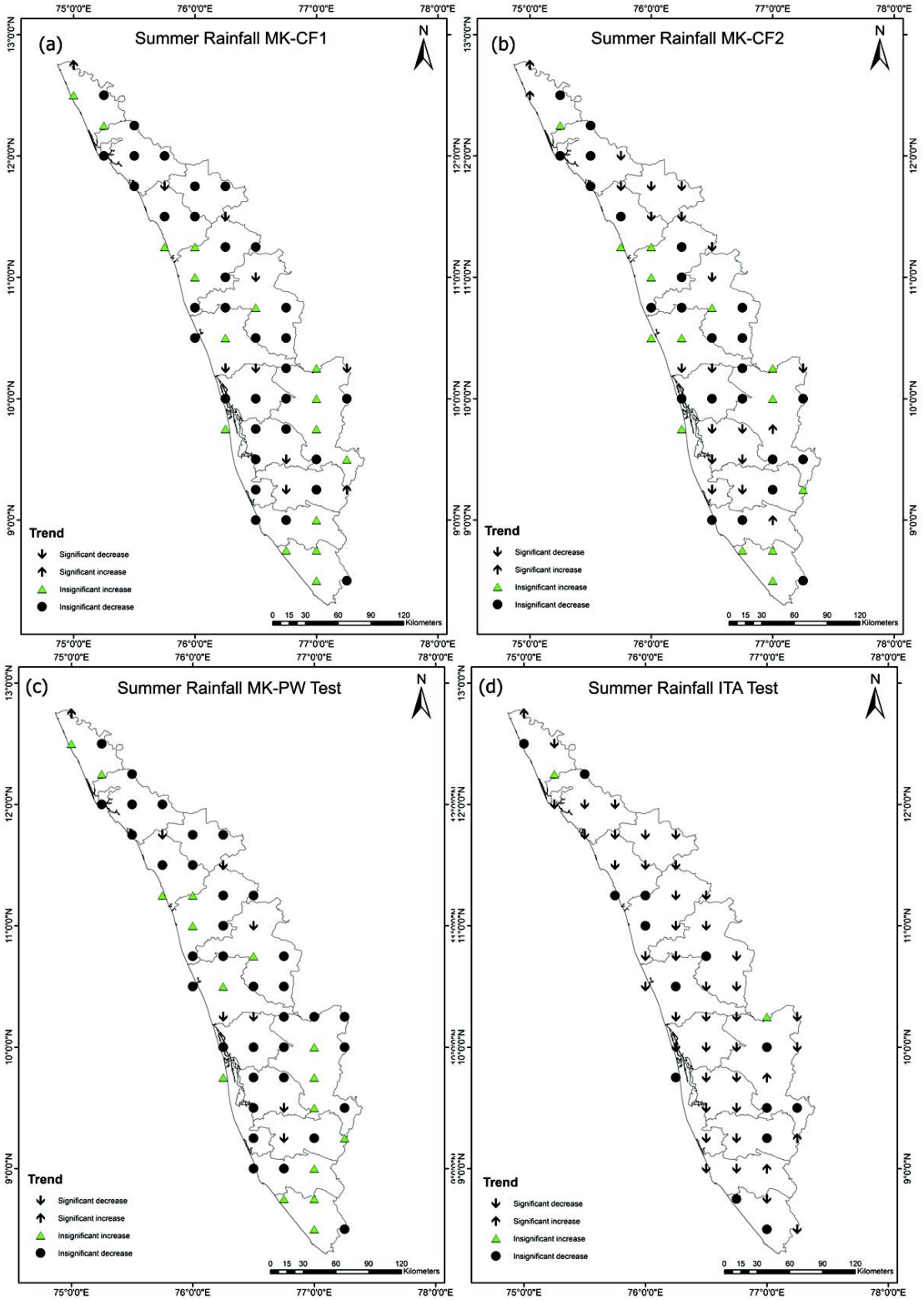

Figure 5.15. Results of (a) MK-CF1 (b) MK-CF2 (c) MK-PW (d) ITA tests of summer rainfall

In the annual and south-west monsoon rainfall series, it is shown that more than 83% of grid points exhibit negative trends, whether significant or non-significant. However, in the case of north-east monsoon and winter rainfall, more than 90% of the grid points show a negative trend (both significant and non-significant), making it a subject of concern. On the contrary, compared to other seasons, the grid points (69%) corresponding to the decreased rainfall in summer are fewer. Over 30% of the grid points show increasing precipitation during the summer season.

5.4 LONG-TERM TREND OF ANNUAL AND SEASONAL RAINY DAYS

Results of five trend analysis techniques indicating a significant and non-significant trend in annual rainy days are depicted in Figure 5.16 and Figure 5.17. In the annual rainy days series, the significantly decreasing trends at a 5% significance level are identified for 44 (75%), 36 (61%), 31 (53%), 42 (71%), and 47 (80%) grids from the results of Mann-Kendall test, MK-CF1, PWMK, MK-CF2, and ITA test respectively. However, at α =5%, 4 (7%) and 3 (5%) grids had significantly increasing trends based on the results of the Mann-Kendall test and ITA test, whereas MK-CF1, PWMK, and MK-CF2 detected a significantly increasing trend at two grids (3%). Likewise, the statistically significant decreasing trends in the south-west monsoon (Figure 5.18 and Figure 5.19) rainy days are unveiled for 35 (59%), 34 (58%), 29 (49%), 37 (63%), 45 (76%) grids from the results of the Mann-Kendall test, MK-CF1, PWMK, MK-CF2, and ITA test respectively. The statistically significant rising trends of rainy days in south-west monsoon are perceived from the results of the Mann-Kendall test, MK-CF1, PWMK, MK-CF2, and ITA tests for 4 (7%), 2 (3%), 3 (5%), 3 (5%) and 4 (7%) grids respectively. Similarly, on north-east rainy days (Figure 5.20 and Figure 5.21), a significantly decreasing trend is evident for 29 (49%), 33 (56%), 26 (44%), 42 (71%), and 48 (81%) grids from the results of the Mann-Kendall test, MK-CF1, PWMK, MK-CF2, and ITA tests respectively. The Mann-Kendall test, MK-CF1, and PWMK identified a statistically significant increasing trend in north-east rainy days at 1 (2%) grid, whereas both MK-CF2 and ITA tests unveiled the trend at 2(3%) grids. In winter rainy days (Figure 5.22 and Figure 5.23), the Mann-Kendall test, MK-CF1, PWMK, MK-CF2, and ITA tests discovered a statistically significant decreasing trend for 34 (58%), 34 (58%), 24 (41%), 43 (73%) and 42 (71%) grids respectively at α=0.05.

However, the Mann-Kendall test, MK-CF1, and PWMK could not find any significant increasing trend, whereas MK-CF2 and ITA tests confirmed statistically significant increasing trends for 1(2 %)and 4 (7%)grids at a similar significance level.

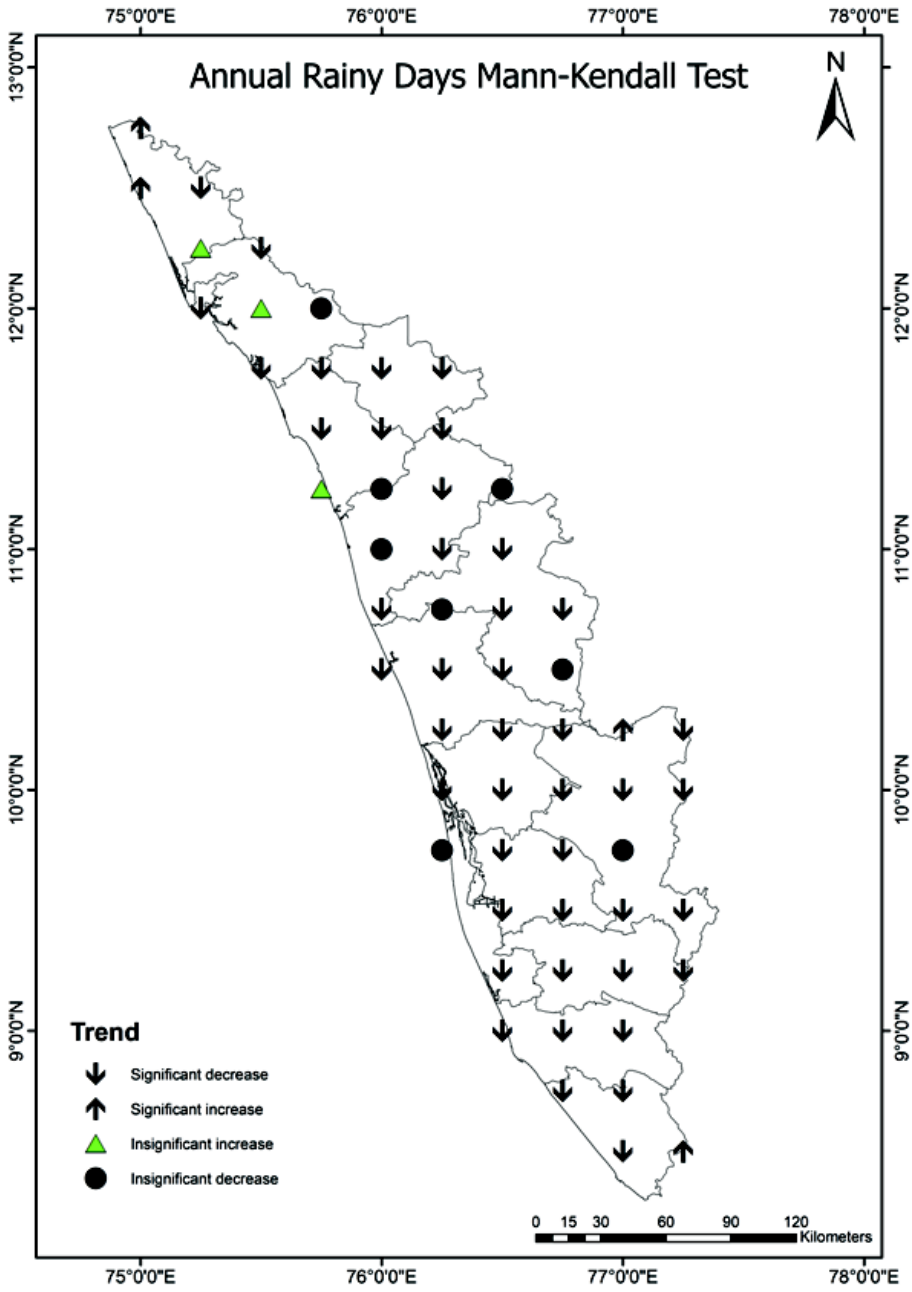

Figure 5.16. Mann-Kendall test results of annual rainy days

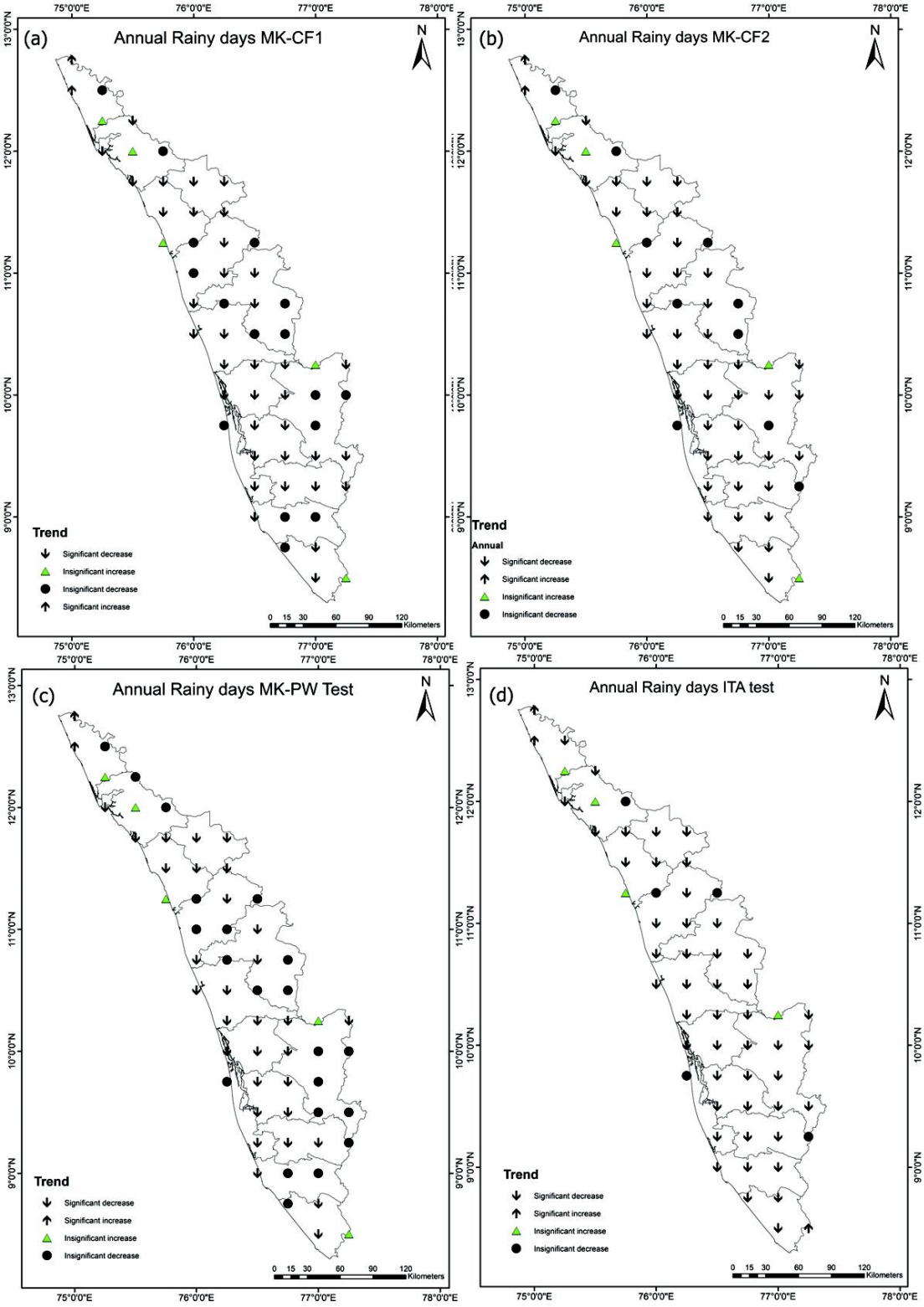

Figure 5.17. Results of (a) MK-CF1 (b) MK-CF2 (c) MK-PW (d) ITA tests of annual rainy days

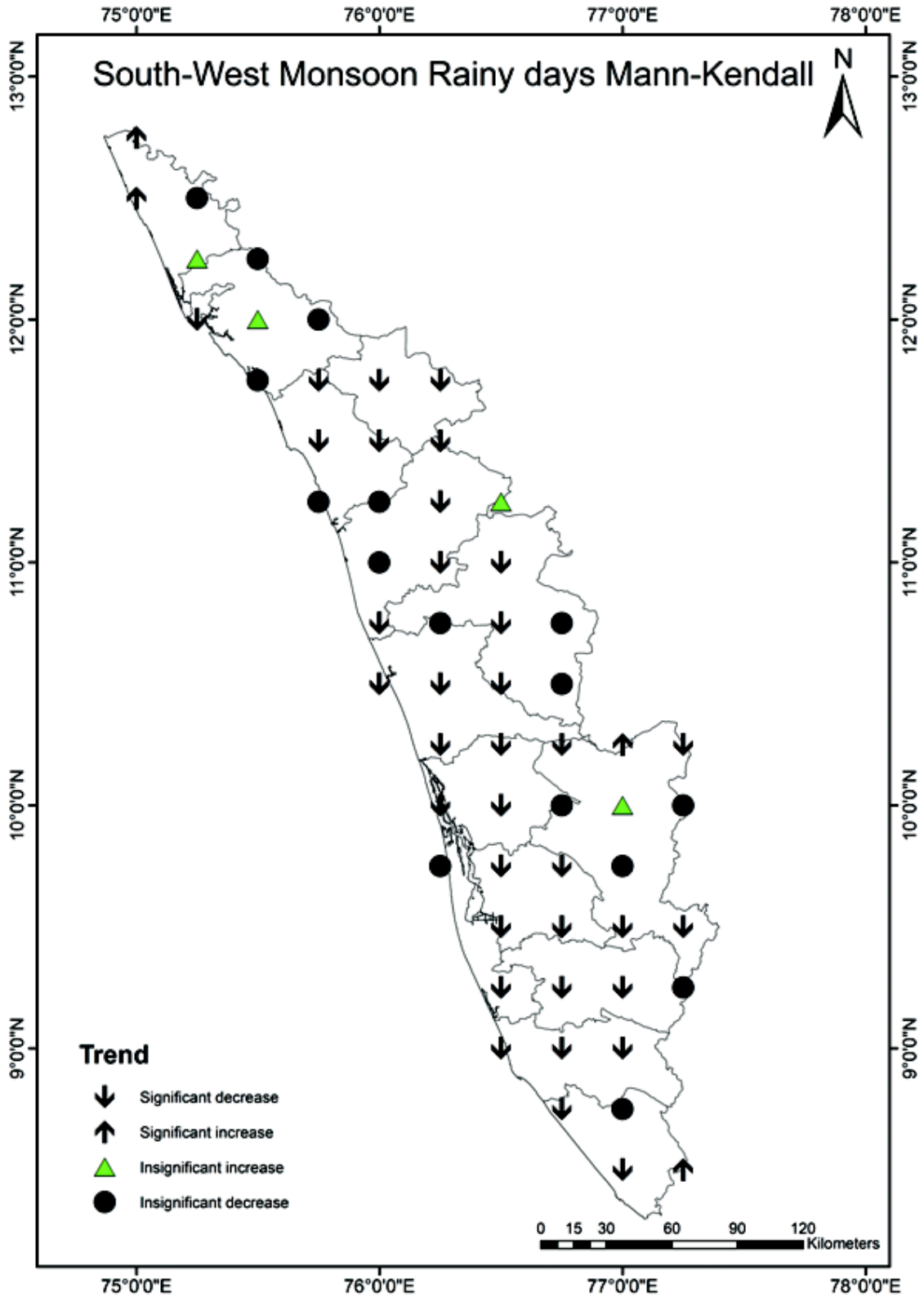

Figure 5.18. Mann-Kendall test results of south-west monsoon rainy days

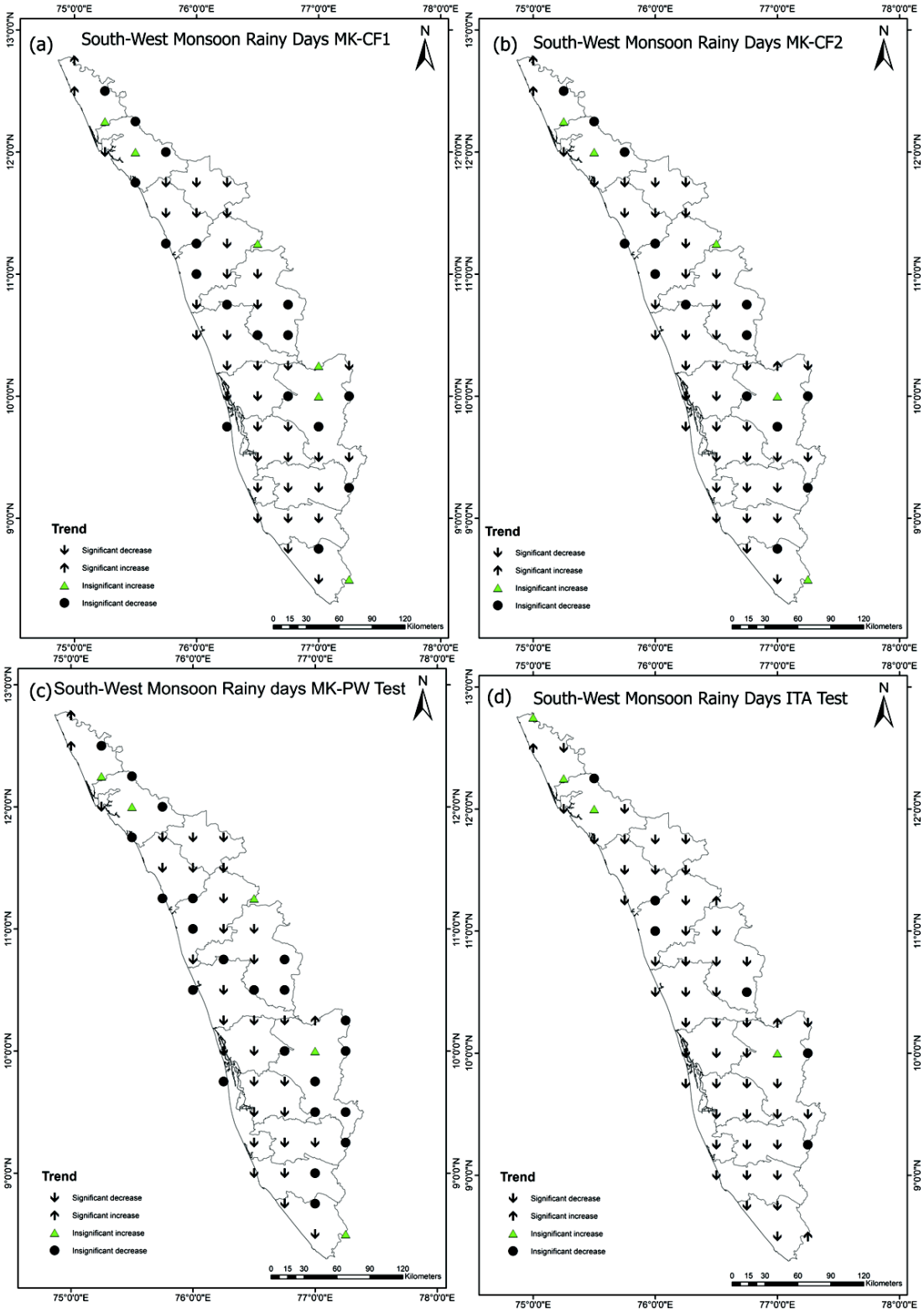

Figure 5.19. Results of (a) MK-CF1 (b) MK-CF2 (c) MK-PW (d) ITA tests of south-west monsoon rainy days

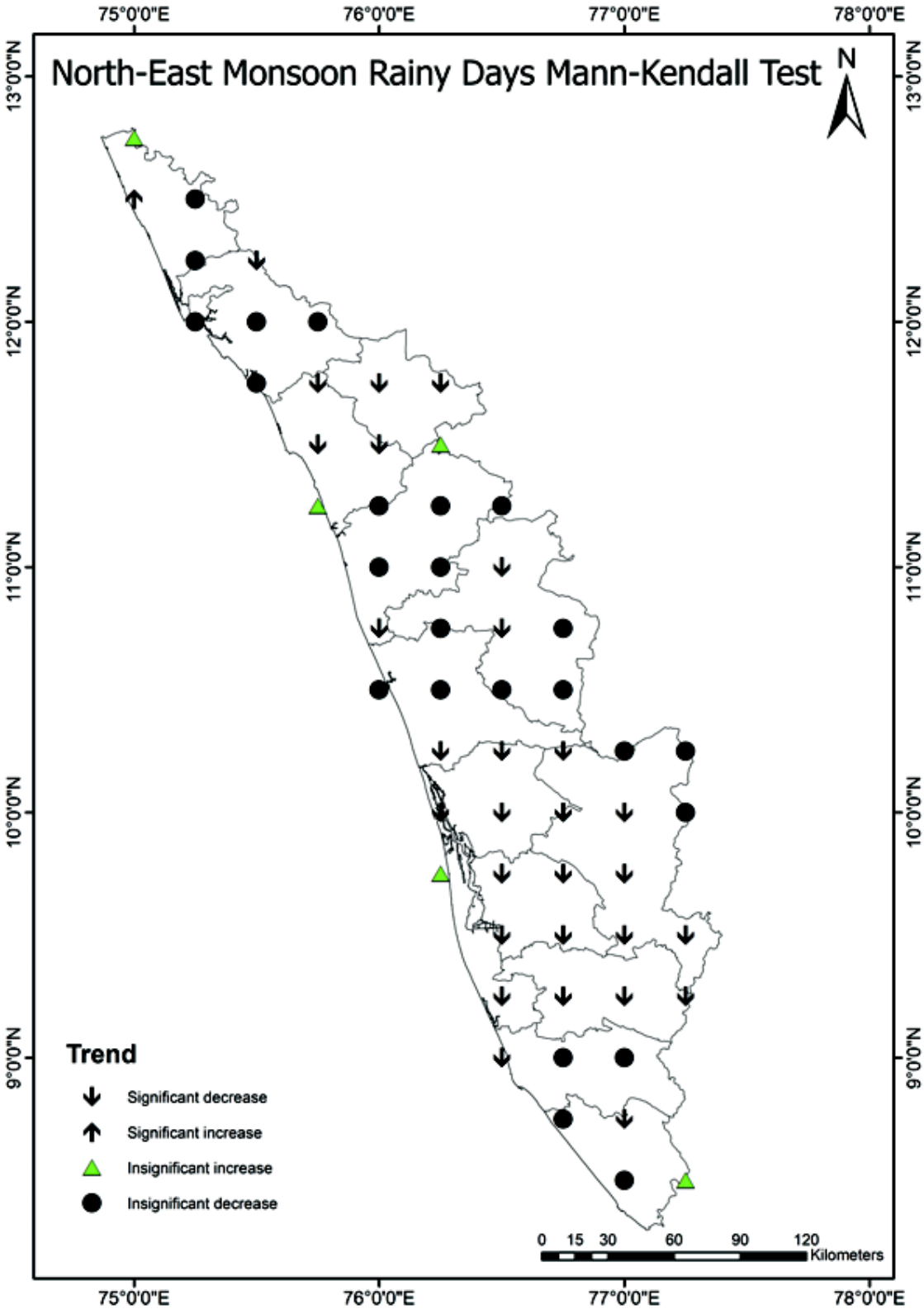

Figure 5.20. Mann-Kendall test results of north-east monsoon rainy days

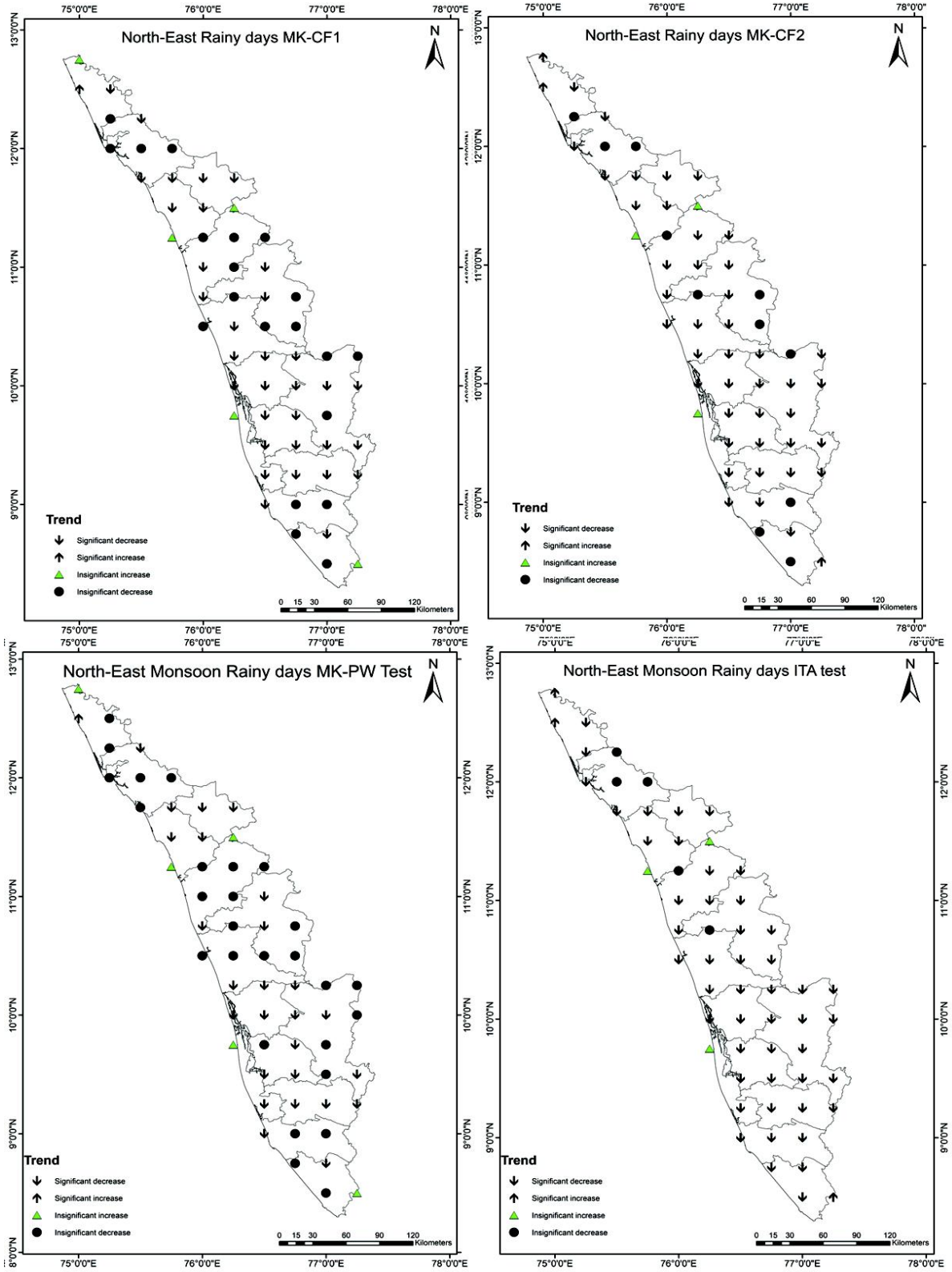

Figure 5.21. Results of (a) MK-CF1 (b) MK-CF2 (c) MK-PW (d) ITA tests of north-east monsoon rainy days

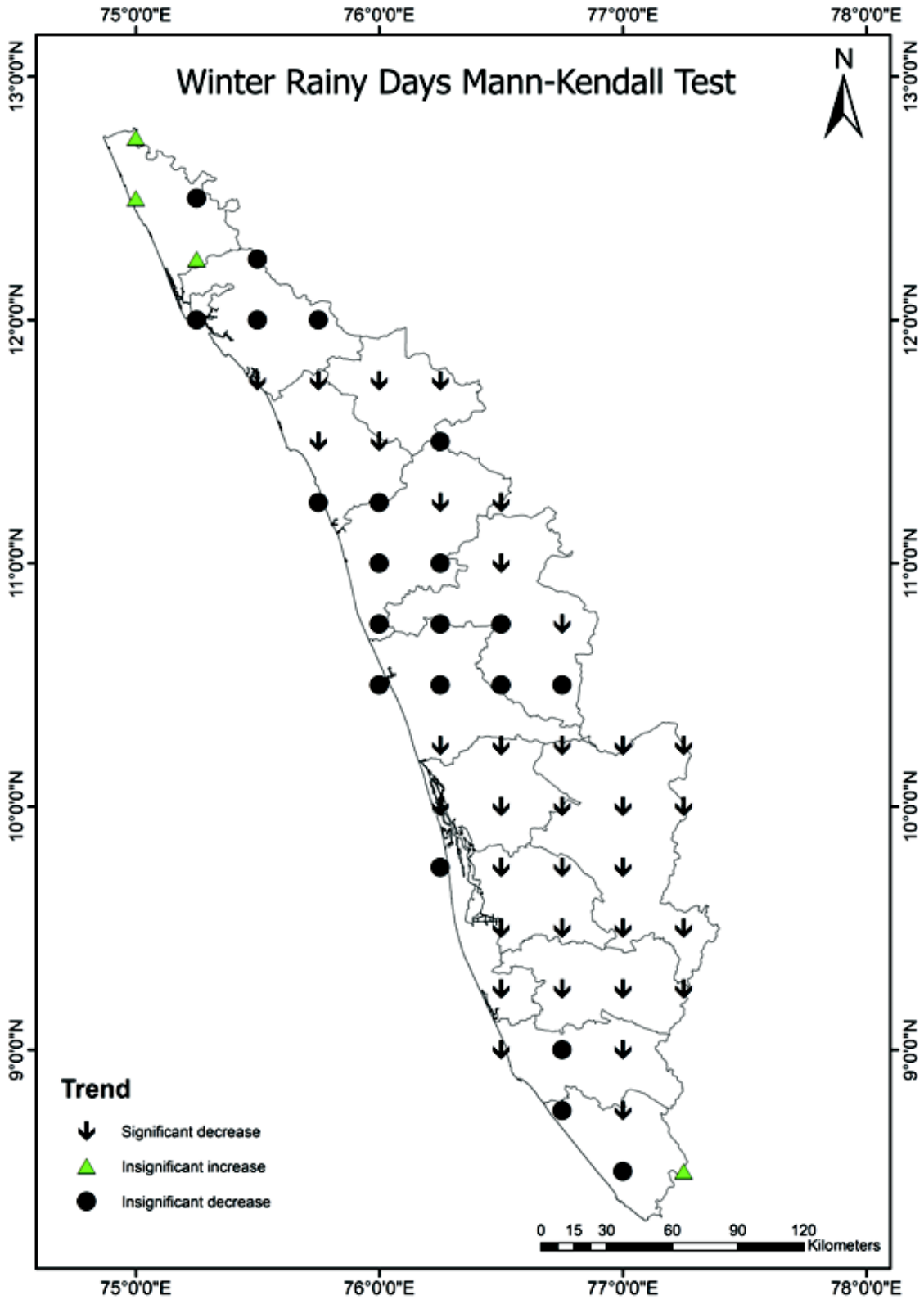

Figure 5.22. Mann-Kendall test results of winter rainy days

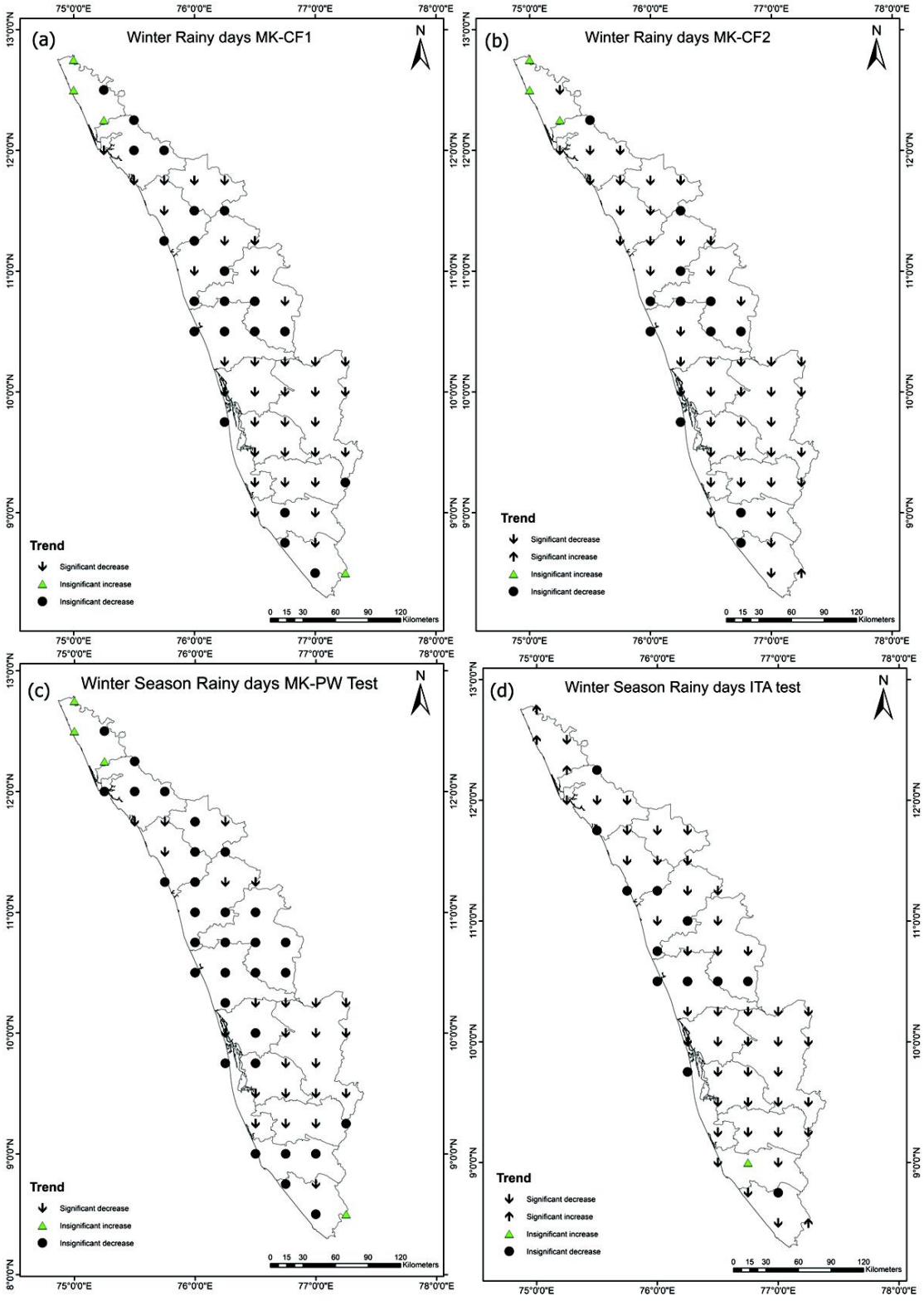

Figure 5.23. Results of (a) MK-CF1 (b) MK-CF2 (c) MK-PW (d) ITA tests of winter rainy days

The rainy days in the summer (Figure 5.24 and Figure 5.25) season were found to be significantly decreasing for 17(29%), 16 (27%), 16 (27%), 20(34%), and 39(66%) grids by Mann-Kendall test, MK-CF1, PWMK, MK-CF2 and ITA tests at 5% significance level. The Mann-Kendall test, MK-CF1, and PWMK identified a statistically significant increasing trend in summer rainy days at 2(3%) grids, whereas both MK-CF1 and ITA tests unveiled the trend at 6(10%) grids.

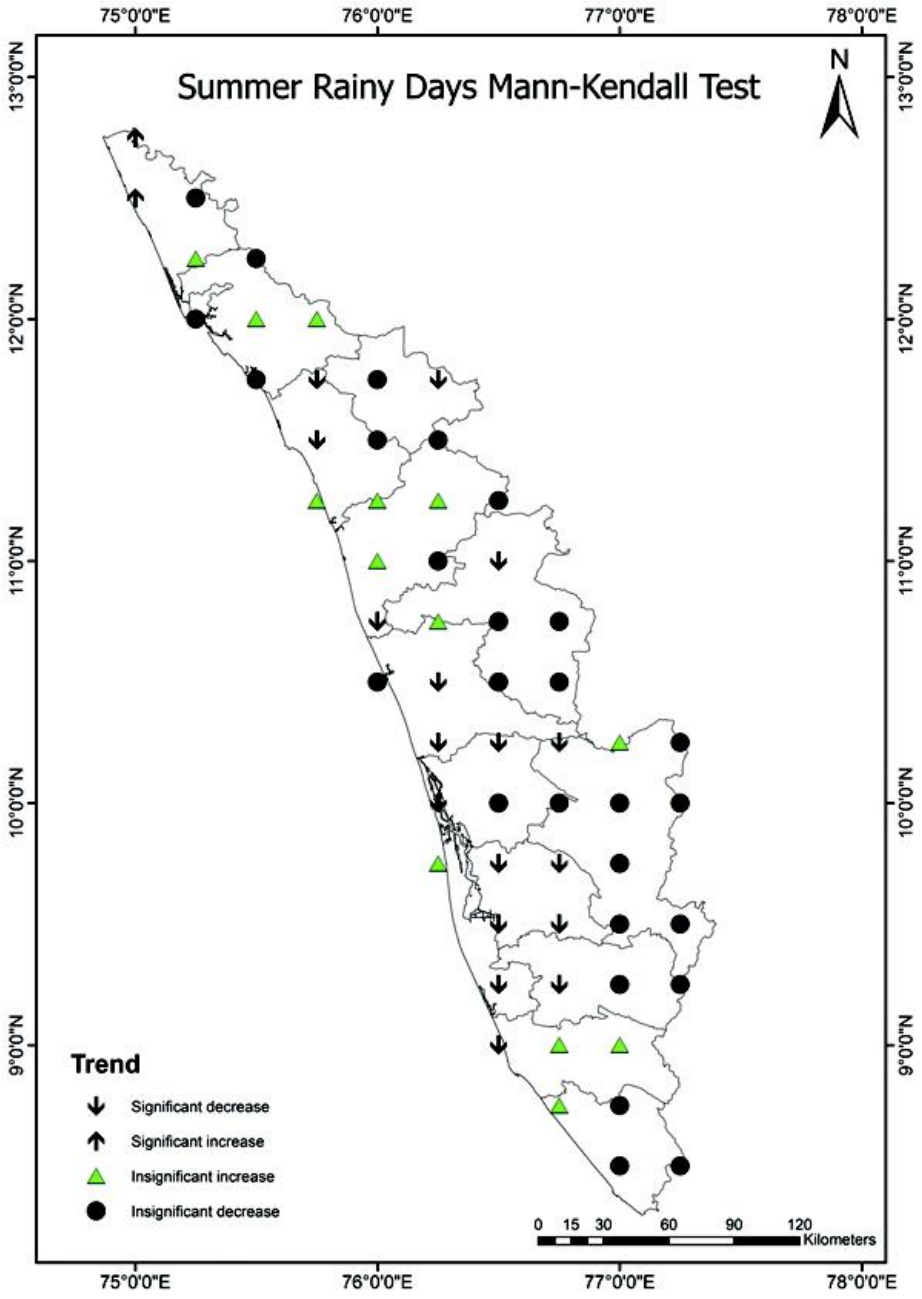

Figure 5.24. Mann-Kendall test results of summer rainy days

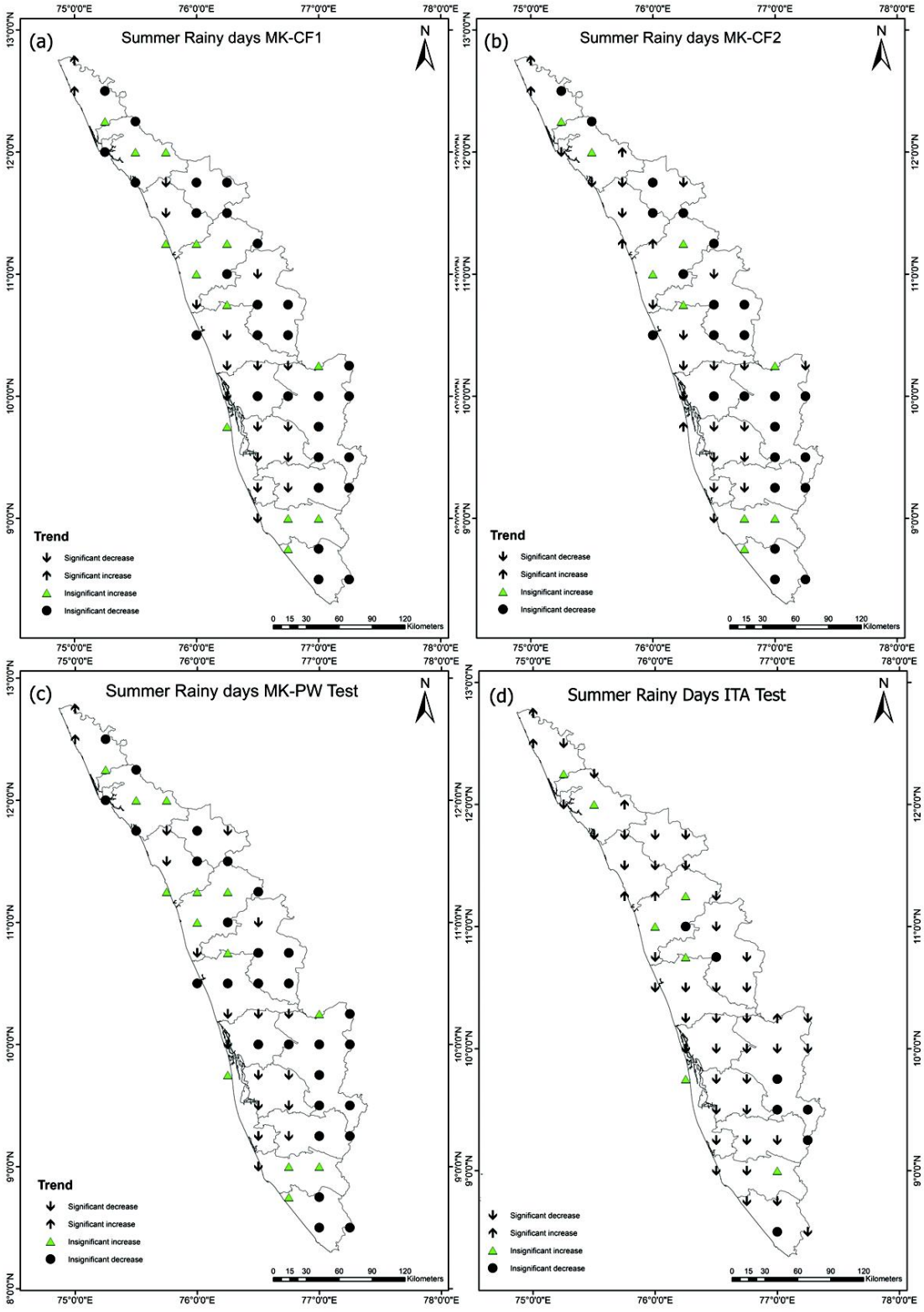

Figure 5.25. Results of (a) MK-CF1 (b) MK-CF2 (c) MK-PW (d) ITA tests of summer rainy days

The above results indicate that a significant majority, precisely over 88%, of grid points exhibit negative trends in annual and south-west monsoon rainy days series, irrespective of whether these trends are statistically significant or non-significant. However, more than 90% of the grid points show a negative trend (both significant and non-significant) in the north-east monsoon and winter rainy days. Contrariwise, compared to other seasons, the grid points (75%) corresponding to the summer season rainy days show a decreasing trend. In contrast, the increasing trends are evident for more than 25% of the grid points.

5.5 MAGNITUDE OF RAINFALL AND RAINY DAYS TREND

Table 5.2 shows the magnitude of the increasing and decreasing trend in annual and four seasonal time series of rainfall and rainy days calculated using Sen's slope test for 59 grids. It is seen from Table 5.2 that annual rainfall is varying at range from -17.38 mm/year to 7.6 mm/year with a mean value of -3.97 mm/year. The rainfall during the south-west monsoon, north-east monsoon, winter, and summer season changes at rates varying from -15.3–8.0, -7.0 – 0.48, -1.16 –0.39, -1.74 – 0.7 mm/year, respectively with the mean values of -2.83, -0.79, -0.31 and -0.26 mm/year.

Table 5.2 Trend magnitude in rainfall and rainy days at 59 grid points (1901-2019)

Grids	**Annual**		**South-west monsoon**		**North-east monsoon**		**Winter**		**Summer**	
	Rain	**R.D**	**Rain**	**RD**	**Rain**	**RD**	**Rain**	**RD**	**Rain**	**RD**
1	-1.5	-0.1	-1.1	-0.07	-0.1	-0.01	-0.21	-0.01	0.13	0
2	-0.7	0.16	-0.16	0.1	0.17	0.04	0.39	0.01	-0.47	-0.02
3	-2.1	-0.1	-2.29	-0.11	-0.26	-0.01	-0.17	0	0.34	0
4	-2.1	-0.19	-0.79	-0.08	-0.66	-0.04	-0.72	-0.06	0.03	-0.01
5	-3.9	-0.28	-2.74	-0.13	-0.6	-0.06	-0.28	-0.02	-0.24	-0.05
6	-6.2	-0.11	-4.43	-0.1	-1.16	-0.02	-0.24	0	-0.55	0
7	-3.1	-0.11	-2.82	-0.06	-0.84	-0.02	-0.61	-0.03	0.5	0.01
8	-6.8	-0.34	-4.3	-0.15	-1.09	-0.07	-0.49	-0.04	-0.89	-0.07

Grids	Annual		South-west monsoon		North-east monsoon		Winter		Summer	
9	-6.1	-0.41	-4.13	-0.17	-0.96	-0.08	-0.49	-0.04	-1.04	-0.11
10	-4.5	-0.33	-2.2	-0.17	-1.49	-0.06	-0.89	-0.05	-0.27	-0.03
11	-0.9	-0.08	-0.08	0	-0.83	-0.03	-0.87	-0.02	0.17	0
12	-7.7	-0.39	-4.52	-0.15	-1.42	-0.08	-0.64	-0.05	-1.02	-0.1
13	-15	-0.6	-11.8	-0.21	-2.25	-0.12	-0.82	-0.08	-1.74	-0.17
14	-3.1	-0.19	-2.37	-0.12	-0.47	-0.04	-0.8	-0.04	-0.08	0
15	-1.3	-0.1	-0.2	-0.05	-0.77	-0.04	-0.77	-0.03	0.02	0
16	-1.4	-0.05	-1.07	-0.04	-0.18	0	-0.1	0	0.59	0.02
17	-6.4	-0.31	-4.95	-0.16	-0.74	-0.04	-0.37	-0.02	-0.73	-0.08
18	-4.7	-0.44	-1.98	-0.14	-1.28	-0.1	-0.83	-0.07	-1.03	-0.12
19	2.13	-0.07	1.71	-0.01	0.15	-0.04	-0.58	-0.05	0.51	0
20	-2.9	-0.3	-2.44	-0.14	-0.26	-0.05	-0.15	-0.03	-0.53	-0.06
21	-5.8	-0.25	-3.92	-0.12	-0.88	-0.05	-0.27	-0.02	-0.36	-0.03
22	0.83	-0.19	2.82	-0.04	-0.81	-0.07	-0.57	-0.05	-0.32	-0.03
23	4.54	-0.13	6.2	0.04	-0.98	-0.07	-0.81	-0.07	0.18	-0.01
24	-1.3	-0.13	-0.04	-0.02	-0.29	-0.03	-0.58	-0.03	-0.26	-0.02
25	-6.1	-0.32	-4.42	-0.16	-0.75	-0.06	-0.2	-0.02	-1.17	-0.08
26	-7.1	-0.28	-3.9	-0.13	-1.98	-0.08	-0.1	-0.02	-1.61	-0.06
27	4.14	-0.39	5.38	-0.11	-1.01	-0.13	-0.41	-0.04	-0.32	-0.09
28	3.87	0.31	5.12	0.3	-0.78	-0.04	-0.67	-0.04	0.05	0.03
29	-1.3	-0.16	-0.43	-0.06	-0.34	-0.03	-0.89	-0.05	-0.43	-0.02
30	-4.3	-0.1	-3.7	-0.06	-0.77	-0.02	-0.02	0	-0.08	-0.01
31	-2.5	-0.16	-2.63	-0.08	-0.24	-0.03	-0.04	0	0.18	-0.04
32	-3.4	-0.11	-2.42	-0.07	-0.65	-0.03	-0.09	0	-0.1	0
33	-0.9	-0.06	0.5	0	-0.33	-0.03	-0.17	-0.01	-0.08	0
34	-3.9	-0.2	-2.94	-0.1	-0.63	-0.05	-0.08	0	-0.49	-0.05
35	-1.9	-0.04	-1.63	-0.02	0.01	0	-0.06	0	-0.06	0
36	-3.3	-0.15	-2.6	-0.1	-6.99	-0.05	-0.09	0	0.07	0
37	-2.5	-0.16	-1.44	-0.07	-0.55	-0.04	-0.15	-0.01	-0.24	0

Grids	Annual		South-west monsoon		North-east monsoon		Winter		Summer	
38	-1.8	-0.04	-1.82	0	-0.54	-0.02	-0.08	0	0.15	0
39	-5.6	-0.11	-4.81	-0.07	-0.73	-0.02	-0.07	0	-0.36	-0.01
40	-10	-0.29	-8.18	-0.17	-1.2	-0.06	-0.17	-0.01	-0.6	-0.04
41	-1.2	0	-1.54	-0.01	0.19	0	-0.1	0	0.21	0.03
42	-3.4	0	-2.61	-0.02	-0.6	0	-0.08	0	0.06	0.01
43	-6.5	-0.15	-5.42	-0.11	-0.63	-0.02	-0.21	-0.03	-0.16	0
44	-0.7	-0.07	1.01	0.03	-0.48	-0.03	-1.16	-0.05	-0.3	-0.01
45	-15	-0.22	-12.6	-0.09	-1.58	-0.07	-0.24	-0.02	-0.46	-0.05
46	-17	-0.19	-15.3	-0.14	-1.23	-0.04	-0.11	0	-0.34	-0.01
.47	-15	-0.18	-13.5	-0.15	-0.55	0	-0.12	0	-0.59	0
48	-5.6	-0.12	-3.98	-0.03	-0.67	-0.03	-0.17	-0.01	-0.45	-0.03
49	12.2	-0.22	-9.28	-0.08	-1.88	-0.09	-0.23	-0.02	-0.83	-0.04
50	-16	-0.23	-14.7	-0.15	-0.94	-0.05	-0.08	-0.01	-0.3	-0.01
51	-12	-0.6	-10.4	-0.48	-1	-0.07	-0.16	-0.02	-0.41	-0.03
52	-2.3	-0.1	-2.17	-0.05	-0.04	-0.01	-0.03	0	-0.21	-0.02
53	-5	0.01	-4.06	0.02	-0.7	0	-0.04	0	-0.42	0
54	7.6	-0.01	7.99	0	-0.46	-0.01	-0.01	0	-0.18	0.03
55	1.68	0	1.46	0	0.2	0	0.02	0	0.26	0
56	2.87	-0.1	3.9	-0.02	-0.95	-0.05	-0.04	0	-0.2	0
57	-8.5	0.24	-7.84	0.08	-0.45	0	-0.01	0	-0.22	0.07
58	0.59	-0.08	-0.37	-0.02	0.48	-0.03	0.01	0	0.37	-0.03
59	0.9	0.16	0.05	0.04	-0.02	0.03	0.02	0	0.7	0.08

It is interesting to note that annual rainfall was found to be significantly decreasing for more than 70% of the grid points in cluster 2, 3, and 4. Most of these points are located along the coastal region and midland, whereas some grid points in cluster 5 show an increasing trend in annual rainfall. On the other hand, 11 grids were increasing in the south-west monsoon located near the Western Ghats. The annual rainfall is varying at range from -15.16 mm/year to 2.87 mm/year with a mean value of -4.26 mm/year in cluster 1, whereas it changes from -17.38 mm/year to 7.60 mm/year with a mean value

of -5.55 mm/year in cluster 2. Likewise, south-west monsoon rainfall is found to be deviating at a mean rate of -12.62 mm/year to 3.90 mm/year with a mean value of -3.49 mm/year in cluster 1, whereas it varies at a range from -15.30 mm/year to 7.99 mm/year with a mean value of -4.74 mm/year in cluster 2. The decrease in annual and south-west monsoon rainfall is more in clusters 1 and 2, whereas the reduction in north-east monsoon rainfall is found to be high in clusters 2 and 3 compared to the other clusters. The average magnitude of decrease in north-east monsoon rainfall over cluster 2 and 3 was found to be 0.99 and 1.05 mm/year, respectively. Furthermore, it is worth noting that in cluster 3 and 4, the average values of winter and summer rainfall display a noticeable decline. Specifically, cluster 3 decreases -0.40 mm/year and -0.74 mm/year in winter and summer rainfall, respectively.

Similarly, cluster 4 declines -0.74 mm/year and -0.25 mm/year in winter and summer rainfall, respectively. These reductions are relatively higher when compared to the corresponding changes in other clusters. Moreover, the annual rainy days vary in a range from -0.6 – 0.31 days/year with a mean value of -0.15 days/year. Similarly, the rainy days during the south-west monsoon, north-east monsoon, winter, and summer season alter within -0.48–0.3, -0.13– 0.04, -0.08 –0.01, -0.17–0.08 days/year respectively with the mean rates of -0.07, -0.04, -0.02 and -0.02 days/year respectively. Although the highest number of rainy days are experienced by cluster 1 and 3, there is a considerable reduction in the number of rainy days from 1901 to 2019. The number of rainy days during winter and the north-east monsoon has considerably decreased in all 5 clusters. The reduction in annual and seasonal rainy days is higher in clusters 3 and 4 than in the other clusters. The annual rainy days are decreasing at a mean value of 3.20 days/decade and 2.20 days/decade in cluster 3 and cluster 4, respectively. Likewise, rain days of the south-west monsoon were declining at a rate of 1.20 days/decade in cluster 3 and 4. Even though there is a reduction in the rainy days in cluster 3, annual rainfall does not show a profound reduction. This indicates the possible occurrence of high-intensity rainfall for a short duration in the regions mentioned above. The increase in the frequency of climate extremes across peninsular India was reported by various researchers (Dash et al. 2009; Goswami et al. 2006; Malik

et al. 2016; Mukherjee et al. 2018). These results can be validated with the 2018, 2019, and 2020 Kerala floods which occurred over a few days.

It has been observed that between 1901 to 2019, there has been a significant increase in dry days, with the highest number recorded in clusters 4 and 5. The growth rate in annual dry days is higher in cluster 3(from 137 days in 1901 to 173 days in 2019) and 4 (from 134 days in 1901 to 210 days in 2019) than in the other clusters. There has been a significant rise in dry days in all clusters, particularly during the south-west and north-east monsoon periods. This increase has substantial implications for the various water sources within the state. The increase in dry days during non-rainy seasons has resulted in severe water scarcity and a decline in groundwater levels due to uneven rainfall distribution. Most rainwater discharges to the Arabian Sea within 48 to 72 hours of the occurrence due to the complexity of the state's topography (Dash et al. 2018).

5.6 TEMPERATURE CHARACTERISTICS

The summary statistics of monthly, seasonal, and annual temperature (mean temperature, maximum temperature, and minimum temperature) for 1951 to 2019 are presented in Table 5.3. From Figure 5.26, it is evident that there is a strong gradient in mean temperature over Kerala from Northern Kerala to Southern Kerala.

Table 5.3 Monthly and seasonal means of temperature (°C) over Kerala for 69 years (1951-2019).

Seasons	Mean (° C)			Maximum (° C)			Minimum (° C)		
	Max	Min	Avg	Max	Min	Avg	Max	Min	Avg
January	25.3	23	24.2	30.8	28.5	29.7	20.1	17.1	18.6
February	26.5	24.3	25.3	32.3	29.6	31	20.8	18	19.6
March	28.4	25.5	26.8	34.1	30.5	32.4	22.7	20	21.2
April	29.6	26.6	27.7	35	31	32.7	24.3	21.6	22.6
May	28.8	25.7	27.4	33.7	29.7	32	24	21.7	22.8
June	27.1	24.2	25.5	31.1	27.3	29.2	23	21	21.8
July	26.1	23.7	24.8	30.1	26.6	28.2	22.2	20.7	21.4
August	26.2	24.2	24.8	30.1	27.1	28.3	22.2	20.8	21.4

Seasons	Mean (° C)			Maximum (° C)			Minimum (° C)		
	Max	Min	Avg	Max	Min	Avg	Max	Min	Avg
September	26.3	24.3	25.3	30.6	27.6	29.1	22.2	20.8	21.3
October	26.1	24.2	25.2	30.6	27.5	29.3	22	20.3	21.2
November	25.8	23.8	24.7	30.6	27.3	29.1	21.5	18.7	20.4
December	25.5	23.2	24.3	30.4	27.7	29.2	21.2	17.5	19.3
Annual	26.5	24.7	25.5	31.2	28.8	30.1	21.7	20.4	21
South-west monsoon	26.1	24.2	25.1	30.1	27.2	28.7	22.3	21	21.5
North-east monsoon	25.8	24.2	25	30.6	27.7	29.2	21.6	19.7	20.8
Winter	25.6	23.9	24.6	31.1	28.9	30	21.1	18.1	19.2
Summer	28.7	26.3	27.3	34	31	32.3	23.4	21.4	22.2

The spatial variation of mean temperature is well illustrated in Figure 5.26, and the magnitude steps down from the southern part to the northern part of the state. At the annual scale, the average mean, maximum and minimum temperature ($T_{mean,}$ $T_{max,}$ and $T_{min)}$ for 69 years were 24.7 ℃, 28.8 ℃, and 20.4 ℃, respectively. It is important to note that the highest temperature is usually experienced between April and May, and the lowest temperature is registered during December and January. The ever-recorded maximum temperature is 37.6 ℃, measured in 2016, whereas 20.8 ° C (1956) is the lowest temperature from 1951 to 2019. Detailed analysis showed that 2016 was the warmest year since 1901, and the value was 0.71 ℃ above the 1981-2010 average. According to IMD 2020, the warmest years were 2016 (0.71 ℃), 2009 (0.55 ℃), 2017(0.54 ℃), 2010 (0.53℃) and 2022 (0.71 ℃).

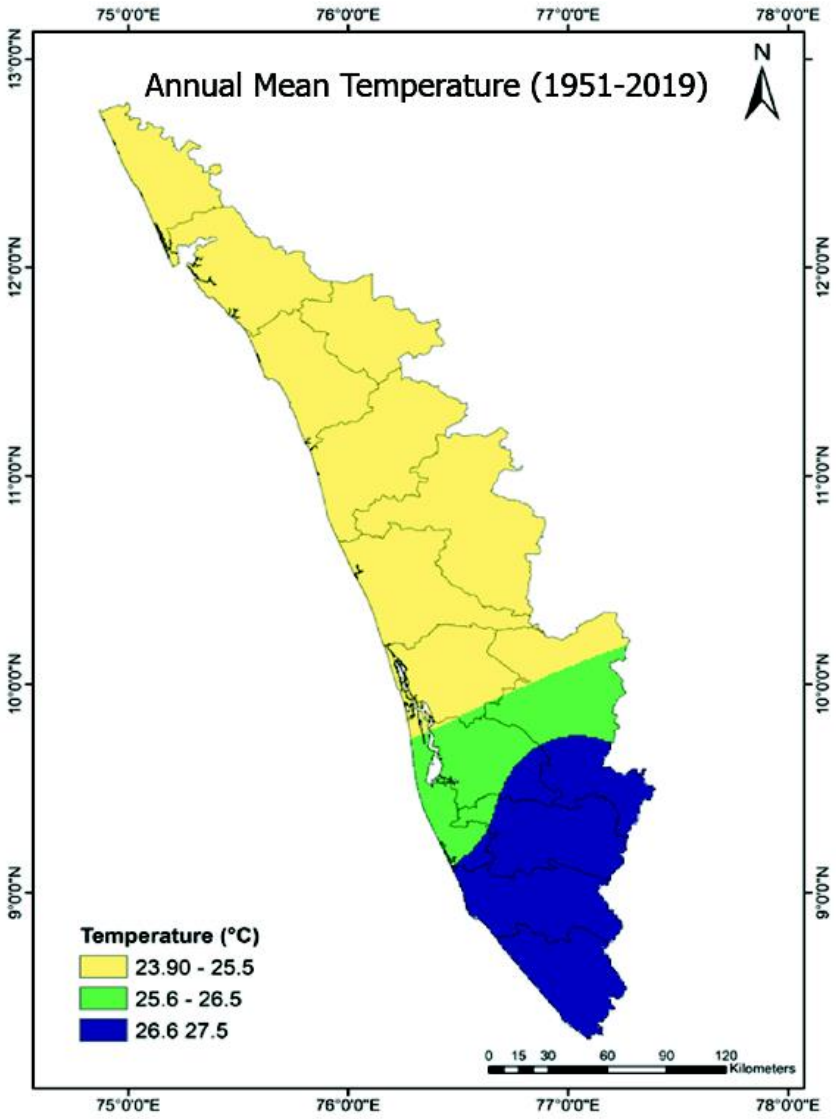

Figure 5.26 Spatial variation of mean annual temperature.

5.7 LONG-TERM TREND OF ANNUAL AND SEASONAL TEMPERATURE

Figure 5.27 shows that the annual and seasonal mean temperature at all five grids is increasing. Compared to other grids, the mean temperature is high in grid 4 and 5, mainly situated towards the southern parts of the state. The lowest temperature in grid 3 is in the state's central part. A continual rise in mean temperatures over time is noted in Figure 5.27, even though the rate of increase is almost uniform in all grids. The highest and lowest temperature were observed in the state's southern parts (grid 4 and

5) and central parts (grid 3), respectively. The highest mean temperature increase rate is registered during the south-west monsoon season in grid 2, 4, and 5. Interestingly, the north-east monsoon season grid shows a slight increase compared to other grids.

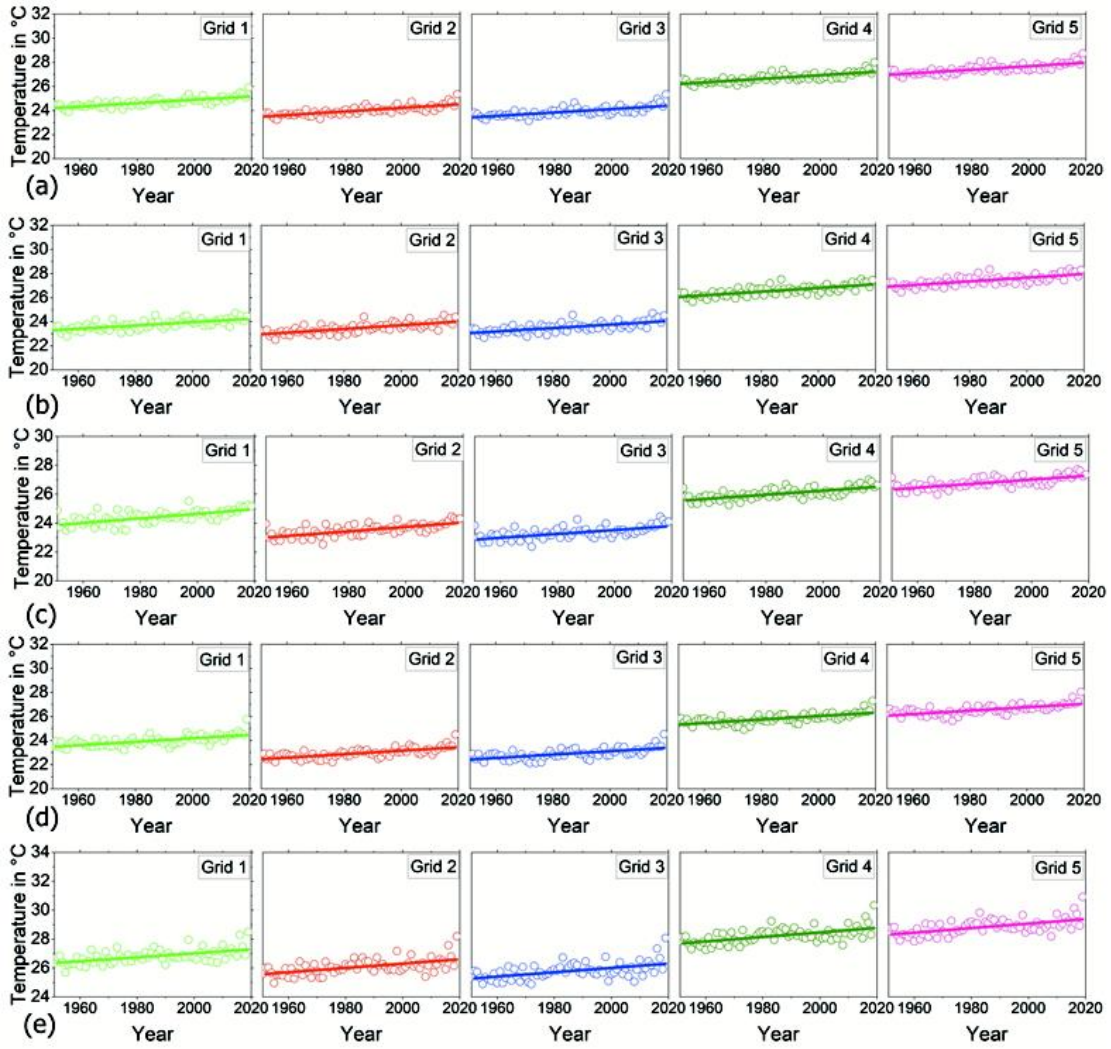

Figure 5.27. Scatter plots of long-term mean temperature for (a) annual. (b) south-west monsoon. (c) north-east monsoon (d) winter. (e) summer

Results of 5 trend tests for the mean temperature of annual and seasonal time series in the study are presented in Figure 5.28 to Figure 5.37. It is seen that in annual as well as four seasonal (south-west monsoon, north-east monsoon, winter, and summer) mean temperature series, Mann-Kendall test, MK-CF1, PWMK, MK-CF2 and ITA tests at 5% significance level uncovered statistically significant increasing trends for all five grids.

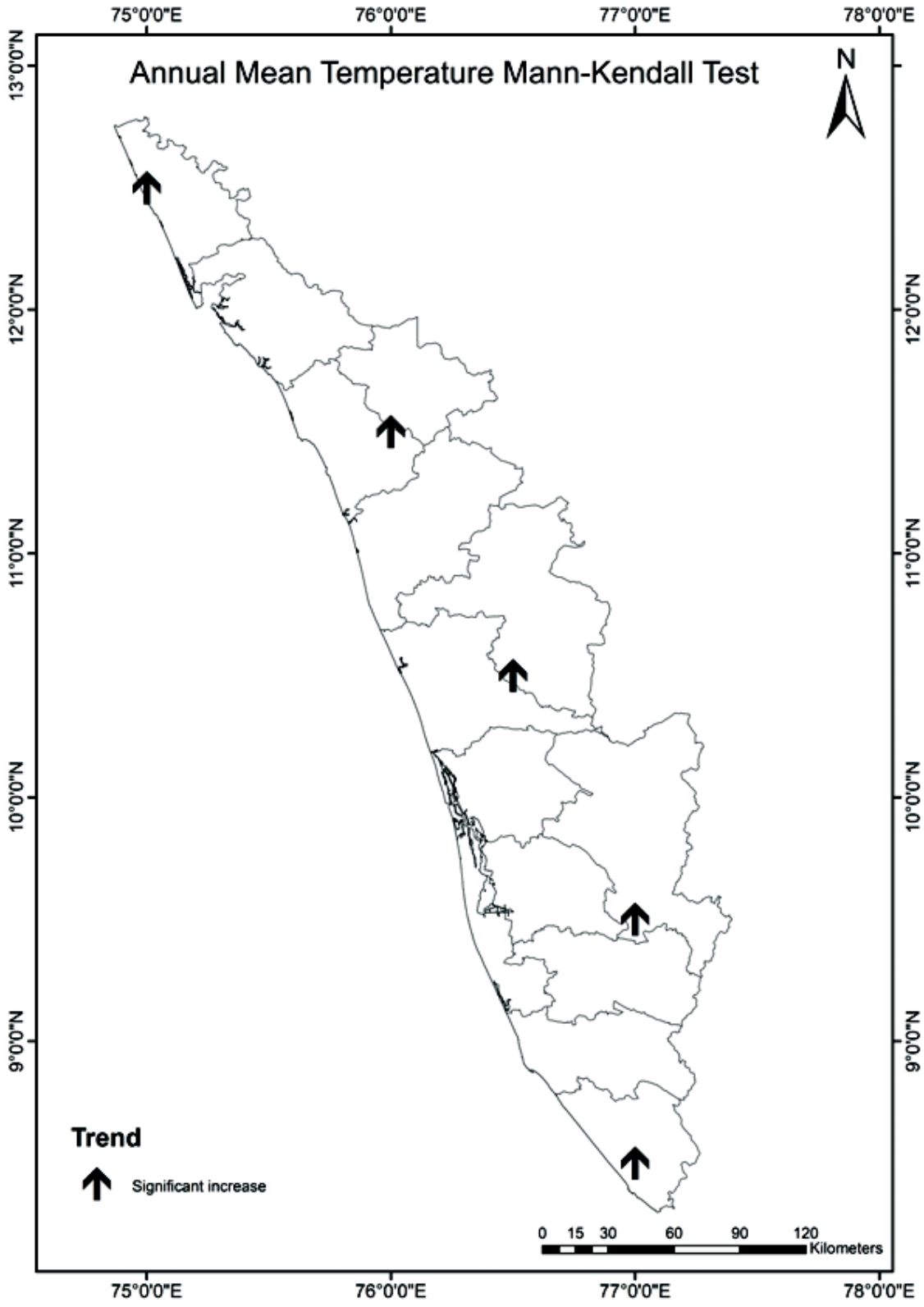

Figure 5.28. Mann-Kendall test results of annual mean temperature

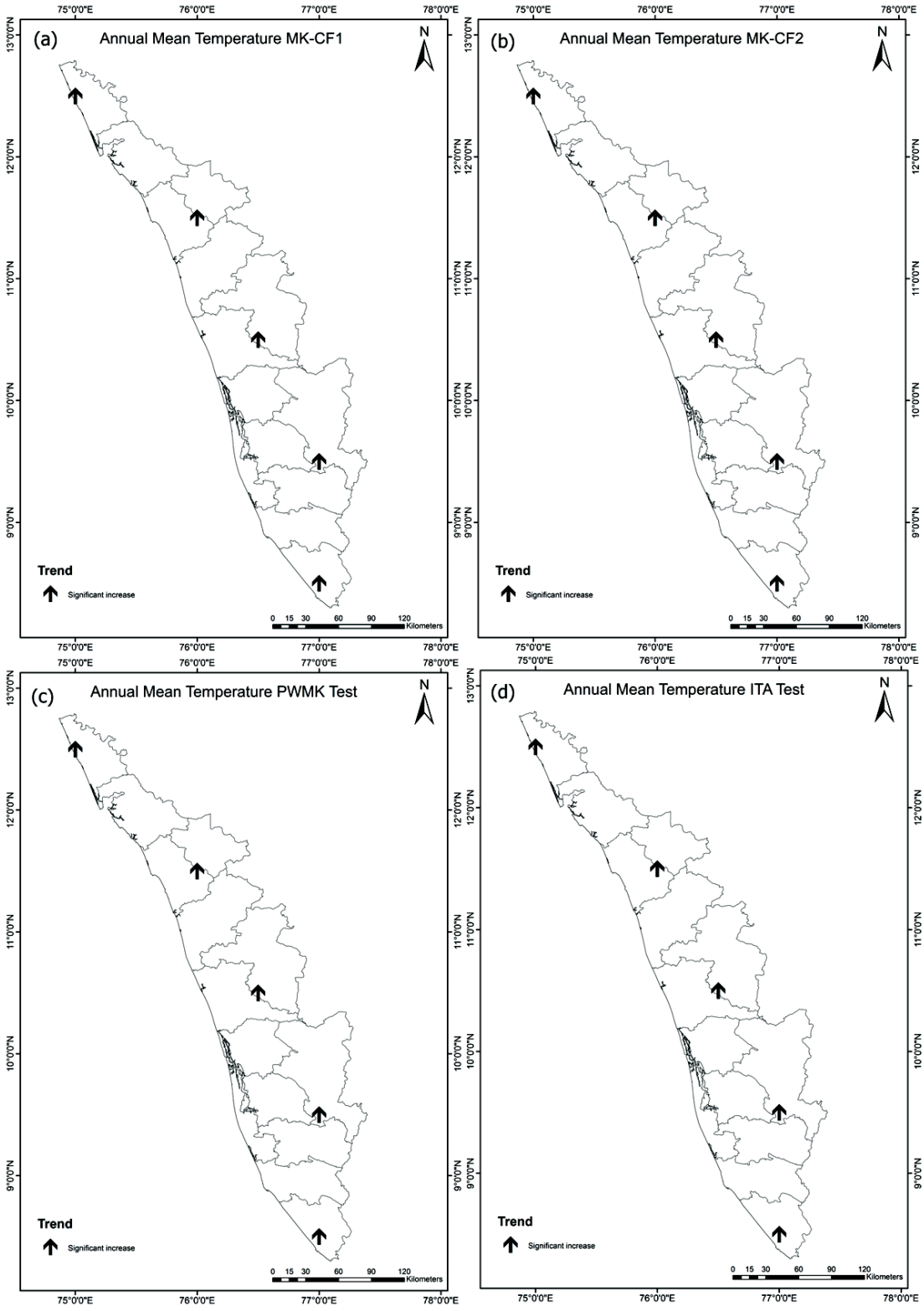

Figure 5.29. Results of (a) MK-CF1 (b) MK-CF2 (c) MK-PW (d) ITA tests of annual mean temperature

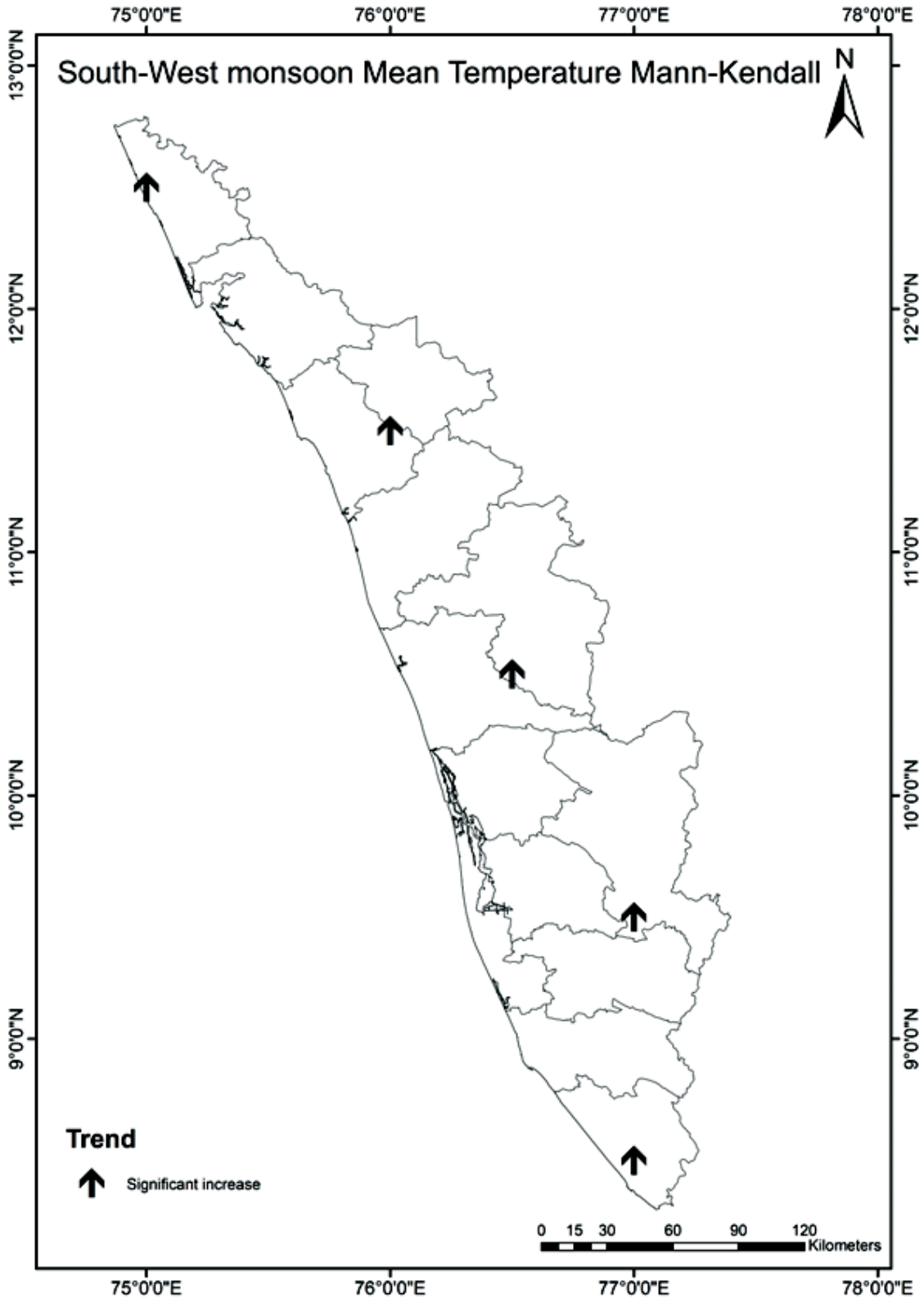

Figure 5.30. Mann-Kendall test results of south-west monsoon mean temperature

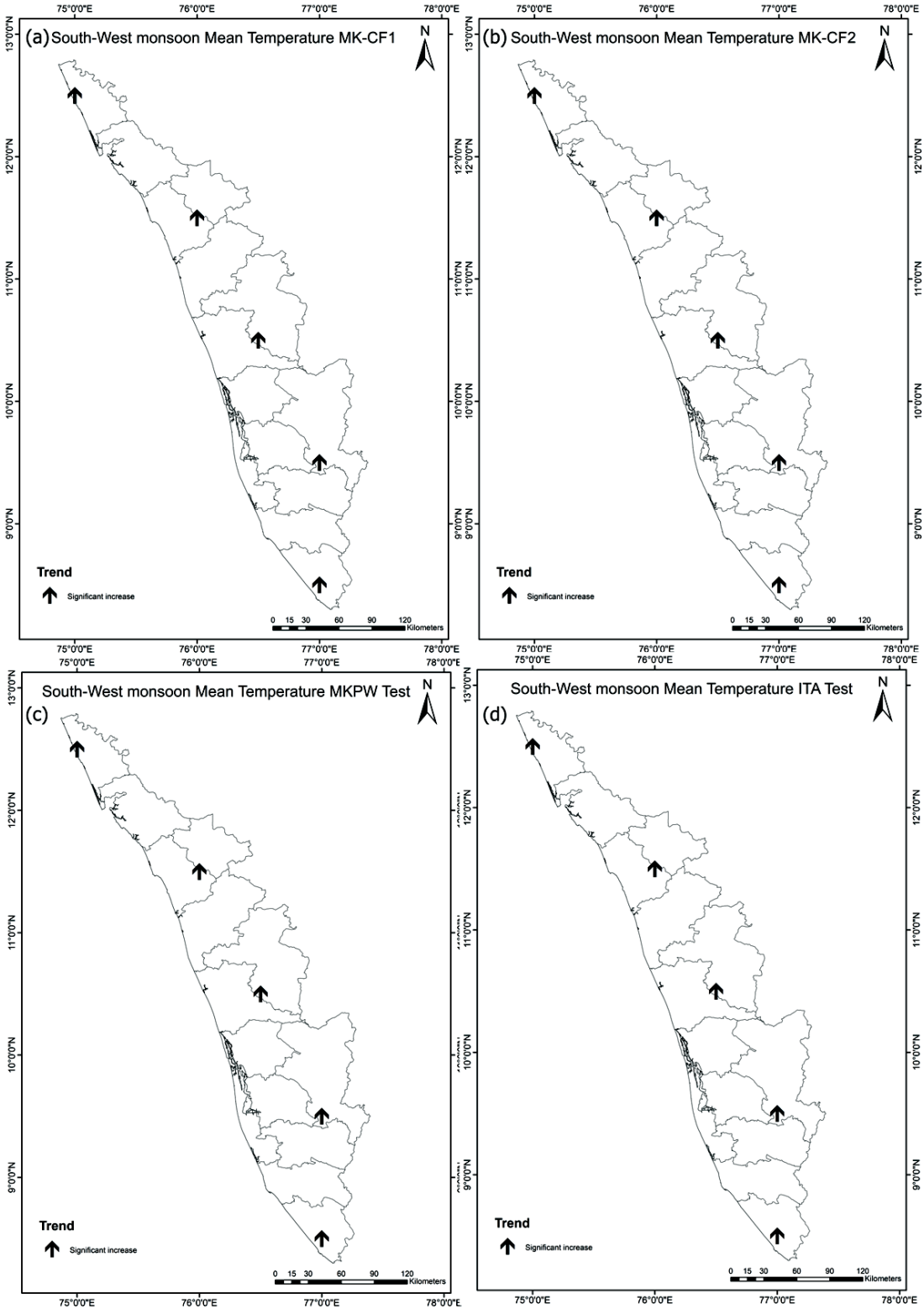

Figure 5.31. Results of (a) MK-CF1 (b) MK-CF2 (c) MK-PW (d) ITA tests of South-west monsoon mean temperature

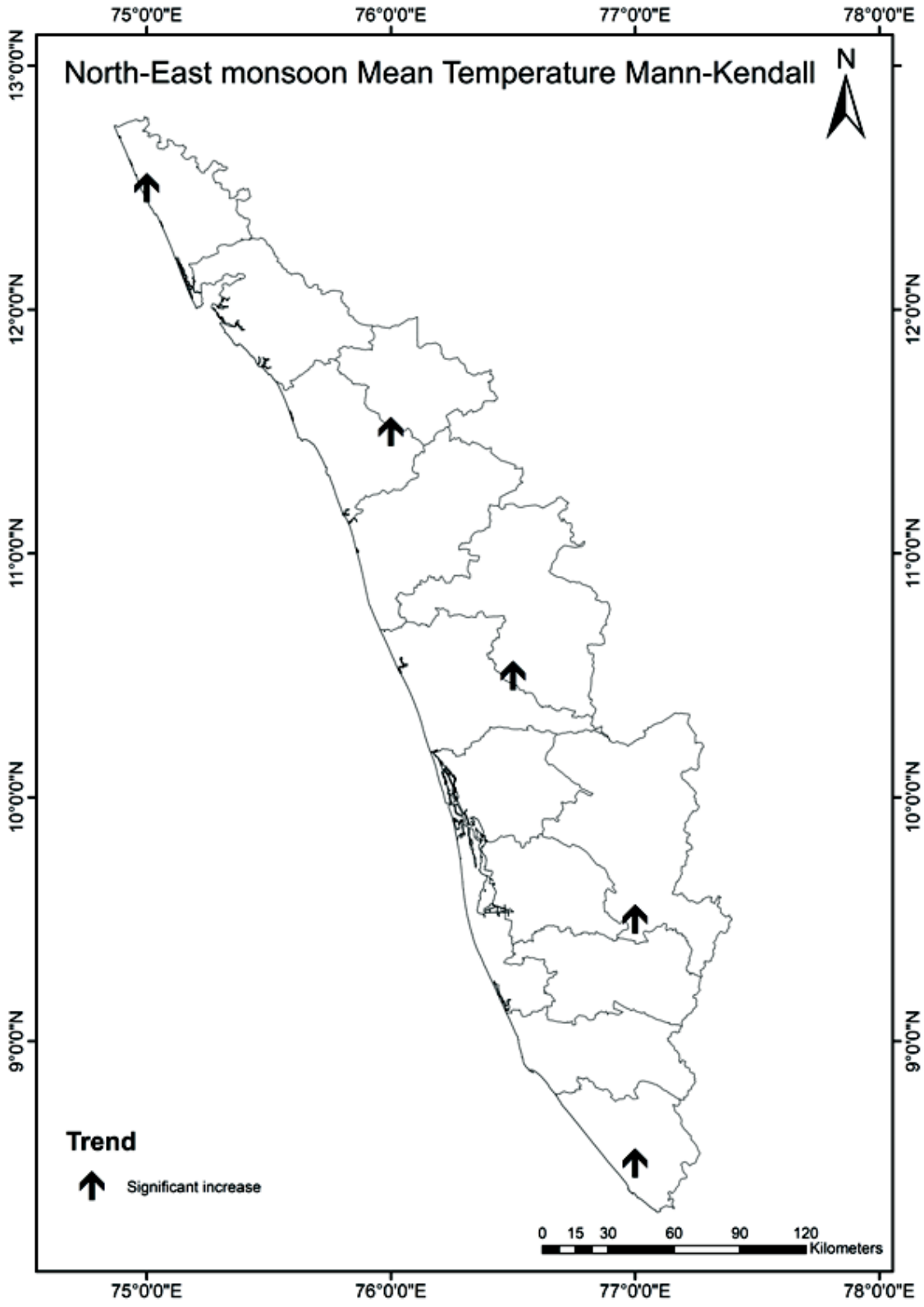

Figure 5.32. Mann-Kendall test results of north-east mean temperature

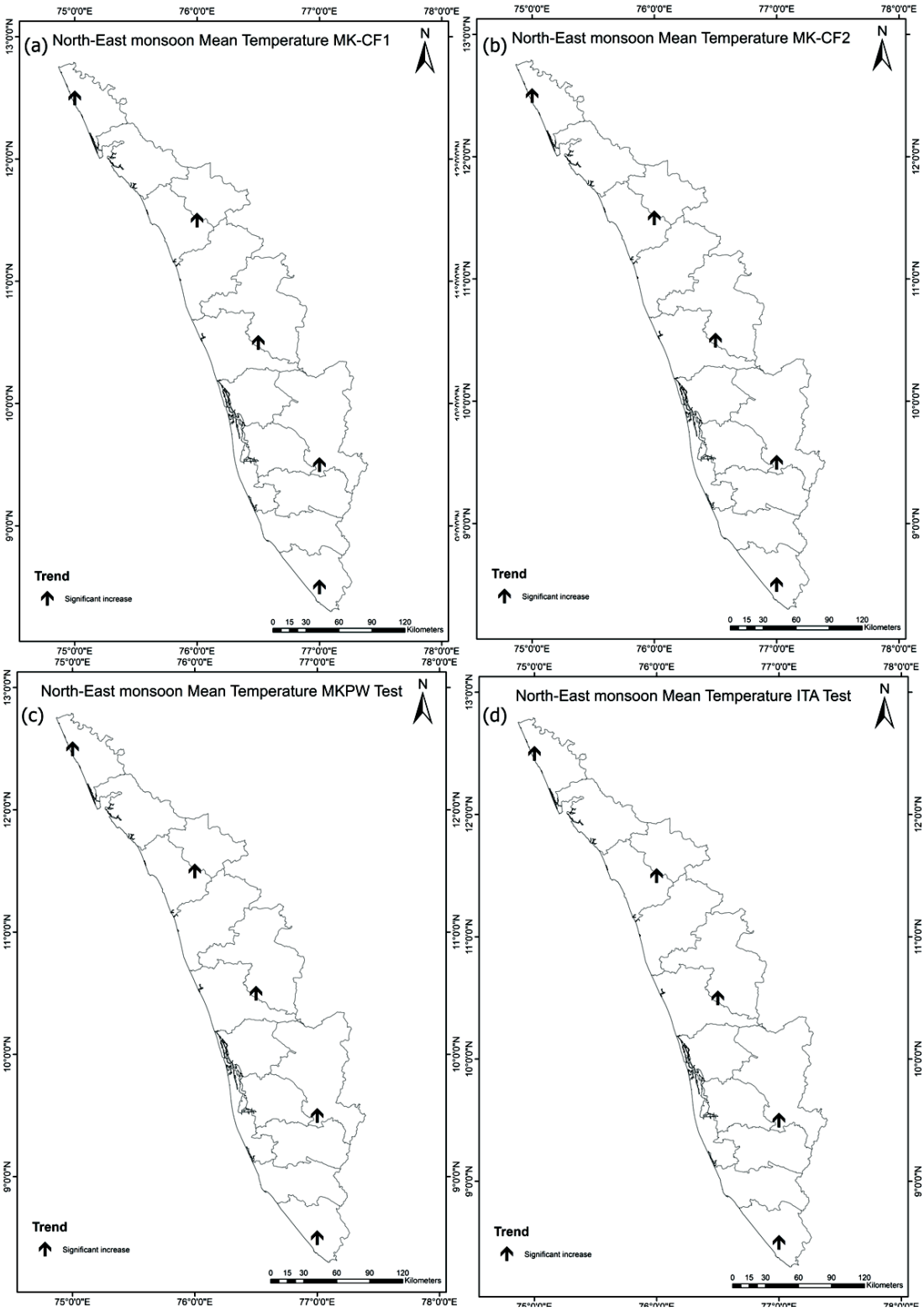

Figure 5.33. Results of (a) MK-CF1 (b) MK-CF2 (c) MK-PW (d) ITA tests of north-east mean temperature

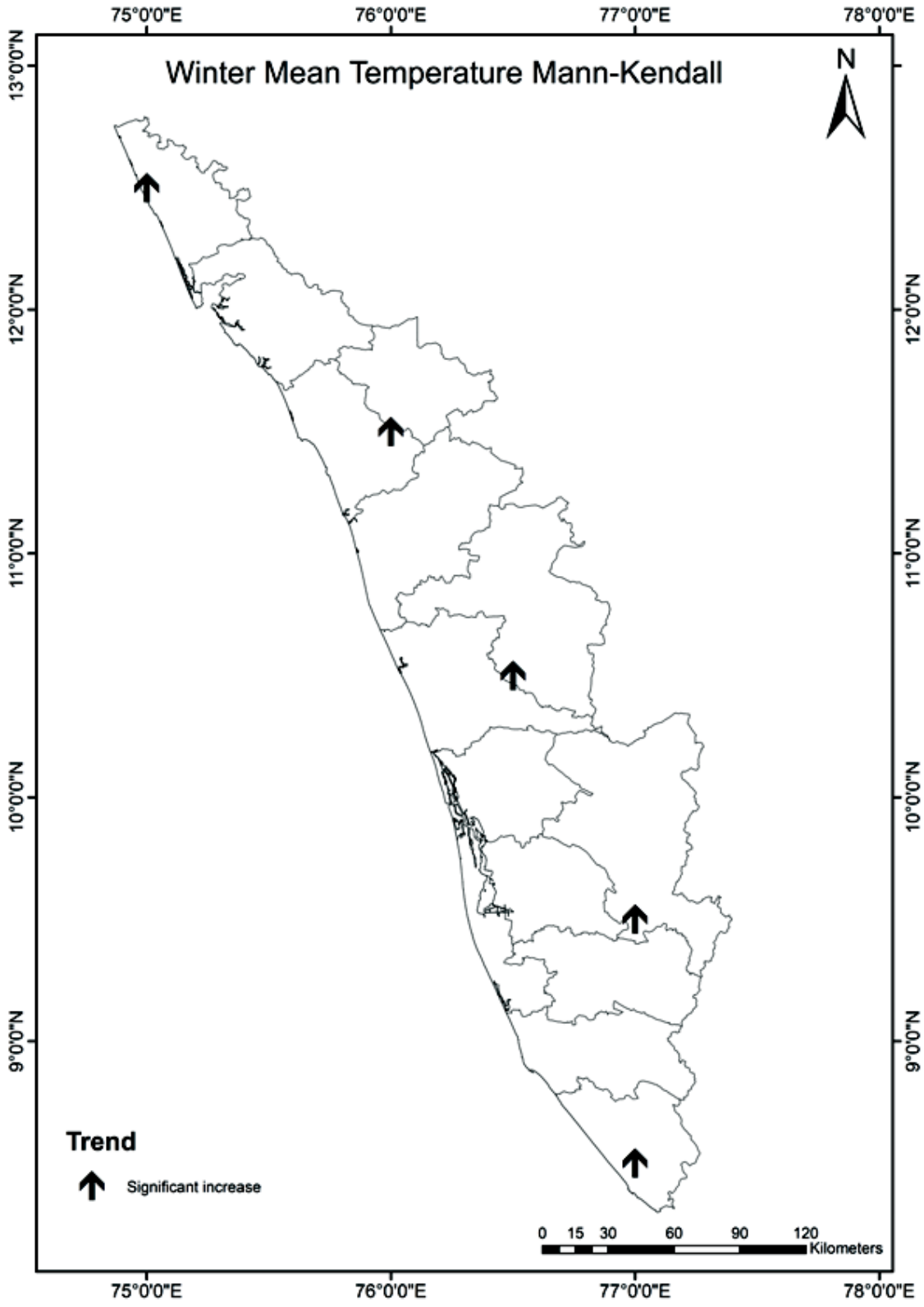

Figure 5.34. Mann-Kendall test results of winter mean temperature

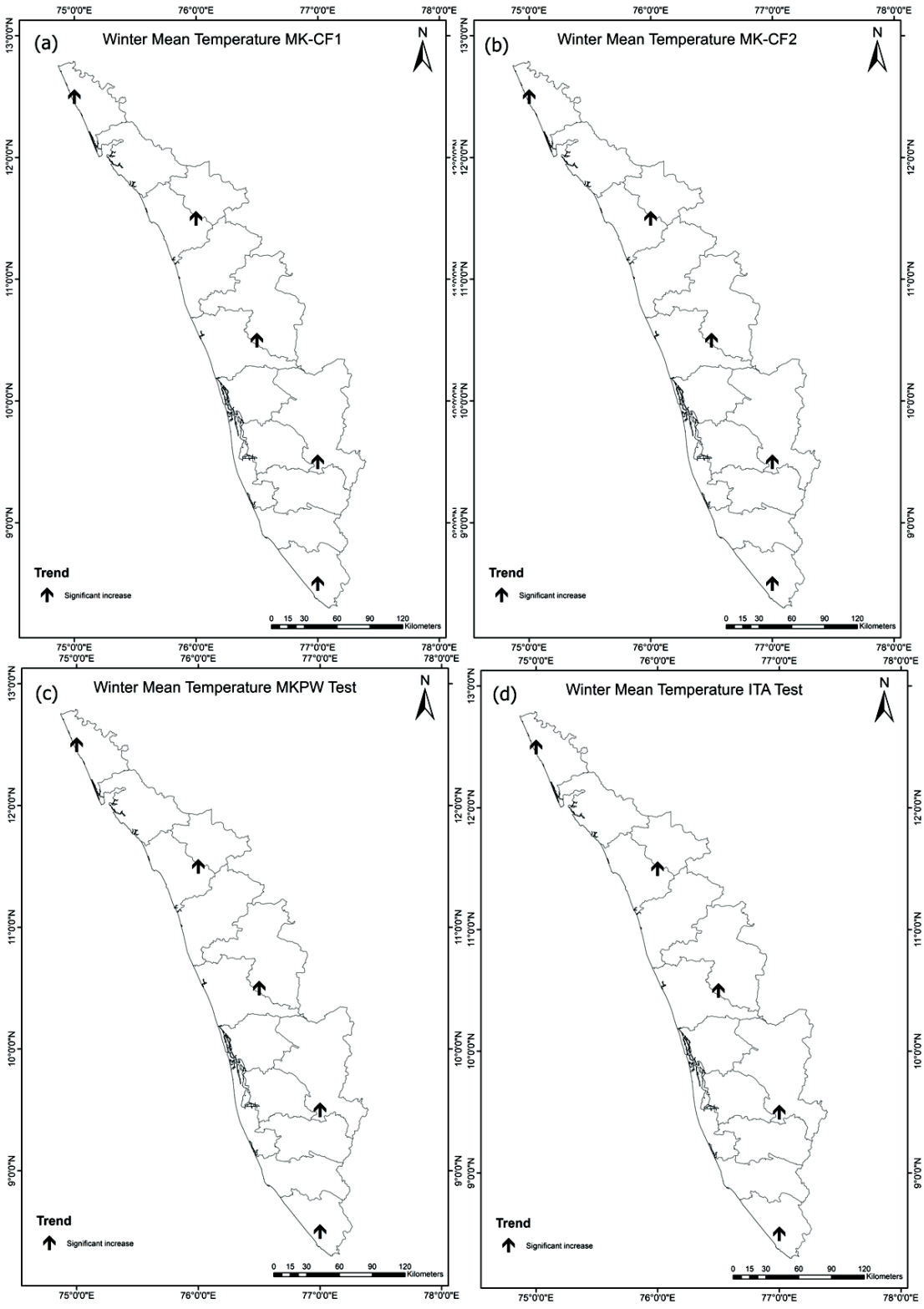

Figure 5.35. Results of (a) MK-CF1 (b) MK-CF2 (c) MK-PW (d) ITA tests of winter mean temperature

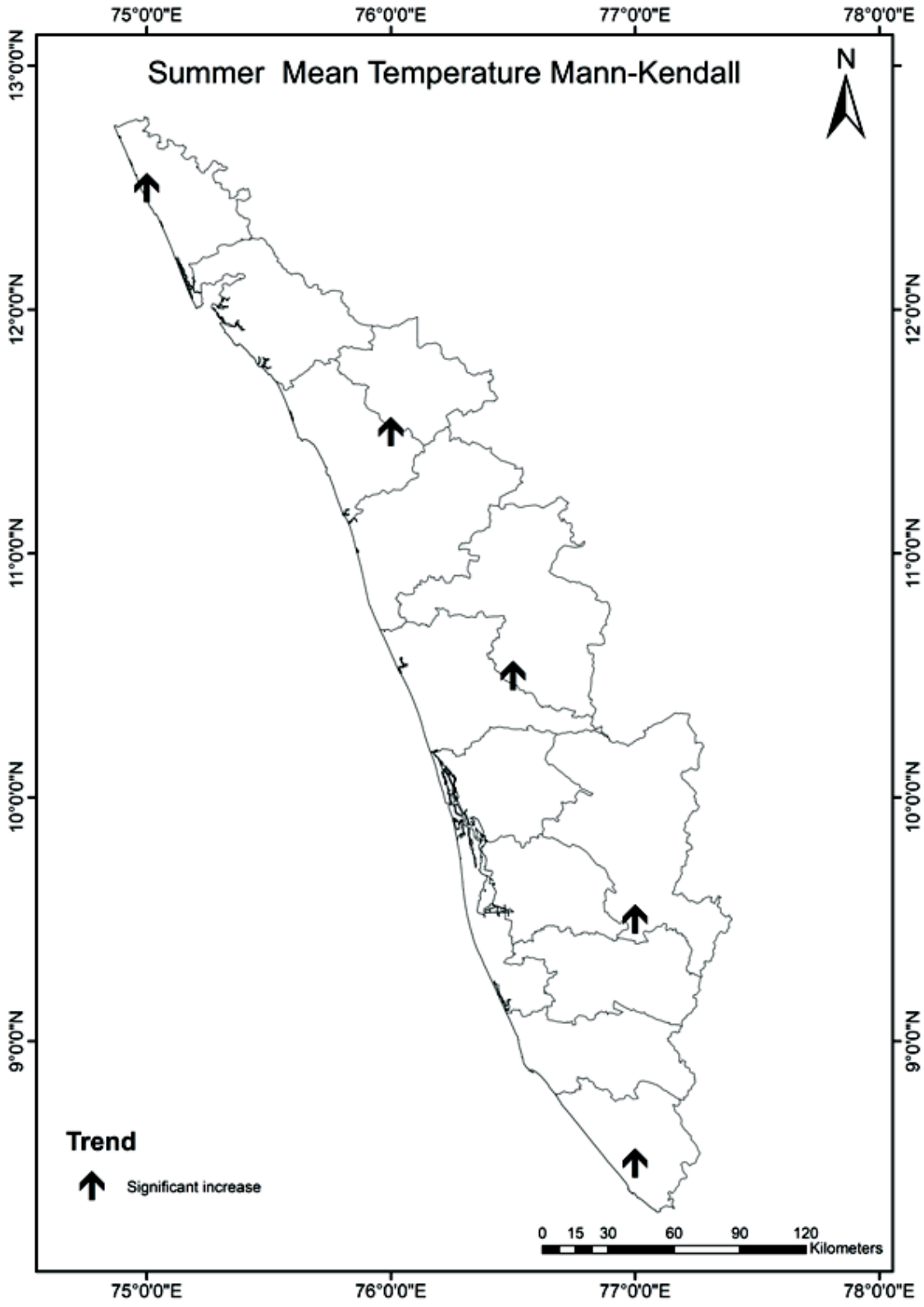

Figure 5.36. Mann-Kendall test results of summer mean temperature

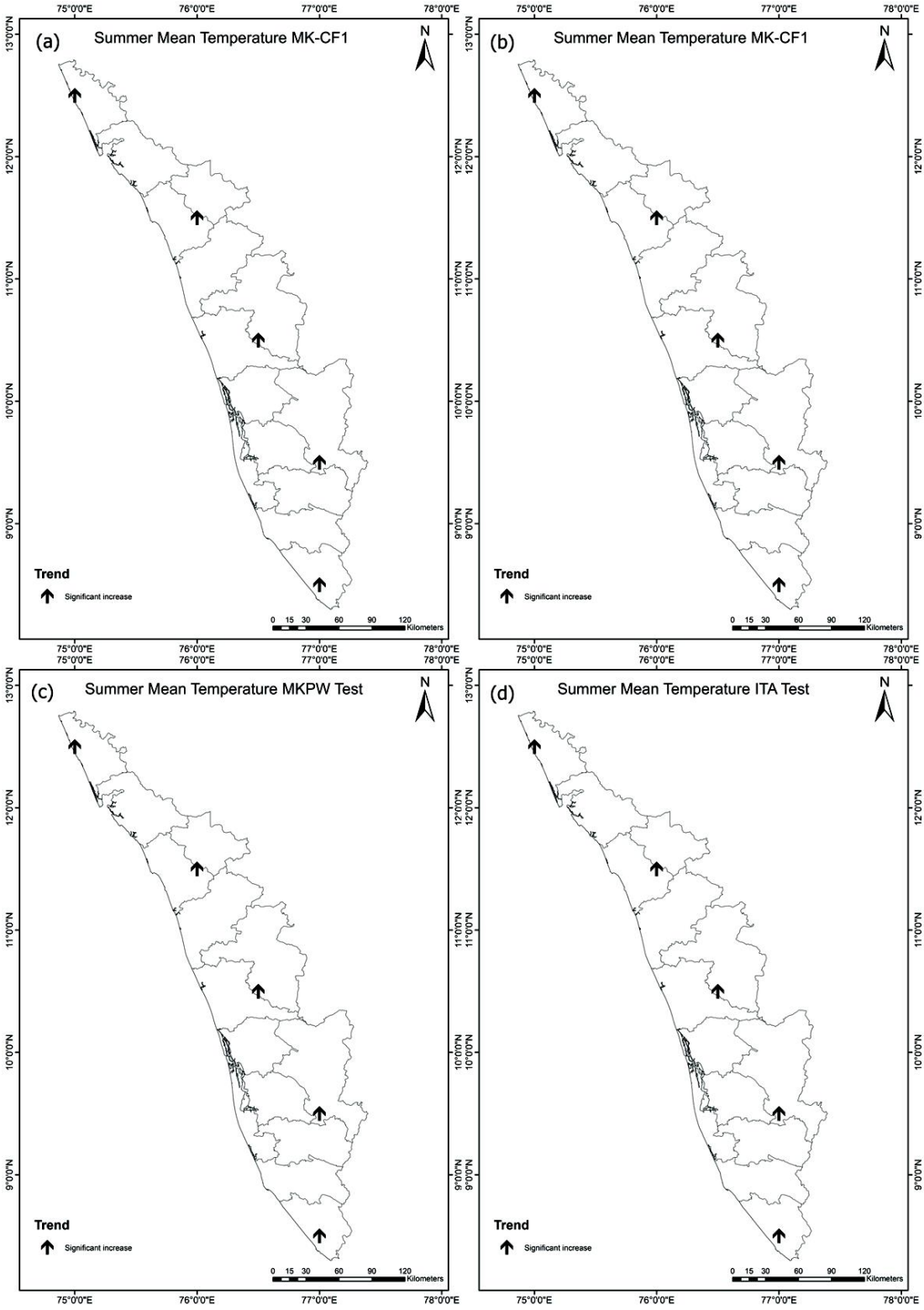

Figure 5.37. Results of (a) MK-CF1 (b) MK-CF2 (c) MK-PW (d) ITA tests of summer mean temperature

Likewise, in the case of annual and four seasons, the Mann-Kendall test, MK-CF1, PWMK,

MK-CF2, and ITA tests evidenced the statistically significant increasing trends in the maximum temperature series of all 5 (100%) grids at α=5% (Figure 5.38 and Figure 5.39).

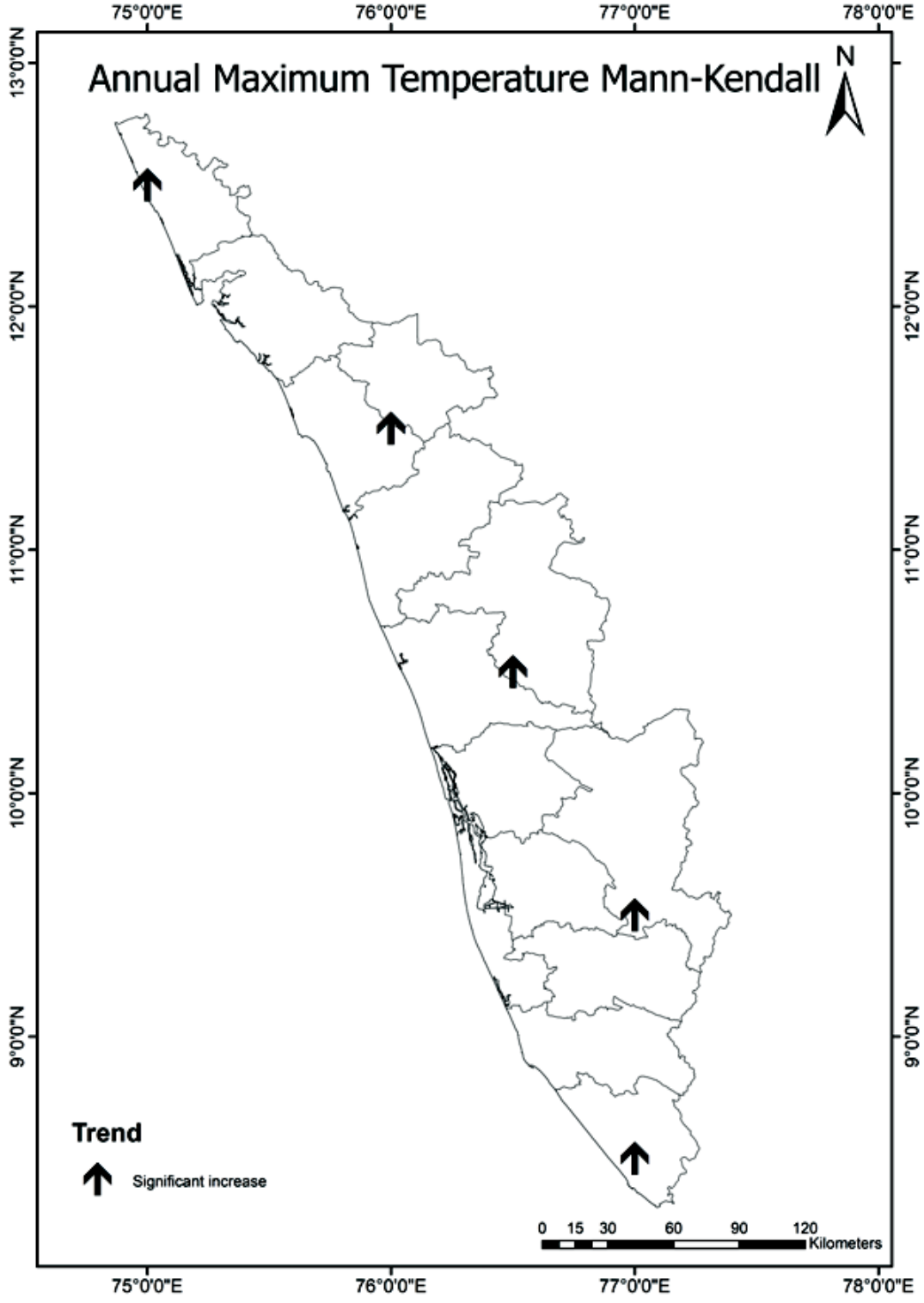

Figure 5.38. Mann-Kendall test results of annual maximum temperature

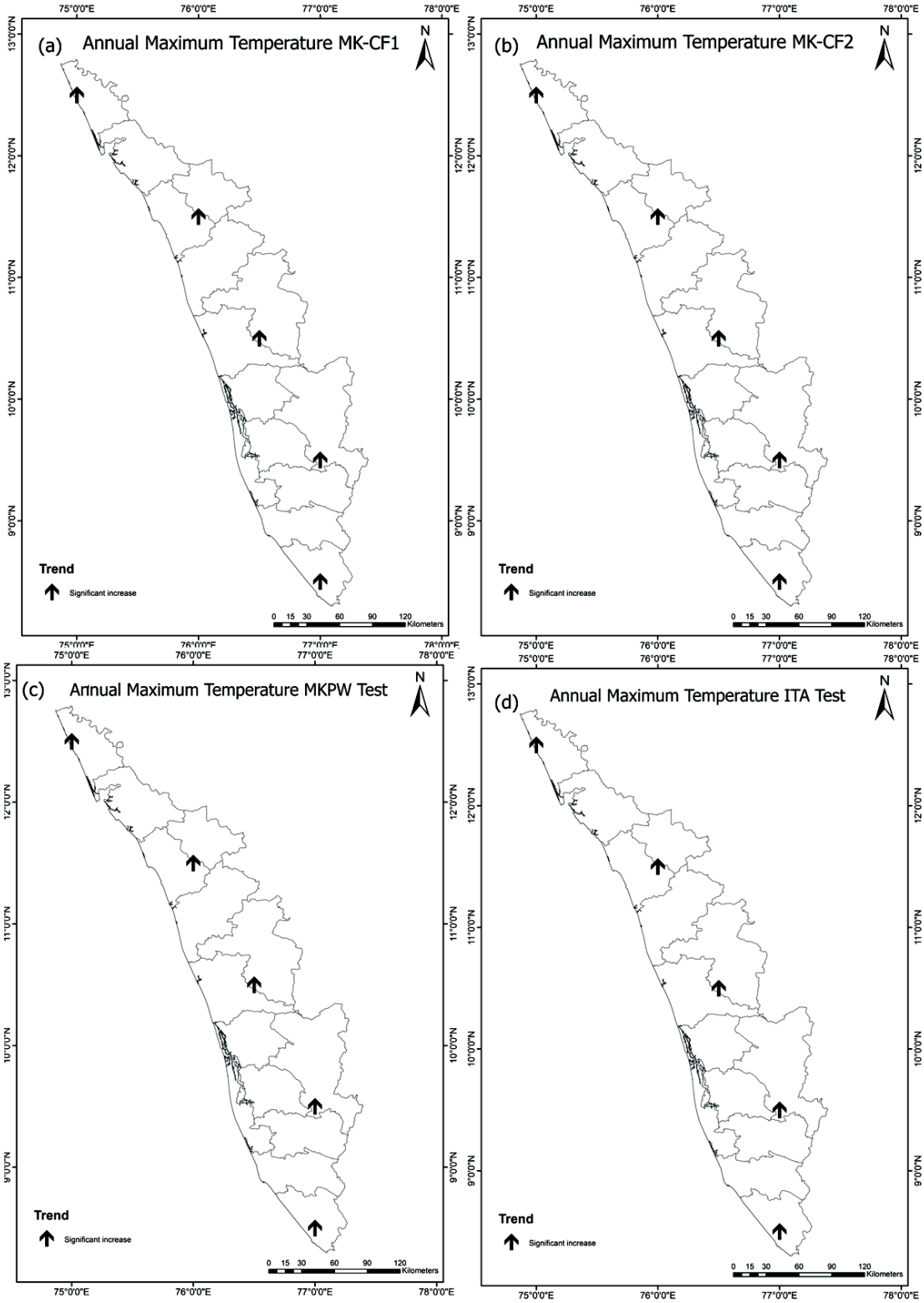

Figure 5.39. Results of (a) MK-CF1 (b) MK-CF2 (c) MK-PW (d) ITA tests of annual maximum temperature

It is seen that the minimum temperature in annual, south-west monsoon, and north-east monsoon was found to be significantly increased for all grids by the Mann-Kendall test, MK-CF1, PWMK, MK-CF2, and ITA tests at α=5% (Figure 5.40 and figure 5.41).

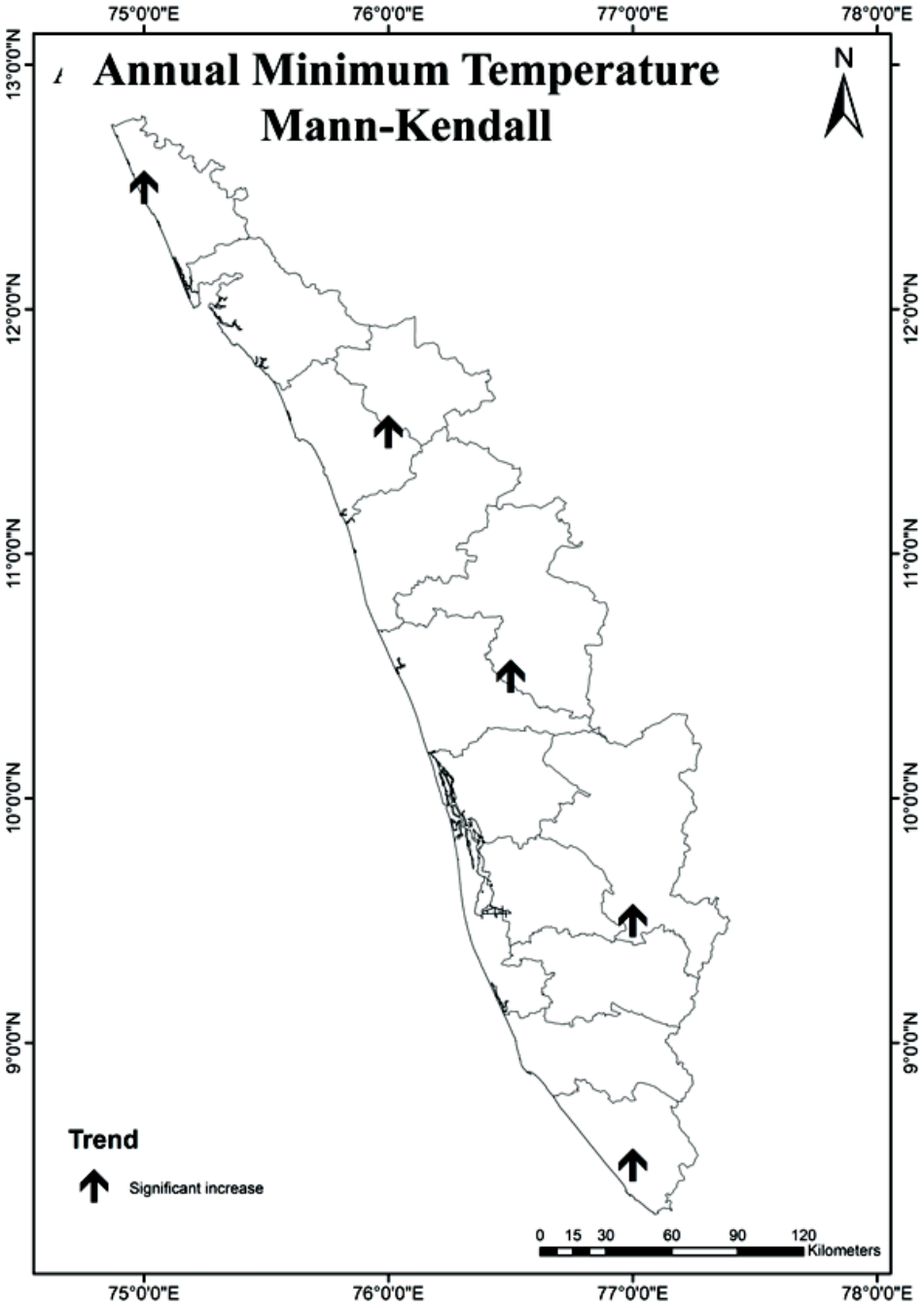

Figure 5.40. Mann-Kendall test results of annual minimum temperature

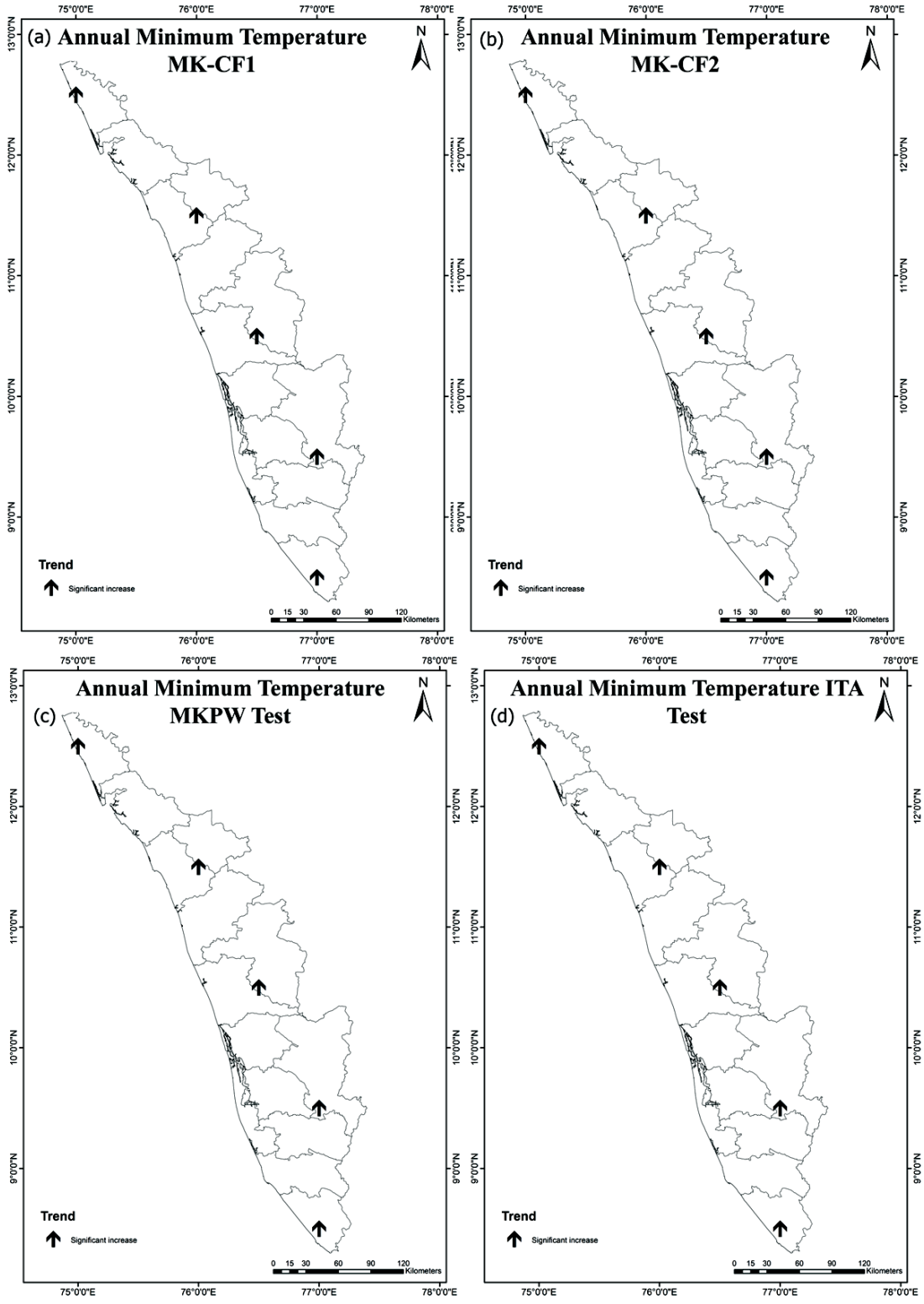

Figure 5.41 Results of (a) MK-CF1 (b) MK-CF2 (c) MK-PW (d) ITA tests of annual minimum temperature

The Mann-Kendall test, MK-CF2, and ITA tests identified a statistically significant increasing trend in winter season minimum temperature at 4 (80%) grids, whereas PWMK only discovered a significant trend at 2 (40%) grids**.** Likewise, the MK-CF1 unveiled a statistically significant increasing trend at one grid (5% significance level**).** The summer season minimum temperature is significantly increasing at all five grids (100%), as revealed by MK-CF2 and ITA tests at α=5%. On the contrary, MK-CF1 and PWMK resulted in statistically significant increasing trends for 2 (40%) grids, whereas the Mann-Kendall test discovered a significant trend at three grids at a similar significance level.

5.8 MAGNITUDE OF THE TEMPERATURE TREND

The magnitude of increasing trends in annual and seasonal time series of mean, maximum, and minimum temperatures was quantified by Sen's slope test and summarized for five grids in Table 5.4. It is seen from the table that annual as well as seasonal mean temperature is increasing at a rate ranging from 0.1 to 0.2 °C/decade. Likewise, the maximum temperature in the annual, south-west monsoon, north-east monsoon, winter, and summer seasons is increasing at a rate of 0.2 °C/decade.

Table 5.4. Trend magnitude in temperature at five grid points (1951-2019)

Season	**Temperature/Grids**	1	2	3	4	5
Annual	Mean	0.01	0.01	0.01	0.01	0.01
	max	0.02	0.02	0.02	0.02	0.02
	min	0.01	0.01	0.01	0.01	0.01
South-west monsoon	Mean	0.01	0.02	0.01	0.02	0.02
	max	0.02	0.02	0.02	0.02	0.02
	min	0.01	0.01	0.01	0.01	0.01
North-east monsoon	Mean	0.02	0.01	0.01	0.01	0.01
	max	0.02	0.02	0.02	0.02	0.02
	min	0.01	0.01	0.01	0.01	0.01
Winter	Mean	0.01	0.01	0.01	0.01	0.01
	max	0.02	0.02	0.02	0.02	0.02
	min	0.01	0.01	0.01	0.01	0.01

Season	**Temperature/Grids**	1	2	3	4	5
	Mean	0.01	0.01	0.01	0.01	0.01
	max	0.02	0.02	0.02	0.02	0.02
Summer	min	0.01	0.01	0.01	0.01	0.01

Similarly, the minimum temperature magnitude is increasing in the annual, south-west monsoon, north-east monsoon, winter, and summer seasons at a magnitude of 0.1 °C/ decade. However, the winter and summer minimum temperature at 1 of 5 grid points has no change. This study revealed a rapid increase in maximum and mean temperatures which indicates a severe concern that possibly impacts the paddy cultivation of the state, which is the backbone of Kerala's economy. Studies pointed out that a warming climate causes an increasing tendency of extreme precipitation indices as well as the quantum of precipitation, implying an increase in the frequency of high-intensity rainfall events (Mukherjee et al. 2018; Rao et al. 2020; Wang et al. 2020). The results of the current study can be correlated with the recent Kerala floods.

5.9 RAINFALL CONCENTRATION AND PATTERN CHANGE

The annual scale of precipitation concentration index (PCI) calculated for 5 clusters in the study area varies from a minimum of 13 (moderate concentration) in cluster 4 to a maximum of 28 (high concentration) in cluster 1, which indicates that PCI distribution is not uniform over the state **(**Figure 5.42**).** Generally, if the PCI value is less than 10, it represents the uniform rainfall distribution in all months. In contrast, if the PCI values vary from 11 to 20, it indicates the seasonality of rainfall distribution, and values above 20 indicate substantial irregularity in rainfall distribution (De Luis et al. 2011; Thomas and Prasannakumar 2016; Zhang et al. 2019). It is noted that, in general, higher values of PCI are observed in cluster 1, 2, and 5, while lower values are detected in cluster 3 and cluster 4. A significant variation in PCI values is noticed in clusters 1, 2, and 5**.** A clear gradient of change in the PCI values as moving from southern Kerala to northern Kerala (Figure 5.42) is noted. Mean PCI (21-23) values in the northern parts of the state are higher than in the southern and central regions (13.7 to 20). The high value of PCI in the northern parts of the state indicates that the majority of the annual rainfall occurs in a few months of the year, and it will lead to an increase in dry days, leaving the area

vulnerable to water scarcity in non-rainy seasons. Interestingly, there was an unusual rise in PCI values in all clusters after 2016**.**

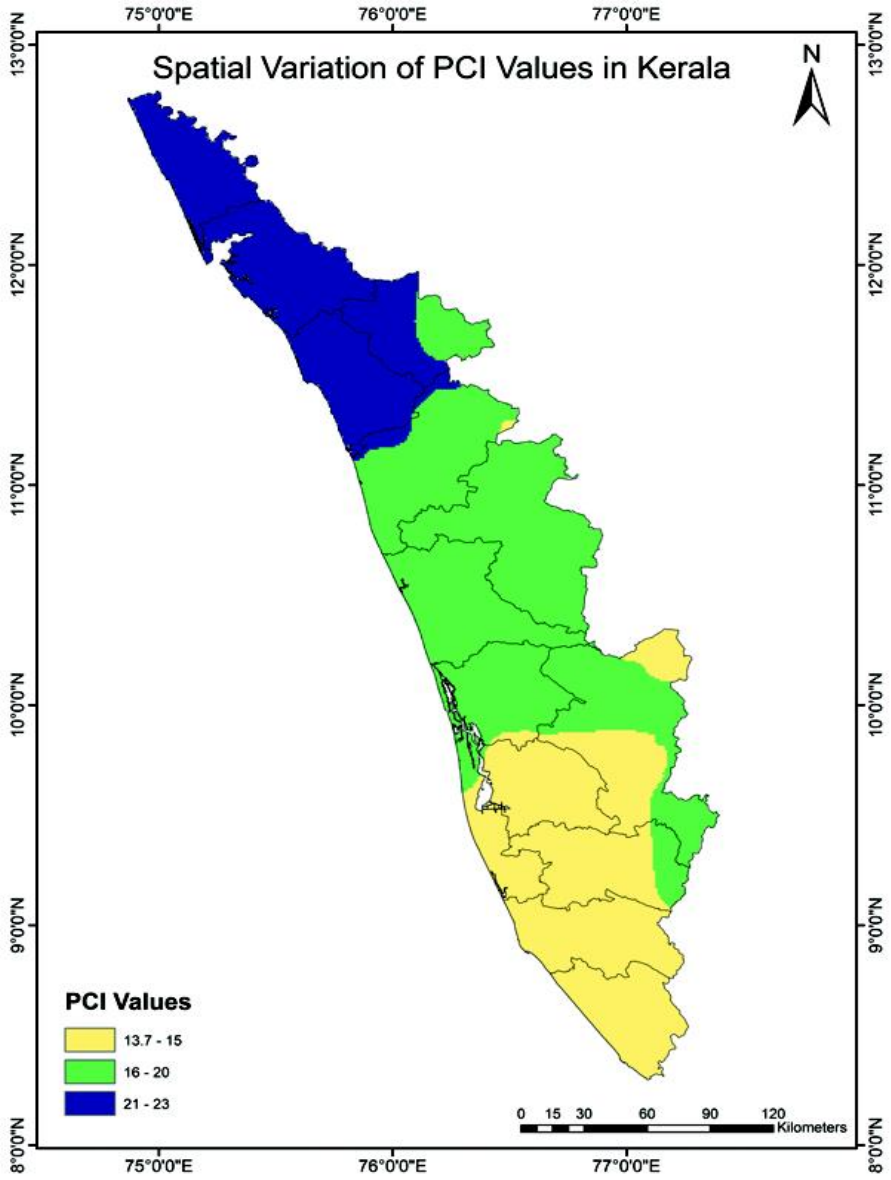

Figure 5.42. Spatial variation of mean PCI values

The PCI values were calculated seasonal-wise to know the pattern of seasonal rainfall distribution in these periods (Figure 5.43). On the seasonal scale, the south-west monsoon shows the least variability compared to other seasons. In all 5 clusters, the PCI value was less than 12 during the study period (8.3 to 12). This indicates that rainfall concentration is uniform during the south-west monsoon in all 5 clusters. But

PCI values of north-east monsoon, winter season, and summer vary from 8.3 to 25 in all clusters. This gives an insight into the highly irregular rainfall pattern during the season.

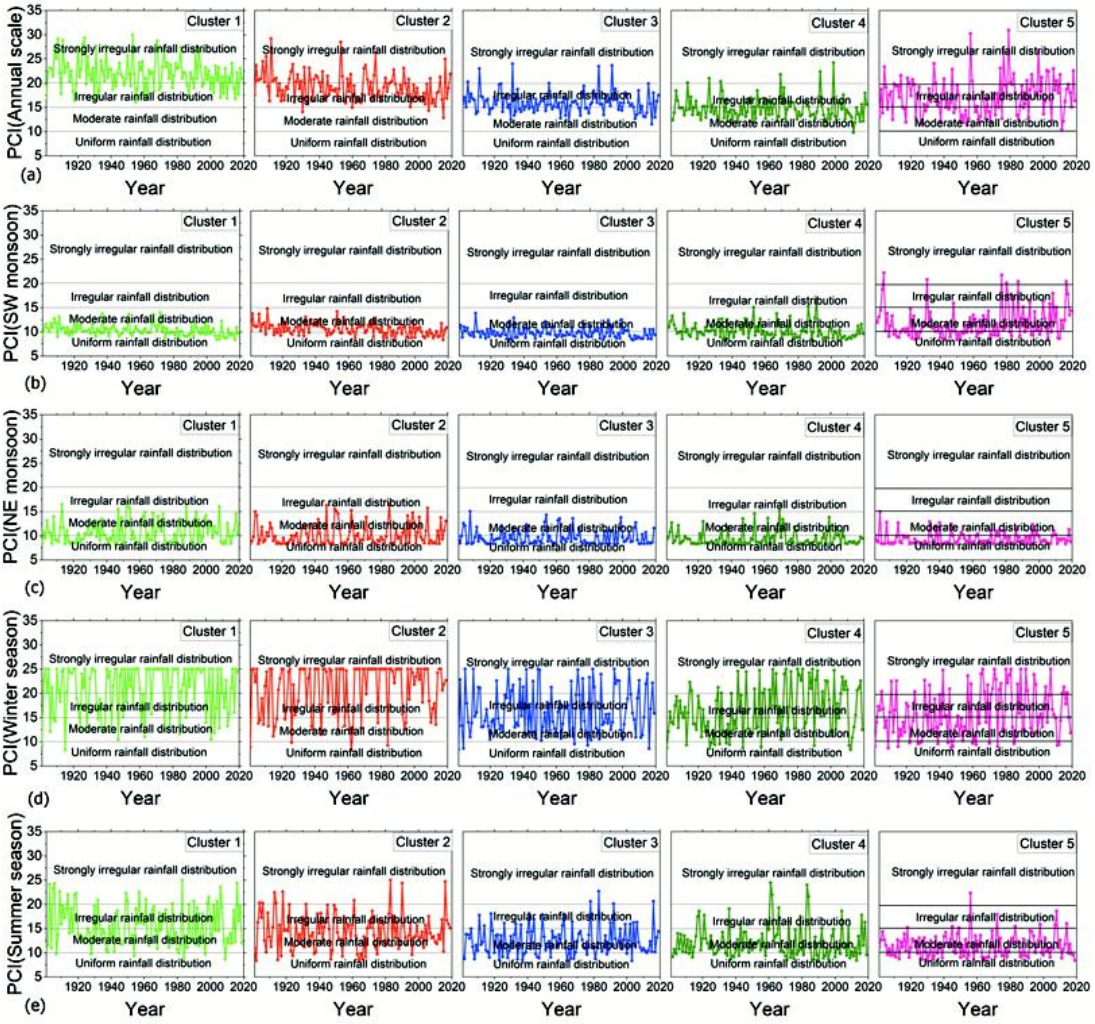

Figure 5.43 Temporal variation of precipitation concentration index (PCI) of (a) annual rainfall (b) south-west monsoon. (c) north-east monsoon (d) winter (e) summer

It is noted that in cluster 1 and cluster 2, very strong irregularity in rainfall distribution was detected in 46 and 85 years, respectively, mostly between 1910-1930 and 1985-2000. The irregularity in rainfall concentration is associated with a high contribution of the south-west monsoon rainfall (Thomas and Prasannakumar 2016). In the case of cluster 1, years show very strong irregularity in rainfall concentration, and it has

received more than 75% of the annual rainfall during the south-west monsoon (mean=70.6%, range=24 to 86%). In cluster 1, none of the PCI values falls below 15 (moderate precipitation concentration) during the study period. But among the study time, 85 years in cluster 2, which showed strong irregularity, has also received nearly 83% annual rainfall during south-west monsoon (mean=80%, range=45.6 to 93%). It is noted that in both clusters, more than 70% of the annual rainfall is received during the south-west monsoon, and it indicates the concentration of the majority of the annual rainfall falls in a few months of the year. The rainy season in cluster 1 and 2 are very short, and heavy rainfall is confined in the quarter part of the year. This indicates that the economy of Kerala largely depends upon the monsoon-driven climate. But as we go to cluster 3 and 4, an extreme irregularity was identified only in 5 and 6 years, respectively. In cluster 3, the contribution of the south-west monsoon to the annual rainfall budget is in the range of 70 to 85% during the years where the PCI value is more than 20*(*mean=65%, range=26 to 85%) whereas, in *t*he case of cluster 4, a substantial irregularity was found only in 6 years in which the contribution of the south-west monsoon was more than 60 % (mean =50%). The contribution of the north-east monsoon to annual rainfall in grids of cluster 5 is more than 45%. 25 years show strong irregular rainfall in cluster 5, mostly between 1915-1945 and 1975-2018. It is worth mentioning that in these 25 years, the contribution of the north-east monsoon was more than 55%. This could be due to the absence of the Western Ghats barrier against the north-easterly winds.

The degree of variability in monthly rainfall can also be estimated using the seasonality index. Figure 5.44 presents the spatial variation of SI values over Kerala from 1901 to 2019, which depicts the substantial variation in rainfall distribution throughout the year. The value of SI ranges from a minimum of 0.45 in the southern part of Kerala (short dry seasons) to a maximum of 0.95 in the northern parts of the state (long dry season). The lower value of the SI indicates a better distribution of rainfall. These findings support the spatial variation of PCI over the state. The seasonality of rainfall is vital in deciding the calendar of agricultural activities. Calculating the seasonality of rainfall is necessary as it directly impacts extreme events like floods and drought. In the southern

part of the state, the SI value ranges from 0.4 to 0.59, which indicates seasonal rainfall with short dry seasons.

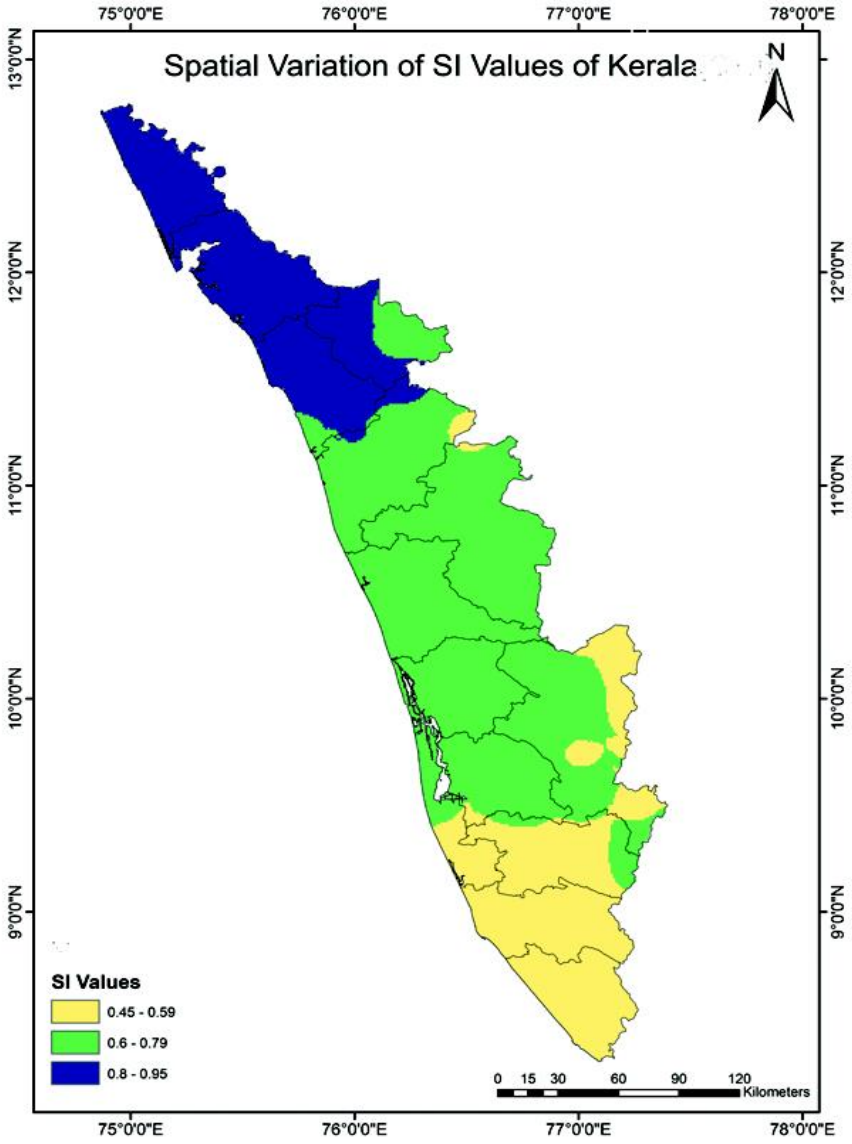

Figure 5.44 Spatial variation of SI values over Kerala

In the case of southern parts of Kerala, the contribution of the south-west monsoon rainfall to the annual rainfall budget is near 50 to 55% only. So the north-east monsoon and summer rainfall significantly influence the southern part of the state. In the central part of the state, the value ranges from 0.6 to 0.79, indicating that rainfall distribution is seasonal, where the rainfall contribution from the south-west monsoon is in the range of 60 to 70%. Moreover, the SI values of the northern part of Kerala vary from 0.8 to

0.95, reflecting the rainfall distribution in these areas is seasonal, with long and drier seasons. This is mainly because the south-west monsoon contributes more than 75% of annual rainfall, and the rest of the seasons have minimal impact on the northern part of the state. This explains the increasing rate of dry days in other seasons. These findings support the spatial variation of PCI over the state.

5.10 LAND USE LAND COVER MAPPING

The classified LULC maps of the Kerala state showing the distribution of five LULC classes (urban, water, forest, vegetation, and barren land) using random forest algorithm and CART for the years 1990, 2000, 2013, and 2020 are produced. One image was taken from each decade to understand the decadal transformations in land cover. However, Landsat image 2013 (Landsat 8 series) was used instead of Landsat 7 image series to avoid stripping in the imagery. The complex topography of the study area made it very difficult to differentiate various land cover classes. The identified classes for this study were (1) urban, (2) water, (3) vegetation, (4) forest, and (5) barren land. A single index with a fixed threshold value can determine the change of one particular land class. The indices used in the study aid in accurate image classification using various methods.

NDVI measures the amount and health of vegetation cover in a given area. NDVI values range from -1 to +1, with higher values indicating healthier and more abundant vegetation. When the NDVI value is -1, it indicates no vegetation or water bodies in the area. Areas with negative values could also be shadows or artificial surfaces that do not reflect much light. When the NDVI value is 0, it indicates bare soil or rock surfaces with little to no vegetation cover. This could also be the case for areas with clouds or snow cover, which can affect the reflectance values of the bands used to calculate NDVI. The NDVI value implies dense and healthy vegetation cover between 0 and 1. This could include tropical rainforests, mature forests, or well-managed agricultural fields. It is important to note that NDVI values vary depending on the type of vegetation, the time of year, and the environmental conditions of the studied area. Even though Kerala state has undergone rapid urbanization, which led to the loss of vegetation in the last three decades, the NDVI (Figure 5.45) values remain unchanged.

The NDVI value ranges from -0.62 to 0.82 during the 1991 year. Subsequently, in 2000, 2013, and 2020 the value varied from -0.42 to 0.86, -0.39 to 0.84, and -0.46 to 0.85, respectively. The slight changes in the values of NDVI after 2013 point out the clearing of semi-dense vegetation for the urban area expansion. It is also noted that there is a reduction in grasslands and croplands in the state, whereas NDVI values were increasing in the Western Ghats region. The decrease of NDVI values in Kerala over human habited areas shows the declining rate of agriculture in the state. It is evident from the figures that vegetation cover in Kerala was hugely destroyed from 2013 to 2020 for urban development. However, the overall increase in the NDVI values suggests that the density of vegetation and biomass is increasing in certain areas like the Western Ghats Forest regions.

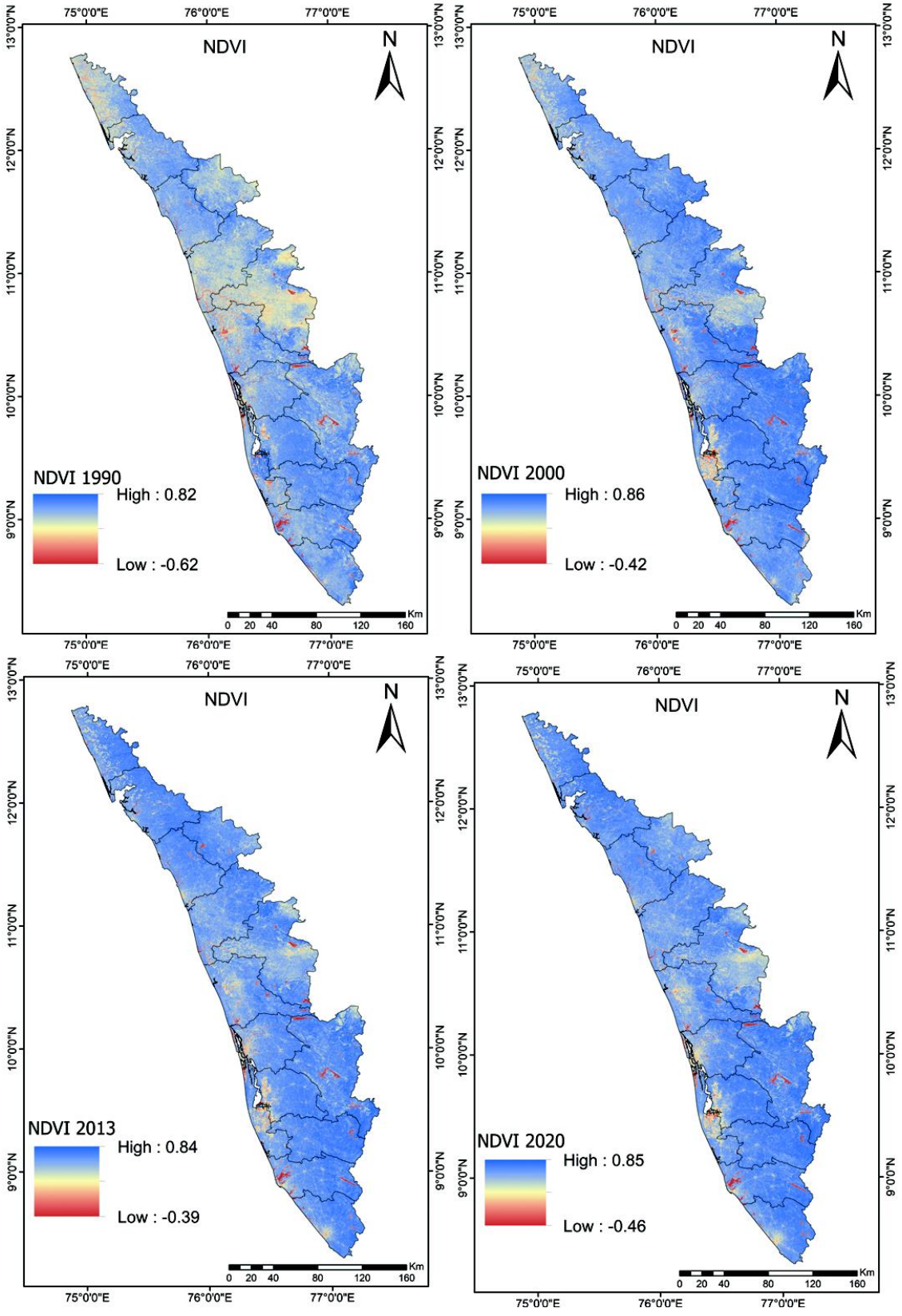

Figure 5.45. NDVI maps of Kerala from 1990 to 2020

NDBI is a remote sensing index used to detect and map the level of built-up in a given region. NDBI values range from -1 to +1, with higher values indicating a higher probability of built-up areas. When the NDBI value is -1, it means no built-up areas or water bodies in the area. Areas with negative values could also be shadows or artificial surfaces that do not reflect much light. When the NDBI value is 0, it represents a mix of built-up and non-built-up areas. This could be the case for areas with sparse or low-rise buildings or a combination of urban and rural land cover. When the NDBI value ranges between 0 and 1, it shows an increased probability of built-up areas. This could include urban areas with medium- to high-density buildings and industrial or commercial areas. Results showed that the NDBI (Figure 5.46) value for 2020 ranges from -0.79 to 0.59. The lower and upper limits of NDBI values increased from 1990 to 2020. This signals the level of urbanization happening in Kerala. Results showed that the till 2013, the rate of urbanization was slow, and most of the areas were moderately developed, whereas 2020 NDBI results pointed out the sudden rise in NDBI values in the state, indicating high-density built-up regions.

Bare Soil Index (BSI) is a remote sensing index that detects and maps areas of bare soil or exposed ground. The BSI formula uses the Red, Blue, middle infrared band (MIR), and near-infrared (NIR) electromagnetic spectrum bands, typically captured by remote sensing platforms such as satellites or drones. The BSI scale ranges from -1 to 1, with values closer to 1 suggesting a higher likelihood of exposed ground or bare soil. When the BSI value is -1, it signals no bare soil or exposed land in the area. Areas with negative values could also be shadows or artificial surfaces that do not reflect much light. When the BSI value is 0, it points to a mix of vegetated and non-vegetated areas. This could be the case for areas with sparse vegetation or a combination of land cover types. When the BSI value is between 0 and 1, this range indicates an increased probability of bare soil or exposed ground. This could include areas with low vegetation cover and areas where vegetation has been removed or disturbed, such as agricultural fields or construction sites. The BSI value (Figure 5.47) ranges from -0.72 to 0.50 during 1991. Subsequently, in 2000, 2013, and 2020, the value varied from -0.59 to 0.20, -0.64 to 0.44, and -0.62 to 0.43, respectively. A slight increase in the BSI values indicates an increase in the barren land or exposed areas.

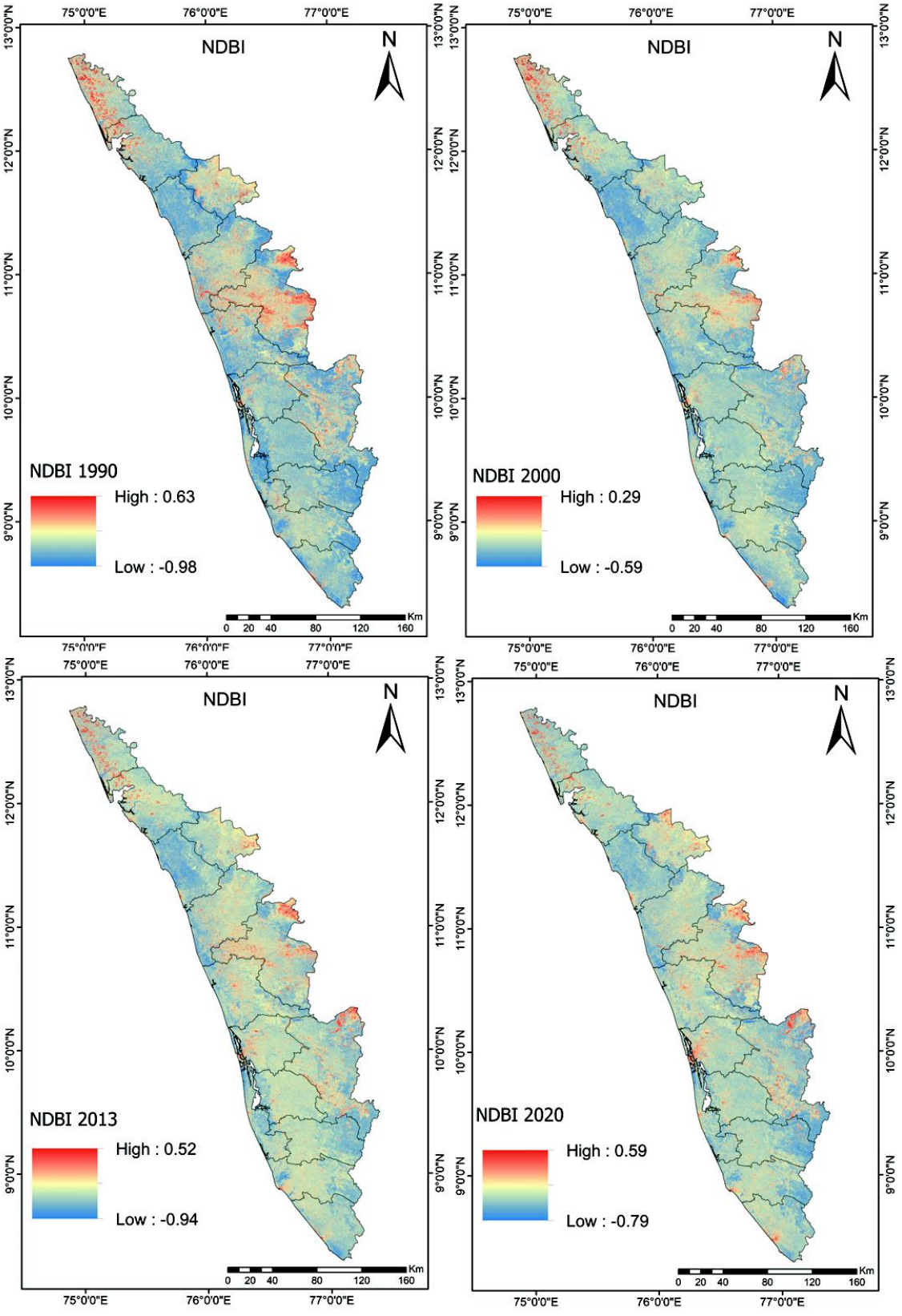

Figure 5.46. NDBI maps of Kerala from 1990 to 2020

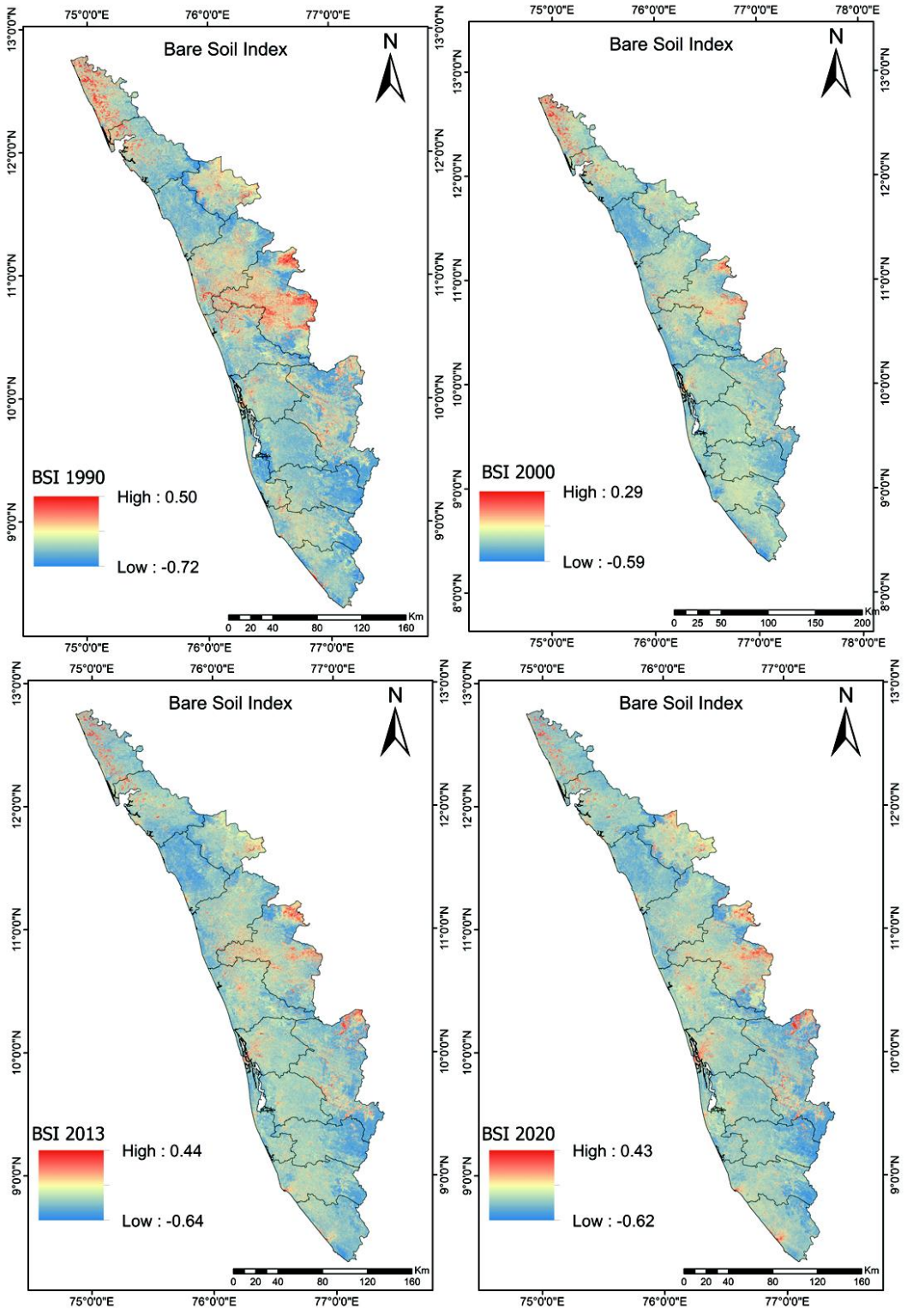

Figure 5.47. BSI maps of Kerala from 1990 to 2020

MNDWI is used to detect open water bodies, such as lakes, rivers, and oceans. The Changes in the MNDWI values from 1990 to 2020 are depicted in Figure 5.48.

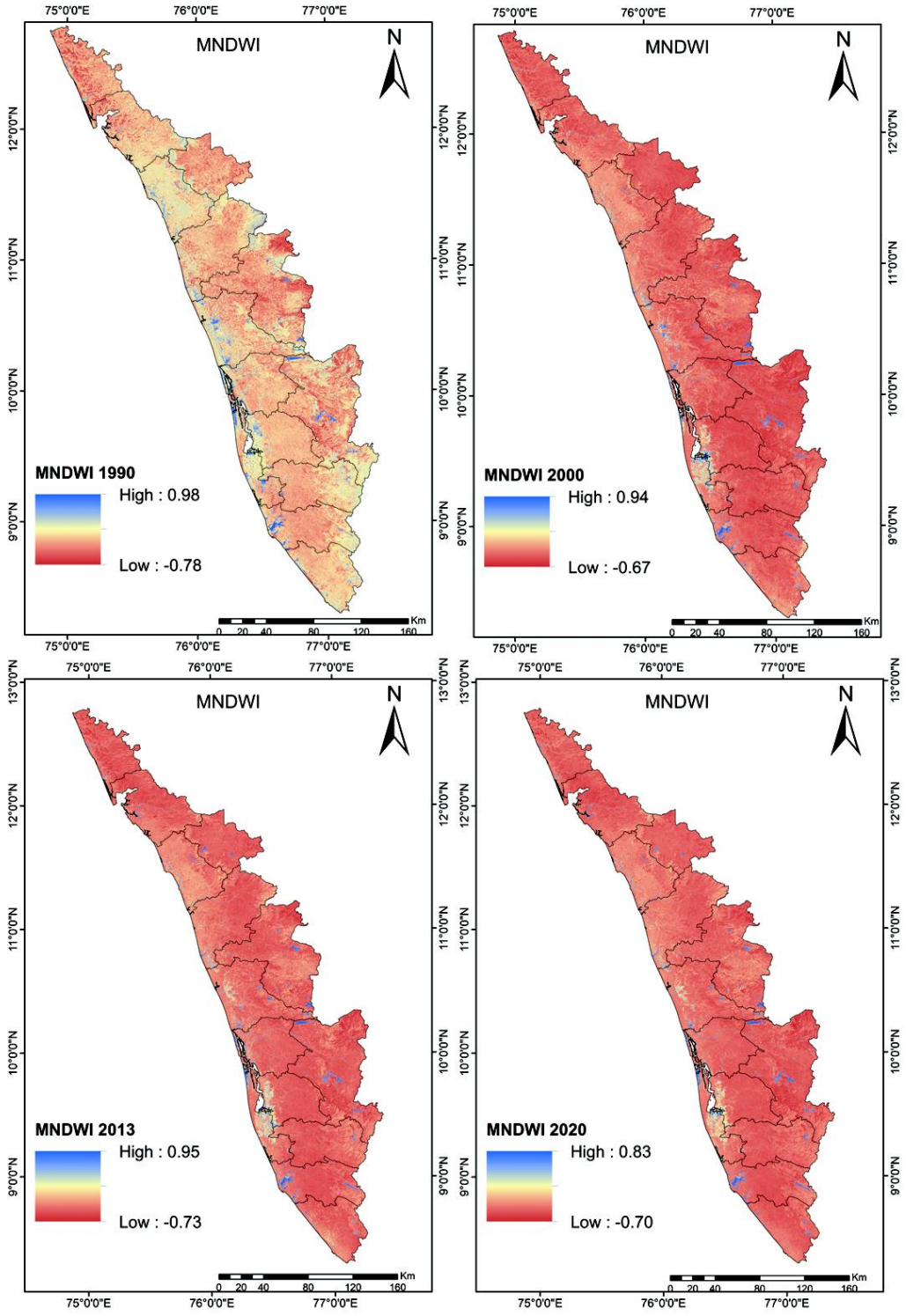

Figure 5.48. MNDWI maps of Kerala from 1990 to 2020

The output of the MNDWI ranges from -1 to 1, with values closer to 1 indicating a higher probability of open water bodies. When the MNDWI value is -1, it indicates no water bodies in the area. Areas with negative values could also be shadows or artificial surfaces that do not reflect much light. When the MNDWI value is 0, it indicates a mix of water and non-water areas. This could be the case for areas with a combination of land cover types, including water bodies and vegetation. When the MNDWI value is between 0 and 1, this range indicates an increased probability of open water bodies. This could include areas with low vegetation cover and areas with high vegetation cover where water is still visible, such as wetlands or flooded forests. The MNDWI value ranges from -0.78 to 0.98 during the 1991 year. Likewise, in 2000, 2013, and 2020, the value varied from -0.67 to 0.94, -0.73 to 0.95, and -0.70 to 0.85, respectively. The slight reduction in the value of MNDWI after 2010 indicates the drop in water bodies in the state.

This study used two supervised machine learning classifiers with the same training data to investigate the region's LULC changes. The same training and validation points were given as input to both algorithms to prevent bias in the results. The classification process involved training each class with 90-100 regions of interest (ROIs) and validating with 60-70 ROIs. A training data set was created by randomly choosing 70% of the observations used in the classifier algorithm. In comparison, the remaining 30% of the observations were utilized to form the validation data set (Devkota et al. 2023). The supervised classifier algorithm was enhanced using the training dataset, and the accuracy assessment of the generated land cover classification maps was evaluated using the validation dataset. Validating the results is crucial because the classified map alone cannot provide sufficient information. The accuracy of both algorithms was tested using a confusion matrix, without which the conclusions from the results cannot be valid. The producer’s accuracy and consumer’s accuracy were calculated for each class, while the overall accuracy and kappa coefficient were computed for each image in both models.

The study done by Kulithalai Shiyam Sundar and Deka 2022 pointed out that the performance of the RF model is better when n_{tree}= 30, whereas another study done in

one of the river basins in Kerala by Abraham and Kundapura 2022 considered n_{tree}= 10 for good accuracy. The current study considered n_{tree}=10 for the RF model, which gives excellent accuracy. Both classifiers were well-trained in the GEE platform with training datasets to obtain the above-mentioned land cover classes. Table 5.5 shows the consumer's and producer's accuracy for the RF classifier. Interestingly, the consumer's and producer's accuracy for water and forest classes is relatively high for the RF model compared to other classes. The consumer's accuracy ranges from 91.8% to 100%, whereas the producer's accuracy extends from 90.65% to 100%. Producer's and consumer's accuracy for all classes was more than 90% on all classified images. The consumer's accuracy for all classes was more than 91% for all years. The lowest value of the consumer's accuracy and the producer's accuracy of the RF model was marked for the urban class. Results from the table show that all the accuracy values are above 90%, indicating the strength of the RF model.

The CART algorithm is a non-parametric pattern classification technique using a binary decision tree model. This algorithm uses a set of predictor variables to split the data into subsets, creating a tree-like structure. In constructing a decision tree, the CART algorithm employs training samples, although the identification and construction of the tree are unknown. To address this, the CART algorithm grows a large tree and then prunes it to a smaller size to reduce the lowest cross-validation error estimate. The innovative pruning process is based on the concept of weakest-link-cutting, with the links indexed by a cost-complexity parameter's values.

Table 5.5. The consumer's and producer's accuracy for RF for various years of LULC

LULC	Consumer's accuracy (%)				Producer's accuracy (%)			
	1990	2000	2013	2020	1990	2000	2013	2020
Urban	92.6	91.8	92.3	95.6	90.65	92.4	92.78	93.54
Water	100	95.21	97.85	98.3	100	96.8	100	100
Forest	95.41	94.42	93.38	92.3	94.6	93.25	100	100

LULC	Consumer's accuracy (%)				Producer's accuracy (%)			
	1990	2000	2013	2020	1990	2000	2013	2020
Vegetation	93.3	96.54	100	94.21	92.66	94.8	98.36	92.66
Barren land	94.67	94.2	100	93.79	92.18	92.11	100	91.96

The CART model in GEE uses a set of predictor variables to build a decision tree and classify pixels into different land cover classes. In GEE, the CART algorithm can be implemented using taking the input data, predictor variables, and parameters for tree construction and pruning as arguments. The resulting model can then be applied to classify pixels in an image or image collection. A minor alteration in the training data can significantly impact the results of the decision tree, as it is highly sensitive to it (Bar et al. 2020).

Table 5.6 depicts the accuracy statistics of the CART model for different years. Results show that, like the RF model, the accuracy value of the water and forest classes is relatively higher than other classes. The consumer's and producer's water class accuracy were more than 95% for all years. The producer's accuracy of water class and forest class was obtained as 100% in 2020. The consumer's accuracy for the CART model varies from 86.43% to 100 %, whereas the producer's accuracy ranges from 87.64% to 100%. The lowest value of consumer accuracy, as well as the producer's accuracy, was obtained for the forest class in 2000.

Table 5.6. The consumer's and producer's accuracy for CART for various years of LULC

LULC	Consumer's accuracy (%)				Producer's accuracy (%)			
	1990	2000	2013	2020	1990	2000	2013	2020
Urban	91.5	90.4	91.69	93.5	88.65	91.28	94.8	92.18
Water	97.59	100	95.23	100	98.6	100	96.4	100

LULC	Consumer's accuracy (%)				Producer's accuracy (%)			
	1990	2000	2013	2020	1990	2000	2013	2020
Forest	92.87	86.43	91.38	90.4	93.05	87.64	100	100
Vegetation	91.27	94.87	93.36	92.5	91.12	88.68	92.37	91.66
Barren land	92.27	92.3	88.9	91.5	88.7	92.36	96.77	90.96

The comparison between the RF model and CART results indicated that the RF model performed relatively better than CART even though the same training and testing points were employed for both models for the respective years. Interestingly, the consumer's accuracy of the CART model for water class is higher than that of the RF model. All classes except urban showed higher consumer and producer accuracy for the RF model. The CART model and RF performed well in 2013 and 2020, whereas the 1990 and 2000 RF models outshined the CART. Table 5.7 summarises the comparison of overall accuracies and Kappa coefficient (κ) for the RF model and CART. It is very clear from the outcomes that the RF model performs better than CART. The overall accuracy and Kappa coefficient (κ) value range from 87.85% to 93.06%. Likewise, the Overall accuracies and kappa coefficient of the RF model are higher than CART. It is interesting to note that overall accuracies and the Kappa coefficient of the RF model are higher than 90% for all years. The overall accuracy and kappa coefficient were the highest in 2013 for both models. Both models had a kappa coefficient (κ) of over 85%, showing that the classified image and the reference data agree. This aligns with research suggesting that a kappa coefficient more significant than 85% signals an excellent level of agreement (Abraham and Kundapura 2022a). Likewise, the highest value for the kappa coefficient was obtained in 2013 for the RF model (92.83%) and CART (92.05%), while the lowest values were 90.1% and 87.85% for the RF model and CART, respectively.

Table 5.7. Overall accuracy and Kappa coefficient for RF and CART model for each year

Year	RF		CART	
	OA (%)	Kappa (%)	OA (%)	Kappa (%)
1990	92.7	92.38	89.94	88.9
2000	91.72	90.1	89.08	87.85
2013	93.06	92.83	92.44	92.05
2020	91.8	91.2	91.16	90.45

Results indicate that the highest overall accuracy observed was 93.06 % for the year 2013 for the RF model, whereas the lowest overall accuracy was 89.08% in 2000 for the CART model. The overall accuracy was higher than 90% in 2020 for both models. Likewise, the overall accuracy was relatively low in 2000 compared to other years. The consumer's accuracy and producers' accuracy of forest class and vegetation class in 2000 were relatively low for both models compared to other years. Likewise, the highest value for the kappa coefficient was obtained in 2013 for the RF model (92.83%) and CART (92.05%), while the lowest values were 90.1% and 87.85% for the RF model and CART, respectively. There is a substantial difference in the performance of the classifiers in the forest and vegetation class. The most accurate LULC classification was for 2013 and 2020, where both the consumer's and producer's accuracy was higher than 90% for all land classes. The analysis is carried out using the RF model, as the performance of the classification is found to be better than the CART. The individual land use class area for the above-mentioned years is summarised in Table 5.8. Figure 5.49 displays the LULC maps of the Kerala state during the study period.

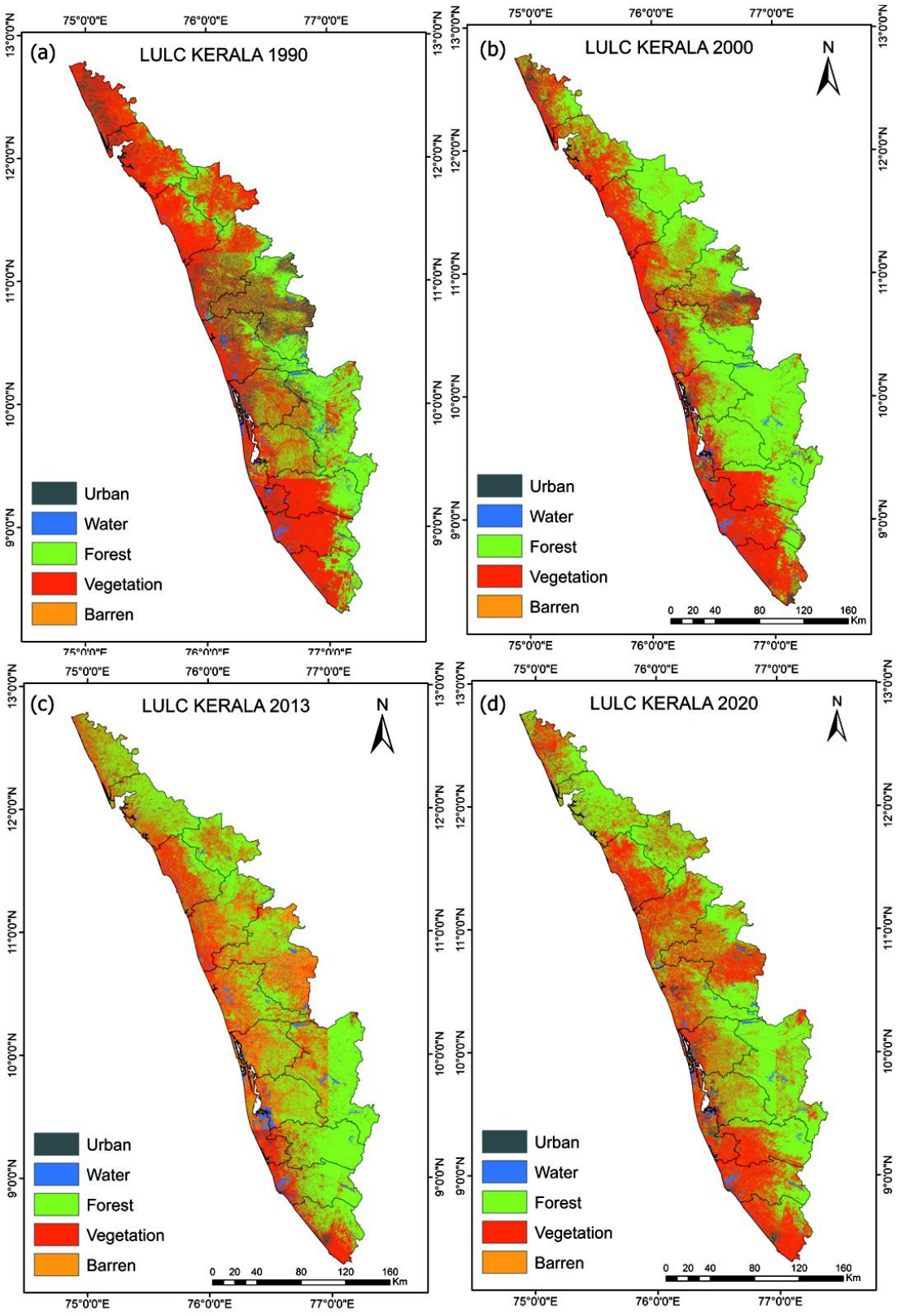

Figure 5.49 Lad use land cover maps of Kerala for (a) 1990 (b) 2000 (c) 2013 (d) 2020

The LULC classes of the state show that vegetation has been the dominant class for the last three decades, followed by the forest class. The results show that Kerala state has changed drastically between 1990 and 2020, spanning three decades. The urban areas and infrastructure has continuously increased over time, whereas vegetation areas have decreased. Across various regions of Kerala state, the rate of LULC changes varied during different periods.

Table 5.8. Areal statistics of different land use classes of Kerala during 1990-2020

Land class	1990	2000	2013	2020
Urban	613.141	917.352	1090.61	1583.03
Water	985.7	825.954	792.1	688.479
Forest	13597	13850.1	15543.1	16432.9
Vegetation	21763.5	21391	19589.5	18383.7
Barren	736.37	711.4	680.5	607.67
Total	37695.8	37695.8	37695.8	37695.8

The above results show that the urban area in 1990 was 613 $km^{2,}$ and it increased to 1583.03 km^2 in 2020 showing a growth of 158.2%. Kerala has undergone significant socioeconomic changes, leading to an increased urban population and substantial infrastructure growth. It is observed that the area of water class shows a considerable reduction in the area within three decades. The water bodies declined by 30.15% during the study period, the highest reduction in the area compared to other land classes. The most significant decrease in the area of water bodies occurred from 1990 to 2000, with a reduction of 16.23%, followed by a decline of 13.08% between 2013 and 2020.

Interestingly, the forest class in the study area showed steady growth throughout the study period, which is a positive sign. The forest area has grown by 20.85%. The highest increase in the forest area was registered from 2000 to 2013 (12.23%), followed by 2013 to 2020 (5.72%). The distinction between forest and vegetation was sharp and

accurate when Landsat 8 images were employed, possibly due to the higher radiometric resolution of Landsat 8 (level 1 products), which is twice that of its predecessor Landsat 7 (Kulithalai Shiyam Sundar and Deka 2022).

The vegetation class showed a reduction in area from 21763.545 km^2 (in 1991) to 18383.695 km^2 (in 2020). Vegetation is the predominant class in Kerala state which showed a decrease of approximately 15.52% during the study period. It is noted that the vegetation area from 2000 to 2013 was reduced to 19589.5 km^2 (8.42 %), and later the area shrank to 18383.7 km^2 (6.15 %). The barren land class area decreased from 736.37 km^2 to 607.67 km^2, marking a reduction of 17.47% during the period. The most significant reduction in barren occurred between 2013 and 2020, with a decrease of 10.70%. The conversion of land use classes from water, vegetation, and barren to urban areas was the most significant, possibly due to population growth and subsequent urban sprawl. It is worth mentioning that the cultivated land in the study region has decreased over the years. This may be due to the poor returns from the cultivation that led to the conversion of agricultural land to non-agricultural use. The effect of land use changes at a particular location can vary from the other location depending upon the geographic location and scale. The built-up area of road networks and buildings has considerably increased over the past three decades. It is also noted that forest area has increased during the study period. The Kerala state is top-ranked in expanding forest cover, according to the India State of Forest Report 2019 (FSI 2019). One of the primary reasons for the increase in forest cover in the era of urbanization is mainly attributed to the conservation activities run by authorities and strict laws imposed by the government (FSI 2019).

Land use change is considered the most significant anthropogenic component influencing the climate. The LULC pattern changes significantly with time due to urbanization, affecting the physical and social environment. The unplanned growth of urban areas can lead to the destruction of natural habitats and biodiversity loss. Urbanization has significant adverse environmental impacts, including resource depletion, forest conversion, environmental pollution, and land degradation, even though it accounts for a very small percentage of the total land surface area (Arowolo

et al. 2018; Liu et al. 2019). Conversion of natural ecosystems into human land uses, like agriculture or urban areas, releases carbon stored in vegetation and soil into the atmosphere, contributing to global warming. The impact of LULC change on climate extends to alterations in the surface energy balance and hydrological cycle. The destruction of natural forests decreases evapotranspiration and increases surface absorption of solar radiation, altering rainfall patterns and raising temperatures (Chapman et al. 2017; Kishtawal et al. 2010; Mohan and Kandya 2015; Shastri et al. 2015; Xu and Zhao 2016; Yang et al. 2017a; Zhang 2020). Studies have shown that one of the main factors contributing to the current temperature increase is human-induced changes in LULC. The changes in LULC have been associated with aerosol levels which can alter the surface temperature through direct and indirect effects. These changes can also modulate rainfall and, under certain favourable circumstances, result in droughts or floods by altering extreme events (Gogoi et al. 2019; Mohan and Kandya 2015). Thus, assessing and monitoring the LULC changes for integrating natural resources management strategies is essential.

The unplanned and unsustainable LULC transformation is a major problem in developing countries like India. For over 140 years, India has undergone significant changes in LULC, including deforestation and urban expansion (Roy et al. 2015). The Green Revolution in the 1960s brought a lot of development in the agriculture sector of India through the use of high-yield crops and chemical fertilizers. Even though the movement helped to increase agricultural production in the country, it led to the loss of biodiversity, natural ecosystem, and forest areas (John and Babu 2021; Singh 2000). Industrialization and quick economic growth have substantially impacted LULC in India, leading to increased built-up areas and declining biodiversity throughout the nation. Kerala is highly vulnerable to climate change due to its state's geographic location. The state had undergone tremendous changes in the land use classes, with vegetation and forest areas replaced by agriculture and built-up areas in hotspots like the Western Ghats (Kumar 2006; Kumar and Nair 2004).

The major observations from this study are the accelerated growth of the built-up class and forest class, whereas decreasing vegetation class in Kerala from 1990 to 2020.

These results are consistent with earlier studies on the LULC variations in Kerala (Abraham and Kundapura 2022a; Kulithalai Shiyam Sundar and Deka 2022; Skariah and Suriyakala 2022). The area of barren land and water bodies decreased during the study period (ENVIS 2021). The conversion of these lands to industrial zones and human settlement is one of the primary reasons for the decrease in the extent of bare land. Most of Kerala's water bodies are rain-fed, and the reduction of their area can be related to both anthropogenic activity and climate change. During extreme rainfall events, the runoff can be intensified by the adverse effects of increasing built-up areas and decreasing the carrying capacity of water bodies (Miller et al. 2014; Xu and Zhao 2016). It is observed that impervious surfaces of built-up areas reduce the infiltration, leading to increased surface runoff (Saravanan and Abijith 2022). Simultaneously the shrinking of water bodies decreases the capacity of the land to store rainwater, resulting in more runoff going into the water bodies and causing them to overflow. Various researchers have reported that the hydrological cycle, including surface runoff, groundwater recharge, and other terrestrial fluxes infiltration, is significantly impacted by LULC (Dixit et al. 2022; Zhu and Li 2014). In addition, this study done by Boyaj et al. 2020 revealed that about 20–25% of the rainfall seen in heavy rainfall events was caused by variations in LULC in South India over the last ten years.

Gadgil et al. 2011 analyzed the human interventions in the eco-sensitive zones of Kerala and reported that they pose a significant threat to the ecological development of the region. The changes in the LULC patterns in the Western Ghats have resulted in fluctuations in the runoff, reduced water tables, and deterioration in water quality. Human encroachments, like dam construction, have entirely changed the course of rivers (Gadgil et al. 2011). The Kerala state experienced extreme rainfall events that led to landslides and severe floods, causing many fatalities in four consecutive years (2018, 2019, 2020, and 2021). Many studies were carried out regarding the potential contributions of climate change and LULC to these events, leading to a need for restructuring of policies and practices (Dixit et al. 2022; Hao et al. 2022; Skariah and Suriyakala 2022). Changes in the LULC, such as large-scale deforestation in the drainage basins of rivers that originate in the Western Ghats region, as well as urban growth, were considered the main reason for August 2018 flooding (Dixit et al. 2022;

Skariah and Suriyakala 2022). The increase in impervious surfaces like built-up areas stops runoff from infiltrating into the ground, which can increase the intensity of floods (Skariah and Suriyakala 2022). The findings from the study will help policymakers in decision-making and strategy planning for future development.

5.11 CLASSIFICATION OF URBAN AND RURAL GRIDS

The contribution of urbanization to the changes in extreme climate is typically investigated using two primary methods: physical modelling and statistical tools. These approaches provide valuable insights into the relationship between urban development and extreme climate events. Physical modelling includes the development of computer simulations that include elements like the effects of UHI and changes in land use patterns. These simulations enable researchers to understand how urbanization affects variables such as temperature, precipitation, and wind patterns. However, in physical modelling, the uncertainties will likely persist in the simulation results due to the existing uncertainties in the parameters and driving fields. These uncertainties arise from the complexities and variability inherent in urban environments, making it challenging to accurately determine the input parameters and areas required for physical models.

On the other hand, statistical tools analyze meteorological data from urban and non-urban areas to identify statistical relationships between urbanization and extreme weather events. It is commonly accepted that using observations as a direct indicator of climate change is a trustworthy and practical strategy. It can provide essential and impartial proof of the actual climate conditions and changes in the real world. Researchers can quantify the influence of urban development on observed extremes by employing techniques such as regression analysis and time series analysis. This study used the dynamic classification approach to categorize IMD grids into urban and rural categories. The dynamic classification approach considers various factors and criteria to determine whether a grid belongs to an urban or rural category. These criteria may include population density, land use patterns, infrastructure development, satellite imagery, and other relevant data sources. This classification approach provides a valuable framework for investigating the influence of urbanization on climate variables

and extreme climate events. It helps in understanding the spatial patterns and dynamics of urban development.

Utilizing time-varying land cover data, the study implemented a dynamic classification method to categorize urban and rural grids in Kerala. This approach provided better insights into the urbanization process in Kerala over the past 30 years. This classification of urban and rural grids is conducted by utilizing LULC maps spanning 1990 to 2020. It is crucial to carefully select the optimal number of urban sites for reliable results. It is observed that some of the rural areas have converted into urban areas within a short time because of the rapid urbanization that happened in the state after 2000. A circular buffer zone with a radius of 7.5 km was constructed around each grid, and the proportion of built-up area was calculated within the buffering region. The radius value for the buffering process was chosen based on the correlation coefficient between the urban expansion rate around the grid point and the climate change during the period. If the built-up area is more, it shows the level of urbanization around the grid point. For the current study, grid points with built-up areas more than or equal to 33.33% are considered urban, otherwise are considered as rural type. The built-up area around each grid for 1990, 2000, 2013, and 2020 was calculated separately and classified the grids into urban-rural types as per the process mentioned above. Various researchers have employed the methodology discussed above for urban-rural studies (Lin et al. 2018; Wu et al. 2020b; Zhao et al. 2019). As per the dynamic classification scheme, Figure 5.50 shows the change in the number of urban and rural grids in Kerala from 1990 to 2020. It is evident from Figure 5.50 that many regions have been converted to urban from rural type within 30 years of the period.

Compared to other methods, utilizing LULC mapping provides a superior representation of the rural-urban transition as it directly captures the information and progress of urbanization. LULC mapping offers a more accurate and comprehensive understanding of the changing landscape, allowing for a detailed analysis of the transition from rural to urban areas. The number of urban grids was only four during the 1990s, accounting for only 6.70% of all grids, and the rest of the state was classified as forest and rural areas. The number of urban grids has increased to 22 in 2020, and

the proportion of total grids raised to 37.28%. A total of 36 rural grids were also identified, in which most of the grids were not well spatially distributed over the whole state and were situated at different latitudes. As per the classification results, more urban grids are located near the coastal region in Kerala, whereas the grids near the Western Ghats are mostly grouped as rural grids. Most of the developments in Kerala are happening near coastal areas. The state has a long coastline of 589.50 km, India's fifth most extensive coastline. The grids nearby the Western Ghats are grouped into rural grids because of the low rate of urbanization and impervious region.

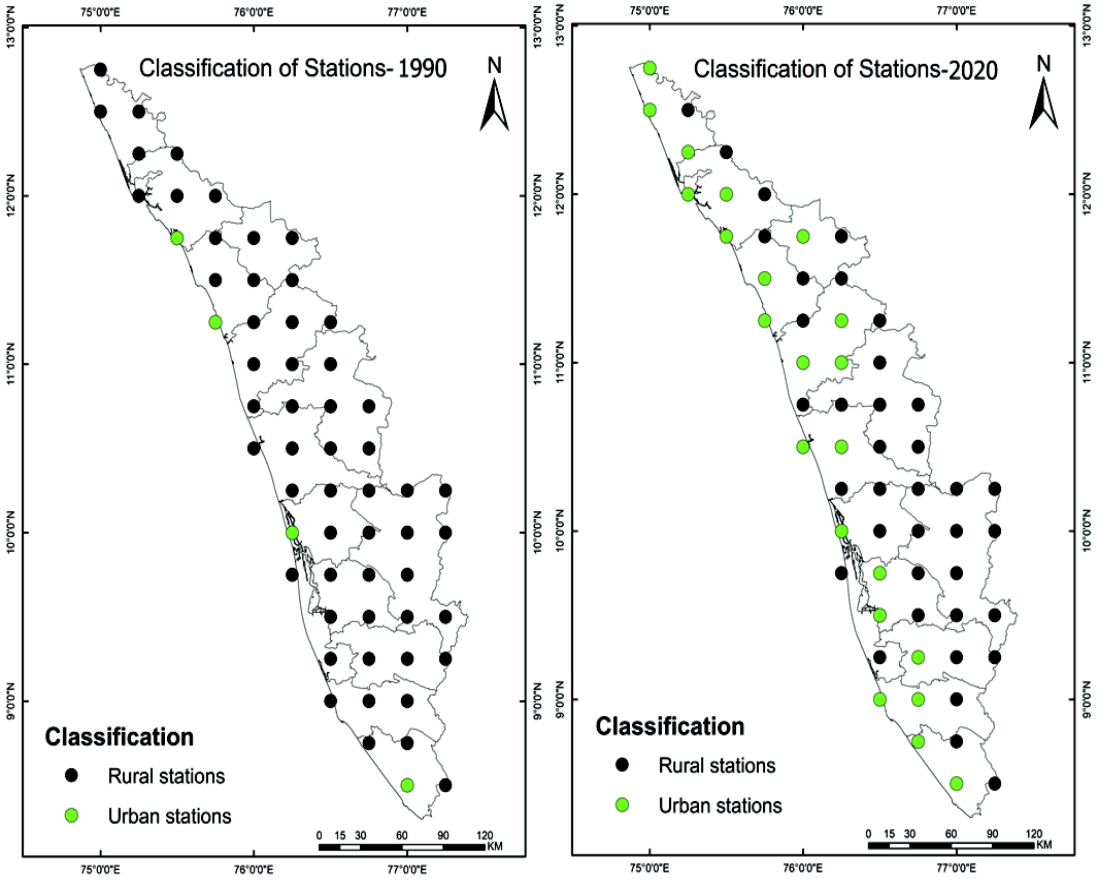

Figure 5.50. Distribution of urban and rural grids in Kerala -1990 to 2020

5.12 EXTREME CLIMATE INDICES

The extreme precipitation indices from 1951 to 2020 were computed at the annual scale using RClimdex, and trend analysis results are depicted in Figure 5.51, Figure 5.52, and Figure 5.53. The modified version of the Mann-Kendall test (MK-CF1), which was

proposed by Hamed, K. H., & Rao 1998, had employed for doing the trend analysis of the extreme climate indices at 95% confidence level. Consecutive wet days (CWD), R10, R20, R25, RX5 day, annual total wet-day precipitation (PRCPTOT), and SDII are decreasing at more than 60% of the grids in Kerala. Detailed analysis showed that 61 to 80% of grid points show an increasing trend in R95p, R99p, RX1 day, and R50 during the study period varying at 95% confidence level. Interestingly more than 60 % of the grids show a downward trend in consecutive dry days (CDD), suggesting a wetting trend in the study region, especially over the northern part of Kerala. The variations in precipitation trends mainly depend on regional characteristics, unlike trends in temperature. The extreme precipitation indices (R95p, R99p, RX1 day, and R50) exhibit an increasing trend in most of the grid points in Southern Kerala. At the same time, it shows a notable increasing trend in consecutive dry days (CDD) in the region. This will lead to high-intensity rainfall events during the rainy season despite the reduction in rainy days. It is worth mentioning that extreme precipitation intensities and extreme precipitation frequencies are significantly increasing over Kerala state. This aligns with previous studies on extreme precipitation in India (Falga and Wang 2022; Kumar et al. 2020; Mukherjee et al. 2018). Kerala witnessed subsequent major flood events in 2018, 2019, and 2020 August month.

The CDD values showed a distinct shift gradient from southern to Northern Kerala. The CDD shows a significantly varying trend, with values varying between 1.8 (Southern Kerala) and -4.5 days/decade (Northern Kerala). In Southern Kerala, the CDD value has increased from 24 days in 1951 to 57 days in 2020. Similarly, in Central Kerala, the CDD value increased from 44 days in 1951 to 112 days in 2020. However, in Northern Kerala, the CDD value has decreased from 85 days in 1951 to 56 days in 2020. This indicates the chances of occurrences of droughts in the Central Kerala as well as Southern Kerala. The number of consecutive wet days is decreasing everywhere in the study area, with the highest in Northern Kerala (4.8 days/decade) and the lowest in Southern Kerala (2.6 days/decade). From 1951 to 2020, there has been a decrease in the CWD (93.22% of the grids) value in all parts of Kerala, but to varying degrees. Southern Kerala has decreased from 43 to 16 days, Central Kerala from 48 to 26 days, and Northern Kerala from 83 to 55 days. There are significant variations in the trend of

CWD in Southern Kerala, Central Kerala, and Northern Kerala. Southern Kerala is experiencing a decrease of 2.6 days/decade, while Central Kerala is experiencing a reduction of 3.3 days/decade. In contrast, Northern Kerala is seeing a much more significant decrease of 4.8 days/decade. An increasing number of CDD and a decreasing number of CWD in the state supports the results obtained for PCI and SI values of the state.

More than 80% of the grids show a negative trend in R10, whereas the grids show an increasing trend in R10 situated along the Western Ghats. It is worth mentioning that there is a statistically significant increasing trend in R10 identified in 2 grids located in the Northern parts of Kerala, where the value has risen from 82 days in 1951 to 107 days in 2020. In contrast, it is decreasing in Southern Kerala (119 days in 1951 to 97 days in 2020) and Central Kerala (103 days in 1951 to 88 days in 2020). Significant variation in trend was observed in the R10 values, ranging from 6.25 days/decade in Northern Kerala to -5.41 days/decade in Southern Kerala. But it is interesting to note that indices like R20 and R25 are decreasing all over the state. It is noted that more than 80% of grids are showing a negative trend (significant and non-significant) in R20 and R25. The R25mm index shows a similar pattern to R20mm, exhibiting a significant decreasing trend in most grids. It is worth mentioning that while most grids in Kerala have revealed a significant decrease in R10, R20, and R25 values, the grids along the Western Ghats have shown a noticeable increase in these indices. This indicates a distinct trend of increased light rainfall in these specific areas. The Western Ghats region, known for its unique topography and biodiversity, appears to be experiencing a shift towards more frequent occurrences of lighter rain events compared to the rest of the parts of the state. This variation highlights the complexity of rainfall patterns within Kerala and the influence of local geographical features on precipitation distribution. For over 80% of the grids in Kerala, there has been a noticeable decrease in indices indicating light to moderate rainfall, namely R10, R20, and R25, signalling a concerning trend of diminishing light precipitation in the region.

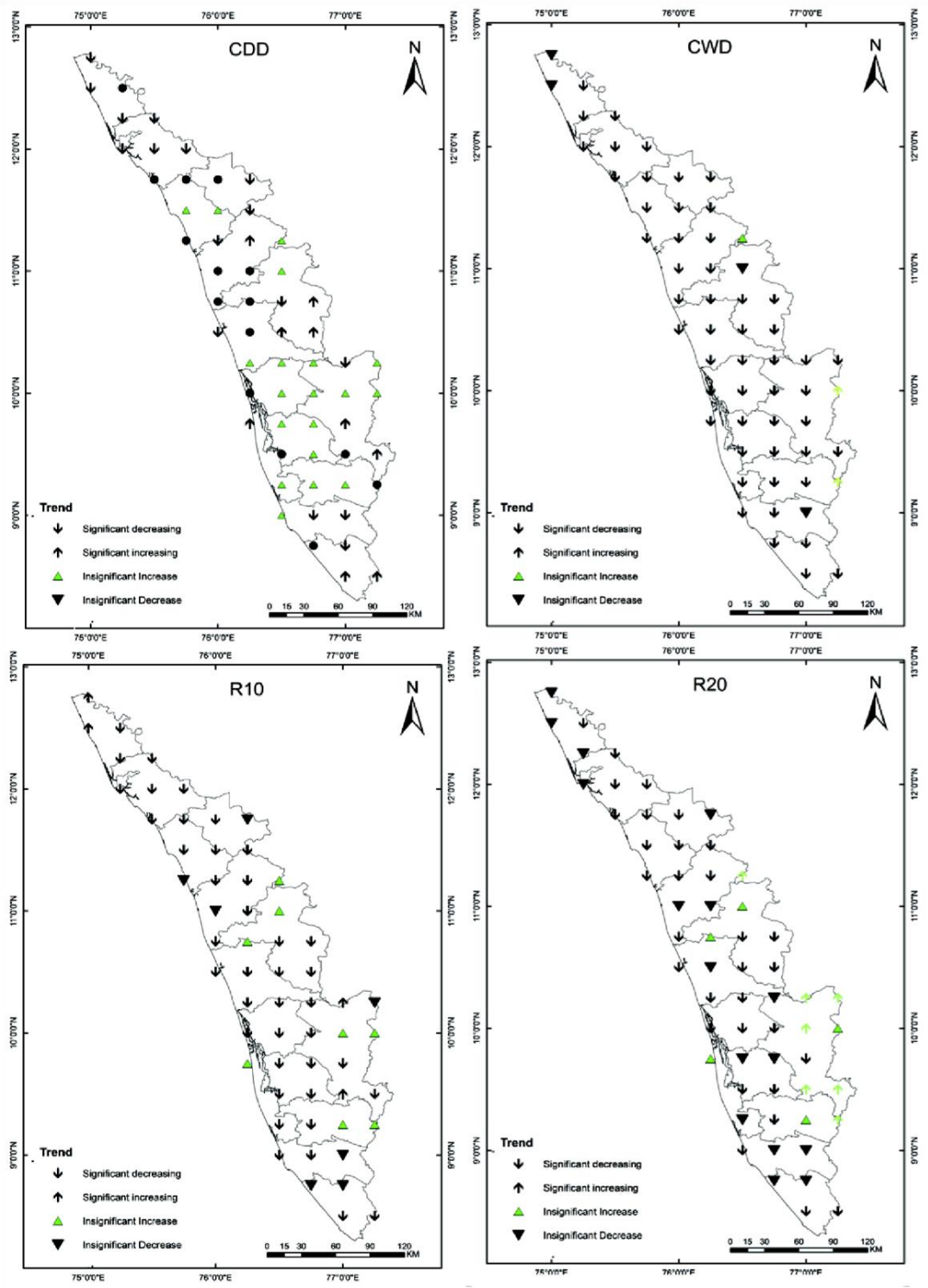

Figure 5.51. Long-term trends of extreme precipitation indices from 1951 to 2020 using the modified Mann-Kendall test

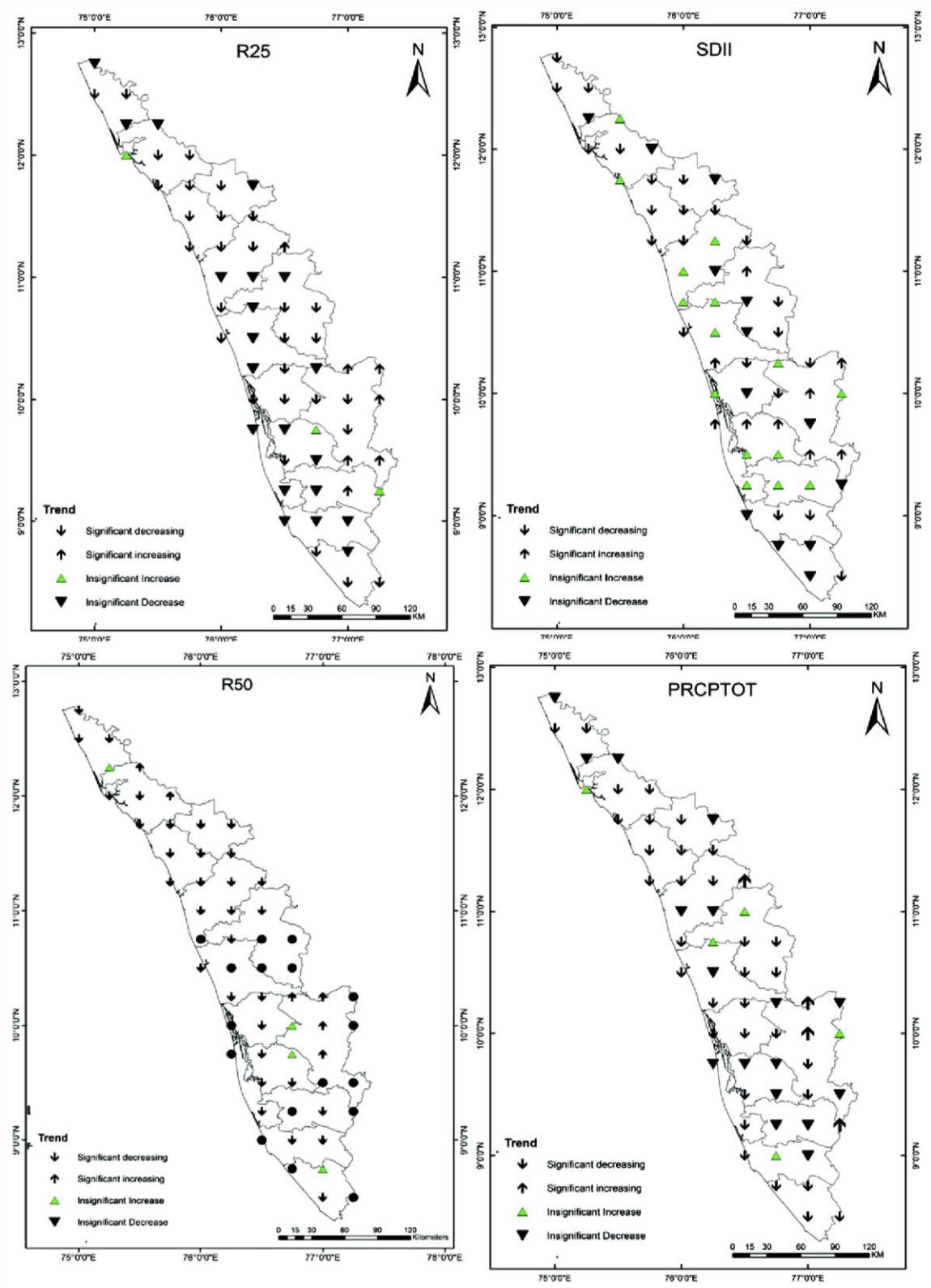

Figure 5.52. Long-term trends of extreme precipitation indices from 1951 to 2020 using the modified Mann-Kendall test

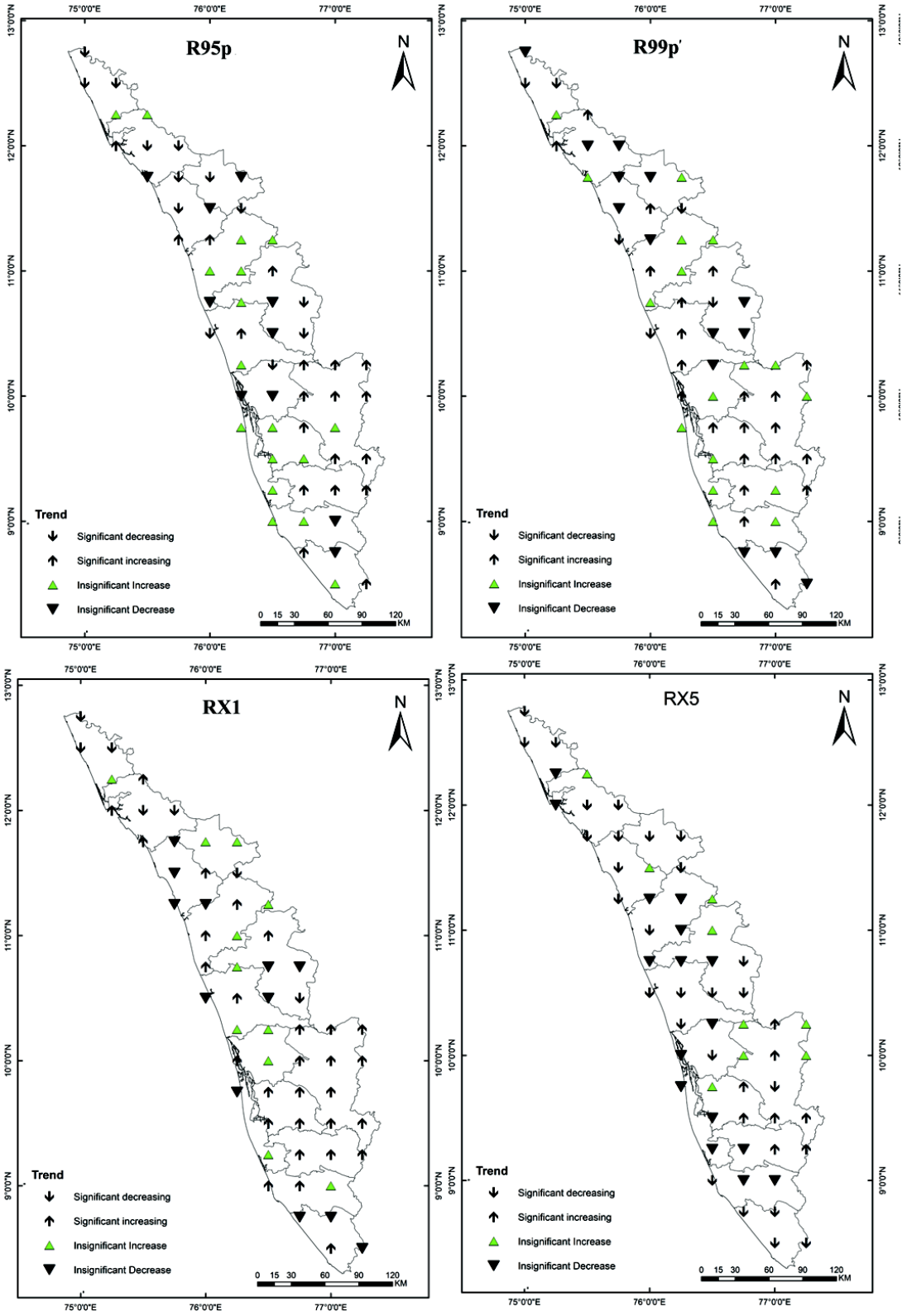

Figure 5.53. Long-term trends of extreme precipitation indices from 1951 to 2020 using the modified Mann-Kendall test

A significant increase in R50 values, especially in the Western Ghats and high-altitude areas of Central Kerala. Notably, after 2010, R50 values have risen in most of the grids throughout Kerala, indicating a notable escalation in extreme rainfall events within the state. This trend highlights the intensification of heavy precipitation. It underlines the need to closely monitor and comprehend extreme rainfall patterns, particularly in regions characterized by high elevations and complex terrains like the Western Ghats and central high-altitude areas of Kerala.

The trend of R50 is increasing in Central Kerala at a rate of 0.9 days/decade, while it is decreasing in Southern Kerala at a rate of -2.5 days/decade and in Northern Kerala at a rate of -1.6 days/decade. The SDII measures the observed intensity of rainfall over a year. It has been observed that the SDII is decreasing in 35 grids, which account for approximately 60% of the total grids in both Northern and Southern Kerala. This indicates a decreasing trend in the intensity of rainfall events in these regions. An interesting observation is that the SDII values in Central Kerala are increasing, including both significant and non-significant increases. The increase in SDII by a rate of 5 mm/year in Central Kerala is indeed a cause for concern. This rise indicates a growing occurrence of high-intensity rainfall events in the region. The disastrous floods experienced in 2018, 2019, and 2020 can be attributed, at least in part, to these increased rainfall intensities. The index PRCPTOT (annual total precipitation in wet days with Pr≥1) is decreasing for more than 84% of the grids in Kerala, whereas it showed a significant increase in the value over the Western Ghats. After 2010, a sudden rise in PRCPTOT was observed in Northern Kerala, where the value in this region rose from 3009.8 mm in 1951 to 4265.8 mm in 2020. In contrast, Southern Kerala is experiencing a decrease, with a decline from 2063.7 mm in 1951 to 1070.8 mm in 2020. The trend of PRCPTOT varies significantly, with Southern Kerala experiencing -12.76 mm/year while Northern Kerala experiences -4.27 mm/year. These indices are very helpful in the agricultural sector as these are the key indicator of meteorological drought at various locations in Kerala.

It is also noted that there is a spike in RX1 value after 2014 in most grids (increasing from 114 mm in 1951 to 252.4 mm in 2019). These findings highlight an increased

tendency for heavy and intense rainfall, which can be correlated with the 2018 and 2019 Kerala floods. In Central Kerala, particularly in high-altitude regions like the Western Ghats and some parts of Southern Kerala, the RX1 index is increasing (68% of the grids). This indicates a rise in the maximum one-day precipitation observed in a year for these areas. In contrast, the grids located in Northern Kerala display a decreasing trend in the RX1 index. Central Kerala and Northern Kerala are experiencing significantly different trends in RX1. The former is seeing an increase of 9.5 mm/year, while the latter is experiencing a decrease of -2.6 mm/year. Interestingly RX5 showed a decreasing trend in more than 70% of the grids, as it doesn't follow the pattern of RX1. Although the trend of RX5 is decreasing in most parts of the state, there has been a spike in its values after 2014, similar to RX1. The value of RX5 in Central Kerala was 267 mm in 1951, which increased to 362 mm in 2014 and rose to 511mm in 2020. From 1951 to 2020, the value of RX5 rose from 499.8 mm to 506 mm in 2014 in Northern Kerala and then further increased to 714.5mm. An interesting observation is the unusual increase in RX5 values at grid points located in the Western Ghats, from 219 mm in 1951 to 535.3 mm in 2020. RX5 index has been increasing at an average rate of 10.93 mm per decade in this region.

The R95p and R99p indices are used to assess the occurrence of very wet and extremely wet days. These indices provide a measure of precipitation behavior on days with high levels of rainfall. The R95p and R99p are increasing at more than 66% of the grids located in Central Kerala and Western Ghats. Over 70 years, from 1951 to 2020, the R95p index in Southern Kerala underwent a significant increase from 381.4 mm to 1249.3 mm. In Central Kerala, the index rose from 485.1 mm to 1471.2 mm between 1951 and 2014, and in Northern Kerala, the index increased from 742.2 mm in 1951 to 1306.8 mm in 2020. Although the R95p index has increased across the state, the most significant rise has been observed in Central and Southern Kerala urban areas. The trend of R95p exhibits distinct patterns in different regions of Kerala. In Southern Kerala and Central Kerala, the R95p is increasing at 12.91 mm/decade and 22.50 mm/decade, respectively. However, in Northern Kerala, there is a decreasing trend in R95p at a rate of 5.96 mm/decade. Likewise, the trend of R99p displays distinct patterns across different regions of Kerala. In Southern Kerala, there is an observed increasing trend in

R99p, with a 1.09 mm/decade rate. In Central Kerala, the increase in R99p is more significant, with a higher rate of 43.98 mm/decade. However, Northern Kerala exhibits an opposite trend, with a decreasing R99p rate of 12.25 mm/decade. The rise in extreme precipitation indices such as R95p, R99p, Rx1 day, and Rx5 day could trigger flood events. The increase in the intensity of rainfall and a decrease in the number of consecutive rainy days suggests a potential for extreme events during the monsoon season (Abraham and Kundapura 2022b; George 2020). At the regional scale, precipitation variations are more influenced by internal climate variability compared to temperature (Dai et al. 2018). The results of this study may be significantly relevant to the rainfall-induced natural disasters that have already taken place in the state between 2018 and 2021 (Hao et al. 2022; Hunt and Menon 2020; Mishra et al. 2018; Mishra and Shah 2018; Wadhawan et al. 2020).

Figure 5.54, Figure 5.55, and Figure 5.56 illustrate the long-term trend analysis test results of 12 extreme temperature indices from 1951 to 2020. Hot extreme temperature indices (TXx, TXn, TNx, TNn, TX90p, TN90p, WSDI, SU35, and TR20) display increasing trends, whereas all cold extreme indices (TX10p, TN10p) exhibit decreasing trends. An alarming rate of decrease in the cold extremes and an increase in the warm extremes is also noted. Throughout the study period in Kerala, the TXx ranged from 32.64°C to 36.65°C whereas TXn varied from 21.64°C to 29.32°C. For the study period in Kerala, TNx ranged from 21.50°C to 27.2°C whereas TNn varied from 13.5°C to 21.25°C. While temperature extremes do not show as much regional variation as precipitation extremes, their rates of change are still not uniform across the state. Despite relatively higher temperatures in Southern Kerala than in Northern Kerala, the rate of change in temperature extremes is higher in Northern Kerala than in Southern Kerala. It is seen that the TXx value is increasing at the rate of 0.14°C/decade in Northern Kerala, whereas it is rising at the rate of 0.12°C/decade in Southern Kerala. In Northern Kerala, the TXn value is increasing at a rate of 0.20°C/decade, while in Southern Kerala, it is rising at a slightly lower rate of 0.17°C/decade. Compared to the rate of 0.07°C/decade in Northern Kerala, the TNx value is increasing at a much lower rate of 0.01°C/decade in Southern Kerala. Likewise, the rate of TNn value increase in Southern Kerala is much lower at 0.03°C/decade, compared to the 0.07°C/decade

increase observed in Northern Kerala. The lower limit of daily minimum and maximum temperature increases faster than the upper limit of daily minimum and maximum temperature.

The southern part of the state is experiencing more hot days than other regions. It is also noted that there was an increase in TX90 values from 1951 to 2020 (TX90 values increased from 12 days in 1951 to 105 days in 2019). The mean increasing trend of TX90 (TN90) is 4.76 days /decade (2.0 days /decade), while TX10p (TN10p) has a mean declining trend of 2.4 days /decade (0.9 days/decade). The warm days and nights (TX90p and TN90p) have increased from their initial percentages in the state. The TX90p has significantly increased from 2.74% to 49.32%, while the TN90p has also increased from 17.53% to 49.33%. In Southern Kerala, the TX90p is increasing at 5.2 days/decade. The increase is slightly lower for Central Kerala at 4.4 days/decade. In Northern Kerala, the rate of increase is 4.9 days/decade. The rate of increase in TN90p varies across different regions of Kerala. In Southern Kerala, the TN90p is increasing at 2.2 days/decade. Central Kerala experiences a slightly lower increase, with a rate of 1.8 days/decade. Northern Kerala has a rate of increase in TN90p at 2.1 days/decade. Similarly, in Southern Kerala and Northern Kerala, the TX10p is decreasing at a rate of 2.4 days/decade, whereas in Central Kerala, there is a decrease in TX10p at a rate of 2.1 days/decade. The rate of reduction in TN10p varies across different regions of Kerala, with Southern Kerala experiencing a decrease at a rate of 1.1 days/decade, Central Kerala showing a decline at a rate of 0.9 days/decade, and Northern Kerala exhibiting a reduction in TN10p at a rate of 0.7 days/decade.

Generally, warm temperature extremes have consistently increased intensity, duration, and frequency, whereas cold temperature extremes have shown the opposite trend. Although the direction of change of various indicators was similar across regions, the rate of change varied. Both cold days (TX10p) and cold nights (TN10p) have decreased in frequency from their initial percentages. The TX10p has experienced a substantial decrease, dropping from 16.4% to 3.56%, while the TN10p has also reduced significantly, falling from 7.4% to 0.55%.

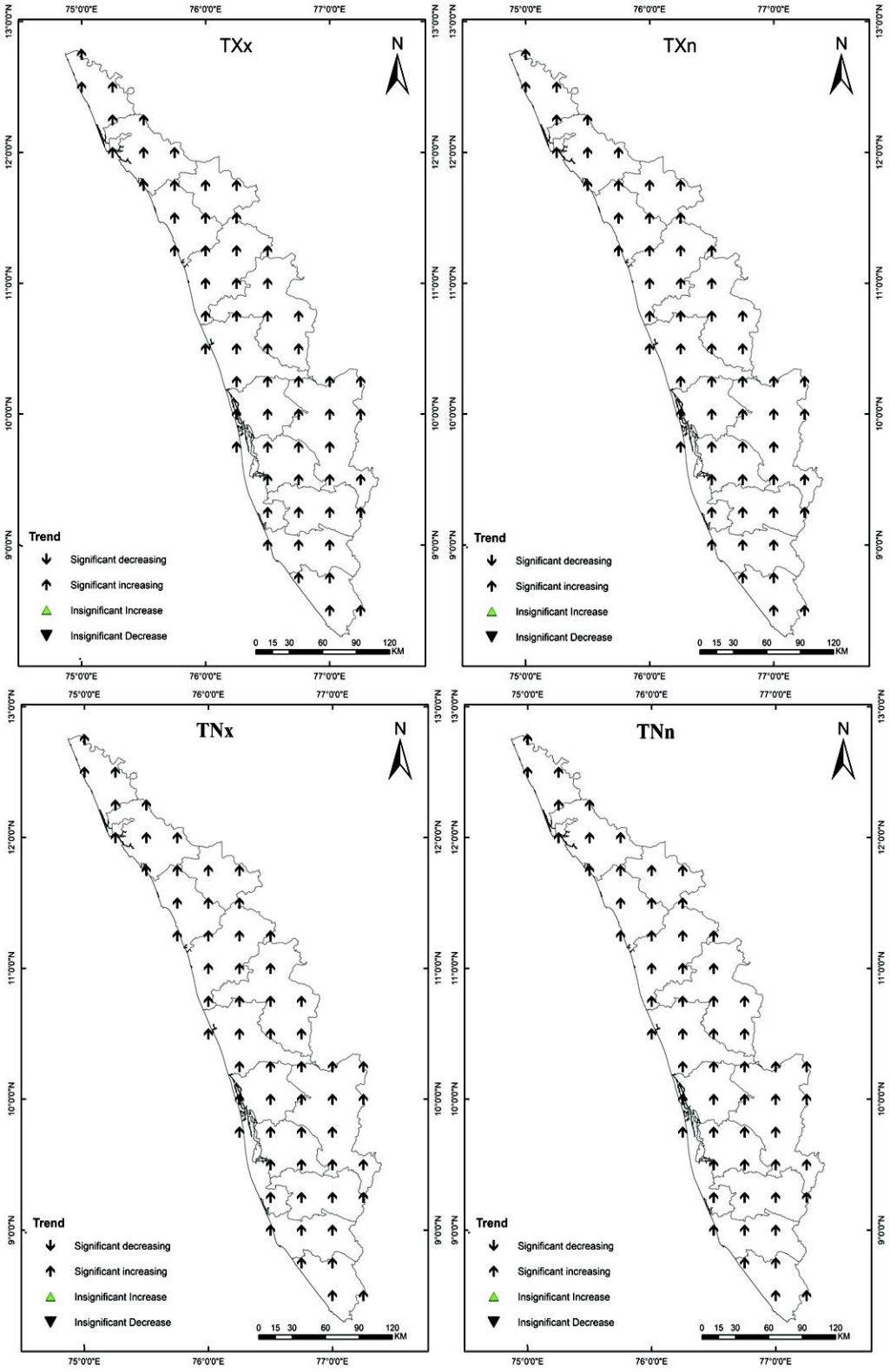

Figure 5.54. Long-term trends of extreme temperature indices using the modified Mann-Kendall test

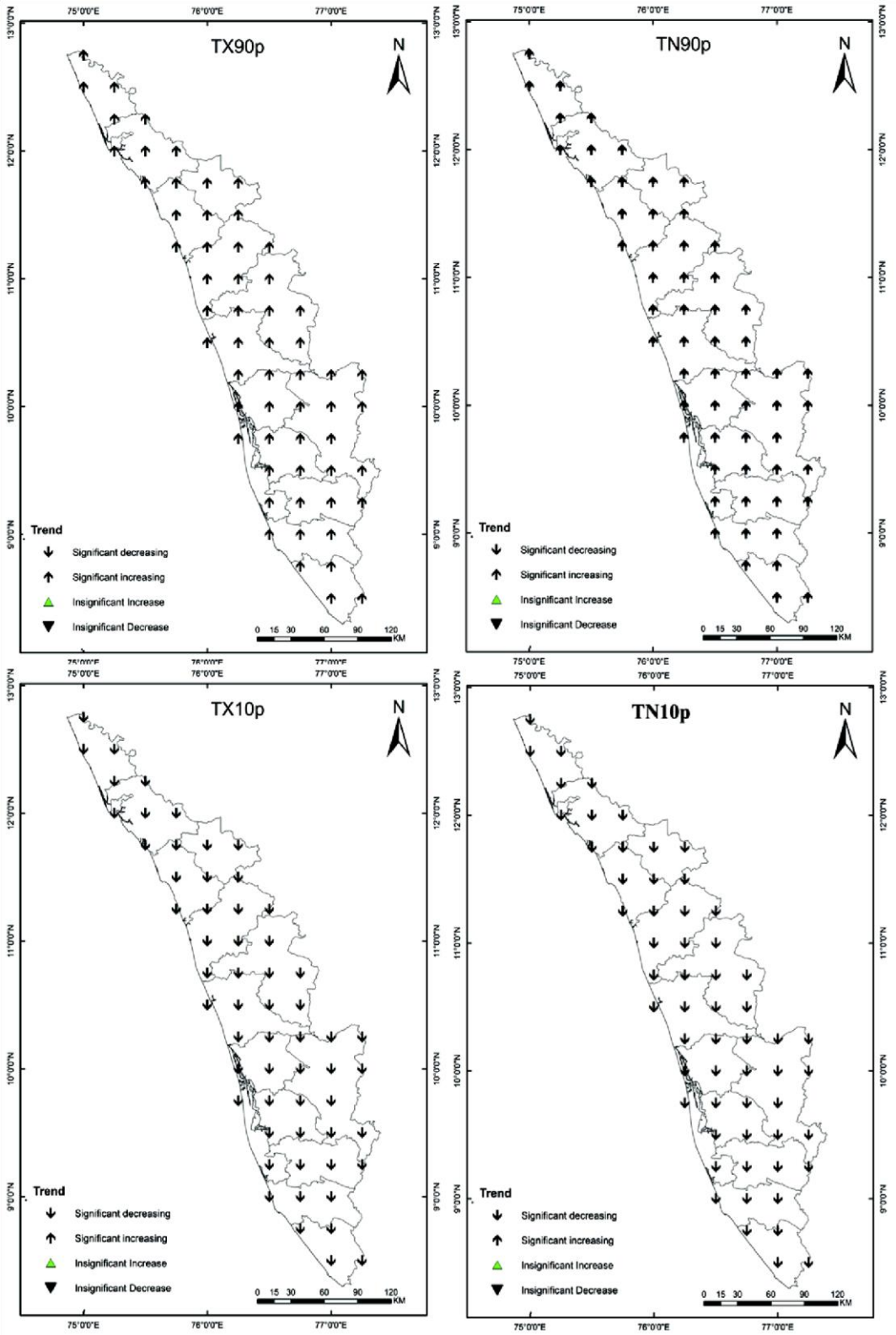

Figure 5.55 Long-term trends of extreme temperature indices using the modified Mann-Kendall test

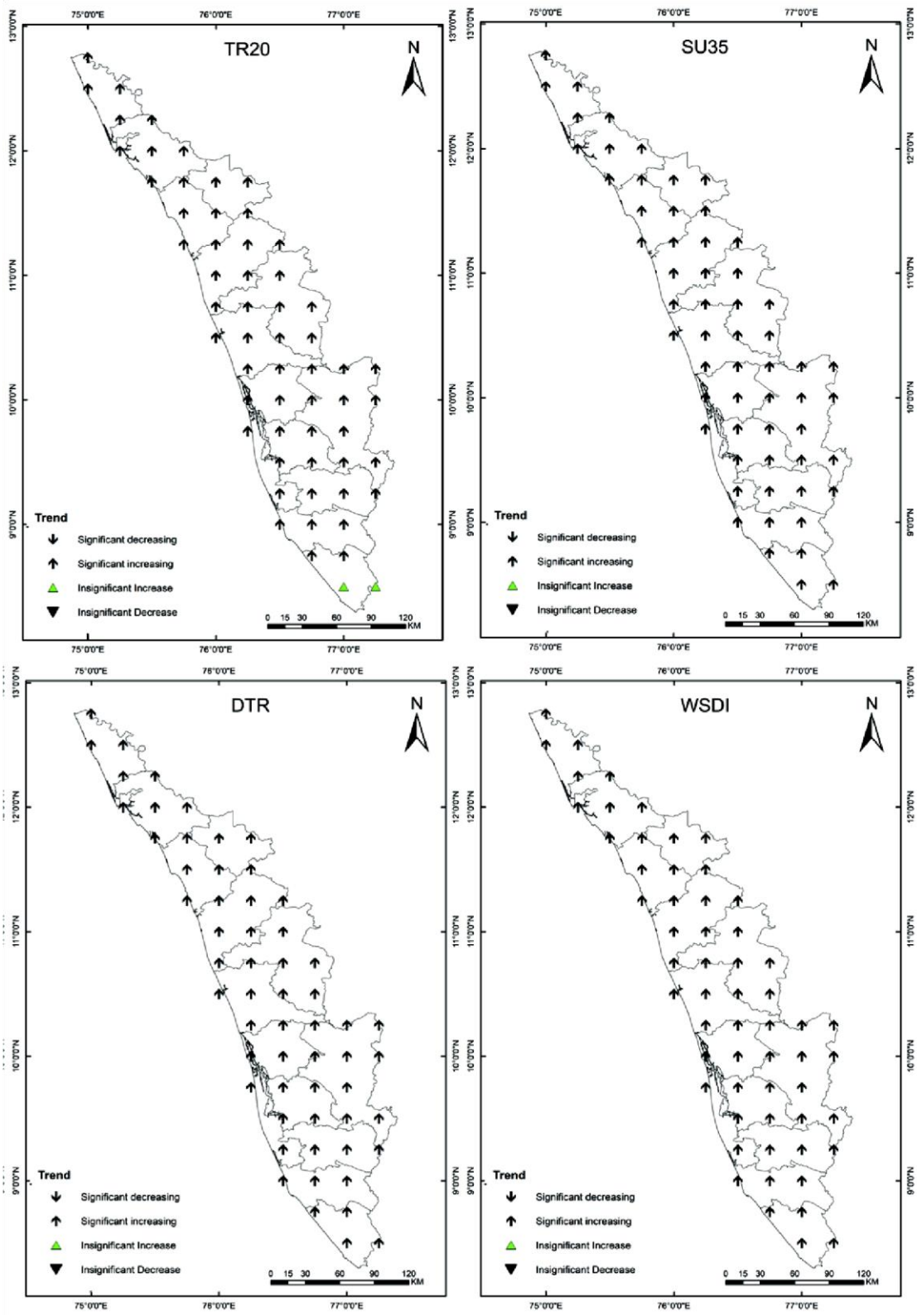

Figure 5.56. Long-term trends of extreme temperature indices using the modified Mann-Kendall test

Over the last 70 years, the results revealed a significant reduction in cold days and nights and an increase in warm days and nights. Generally, warm temperature extremes have consistently increased intensity, duration, and frequency, whereas cold temperature extremes have shown the opposite trend. Although the direction of change of various indicators was similar across regions, the rate of change varied. Results showed that SU35 shows a statistically significant increasing trend in the state in all grids. The increase in the SU35 index from 0 days in 1951 to 44 days in 2016 could indicate the warming climate experienced in the state. The TR20 index measures the number of tropical nights in the state, and the minimum temperature has crossed 20°c in 80% of the year. Interestingly, WSDI and TR20 have a prominent upward trend of 6.5 and 9.5 days/decade, respectively. Over time, WSDI increased significantly in the state from 0 days in 1951, but by 2016, WSDI had risen to 188 days. In addition, it was found that the diurnal temperature range is increasing significantly over the state.

The present study's findings agree with the results of Roy 2019 pointed out the rising trend of warm temperature extremes in India. Compared to hot temperature extremes, the cold temperature extremes decline at higher rates in all grids, which shows the overall warming tendency. The findings also give an insight into the substantial variations in Kerala's extreme temperature towards the warmers conditions, where hot extremes were more pronounced. The alarming shifts associated with the upper tails of maximum and minimum temperature show the overall warming in the region, which aligns with the global mean temperature changes. Under RCP4.5 and RCP8.5 scenarios, significant increases are projected for rainfall extremes, including PRCPTOT, R20MM, R95P, R99P, RX1day, and RX5day, over Southern India and the Western Ghats (Yaduvanshi et al. 2021). In 2021, Kerala state recorded the highest annual rainfall in the last 60 years and the sixth-highest annual rainfall since 1901(IMD 2021).

5.1 URBANIZATION EFFECTS AND CONTRIBUTION

The temporal variation of extreme precipitation indices for urban and rural grids in Kerala from 1951 to 2020 are constructed and depicted in Figure 5.57 and Figure 5.58.

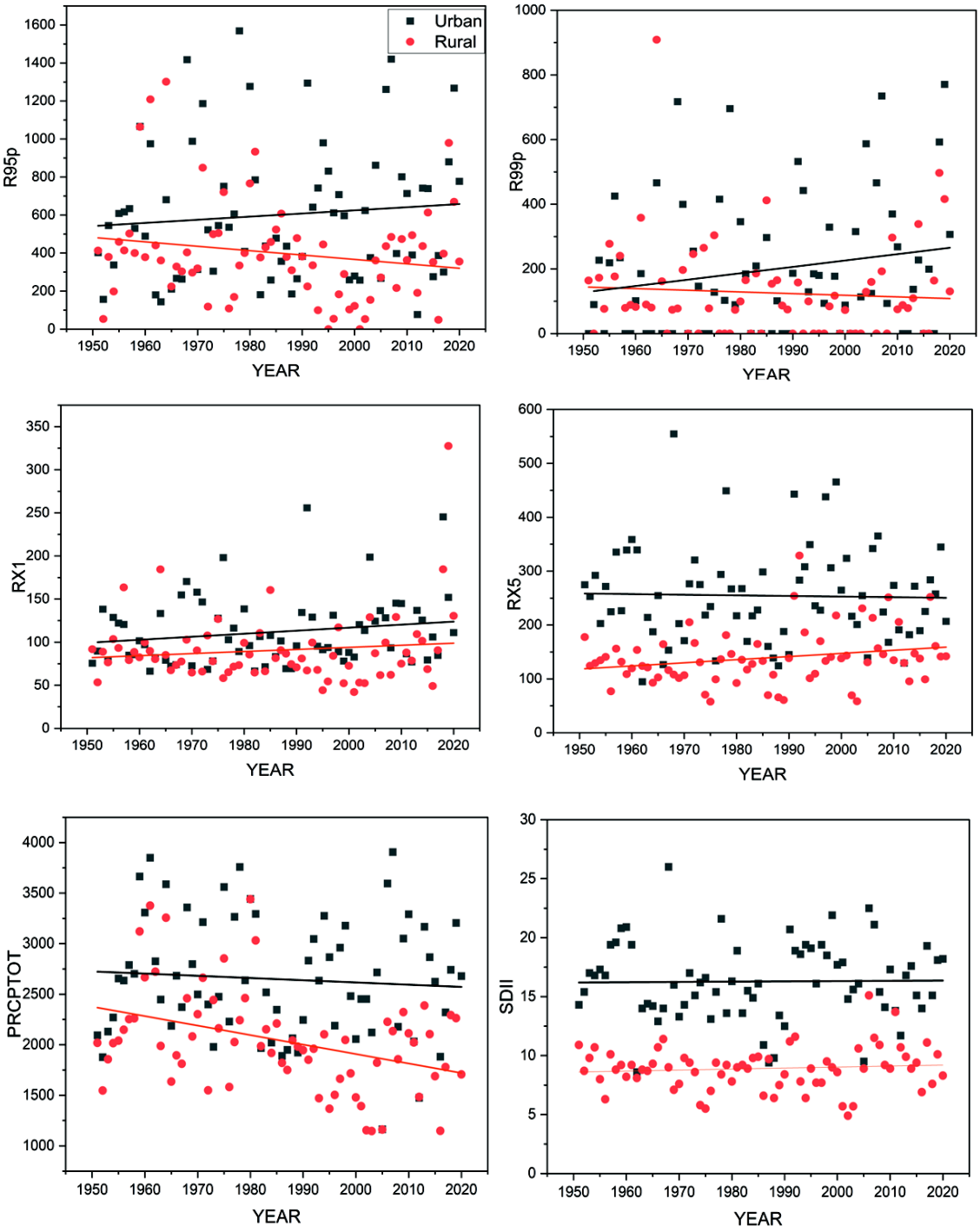

Figure 5.57. Temporal variation of extreme precipitation indices in the urban and rural grids of Kerala –from 1951 to 2020

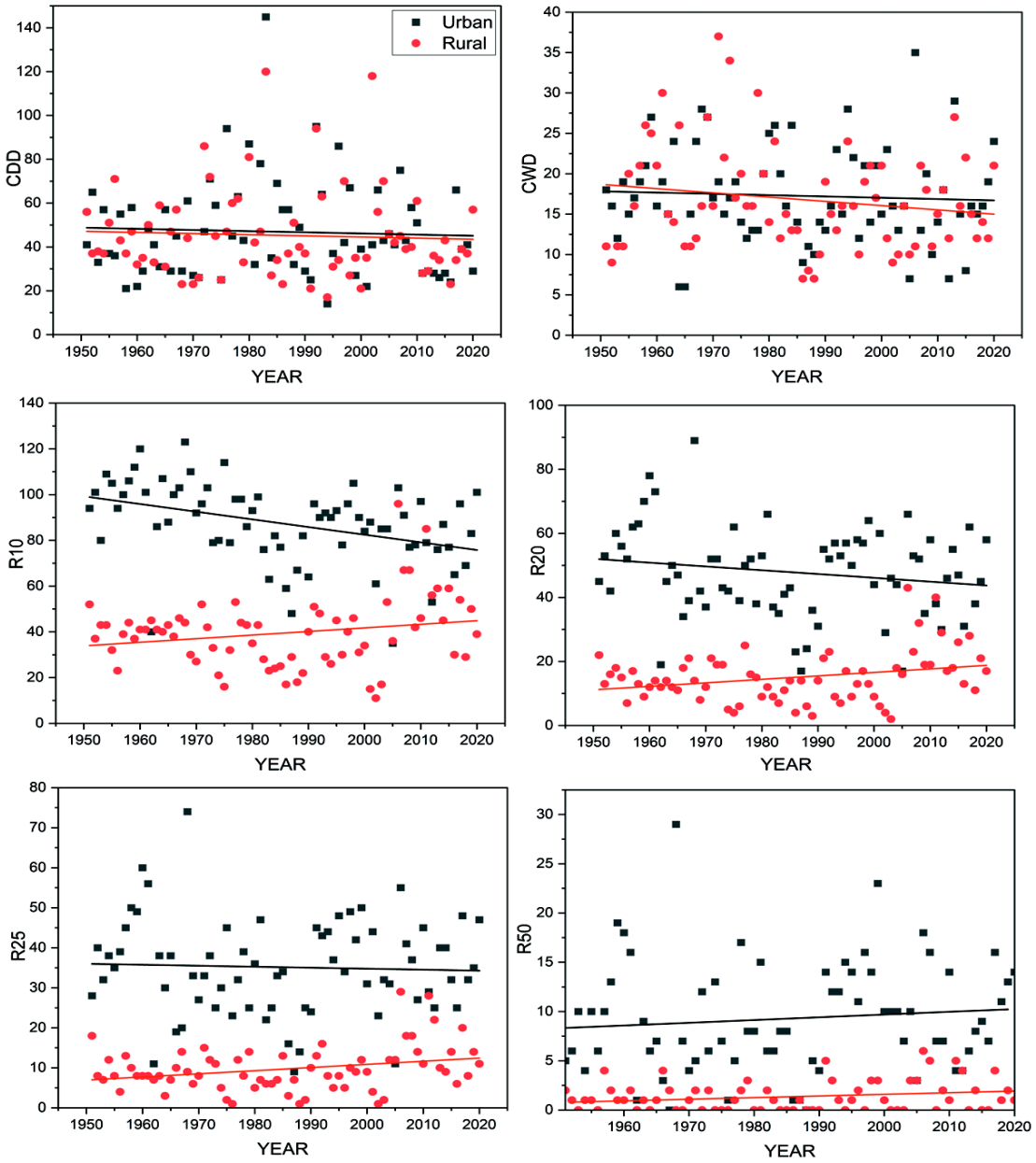

Figure 5.58. Temporal variation of extreme precipitation indices in the urban and rural grids of Kerala –from 1951 to 2020

Notably, the urban series generally exhibits steeper slopes for most extreme climate indices than the rural series. From the analysis, it is clear that the urbanization has a significant impact on most of the extremes. It is seen that indices like R50, SDII, R95p, R99p, RX1 day, and RX5 day are exhibiting a slightly larger upward trend in urban areas compared to surrounding rural areas. Interestingly, R95p, R99p, PRCPTOT,CDD and CWD are decreasing in rural areas. The differences in the trends between urban and rural grids for indices like CWD, CDD, and RX1 are marginal, and it may be

because extreme precipitation events are complex and regionally dependent (Gu et al. 2019; Lin et al. 2020). Increasing urbanization has a crucial role in extreme rainfall events. The indices like R10mm, R20mm, and R25mm (indicates the light to medium rain) showed a statistically significant negative trend on most urban grids. It is interesting to note that some grids show a statistically significant increasing trend for CWD. Table 5.9 lists the urbanization effects on trends of rainfall extremes in all urban grids across the state from 1951 to 2020. The results showed that impact of urbanization on extreme rainfall indices was statistically significant in most grids. The effect of urbanization on different extreme rainfall indices varied, with some indices showing a negative effect while others showed a positive effect. It is seen that CDD showed a negative effect, while indices like RX1, RX5, SDII, PRCPTOT, R95p, and R99p exhibited a positive effect. Over 60% of the grids show statistically significant trends for these indices. The urban grids in Northern Kerala have shown statistically significant increases in CWD, while most grids across the state have exhibited a statistically significant decrease in CDD. The results indicate a statistically significant negative effect of urbanization on light rainfall indices like R10, R20, and R25 on most of the grids in the state, suggesting that urbanization has led to the decrease in light rain in urban areas. Previous research has indicated that urbanization has caused a reduction in light rain as well as increased extreme rainfall events in urban areas (Huang et al. 2023; Yu et al. 2022). The analysis revealed that grids in Southern Kerala and Central Kerala had experienced significant positive effects of urbanization on extreme rainfall indices such as RX1, RX5, R95p, and R99p. These indices represent the frequency, intensity, and magnitude of extreme rainfall events, and their positive trends are consistent with urbanization trends over the past 70 years. Results revealed significant urban-induced changes in the southern and central parts of the state.

Table 5.9 shows the urbanization contribution to extreme rainfall indices. It is seen that more than 70% of grids are showing 100% urbanization contribution for extreme rainfall indices like SDII, PRCPTOT, R95p, R99p, R10mm, R20mm, R25mm, and R50mm, which shows the intensity, frequency and magnitude of rainfall extremes. This directly pointed out that the urbanization process has altered the rainfall regime in the urban region through the increase in the intensity, magnitude, and frequency of extreme events. Earlier research has indicated that urban areas tend to experience increased

levels of precipitation and higher frequency of heavy rainfall events (Kishtawal et al. 2010; Pimonsree et al. 2022; Shastri et al. 2015; Singh et al. 2016; Zhang 2020). Detailed analysis indicated that major urban hubs such as Kochi, Kollam, and Thiruvananthapuram in Southern and Central Kerala have witnessed notable positive impacts of urbanization on extreme rainfall patterns. This result supports the increasing number of extreme rainfall events in the state during 2018, 2019, 2020, and 2021, which has been witnessing heavy rainfall (up to 164% excess of the monthly average) within a short span of days. The stronger precipitation in urban areas may be attributed to local thermodynamics associated with UHI-affected micro-scale circulation patterns, which can lead to a destabilized atmosphere (Shepherd 2006).

Table 5.9 Urbanization effects on trends of rainfall extremes at 22 urban grids in Kerala

Grids	CDD	CWD	R10	R20	R25	R50	R95	R99	RX1	RX5	SDI I	PRCP TOT
1	0.5	0.2	**2.4**	**1.5**	**1.2**	**0.4**	**53.2**	**24.6**	**8.3**	**3.8**	**0.4**	**92.9**
2	0	**1.5**	**6**	**4**	**3.4**	**1.3**	**112.5**	**28.5**	**3.9**	**16.3**	**0.9**	**225.2**
3	0	0.2	0.2	0	0.2	**0.2**	**26.8**	-1.2	-0.3	-0.9	-0.1	**27.7**
4	-0.5	**0.2**	0	0	0	**-0.4**	1.8	0	0.8	**2.4**	**0.2**	-3.8
5	-0.2	**-0.8**	**-4.6**	**-2**	**-0.7**	**0.4**	**27.1**	**11.7**	0.7	**5.5**	0	**50.7**
6	**-1.5**	0.2	**1.9**	**0.7**	**0.4**	**0.7**	**27.1**	**16.3**	**3.4**	**15.2**	-0.2	**20.1**
7	**-1**	-0.5	**-3**	**-1.6**	**-0.6**	**0.4**	**18.2**	**35.7**	**2.3**	**8.2**	**-0.4**	**39.2**
8	**-0.4**	**0.7**	**1.8**	**0.5**	**0**	**0.2**	**18.2**	**9.4**	**2.3**	**3.8**	0	**37.2**
9	**-2.9**	**1.4**	**1.4**	**-0.6**	**-0.9**	**0.3**	**34.3**	**21.3**	**1.3**	**5.8**	**-0.6**	**10.7**
10	**-2.3**	0	**0.8**	**1**	**1.2**	**0.4**	**33.1**	**23.5**	**3.3**	0.6	**0.3**	**71.4**
11	0	**-0.5**	**1.1**	**0.4**	**0.4**	**0.5**	-2.6	-5.5	0.8	0.2	0	21.5
12	0.2	0	**-2.6**	**-1.6**	**-1.3**	**0.2**	**-25.3**	**-25.8**	-0.1	0.6	**-0.5**	**-79.1**
13	0.3	0	0.3	0	0	**0.1**	**-6.1**	-0.9	**-2.2**	**-5.4**	-0.3	2.3
14	**0.5**	**-4.1**	**-2.7**	**-1**	**-0.9**	**0.5**	**-14**	0	0.8	**-6.9**	**0.2**	**-90.5**
15	0	0.4	**2.7**	**0.8**	**0.4**	**0.8**	**-92.7**	**-53.7**	**-8.5**	**-33.2**	**-0.4**	**-27.8**
16	**2.5**	**-1**	**-4.4**	**-3.3**	**-2.4**	**0.3**	**-62.8**	-5	-0.8	**-5.8**	**-0.7**	**-160.4**
17	**-0.6**	-0.5	**2.3**	**1.5**	**1.1**	**0.2**	**74.6**	**31.2**	**2.5**	**5.3**	**0.8**	**106.1**

Grids	CDD	CWD	R10	R20	R25	R50	R95	R99	RX1	RX5	SDI I	PRCP TOT
18	**-0.8**	**1**	0.4	**-1.6**	**1.1**	**-0.5**	**46.1**	**34.4**	**4.3**	**5.8**	**0.4**	62.3
19	**-0.6**	-0.9	**-2.3**	**0.6**	**-1.4**	**-0.4**	**40.7**	**11.1**	0.3	**10.1**	**0.6**	**110.7**
20	**-0.7**	0.2	**1.2**	**0.7**	**0**	**-0.5**	**41.5**	**14.9**	**6.6**	**17.7**	-0.2	-15.4
21	**-2.1**	**1.1**	**3.8**	**2.3**	**1.8**	**-0.6**	**17**	**10.6**	**2**	**8.4**	0.2	**160.3**
22	**-4.4**	**2.5**	**3.3**	**1.8**	**1.9**	**-0.7**	**30.9**	**30.5**	**2.7**	**9**	0	**160.6**

Detailed analysis revealed that most precipitation indices registered 100% urbanization contribution (Table 5.10), indicating urbanization's pivotal role in enhancing the rainfall extremes in this region.

Table 5.10. Urbanization contribution of extreme rainfall events in 22 urban grids

Grids	CDD	CWD	RX1	RX5	R95	R99	R10	R20	R25	R50	SDII	PRCP TOT
1	25.9	12.5	100	100	100	100	100	100	100	100	100	100
2	4.8	100	100	100	100	100	100	100	100	100	100	100
3	100	74.3	40	33.3	100	85.7	6.7	11.6	33.3	100	100	59.5
4	21.8	100	12.2	17.6	100	58.2	30	11	100	100	58	47.5
5	50.3	69.4	22	100	100	47	100	100	100	53.6	100	100
6	100	53.6	100	100	100	100	86.6	60	28.6	100	100	9.2
7	100	1.2	100	100	6.6	100	100	100	60	100	100	100

Grids	CDD	CWD	RX1	RX5	R95	R99	R10	R20	R25	R50	SDII	PRCP TOT
8	100	45.8	61	100	100	72	88.9	50	12.5	100	24.5	83
9	100	94.4	100	67.1	100	100	60	45.9	72.1	80.5	100	20.1
10	100	2.6	41.5	6.3	100	100	46.2	100	100	100	100	100
11	100	27.4	22.2	73.3	100	100	100	42.9	100	100	26.9	64.1
12	100	24.3	20.5	14	100	100	100	100	100	100	100	100
13	65.8	7.7	100	49.3	31.1	74.5	100	1.7	100	100	45.5	9.5
14	100	100	54.8	100	100	30.7	100	100	100	100	100	100
15	59.5	22.9	100	100	100	45.2	58.9	12.1	3.7	13.3	75	28.9
16	100	70.5	4.7	55.6	100	100	100	100	100	80.5	100	100
17	17.4	18.5	53.1	45.9	100	100	70.8	83.7	82.3	100	100	100
18	36.3	46.5	100	100	100	100	40	76.2	100	90	100	100
19	53.7	35.8	53.8	45.1	72.2	58.2	78.1	100	73.7	88.7	14.1	76.5
20	4.3	3.4	100	100	100	100	58.3	100	33.3	100	100	79.5
21	65.2	100	100	78.8	18.8	53.4	100	100	100	100	13.2	100
22	71.3	100	100	47.4	33.4	100	100	100	100	100	14.3	100

Figure 5.59 and Figure 5.60 illustrates the temporal variation of extreme temperature indices for urban and rural grids in Kerala from 1951 to 2020. It is observed that urban time series exhibit steeper slopes than that of rural time series in most of the extreme temperature indices. On the contrary, the rate of increase in cold temperature extremes is higher in rural regions than in surrounding urban areas. Interestingly, trends between urban and rural grids for cold temperature extremes are marginal in some urban grids. In contrast, trends for warm temperature extremes between both grids showed a significant difference. This indicates that the urban-induced impact on daytime extremes is stronger than on night-time extremes.

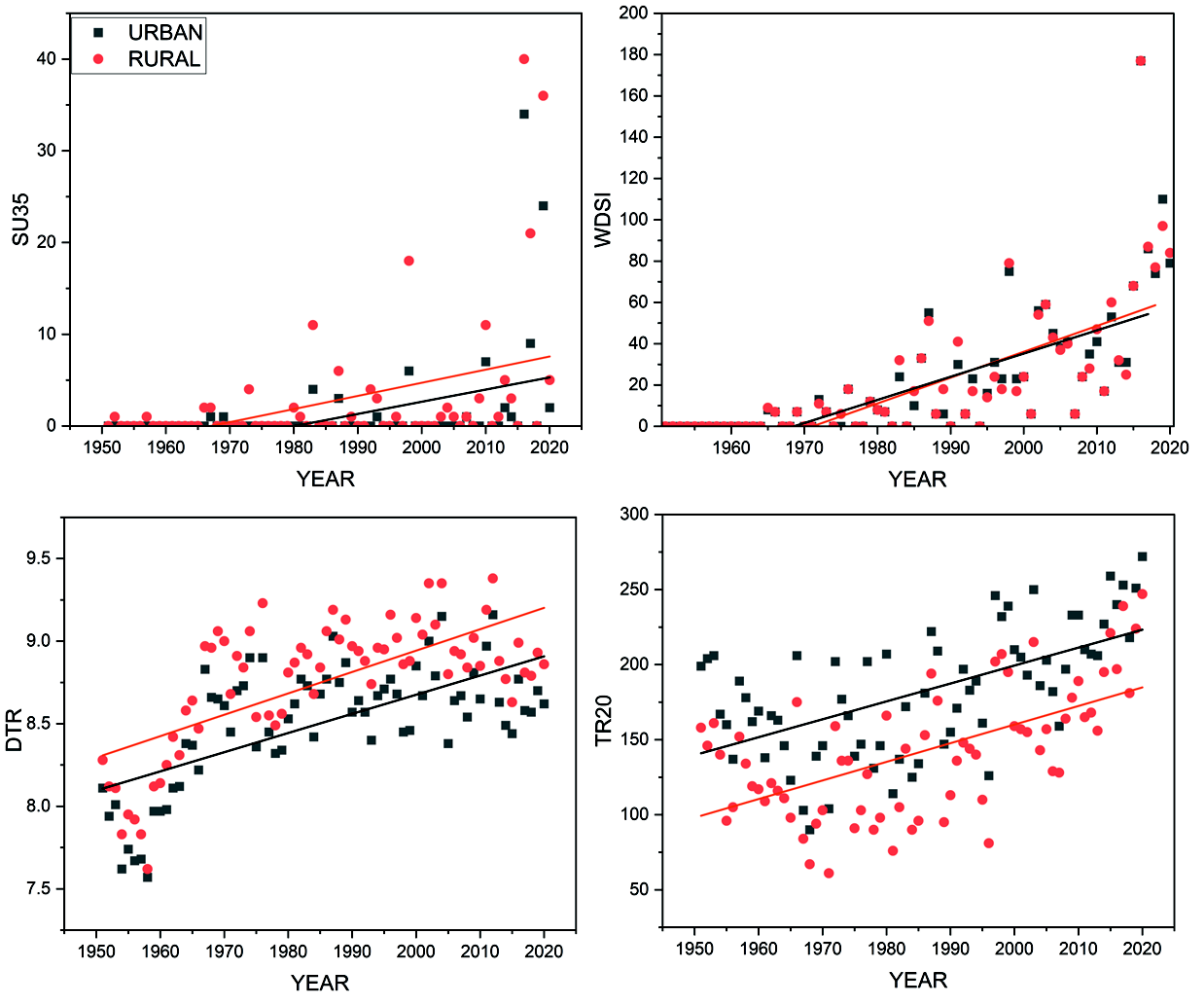

Figure 5.59. Temporal variation of extreme temperature indices in the urban and rural grids of Kerala –from 1951 to 2020

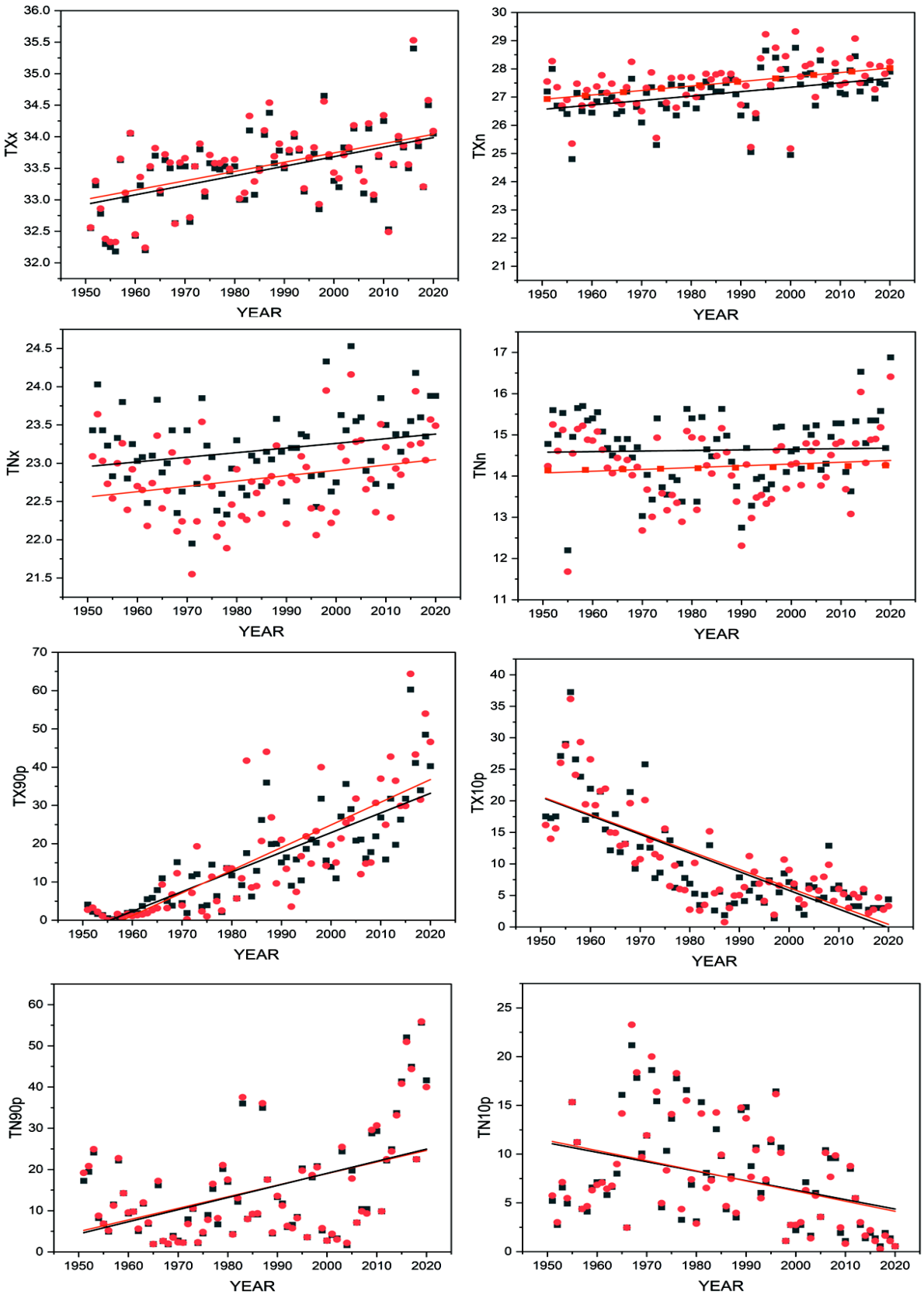

Figure 5.60. Temporal variation of extreme temperature indices in the urban and rural grids of Kerala –from 1951 to 2020

Table 5.11 illustrates the urbanization effects on trends of temperature extremes in all urban grids across the state from 1951 to 2020. As it is seen, many grid points have shown a positive urbanization impact on warm extremes which is statistically significant at 95% confidence level.

Table 5.11 Urbanization effects on trends of temperature extremes at nine urban grids in Kerala

Grids	1	2	3	4	5	6	7	8	9
WDSI	0.74	1.50	**-0.93**	**3.61**	**4.00**	**2.00**	**2.00**	**4.00**	**3.50**
DTR	**0.01**	0.00	0.00	0.01	**0.03**	**0.02**	**0.03**	**0.04**	**0.04**
SU35	0.50	**2.60**	**0.80**	**1.60**	**0.32**	**0.12**	**0.17**	**0.17**	**0.30**
TN10p	-0.10	-0.07	**-0.20**	**-1.24**	**-1.50**	**-0.80**	-0.30	-0.40	**-0.70**
TN90p	**-0.30**	0.20	**-0.70**	**0.60**	**0.50**	0.10	0.30	0.60	**0.90**
TNn	**-0.01**	0.03	0.04	**0.00**	**-0.10**	**-0.02**	**0.01**	**0.04**	**-0.08**
TNx	**-0.01**	0.01	0.01	-0.02	**0.02**	**0.02**	**0.02**	**0.04**	**-0.01**
TR20	**1.01**	**0.40**	0.20	0.33	**0.55**	0.90	**7.80**	**8.00**	**5.10**
TX10p	-0.03	0.05	**-0.03**	**-0.15**	0.03	**-0.17**	**-0.14**	**0.08**	-0.07
TX90p	**0.10**	**0.40**	-0.50	**0.80**	**1.10**	**0.70**	**0.70**	**1.70**	**1.00**
TXn	0.00	**0.09**	0.06	**0.08**	0.02	0.00	**0.07**	-0.03	**0.01**
TXx	**-0.04**	**0.06**	**0.02**	**0.03**	**0.02**	**0.01**	**0.01**	**0.04**	**0.08**

Many grid points have shown a positive urbanization impact on warm extremes, statistically significant from 1951 to 2020. As it shows, urban-induced increasing trends are evident in most extreme temperature indices. Most urban grids exhibit statistically significant positive impacts of urbanization on temperature indices such as WDSI, DTR, SU35, TR20, TX90p, TN90p, TXn, TNx, TNn, and TXx. However, significant adverse effects of urbanization on TX10p and TN10p are also observed in most urban grids. It is noted that WDSI, DTR, and SU35 registered statistically significant positive trends at all grids, whereas TR20 and TXn

exhibited statistically significant positive trends at 7 out of 9 grids. The findings revealed that the indices that demonstrated statistically significant changes across most urban grids were derived with maximum temperature. This suggests that the impacts of urbanization on day-time temperature extremes are more pronounced than on night-time temperature extremes. It is important to note that grids in a state's central and northern parts may exhibit more statistically significant trends in urban grids, either increasing or decreasing, than those in rural areas. All the grids in the northern region of Kerala state show a statistically significant negative trend in TX0p. It is clear from the results that urbanization was the primary cause for the rise in the lower limits of maximum and minimum temperature (TXn and TNn), and these indices exhibit a statistically significant positive urbanization effect.

The results showed that urbanization contribution (Table 5.12) is more discernible at daytime extremes. The rate of extreme temperature events increases in urban areas compared to surrounding rural areas shows that urbanization can intensify the extreme temperature events in the coming decades. The findings revealed that DTR, SU35, TNn, TNx, R20, TX90p, TXn, and TXx had the highest urbanization contributions among the climate variables analysed. Additionally, it was observed that DTR had a 100% urbanization contribution in six out of nine urban grids. TNx and WSDI show the smallest contribution across all grids. Across Kerala, the contribution of urbanization to daytime extreme indices (TX10p and TX90p) was generally more significant compared to night-time percentile-based extreme indices (TN10p and TN90p). Furthermore, the urban grids in Central Kerala and Northern Kerala exhibited the most significant contribution of urbanization to the changes observed in extreme temperature indices. Upon comprehensive analysis, it was found that urban centres in Kochi, Kannur, and Calicut have demonstrated the most significant influence of urbanization on the observed changes in extreme temperature indices.

Table 5.12. Urbanization contribution of extreme temperature events in nine urban grids

Grids	1	2	3	4	5	6	7	8	9
WDSI	15.2	11.7	9.2	37.7	30	21.1	33.2	37.7	38.2
DTR	66.7	**100**	**100**	**100**	**100**	40	55.6	**100**	100
SU35	14.3	74.3	33.3	80	79	46.4	60.4	55.9	42.9
TN10p	50	25.4	40	26.1	27.6	30.6	38.5	16.7	26.8
TN90p	51.5	31	37.1	28.9	25.9	33.9	27.2	29.5	13.6

Grids	1	2	3	4	5	6	7	8	9
TNn	27.2	22.5	30.3	64.5	42.7	30.6	28	22	19.9
TNx	19.7	36	33.8	29.4	22.8	22.4	42.4	36.2	36.5
TR20	38.7	19	27.1	68.1	20.6	26	39.5	27.8	15.6
TX10p	43.4	26.5	23.3	53.3	24.7	25.1	40.5	46.2	36.1
TX90p	21.4	23.5	26	66	69.9	61.5	72.5	72.3	29.4
TXn	45.5	38.2	72.4	53.4	49.8	68.2	77.1	76	68.7
TXx	48.4	25.4	27.4	48.1	51.6	60.2	69.5	42	30.1

India was ranked the fifth most climate-vulnerable country in the world according to the climate risk index 2018 (Eckstein et al. 2018). India has suffered more than 478 extreme climate events since 1970, and the frequency of occurrence of these events has increased since 2005 (Mohanty 2020). Many studies showed the significant influence of urbanization on the changes of extreme climate events under global warming (Kang et al. 2021; Li and Gao 2022; Lin et al. 2020; Oh et al. 2021; Ren et al. 2008; Wu et al. 2019; Zhang 2020; Zhao et al. 2019). Various climate actions are taken globally to limit the increase in earth's temperature to 2°C. Notably, current trends in extreme climate events result from a 0.60 °C rise in the last 100 years. The studies conducted in India on the impact of urbanization on temperature are relatively limited. Still, those that have been done suggest that anthropogenic activities contribute to an increasing trend of night-time temperature extremes. The studies by Mohan and Kandya 2015 and Sussman et al. 2019 both indicate that urbanization and associated factors, such as UHI, are playing a significant role in exacerbating temperature extremes in urban areas in India.

5.2 HEAT WAVES

The spatial variation of Z values modified Mann-Kendall test for all HW measures from 1951 to 2020 are depicted in Figure 5.61 and Figure 5.62. Different regions showed different increased amplitudes. Interestingly, all the HW characteristics show a significant positive trend at 95% confidence level all over the state. HW characteristics in Northern Kerala are alarmingly increasing compared to other parts of the state. It is observed that all of the HW measures have intensifying trends, which signals that HW in the state is becoming increasingly intense, frequent, and lasting. These findings support the increasingly extended periods of HW reported in the past decades. HWA and HWM in Southern Kerala were 33.87°C and 33.85°C, respectively 1951. By 2020, these temperatures had risen to 35.28°C and 34.11°C, respectively.

Similarly, the HWA and HWM temperatures in Central Kerala were 32.57°C and 32.55°C, respectively 1951. Subsequently, there was a gradual increase, with temperatures reaching 33.75°C and 33.0°C by 2020. In Northern Kerala, the HWA and HWM were 32.73°C and 32.55°C, respectively. They have increased to 34.00°C and 33.20°C, respectively. Southern Kerala recorded the highest increase in HWA and HWM, followed by Northern Kerala, while Central Kerala experienced the least increase in these measures. This suggests that the severity of heat waves was the highest in the southern region, with the northern part also experiencing a significant temperature increase.

The HWF in the state has increased significantly over time, from 2 days in 1951 to 72 days in 2019. This increase indicates that heat waves have become more frequent and intense in the region. According to the results, the HWD in Kerala has increased significantly from 3 days in 1951 to 35 days in 2019. This trend suggests that heat waves in the region have been lasting longer over time, indicating an increase in their intensity and severity. In 1951, only some parts of Kerala experienced one heat wave event (HWN), while most areas of the state did not register any events. This was likely because many regions did not experience three consecutive days with a maximum temperature greater than the 95th percentile value. However, in 2020, the number of heat wave events in Kerala increased significantly to seven events in most parts of the state. This rise in HWN is a cause for concern as it can significantly impact public health, agriculture, and the environment. Interestingly, the onset (HWO) and end date (HWE) of HW events exhibit advancing and delaying trends suggesting the longer span of HW season. Over time, there has been a significant increase in the average length of heat wave events (HWL) in the state. In 1951, the HWL was only three days. However, by 2016, the average length of a heat wave had increased to 22 days. In 2017, the HWL decreased slightly to 15 days. This trend highlights the growing impact of climate change on the frequency and severity of heat waves in the region.

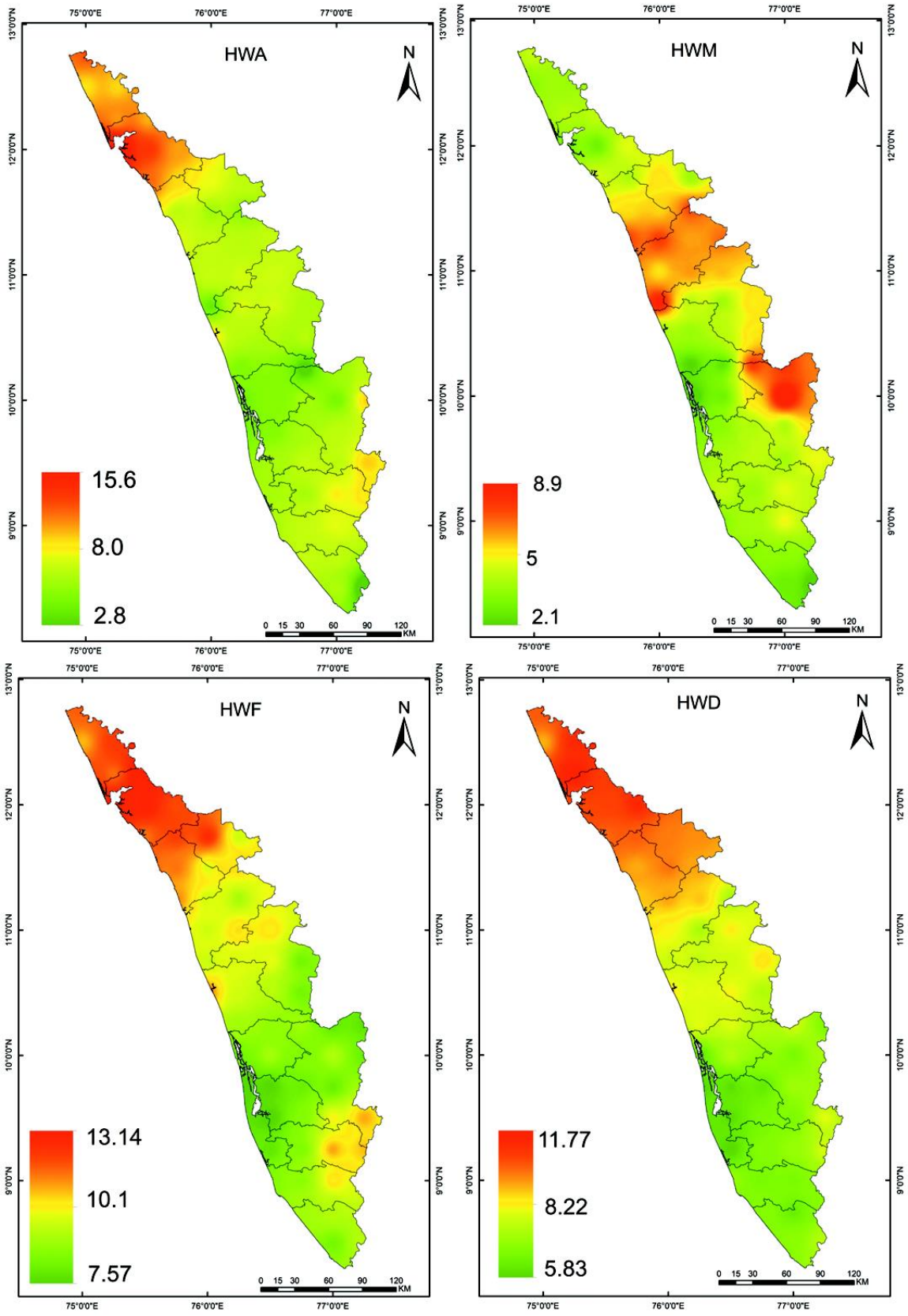

Figure 5.61. Spatial distribution of HW trends from 1951 to 2020 over Kerala

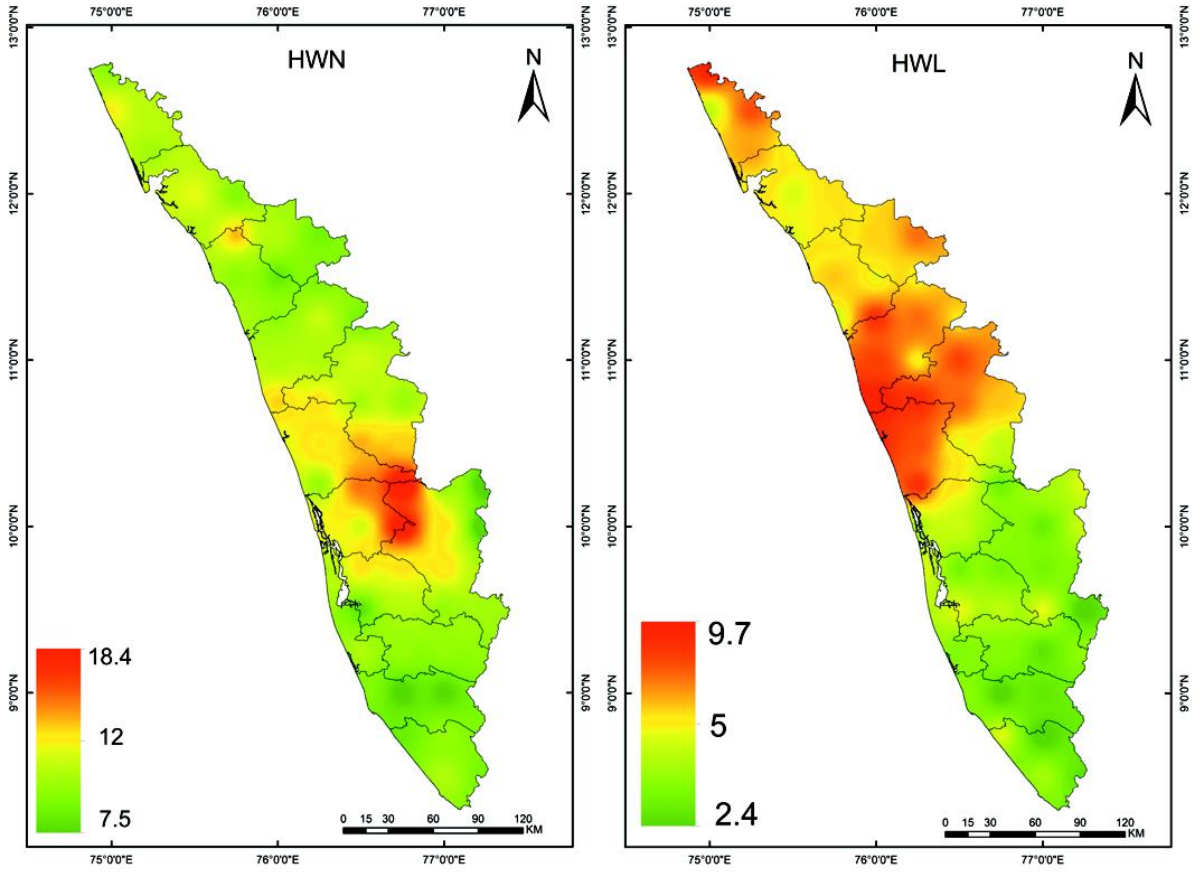

Figure 5.62. Spatial distribution of HW trends from 1951 to 2020 over Kerala

The spatial distribution of HW change trends is illustrated in Figure 5.63 and Figure 5.64. In most of the state, the HWA exhibited a mean upward trend of 0.11°C/decade, whereas HWM exhibited a steadily increasing trend of 0.03 °C/decade. For HWA, the maximum rate of change trends is occurring in the Southern Kerala as well as Palakkad district (0.13 °C/decade), and the least increase is recorded in the Northern and Central regions of the state (0.08°C/decade). In addition to this, an alarming significant trend of 0.13°C per decade in grids located near the Western Ghats is also noted. These all are indications of the increasing severity of HW over the state. The central parts of the state (Thrissur,Palakkad and Alappuzha district) record the highest rate of increase in HWL (1.20 days/decade), followed by grids on the southern coastal sides of the state. These results show HW trends in Kerala have lasted long since 1951. It is important to note that grids in Southern Kerala experience the highest value of HWA and HWN compared to the other parts of the state. Regarding the duration of HW, the mean rate of increase for the occurrence of HWN events in the state is 0.47 events per decade whereas the HWN is increasing at a rate of 0.57 events/ decade in both Northern (Kasargod,Kannur) and Southern Kerala(Thiruvanathapuram,Kollam,Pathanamtitta). However, the increase is slower in Central Kerala at 0.37 events/decade. Central Kerala along with some districts of Northern

Kerala (Calicut,Wayanad,Malappuram) are experiencing an increase in HWD at a rate of 1.8 days/ decade, while in Southern Kerala, the increase is at 1.3 days/ decade.

As observed in Figure 5.63, the mean increasing trend of HWF is 4.6 days/decade in the state. The most significant increase in HWF occurred in Kasargod and Kannur (Northern Kerala), Thrissur (Central Kerala), and Pattanamtitta (Southern Kerala), with a rate of 5.40 days /decade. This indicates an increasing frequency of heat wave events in the state. Besides the frequency and length of heat wave events, it is also noted that HWM and HWA intensified over time. It is concerning to observe a significant increase in HWM and HWA in the Western Ghats. The highest rise of HWM in Kerala is detected in the Western Ghats, escalating at a rate of 0.04°C/decade. Similarly, HWA in the Western Ghats is on the rise, increasing at a rate of 0.13°C/decade. These findings show HW events prolonging and intensifying trends in the study area. HWF days in Southern parts of the state were 5 in 1951 and 73 days registered in 2019. Analysis of the results reveals that HWO exhibited a trend of decreasing duration, with a decline of 2.65 days per decade, indicating the earlier occurrence of HW. Conversely, HWE displayed an increasing trend of 4.6 days per decade, suggesting a delay in the ending date of HW. These trends implied that HW in Kerala became increasingly frequent.

The patterns of heat waves in Kerala are consistent with extreme temperature trend results. These results support the previous studies done in the region (Vijay et al. 2021). It is also noted that the starting date of HW events showed a relatively increasing trend, indicating that they began appearing earlier than in past times. Detailed analysis showed that the ending date of HW events decreased, indicating that the HW's ending got delayed. This is one of the major causes of the delays in the onset of the Indian summer monsoon on the Kerala coast. The results of this study point out that all HW characteristics, including duration (HWL and HWD), frequency (HWN and HWF), and amplitude (HWA and HWM), show intensifying trends in all grid points over the state. There is a minimal number of studies done in India to understand the nature and impact of the heat wave (Bisht et al. 2019; Mishra et al. 2017; Pai et al. 2013; Raghavan 1966; Subbaramayya and Rao 1976). Most of the studies on heat waves are inconsistent in their results due to the selection in the criterion of threshold temperature and inadequate data period. Current study results are in agreement that heat waves are becoming increasingly severe, frequent, and intense in India (Das and Umamahesh 2022; Jaswal et al. 2015; Rohini et al. 2016; Sharma and Mujumdar 2017; Singh et al. 2021).

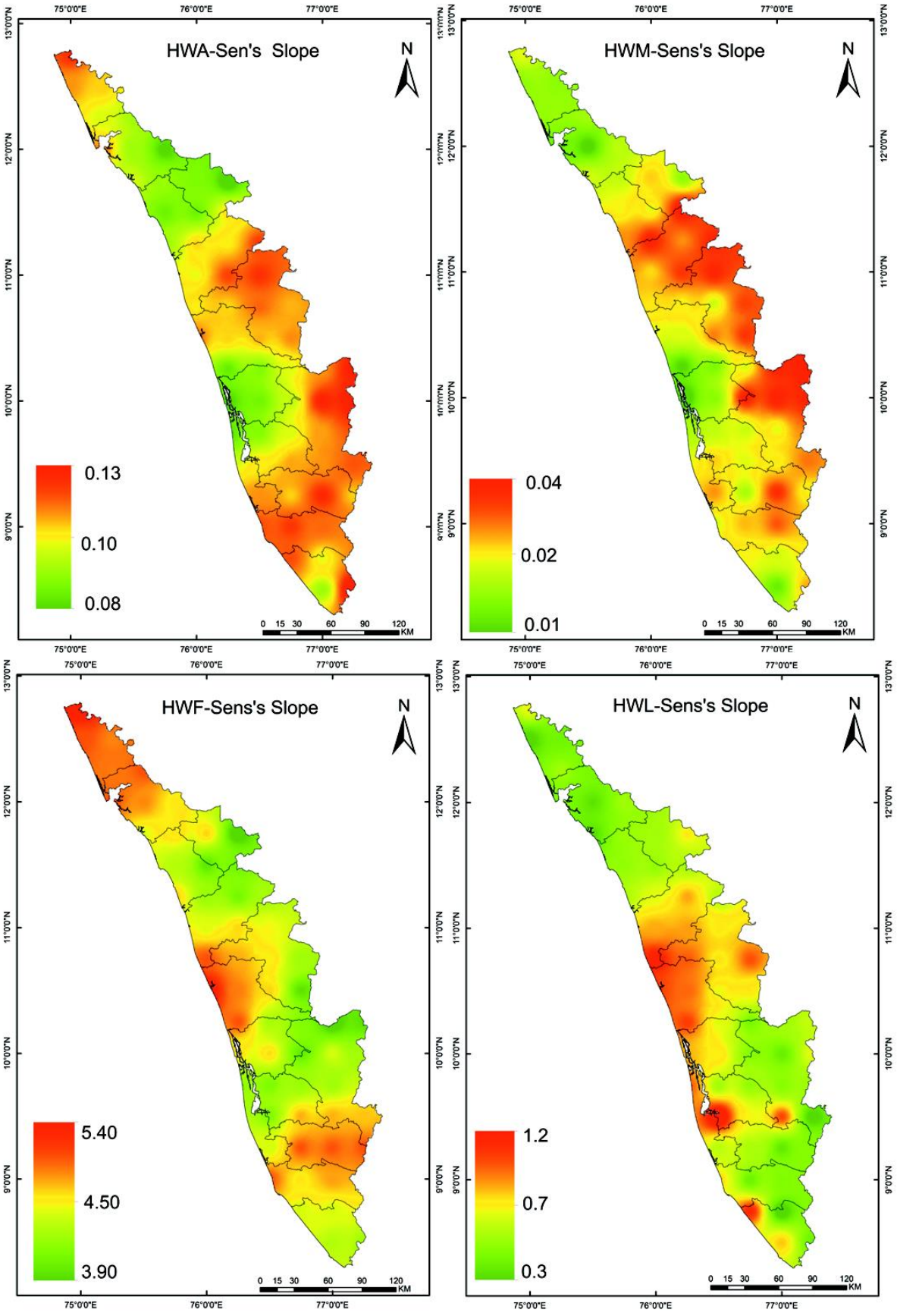

Figure 5.63. Spatial distribution of HW change trends

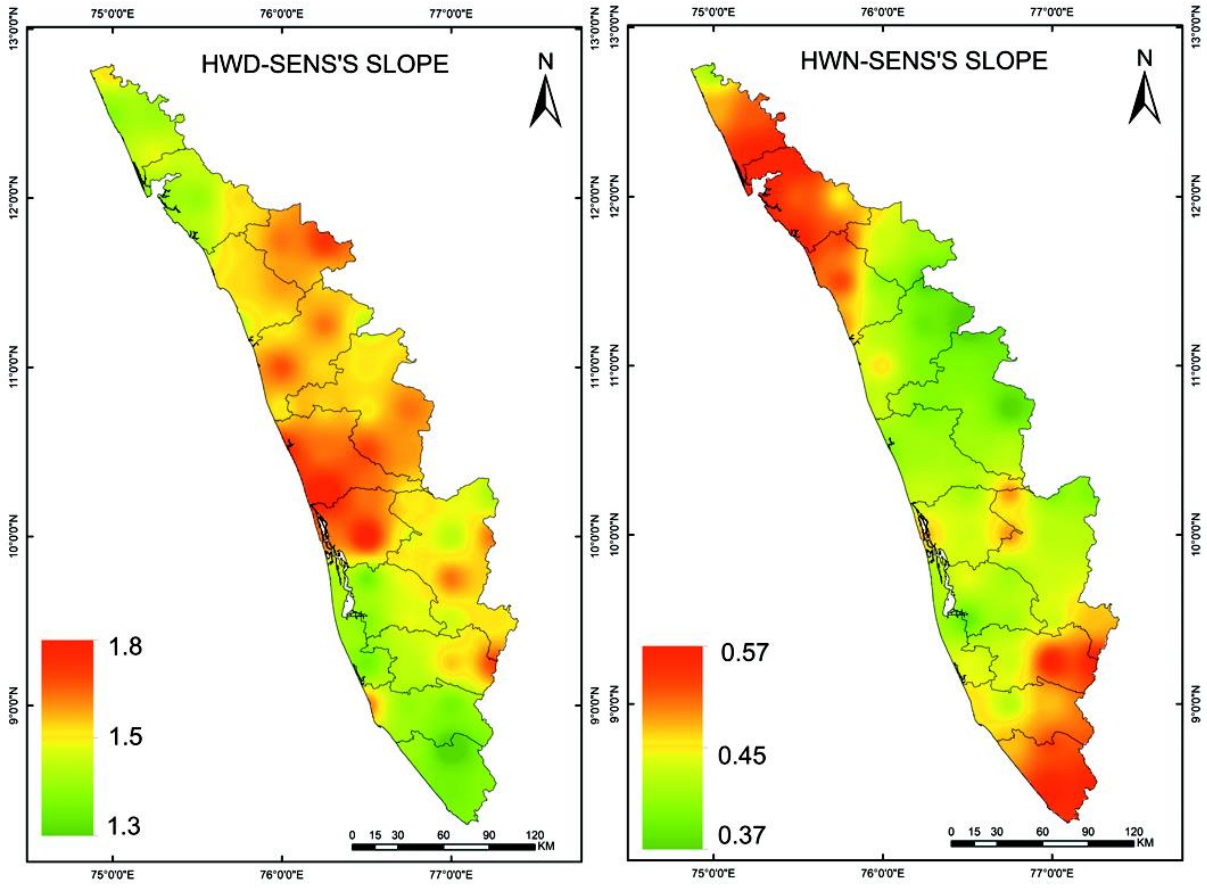

Figure 5.64. Spatial distribution of HW change trends

5.3 URBANIZATION EFFECTS AND THEIR CONTRIBUTION

To estimate the urbanization effects on heat wave characteristics at the local scale, the temporal variation of heat wave occurrence at urban and rural grids in Kerala from 1951 to 2020 is plotted in Figure 5.65. It is observed that heat wave characteristics in urban and rural grids are significantly increasing during the study period. All the HW characteristics in urban grids are more significant than those in rural grids, which shows the intensifying trends of HW characteristics in the urban regions. It is also noted that rural grids show a steeper slope for HWA and HWM than urban grids, which exhibit a steady gradient. The increasing trends in HWF in urban regions are stronger than in rural regions. It is observed that the highest rise in HWN in urban areas are up to 0.57 events/decade, whereas rural area registered an increase of 0.3 events/decade. The rise in HWF in urban areas is 5.40 days/decade, while the trends in rural regions are up to 3 days/decade, which is twice those in urban areas. This shows the pivotal role of urbanization in intensifying HW characteristics. Urban areas show a more

significant increase in HWA than rural regions, with a trend of up to 0.12°C/decade. In contrast, rural areas have a trend of up to 0.08 °C /decade, 1.5 times smaller than urban areas.

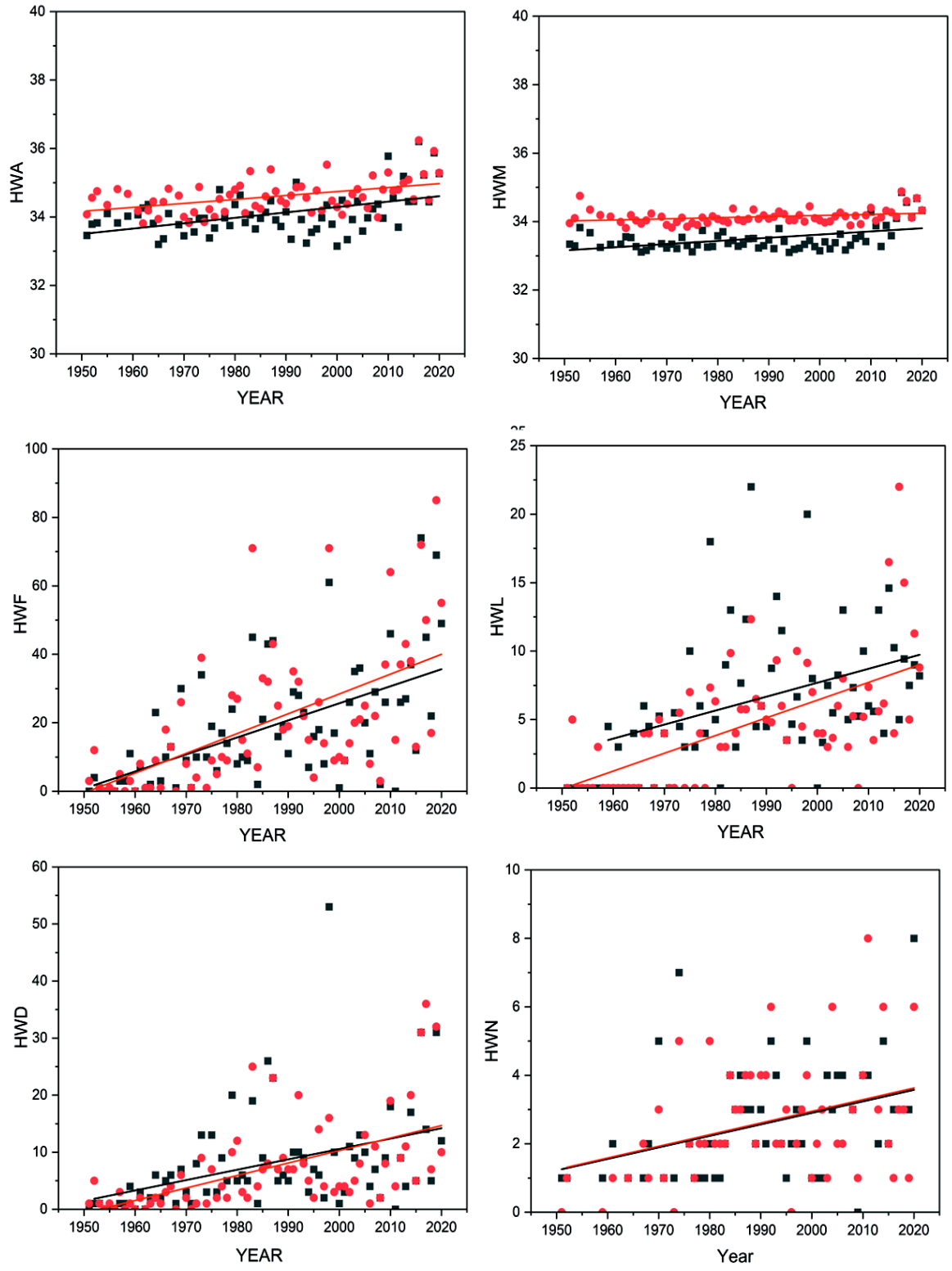

Figure 5.65. Temporal variation of heat waves in the urban and rural grids of Kerala from 1951 to 2020

Similarly, the rise in HWM is up to 0.04 °C /decade in urban areas, while rural regions have a trend of up to 0.02 °C /decade, which is half the trend observed in urban areas. It is essential to note that HWD and HWL exhibit prolonged trends in most urban regions, suggesting a long-lived period of HW in the above-said regions compared to the rural areas. It is observed that in most of the urban grids, HWD exceeded more than one month. Some urban regions registered around 94 total HW days and eight events in 2019 from March to June. Trends of HWD in urban regions (1.82 days/decade) are stronger than those in rural areas (1.3 days/decade). Urban areas exhibit a significantly greater increase in HWL than rural regions, with a trend of up to 1.28 days/decade.In contrast, rural areas show a trend of up to 0.35 days/decade, 3.5 times smaller than those observed in urban areas.

The differences in various characteristics of heat waves between nearby grids can be attributed to the impact of urbanization at the regional level rather than the overall impact of climate change. The effect of urbanization on daytime temperature extremes is more pronounced than on nighttime extremes, which leads to stronger urban-rural contrasts when HW is defined based on maximum temperature. The data analysis reveals that onset date of HW are shifting earlier in urban areas compared to nearby non-urban areas. Conversely, there is a noticeable trend of delayed HW ending dates in urban regions**.** As warming continues, both urban and rural areas will experience more frequent, intense, and longer-lasting HW in the future, with urban regions being more strongly affected. It is worth noting that the years with the highest HWA and HWM coincide with strong El-Nino years (1983, 1998, 2010, 2016, and 2019), highlighting the significant influence of El-Nino on climate extremes.

Table 5.13 shows the urbanization effects on HW characteristics, and it is clear from the results that most grids show a statistically significant positive urbanization effect. The stronger urbanization effect was registered for HWD, HWF, and HWL; the least was marked for HWA. The significant upward trend of HW measures over more than 90% of the state's grids suggests that HW is intensifying. The distribution of the urbanization effect for each HW measure is not uniform across the study area. In Kerala, the urbanization effects on various heat wave characteristics vary across different regions. Central Kerala shows the highest urbanization effects on HWD, HWF, HWL, and HWN. In contrast, the highest urbanization effects on HWA and HWM are observed in Northern Kerala and Central Kerala, where the highest urban population resides. The detailed analysis showed that the increasing trend of HWF in more urbanized areas is higher than in other regions with lower impervious areas. Likewise, HWD

and HWL trends in these regions are also higher than in other areas. This is an indication of the significant influence of urbanization on HW activities. Interestingly, the least urbanization effect is marked in the southern part of the state. Results suggest that HW events in urban land will be more rapid than those in rural lands if warming continues. Urbanization also plays a significant role in advancing the onset date of HW in urban areas compared to surrounding non-urban areas. On the other hand, the delaying trend of the ending date of HW in urban regions is also noted.

Table 5.13 Urbanization effects on trends of HW characteristics at nine urban grids in Kerala

Grid	HWA	HWD	HWF	HWL	HWM	HWN
1	**-0.037**	**-0.65**	**2**	**-0.41**	**-0.01**	0.093
2	**0.062**	**1.43**	**1.9**	**2.41**	**0.021**	**0.238**
3	0.021	**1.35**	**2.3**	**1.4**	**0.03**	0.272
4	0.038	**1.639**	**3.2**	**0.37**	0.027	**0.339**
5	**0.5**	**0.9**	**2**	0.2	**0.7**	**0.1**
6	**0.143**	**1**	**0.9**	**0.22**	**0.022**	0.1
7	**0.1**	**0.8**	**1.6**	**0.0734**	**0.1**	**0.25**
8	**0.026**	**0.8**	**1.9**	0.368	**0.11**	0.21
9	**0.987**	**1.2**	**1.5**	**0.579**	**0.94**	0.287

The contribution of urbanization to six heat wave characteristics at nine grid points is computed and presented in Table 5.14. The results indicate that urbanization had the most significant impact on HWD and HWL, with an average contribution of over 60%. In contrast, the lowest effect was observed for HWF, with an average contribution of 31.78%. The contribution of urbanization to HWD ranges from 47.4% (in Southern Kerala) to 80% (in Northern Kerala), with an average contribution of 61.5%. On the other hand, the contribution of urbanization to HWL ranges from 25% (in Central Kerala) to 100% (in Northern and Southern Kerala), with an average contribution of 71.7%. It is interesting to note that for HWL, some of the grids have reached 100% contribution from urbanization. This shows the pivotal role of urbanization on HW events lasted longer than usual in those regions. It is also seen from the results that both HWA and HWM follow the same trend in urbanization contribution, with a mean value of

40%. The contribution of urbanization to HWA ranges from 17.6% in Southern Kerala to 88.7% in Northern Kerala, with an average contribution of 41.33%.

Similarly, urbanization plays a vital role in HWM, with a contribution ranging from 19.9% in Southern Kerala to 94% in Northern and Central Kerala. The average contribution of urbanization to HWM across the state is 41.34%. The highest urbanization contribution was registered in the northern and central parts of Kerala. The impact of urbanization on heat wave measures in Northern Kerala, with contributions ranging from 19% to 100% and an average of 37%. A thorough examination has unveiled that Kochi, Kannur, and Calicut exhibit the most substantial impact of urbanization on the observed shifts in heat wave charecteristics. Interestingly contribution of urbanization to HW was 17 -100 % for the entire state, which points out the influence of anthropogenic activities on HW events. It is worth mentioning that the contribution of urbanization to all HW measures from 2010 to 2020 was notably higher than in previous periods, indicating a rapid increase in urbanization in Kerala after 2010.

Table 5.14. Urbanization contribution of HW characteristics in nine urban grids

Grids	HWA	HWD	HWF	HWL	HWM	HWN
1	46.3	48.1	10.2	**75.9**	20	48.4
2	40.5	**56.1**	32.8	**100**	27.3	59.5
3	17.6	**51.9**	38.3	**66.7**	37.5	50.7
4	34.5	**72.8**	**58.2**	33.6	45	**84.8**
5	**73.7**	47.4	40	25	**86.4**	25
6	25.7	62.5	20	**100**	19.9	20
7	20	**80**	32	44.1	20	45.5
8	25	**80**	35.8	**100**	22	41.2
9	**88.7**	**54.5**	18.8	**100**	**94**	25.7

Even though many researchers have attempted to study various heat wave characteristics in India, none of them has tried to analyze the role of urbanization on HW characteristics so far. Recent studies reveal the prominent role of urbanization in Heat wave measures in China (Liao et al. 2018; Lin et al. 2018; Wu et al. 2020b, 2021b). Cities with growing infrastructure and large populations will be more vulnerable to heat wave events. The formation of UHI is also considered one of the significant factors for heat wave generation. There is abundant proof that

anthropogenic activities mainly account for the intensification of heat wave events at different spatial scales (Liao et al. 2018; Lin et al. 2018; Luo and Lau 2017; Mishra et al. 2017; Wu et al. 2020b, 2021b). Recent studies in India have also pointed to the country's increasing number of heat wave events. Heat wave occurrence and maintenance are facilitated by the El Niño phenomenon, which strengthens the anticyclone and subtropical high in the western Pacific, and it is observed that heat wave activity tends to increase during the following summer (Luo and Lau 2019). Due to anthropogenic forcing, the twentieth century witnessed a significant increase in heat wave frequency and intensity in India, leading to substantial risks and detrimental effects on human health (Kishore et al. 2022). The heat waves during El Niño years in India exhibit longer durations and higher temperatures, and it caused a delay in the onset of the south-west monsoon (Murari et al. 2016). A study conducted by Saranya et al. 2022 found that marine heat waves have had opposite effects on monsoon rainfall in different parts of India, reducing it over the central sub continent while increasing it over southwest India. The onset of the south-west monsoon varies from year to year. This variability is influenced by the El Niño-Southern Oscillation (ENSO). The delayed onset of the south-west monsoon tends to be associated with warm sea surface temperatures during El Niño events. In contrast, early onsets tend to be related to cool sea surface temperatures during La Niña events (Noska and Misra 2016).

5.4 HEAT WAVE-DROUGHT COMPOUND EVENTS

The spatial variation of the mean fraction of heat wave-drought compounds is illustrated in Figure 5.66. The results showed the frequent occurrence of compound events in the Central and Southern parts of the state, while the fraction was lower in the Northern Kerala. It is important to note that compound events in the state increased significantly after 1985. The mean rate of increase of compound events was 0.20 events/decade. The heat wave analysis showed that the increasing trend of the HW events (0.47 events/decade) is closely associated with the increasing rate of compound events**.** Most grids have marked a significant positive increase at 95% confidence level. Figure 5.66 b and c illustrates the long-term trend analysis test results of compound events and temperature from 1951 to 2020. As it shows, HWA displays statistically significant increasing trends at all 59 grid points during the compound events. Long-term trend analysis of compound events showed a statistically significant increasing trend at all grids in the southern and central parts of the state. In most regions, the number of compound events in Kerala increased from 1 in 1951 to 3 in 2020. Likewise, the

HWA increased remarkably from 1951 to 2020, and the rate of increase of HWA is different in most areas inside the state. In Southern Kerala, the HWA has increased from 33.4°C to 36.15°C. In Central Kerala, it rose from 32.8°C to 34.7°C, while in Northern Kerala, it increased from 32.73°C to 35.25 °C. These trends indicate a significant rise in HWA during compound events across various regions of Kerala over the specified period.

Similarly, the HWM of compound events has increased in various regions of Kerala. In Central Kerala, the value of HWM rose from 32.6°C to 35.18°C, and Southern Kerala witnessed an increase in HWM from 33.4°C to 35.63°C. Likewise, In Northern Kerala, the HWM increased from 32.20°C to 33.93°C. The spatial variation of compound events in Kerala can be attributed to several factors. These include the influence of multiple surface fluxes (Mishra and Singh 2010), which control the occurrence and development of drought and heat waves. The spatial patterns of these fluxes exhibit heterogeneity due to variations in regional precipitation, temperature anomalies, anthropogenic factors, alteration in large-scale climate patterns, and changes in other hydrologic variables (Mukherjee et al. 2020).

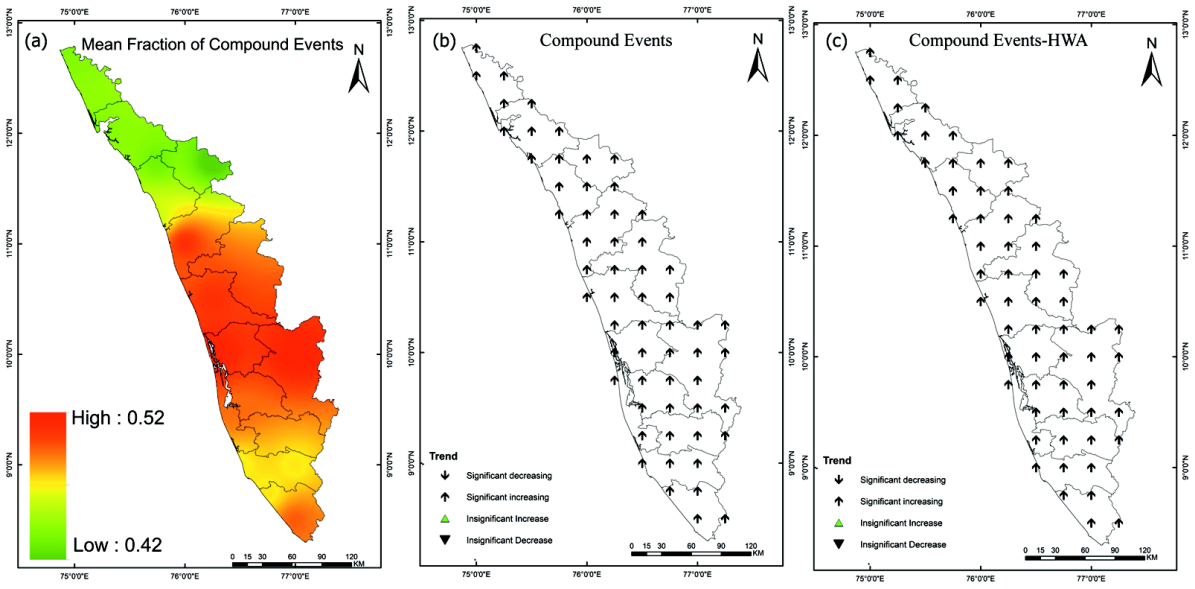

Figure 5.66. (a) Mean fraction of heat wave- drought compound events in Kerala during 1951-2020 (b) trend analysis of compound events (c) trend analysis of HWA

The Sequential Mann-Kendall test is a statistical method employed to estimate the approximate year at which a significant trend initiates within a dataset. The test results graphically showed the upward and backward trend curves of compound events from 1950 to 2020 (Figure 5.67)**.** The analysis revealed more than one change point for most of the grids, and the point at which

the curve falls outside the dotted line indicates the abrupt change in compound events which is significant at 95% confidence level. The majority of the grids showed an abrupt change after 1985. The annual mean occurrence of compound extremes has increased from 0.40 events/year (1951-1985) to 0.60 events/year (1986-2020), indicating a growth of 1.5 times more. It is also important to note that after the abrupt break in 1985, the curve leaned towards a positive trend. The decline in the trend started after 1995 and drastically increased after 2010. The break period in compound events corresponds with the beginning period of Kerala's urbanization. After the breakpoint, the mean rate of HWA increased 2.3 times, rising from 0.06 °C/decade (1951-1985) to 0.14 °C/decade (1986-2020).

The mean rate of HWM has also increased, going from 0.02 °C/decade (1951-1985) to 0.11 °C/decade (1986-2020). These findings strongly suggest that the highest and average temperatures during compound events have experienced a significant increase after the breakpoint. The results indicate that following the change point, both the intensity and occurrence of compound events have increased. Furthermore, it is crucial to understand the role of urbanization in amplifying these compound events as it can have several significant effects that include the UHI effect, changes in local atmospheric conditions, and alterations in the natural ecosystem.

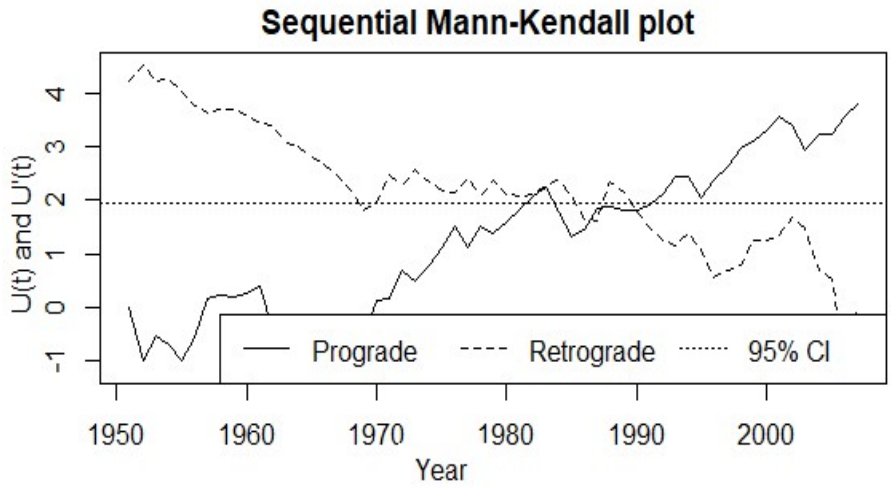

Figure 5.67. Sequential Mann-Kendall test for compound events with progressive trend U(t) and backward trend U´(t)

The two-sample Kolmogorov-Smirnoff test was used to determine the differences in the distribution of compound events between the first half and second half of the periods. The compound events data were divided into two periods based on the results from the sequential

Mann-Kendall test to understand the variations in the frequency of events; 1951 to 1985 and 1986 to 2020. The change was estimated based on the differences in the number of events in 1986 – 2020 relative to 1950 -1985, divided by the total number of events during the study period**.** Various researchers adopted this method to assess the variations in compound events (AghaKouchak et al. 2014; Sharma and Mujumdar 2017; Shi et al. 2021). This study employed empirical cumulative density function (ECDF) to access the changes in the compound events after the abrupt change point relative to the previous time. The ECDFs for HWN of compound events during both periods are illustrated in Figure 5.68.

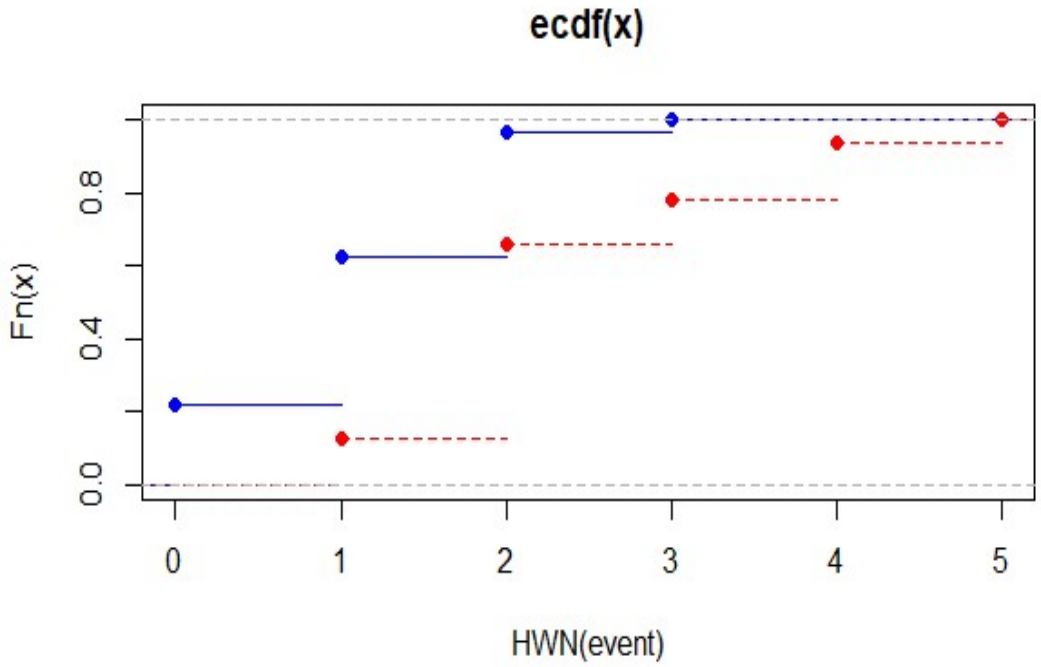

Figure 5.68. The ECDF curve for the HWN of heat wave-drought compound events during 1951-1985(blue line) and 1986-2020 (red line).

The test results show that CDFs of compound events in the second period are substantially different from those in the previous period. The KS test successfully detected statistically significant changes in the occurrence of compound events between two sub-periods at 5% significance level. It is evident from the figure that the upper tail end of 1986-2020 ECDFs had shifted to the right end, proving the increase in the frequency of compound events relative to those in 1951-1985. Results also revealed that compound events during El Niño years were hotter and longer, significantly delaying the onset of the Indian summer monsoon. It is also noted that Previous studies pointed out that large-scale climate oscillation, in particular, ENSO

plays a substantial role in the occurrence of compound events in tropical regions like India (Hao et al. 2018; Mukherjee et al. 2020).

The percentage change of occurrence of compound events, heat waves, and drought during 1986-2020 relative to the base period of 1951-1985 over Kerala state is illustrated in Figure 5.69. The results indicated that the frequency of extreme events is increasing at an alarming rate in Kerala, especially in the southern part of the state. A significant increase of compound extreme events by over 75% was detected in most parts of the state which is a matter of concern. As shown in Figure 5.69, a significant rise of heat wave events by over 85% in southern parts of the state is also noted. The occurrence changes of compound events and heat waves in the southern part of the state were 76.8% and 85.81%, respectively. It is also important to note that changes in drought events are comparatively low concerning other extreme events.

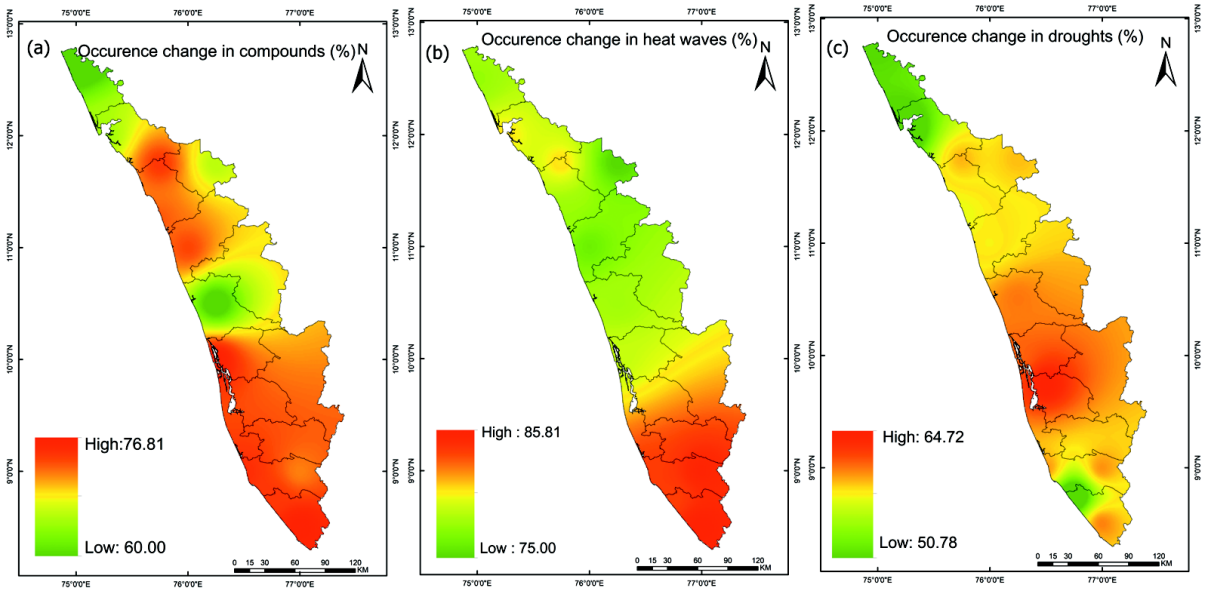

Figure 5.69. Occurrence change in (a) compound events, (b) heat waves, (c) droughts during 1985 – 2020 relative to that during 1951-1985

The results indicated that these events are more frequent in southern and central parts of the state. It is also noted that the intensity of heat waves during the drought period is much higher than in average heat wave conditions, and southern parts of the state registered the highest heat wave intensity in Kerala. This could be attributed to the higher daily maximum temperature variability, especially in the southern region, leading to more temperature threshold exceedance. Compound events and drought events less influence the northern parts of the state than the rest of the state. Results indicated that more than 100% of the grid points with increased compound events also registered an increasing trend in heat wave events. In contrast,

only 55% of the grids reported an increasing trend of compound events accompanied by increased drought events. These analyses suggest that a rising number of heat wave events may be the dominant driving factor of compound extreme events in the state than drought events. The in-depth evaluation of heat wave-drought compound events in Kerala has revealed the amplified severity and duration of heat waves during compound events compared to heat waves. It is seen that HWA and HWM during the compound events were intensified compared to heat wave-alone events. The mean value of HWA was 35.36°C during compound events, while the value was 34.34°C during heat wave events. Likewise, the mean value of HWM in compound events and heat waves were 34.91°C and 33.43 °C, respectively. Compared to heat waves alone, the mean HWA and HWM temperatures during compound events were approximately 1.02°C and 1.48°C higher, respectively. Compared to heat wave-alone events, HWD and HWL last longer during compound events**.** It is also noted that heat wave events lasting more than ten days during compound events occur after 2010 in most parts of the state. Figure 5.70 illustrates the comparison of HWA and HWM between compound events as well as heat wave events.

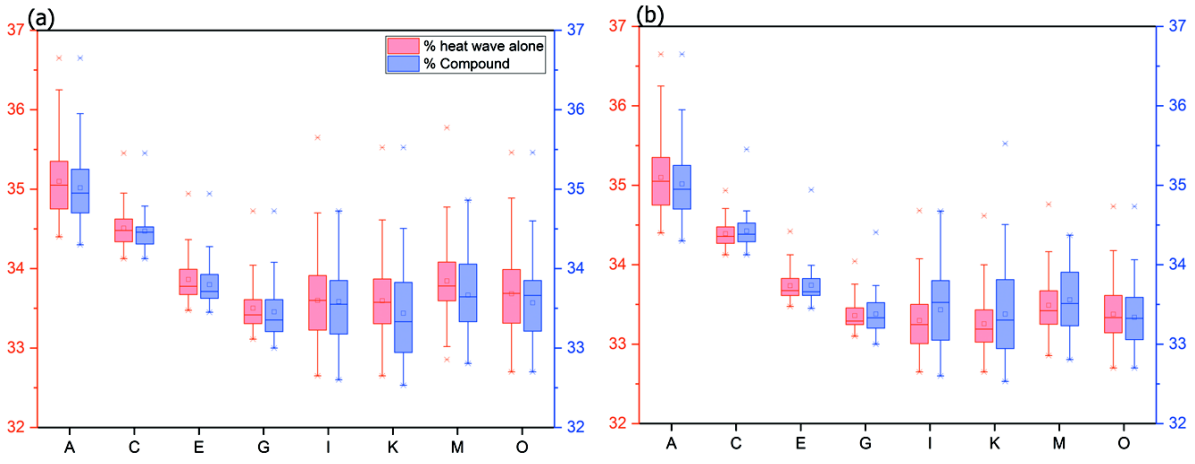

Figure 5.70 a) Comparison of HWA b) HWM between compound events and heat waves

It was found that 48% of the compound events have lasted more than ten days, contrary to 35% in the case of heat waves alone. From 1951 to 2020, there has been a substantial increase in the duration of compound events in most parts of Kerala. The HWD during compound events has risen significantly, escalating from 3 days in 1951 to 34 days in 2020. Similarly, HWL has experienced a notable increase, from 3 days in 1951 to approximately 11.33 days in 2020. Results indicate a pronounced trend towards longer durations for

compound events in Kerala. The data suggests that the region has been encountering more prolonged periods of extreme heat, posing potential challenges and implications for the affected areas.

The primary factor behind the growing prevalence of dry-hot events worldwide has been identified as the escalating temperatures (Das et al. 2022; Feng et al. 2019; Mukherjee et al. 2020). In the current study, the investigation focused on the relationship between the occurrence of compound events and the occurrence of droughts or heat waves individually. The regions experiencing a more significant increase in droughts and heat waves also exhibited a greater increase in compound extremes. Understanding the nonlinear relationship between compound extremes and individual extremes can enhance the predictability of extremes in a changing climate. This understanding also serves as a basis for mitigating the negative effects of compound extremes since their impacts surpass those of individual extremes alone (Shi et al. 2021; Wu et al. 2020a). Mukherjee et al. 2020 established a strong correlation between compound events and El Niño Southern Oscillation (ENSO) in the southern hemisphere, utilizing a Poisson generalized linear model, indicating a connection between compound events and large-scale climate change.

The previous studies on concurrent droughts and heat waves justified these results, indicating a substantial increase in compound events after 1980 (Kripalani et al. 2003; Sharma and Mujumdar 2017). The impact of compound events can be more damaging than their occurrence (Das et al. 2022; Sharma and Mujumdar 2017). So many researchers have attempted to study the effect of compound events on regional as well as global scales since these events can cause significant social and environmental impacts (Das et al. 2022; Kong et al. 2020; Sharma and Mujumdar 2017; Shi et al. 2021; Wang et al. 2020b). Between 1970 and 2019, a significant increase in the frequency of compound extremes was observed in most parts of the world. (Min et al. 2023). Using quantile regression analysis, Kishore et al. 2022 observed a negative correlation between SPI and heat waves, further establishing that drier conditions in India are linked to more intense heat waves. In the near future (2077-2099), there is a projected significant increase in the probability of extreme events over India's western and northern regions. This includes a higher frequency of concurrent droughts and heat waves compared to 2006 to 2030 (Kishore et al. 2022). The results from the current study indicate that the Kerala state has become more prone to heat wave-drought compound events. Considering these compound events is essential when adapting to climate extremes.

5.5 URBANIZATION EFFECT AND CONTRIBUTION

The temporal variation of heat wave-drought compound for urban and rural grids in Kerala from 1951 to 2020 is illustrated in Figure 5.71. Even though it is known that rapid urbanization has a prominent role in local and regional climate under the global warming scenario, the potential impact of the urbanization process on the changes of compound events is never investigated. Results show that urban series generally exhibit steeper slopes for compound events and HWA and HWM during extreme events. It is seen from the analysis that urbanization has a significant impact on compound events. The urban trends for HWA and HWM are 0.20°C/decade and 0.08°C/decade, respectively, while the corresponding rural trends are 0.13°C/decade and 0.05°C/decade respectively, mainly caused by urbanization. Urbanized areas become more prone to the concurrence of heat waves and extended drought events than those surrounding rural areas. The significant regional amplifications of drought and heat wave characteristics observed in this study can be attributed to anthropogenic climate change, as indicated by previous research (Das et al. 2022; Mukherjee and Mishra 2021).

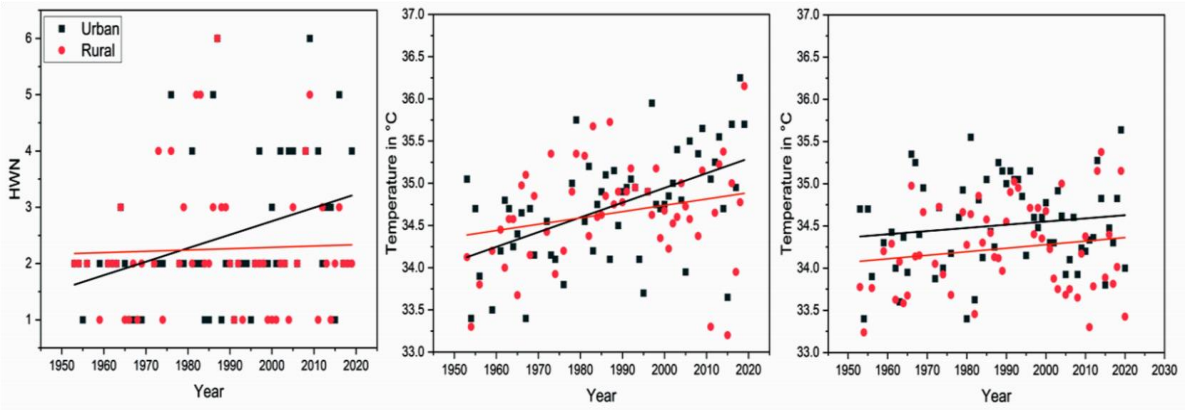

Figure 5.71. Temporal variation of (a) compound events (b) HWA (c) HWM in the urban and rural grids of Kerala –from 1951 to 2020.

Table 5.15 shows the urbanization effects and contribution to compound event characteristics, and it is clear from the results that all grids show a statistically significant positive urbanization effect. The highest rate of urbanization contribution on compound events and HWA was registered at the central part of the state.

Table 5.15. Urbanization effects and contribution of compound events in nine urban grids

Grids	Compound events		HWA		HWM	
	Effect	Contribution	Effect	Contribution	Effect	Contribution
1	**0.02**	64.51	**0.0034**	27.2	**0.004**	41.53
2	0.019	100	0.006	42.85	0.003	55.38
3	**0.014**	87.5	**0.0037**	31.09	**0.0043**	66.22
4	**0.012**	100	**0.008**	76.19	**0.007**	77.5
5	**0.017**	100	**0.0077**	68.5	**0.005**	71.5
6	**0.0086**	100	**0.012**	60	**0.009**	63.4
7	**0.0055**	100	**0.007**	43.75	0.004	50.75
8	**0.0047**	70.8	**0.0064**	44.5	**0.008**	54.9
9	**0.0037**	60.7	**0.0066**	42.8	**0.005**	46.6

The most substantial urbanization effect on compound events was found in the state's central parts, followed by the Northern Kerala, where the highest urban population resides especially in Kollam,Kottayam, Ernamkulam, Thrissur, Malappuram,Calicut, Kannur districts. However, the highest significant influence of urbanization on HWA and HWM was observed in Central Kerala, followed by Northern Kerala. Following an extensive analysis, it has been determined that urban centres including Kochi, Thrissur, Malappuram, Kannur, Kasaragod, and Calicut showcase the most noteworthy influence of urbanization on the observed alterations in HWA and HWM of compound events. Most of the urban grids showed 100% urbanization contribution in increasing the compound events, whereas the average value of urbanization contribution on HWA was 48.6%. This is an indication of the significant influence of urbanization on HW activities. In recent decades, compound events have significantly increased, particularly in areas characterized by large populations and a high level of urbanization (Wu et al. 2021a). Greater increases in the frequency, duration, and intensity of compound events have been observed in most urban areas compared to rural regions(Liao et al. 2021). Without implementing adaptation and mitigation measures, the combination of observed and projected changes in extreme climate events and population and urbanization exert significant pressure on the environment and society.

CHAPTER 6

CONCLUSION

Recent events in Kerala, India, have highlighted the catastrophic impacts of extreme rainfall events, leading to landslides and loss of human lives. This study's primary objective was to understand how urbanization impacts the occurrence of extreme events in Kerala state, India. The study utilized five trend analysis techniques to examine the historical trends of rainfall, rainy days, and temperature. Two standard machine learning techniques were employed on the Google Earth Engine (GEE) platform to investigate the land use and land cover (LULC) dynamics in Kerala state from 1990 to 2020. The study utilized dynamic classification techniques to group the urban and rural grids, leveraging the assistance of Landsat images. The current chapter presents the conclusions derived from the investigation. The key findings from the study are presented sequentially and organized for ease of reference. Additionally, the chapter acknowledges the limitations of the present study and outlines potential avenues for future research.

6.1 SPATIO-TEMPORAL ANALYSIS OF CLIMATIC VARIABLES

The spatial pattern of annual and seasonal rainfall was analyzed by delineating 59 grid points into five clusters through the K-Means algorithm and identifying the influence of geographical and statistical parameters on these clusters by PCA. It is observed that annual mean rainfall is highest in Cluster 1 and Cluster 3 (located in low-altitude areas). In contrast, it remains lowest in Cluster 5 (high-altitude regions) with a high coefficient of variation. Likewise, grids in Cluster 2 are mainly situated towards the northern side of Kerala with high rainfall. In contrast, Cluster 4 is characterized by moderate annual mean rainfall and is located in the region with low altitudes. The declining trend of annual and seasonal rainfall was observed for the entire study area, with the highest in cluster 1 (-4.26 and -3.49 mm/year) and cluster 2 (-5.55 and -4.73 mm/year).

The trend analysis showed that over 83% of the grid points showed decreasing trends (significant and non-significant) in the annual and south-west monsoon rainfall series. However, rainfall during north-east monsoon and winter decreased at more than 90% of the grid points, making it a subject of concern. On the contrary, compared to other seasons, the grid points (69%) corresponding to the decreased rainfall in summer are fewer. Over 30% of

the grid points show an increasing trend in rainfall during the summer season. Trend analysis of rainy days showed that more than 88% of grid points show negative trends, whether significant or non-significant, in annual and south-west monsoon rainy days series. However, in the case of north-east monsoon and winter rainy days, more than 90% of the grid points show a negative trend (both significant and non-significant). These findings indicate the possible occurrence of high-intensity rainfall for a short duration in the cluster 3 and 4. The results of the present study can be correlated to the recent occurrence of extreme rainfall events in the study area.

All trend analysis tests discovered a statistically significant increase in mean and maximum temperature at annual and seasonal scales for all grids. The trend magnitudes in the mean temperature range from 0.1 to 0.2 °C/decade for annual and other seasons, whereas the maximum temperature increases at a rate of 0.2 °C/decade. Similarly, the magnitude of minimum temperature is rising in the annual, south-west monsoon, north-east monsoon, winter, and summer seasons at an extent of 0.1 °C/decade. It is evident from the above results that the climate of the state is significantly changing, which can significantly impact the human health and water resources of the state.

The annual scale of PCI calculated for the state varies from a minimum of 13(moderate concentration) in the southern part of the state to a maximum of 28 (high concentration) in the northern part of the state, which indicates that PCI distribution is not uniform over the state. The value of SI ranges from a minimum of 0.45 in the southern part of Kerala (short dry seasons) to a maximum of 0.95 in the northern parts of the state (long dry season). The rainfall in Cluster 1, 2, and 3 is irregular and total rainfall is concentrated in half of the year.

6.2 SPATIO-TEMPORAL CLASSIFICATION OF LAND USE AND LAND COVER

The LULC dynamics of Kerala state were investigated using two standard machine learning techniques, RF and CART, in the GEE platform from 1990 to 2020. The comparison between the RF and the CART model showed that the RF model outshined the CART with an accuracy of 92.07%, even though the same training and testing points were employed for both models for the respective years. The Overall accuracies and kappa coefficient of the model is higher than the CART. The LULC maps for 1990, 2000, 2013, and 2020 were classified. The results show the urban area's expansion and loss of agricultural fields during the study period. The area of barren lands, as well as water bodies, decreased from 1990 to 2020. The state's urban

area has increased from 613 km^2 (1991) to 1583.03 km^2 (2020). The water bodies declined by 30.15% during the study period, whereas the forest class showed a steady growth (20.85%) throughout the study period. The Vegetation in Kerala state shrunk to 18383.7 km^2 (15.52%) during the last 30 years. The population and subsequent urban sprawl have increased urban areas, adversely affecting the barren vegetation and water bodies. It is important to note that agriculture in the study region has decreased over the years. The growth of the built-up areas reduces the infiltration, leading to increased surface runoff. The current study's findings may have a significant association with rainfall-based natural disasters that have already occurred in the state in 2018, 2019, 2020, and 2021.

6.3 DYNAMIC CLASSIFICATION

The study has utilized a dynamic classification approach to effectively classify urban and rural grids by leveraging time-varying land cover data. By employing LULC mapping, a more precise and comprehensive understanding of the evolving landscape is gained, enabling a thorough analysis of the transformation from rural to urban areas. During the 1990s, there were only four urban grids, making up a mere 6.70% of all grids, while the remaining areas of the state were predominantly classified as forest and rural regions. However, as of 2020, the number of urban grids has risen to 22, constituting a significant increase, with their proportion to the total grids reaching 37.28%. Additionally, the study identified 36 rural grids, but their distribution across the state was uneven, being located at various latitudes and not well spread throughout the region. The classification results reveal a distinct pattern where more urban grids are concentrated in the coastal region of Kerala, while grids near the Western Ghats are predominantly classified as rural.

6.4 EFFECT OF URBANIZATION ON EXTREME CLIMATE EVENTS

The analysis of extreme climate indices in Kerala from 1951 to 2020, at the annual scale using RClimdex and MK-CF1 at a 95% confidence level, reveals that more than 60% of the grids in the region have experienced a decrease in indices such as CWD, R10, R20, R25, RX5 day, PRCPTOT, and SDII, indicating a change in precipitation extremes. In the study period, it was found that 61 to 80% of grid points showed an increasing trend in extreme precipitation indices like R95p, R99p, RX1 day, and R50. The rising incidence of CDD, coupled with a declining number of CWD occurrences in the state, signifies an extended period of drought conditions in Kerala. While most grids in the state have experienced a significant decrease in R10, R20, and R25 values, the grids along the Western Ghats show a distinct trend of increased light

rainfall, indicating a shift towards more frequent occurrences of lighter rain events in this unique region. Kerala is seeing an apparent increase in extreme rainfall events, especially in the Western Ghats and high-altitude portions of Central Kerala, as shown by a significant spike in R50 and RX1 values, with this trend being particularly noticeable after 2010. An increasing trend is observed in the hot extreme temperature indices (TXx, TXn, TNx, TNn, TX90p, TN90p, WSDI, SU35, and TR20), while all cold extreme indices (TX10p, TN10p) demonstrate decreasing trends, indicating a concerning rate of decline in cold extremes alongside the rise in warm extremes. The lower limit of daily minimum and maximum temperature increases faster than the upper limit of daily minimum and maximum temperature. Both warm days and warm nights have shown an increase in their respective percentages in the state, with TX90p experiencing a significant rise from 2.74% to 49.32% and TN90p increasing from 17.53% to 49.33%. Both cold days and cold nights have witnessed significant declines in frequency, with TX10p experiencing a substantial decrease from 16.4% to 3.56% and TN10p showing a significant drop from 7.4% to 0.55%.

In a majority of the grids, the influence of urbanization on extreme rainfall indices was found to be statistically significant, with CDD displaying an adverse effect and indices such as RX1, RX5, SDII, PRCPTOT, R95p, and R99p indicating a positive effect. The results show a statistically significant negative impact of urbanization on light rainfall indices like R10, R20, and R25 on most of the grids in the state, suggesting that urbanization has led to the decrease in light rain in urban areas. Notably, more than 70% of grids exhibit a 100% urbanization contribution to extreme rainfall indices, underscoring the direct impact of urbanization on altering the rainfall regime in urban regions through increased intensity, magnitude, and frequency of extreme events. The comparison between urban and rural grids reveals that the trends in cold temperature extremes show minimal differences in some urban grids. In contrast, significant disparities are observed in warm temperature extremes. This suggests that the impact of urbanization on daytime extremes is more substantial than on nighttime extremes. Urban-induced increasing trends are prevalent in various extreme temperature indices, with the majority of urban grids exhibiting statistically significant positive impacts of urbanization on indices such as WDSI, DTR, SU35, TR20, TX90p, TN90p, TXn, TNx, TNn, and TXx. Conversely, the negative effects of urbanization on TX10p and TN10p are also notable in most urban grids. Notably, the lower limits of maximum and minimum temperature (TXn and TNn) showed a significant urbanization effect, contributing to their rise. Among the climate variables examined, DTR, SU35, TNn, TNx, R20, TX90p, TXn, and TXx exhibited the highest

urbanization contributions, with DTR showing a 100% urbanization contribution in six out of nine urban grids.

6.5 EFFECT OF URBANIZATION ON HEAT WAVES

The long-term trend analysis of HW characteristics from 1951 to 2020 revealed varying increased amplitudes in different regions, with all HW characteristics displaying a statistically significant positive trend at a 95% confidence level throughout the state. Over time, Kerala has witnessed a significant escalation in both the frequency and intensity of heat waves, as indicated by the remarkable increase in HWF from 2 days in 1951 to 72 days in 2019, along with a substantial rise in the HWD from 3 days in 1952 to 35 days in 2019, highlighting their prolonged nature and reinforcing the intensification and severity of such occurrences. Interestingly, the HWO and end date HWE of HW events exhibit advancing and delaying trends suggesting the longer span of HW season. In most of the parts of the state, the HWA exhibited a mean upward trend of 0.11°C/decade, whereas HWM exhibited a steadily increasing trend of 0.030 °C/ decade. These all are indications of the increasing severity of HW over the state.

The study reveals a mean increasing trend of 4.6 days/decade in HWF. It highlights the intensification of HWM and HWA over time, emphasizing the prolonged and intensified nature of heat wave events in the study area. These findings demonstrate intensifying trends in all heat wave characteristics (duration, frequency, and amplitude) across the state, suggesting that urban and rural areas will experience more frequent, intense, and longer-lasting heat waves in the future, with a more substantial impact on urban regions. Additionally, the years with the highest HWA and HWM coincide with strong El-Nino events, underlining the significant influence of El-Nino on climate extremes. The study findings indicate a statistically significant positive urbanization effect on most grids, with stronger impacts observed for HWD, HWF, and HWL than HWA. The upward trend of heat wave measures in over 90% of the grids suggests an intensification of heat waves in the state. Notably, some grids reached a 100% contribution of urbanization to HWL. The contribution of urbanization to heat waves ranged from 17% to 100% across the entire state, indicating the influence of human activities on heat wave events.

6.6 EFFECT OF URBANIZATION ON COMPOUND EVENTS

The spatial variation of the mean fraction of heat wave-drought compounds showed frequent occurrence after 1985 in the Central and Southern parts of Kerala, while the occurrence was

relatively lower in the Northern parts of the state. The mean rate of increase of compound events was 0.20 events/decade, and the analysis of heat waves revealed a closely correlated rising trend (0.47 events/decade), indicating a significant positive increase at a 95% confidence level across most grids. The annual mean occurrence of compound extremes increased from 0.40 events per year (1951-1985) to 0.60 events per year (1986-2020), reflecting a growth of 1.5 times. This break in compound events aligns with the onset of urbanization in Kerala, and following the breakpoint, the mean rate of HWA rose 2.3 times, from 0.06 °C per decade (1951-1985) to 0.14 °C per decade (1986-2020), while the mean rate of HWM also increased from 0.02 °C per decade (1951-1985) to 0.11 °C per decade (1986-2020). The findings indicated that compound events occurring during El Niño years exhibited higher temperatures and longer durations, and they played a significant role in delaying the onset of the Indian summer monsoon.

The analysis of percentage changes in compound events, heat waves, and drought in Kerala during the second half revealed a significant rise of over 75% in compound extreme events over the state, highlighting the alarming trend. Additionally, the intensity of heat waves during the drought period was notably higher than average heat wave conditions, and the southern regions recorded the highest heat wave intensity in Kerala. The results revealed that over 100% of the grid points experiencing increased compound events also exhibited an increasing trend in the heat wave events. In comparison, only 55% of the grids showed a rising trend in compound and increased drought events. These findings suggest that the increasing number of heat wave events might play a more dominant role in driving compound extreme events in the state compared to drought events. The central regions of the state experienced the most pronounced impact of urbanization on compound events, with the Northern Kerala, home to the most significant urban population, following closely. Nearly all urban grids exhibited a 100% contribution to the increase in compound events. In comparison, the average urbanization contribution to HWA stood at 48.6%, emphasizing the substantial influence of urbanization on the occurrence of heatwave activities.

6.7 LIMITATIONS AND FUTURE SCOPE OF THE STUDY

- The current research thoroughly examined the historical trends and spatio-temporal rainfall and temperature variations. Furthermore, there is potential for expanding this study to include projections of future climatic scenarios.

- The current study used the Landsat image series for LULC mapping. The high-resolution satellite image series can be used for detailed mapping.
- The extreme climate events under future LULC and CC scenarios may be investigated.

REFERENCES

Abraham, A., and Kundapura, S. (2022a). "Spatio-temporal Dynamics of Land Use Land Cover Changes and Future Prediction Using Geospatial Techniques." *J. Indian Soc. Remote Sens.*, Springer, 50(11), pp. 2175–2191.

Abraham, A., and Kundapura, S. (2022b). "Evaluating the long-term trends of the climatic variables over three humid tropical basins in Kerala, India." *Arab. J. Geosci.*, Springer, 15(9), pp. 811.

Acharya, T. D., Subedi, A., and Lee, D. H. (2019). "Evaluation of machine learning algorithms for surface water extraction in a Landsat 8 scene of Nepal." *Sensors*, MDPI, 19(12), pp. 2769.

Adarsh, S., and Janga Reddy, M. (2015). "Trend analysis of rainfall in four meteorological subdivisions of southern India using nonparametric methods and discrete wavelet transforms." *Int. J. Climatol.*, Wiley Online Library, 35(6), pp. 1107–1124.

AghaKouchak, A., Cheng, L., Mazdiyasni, O., and Farahmand, A. (2014). "Global warming and changes in risk of concurrent climate extremes: Insights from the 2014 California drought." *Geophys. Res. Lett.*, Wiley Online Library, 41(24), pp. 8847–8852.

Ahmadi, F., Nazeri Tahroudi, M., Mirabbasi, R., Khalili, K., and Jhajharia, D. (2018). "Spatiotemporal trend and abrupt change analysis of temperature in Iran." *Meteorol. Appl.*, 25(2), pp. 314–321.

Ahmed, B., Kamruzzaman, M. D., Zhu, X., Rahman, M., and Choi, K. (2013). "Simulating land cover changes and their impacts on land surface temperature in Dhaka, Bangladesh." *Remote Sens.*, Multidisciplinary Digital Publishing Institute, 5(11), pp. 5969–5998.

Alexander, L. V., Zhang, X., Peterson, T. C., Caesar, J., Gleason, B., Klein Tank, A. M. G., Haylock, M., Collins, D., Trewin, B., and Rahimzadeh, F. (2006). "Global observed changes in daily climate extremes of temperature and precipitation." *J. Geophys. Res. Atmos.*, Wiley Online Library, 111(D5).

Alexander, L. V. (2016). "Global observed long-term changes in temperature and precipitation extremes: a review of progress and limitations in IPCC assessments and beyond." *Weather*

Clim. Extrem., Elsevier, 11, pp. 4–16.

Arowolo, A. O., Deng, X., Olatunji, O. A., and Obayelu, A. E. (2018). "Assessing changes in the value of ecosystem services in response to land-use/land-cover dynamics in Nigeria." *Sci. Total Environ.*, Elsevier, 636, pp. 597–609.

Asfaw, A., Simane, B., Hassen, A., and Bantider, A. (2018). "Variability and time series trend analysis of rainfall and temperature in northcentral Ethiopia: A case study in Woleka sub-basin." *Weather Clim. Extrem.*, Elsevier, 19, pp. 29–41.

Bar, S., Parida, B. R., and Pandey, A. C. (2020). "Landsat-8 and Sentinel-2 based Forest fire burn area mapping using machine learning algorithms on GEE cloud platform over Uttarakhand, Western Himalaya." *Remote Sens. Appl. Soc. Environ.*, Elsevier, 18, pp. 100324.

Barriopedro, D., Fischer, E. M., Luterbacher, J., Trigo, R. M., and Garcia-Herrera, R. A. (2011). "The Hot Summer of 2010: Redrawing the Temperature Record Map of Europe." *Science (80-.).*, 332, pp. 220–224.

Berggren, K., Olofsson, M., Viklander, M., Svensson, G., and Gustafsson, A.-M. (2012). "Hydraulic impacts on urban drainage systems due to changes in rainfall caused by climatic change." *J. Hydrol. Eng.*, American Society of Civil Engineers, 17(1), pp. 92–98.

Bharath, H. A., Chandan, M. C., Vinay, S., and Ramachandra, T. V. (2018). "Modelling urban dynamics in rapidly urbanising Indian cities." *Egypt. J. Remote Sens. Sp. Sci.*, Elsevier, 21(3), pp. 201–210.

Bhutiyani, M. R., Kale, V. S., and Pawar, N. J. (2007). "Long-term trends in maximum, minimum and mean annual air temperatures across the Northwestern Himalaya during the twentieth century." *Clim. Change*, Springer, 85(1–2), pp. 159–177.

Bian, Y., Sun, P., Zhang, Q., Luo, M., and Liu, R. (2022). "Amplification of non-stationary drought to heatwave duration and intensity in eastern China: Spatiotemporal pattern and causes." *J. Hydrol.*, Elsevier, 612, pp. 128154.

Bisht, D. S., Chatterjee, C., Raghuwanshi, N. S., and Sridhar, V. (2018). “Spatio-temporal trends of rainfall across Indian river basins.” *Theor. Appl. Climatol.*, Springer, 132(1–2), pp. 419–436.

Bisht, D. S., Sridhar, V., Mishra, A., Chatterjee, C., and Raghuwanshi, N. S. (2019). “Drought characterization over India under projected climate scenario.” *Int. J. Climatol.*, Wiley Online Library, 39(4), pp. 1889–1911.

Boyaj, A., Dasari, H. P., Hoteit, I., and Ashok, K. (2020). “Increasing heavy rainfall events in south India due to changing land use and land cover.” *Q. J. R. Meteorol. Soc.*, Wiley Online Library, 146(732), pp. 3064–3085.

Breiman, L. (2001). “Random forests.” *Mach. Learn.*, Springer, 45(1), pp. 5–32.

Breiman, L., Friedman, J. H., Olshen, R. A., and Stone, C. J. (1984). “Classification and Regression Trees.”

Burian, S. J., and Shepherd, J. M. (2005). “Effect of urbanization on the diurnal rainfall pattern in Houston.” *Hydrol. Process. An Int. J.*, Wiley Online Library, 19(5), pp. 1089–1103.

Burn, D. H., and Elnur, M. A. H. (2002). “Detection of hydrologic trends and variability.” *J. Hydrol.*, Elsevier, 255(1–4), pp. 107–122.

Caloiero, T., Coscarelli, R., Ferrari, E., and Mancini, M. (2011). “Trend detection of annual and seasonal rainfall in Calabria (Southern Italy).” *Int. J. Climatol.*, Wiley Online Library, 31(1), pp. 44–56.

Cao, W., Zhou, Y., Li, R., Li, X., and Zhang, H. (2021). “Monitoring long-term annual urban expansion (1986–2017) in the largest archipelago of China.” *Sci. Total Environ.*, Elsevier, 776, pp. 146015.

Census. (2001). “Census Commissioner.(2006).” *Census India 2001*.

Census. (2011). “Census of India.”

Chakrabarti, P. G. D. (2001). “Urban crisis in India: New initiatives for sustainable cities.” *Dev. Pract.*, Routledge, 11(2–3), pp. 260–272.

Chapman, S., Watson, J. E. M., Salazar, A., Thatcher, M., and McAlpine, C. A. (2017). "The impact of urbanization and climate change on urban temperatures: a systematic review." *Landsc. Ecol.*, Springer, 32(10), pp. 1921–1935.

Chen, G., Li, X., Liu, X., Chen, Y., Liang, X., Leng, J., Xu, X., Liao, W., Qiu, Y., Wu, Q., and Huang, K. (2020). "Global projections of future urban land expansion under shared socioeconomic pathways." *Nat. Commun.*, 11, pp. 537.

Choudhury, D., Das, K., and Das, A. (2019). "Assessment of land use land cover changes and its impact on variations of land surface temperature in Asansol-Durgapur Development Region." *Egypt. J. Remote Sens. Sp. Sci.*, Elsevier, 22(2), pp. 203–218.

Chu, P.-S., Chen, Y. R., and Schroeder, T. A. (2010). "Changes in precipitation extremes in the Hawaiian Islands in a warming climate." *J. Clim.*, American Meteorological Society, 23(18), pp. 4881–4900.

Chu, Z. Y., and Ren, G. Y. (2005). "Effect of enhanced urban heat island magnitude on average surface air temperature series in Beijing region." *Acta Meteor. Sin*, 63(4), pp. 534–540.

Cyriac, S. (2022). "Dichotomous classification and implications in spatial planning: A case of the Rural-Urban Continuum settlements of Kerala, India." *Land use policy*, Elsevier, 114, pp. 105992.

Dai, A., Zhao, T., and Chen, J. (2018). "Climate change and drought: a precipitation and evaporation perspective." *Curr. Clim. Chang. Reports*, Springer, 4, pp. 301–312.

Das, J., Manikanta, V., and Umamahesh, N. V. (2022). "Population exposure to compound extreme events in India under different emission and population scenarios." *Sci. Total Environ.*, Elsevier, 806, pp. 150424.

Das, J., and Umamahesh, N. V. (2022). "Heat wave magnitude over India under changing climate: Projections from CMIP5 and CMIP6 experiments." *Int. J. Climatol.*, Wiley Online Library, 42(1), pp. 331–351.

Dash, S. K., Kulkarni, M. A., Mohanty, U. C., and Prasad, K. (2009). "Changes in the characteristics of rain events in India." *J. Geophys. Res. Atmos.*, Wiley Online Library,

114(D10).

Dash, Y., Mishra, S. K., and Panigrahi, B. K. (2018). “Rainfall prediction for the Kerala state of India using artificial intelligence approaches.” *Comput. Electr. Eng.*, Elsevier, 70, pp. 66–73.

Deng, K., Yang, S., Ting, M., Zhao, P., and Wang, Z. (2019). “Dominant modes of China summer heat waves driven by global sea surface temperature and atmospheric internal variability.” *J. Clim.*, 32(12), pp. 3761–3775.

Devi, A. B., and Nair, A. M. (2021). “Effects of urbanisation in a shallow coastal aquifer: An integrated GIS-based case study in Cochin, India.” *Groundw. Sustain. Dev.*, Elsevier, 15, pp. 100656.

Devkota, P., Dhakal, S., Shrestha, S., and Shrestha, U. B. (2023). “Land use land cover changes in the major cities of Nepal from 1990 to 2020.” *Environ. Sustain. Indic.*, Elsevier, pp. 100227.

Dey, P., and Mujumdar, P. P. (2019). “On the uniformity of rainfall distribution over India.” *J. Hydrol.*, Elsevier, 578, pp. 124017.

Dhanaraj, K., and Angadi, D. P. (2021). “Urban expansion quantification from remote sensing data for sustainable land-use planning in Mangaluru, India.” *Remote Sens. Appl. Soc. Environ.*, Elsevier, 23, pp. 100602.

Dixit, A., Sahany, S., Rajagopalan, B., and Choubey, S. (2022). “Role of changing land use and land cover (LULC) on the 2018 megafloods over Kerala, India.” *Clim. Res.*, 89, pp. 1–14.

Dong, J., Xiao, X., Menarguez, M. A., Zhang, G., Qin, Y., Thau, D., Biradar, C., and Moore III, B. (2016). “Mapping paddy rice planting area in northeastern Asia with Landsat 8 images, phenology-based algorithm and Google Earth Engine.” *Remote Sens. Environ.*, Elsevier, 185, pp. 142–154.

Dutta, D., Rahman, A., Paul, S. K., and Kundu, A. (2021). “Impervious surface growth and its inter-relationship with vegetation cover and land surface temperature in peri-urban areas

of Delhi.” *Urban Clim.*, Elsevier, 37, pp. 100799.

Eckstein, D., Hutfils, M.-L., and Winges, M. (2018). “Global climate risk index 2019.” *Who Suff. Most from Extrem. Weather events*.

ENVIS. (2021). “Resources: Land – Status of Environment related issues: Kerala ENVIS Centre, Ministry of Environment and Forests, Govt. of India.” *State Environ. Relat. Issues*.

Erumban, A. A., Das, D. K., Aggarwal, S., and Das, P. C. (2019). “Structural change and economic growth in India.” *Struct. Chang. Econ. Dyn.*, 51, pp. 186–202.

Falga, R., and Wang, C. (2022). “The rise of Indian summer monsoon precipitation extremes and its correlation with long-term changes of climate and anthropogenic factors.” *Sci. Rep.*, Springer, 12(1), pp. 1–11.

Feng, S., Hao, Z., Zhang, X., and Hao, F. (2019). “Probabilistic evaluation of the impact of compound dry-hot events on global maize yields.” *Sci. Total Environ.*, Elsevier, 689, pp. 1228–1234.

Feng, X., Porporato, A., and Rodriguez-Iturbe, I. (2013). “Changes in rainfall seasonality in the tropics.” *Nat. Clim. Chang.*, Nature Publishing Group, 3(9), pp. 811–815.

Field, C. B., Barros, V., Stocker, T. F., and Dahe, Q. (2012). *Managing the risks of extreme events and disasters to advance climate change adaptation: special report of the intergovernmental panel on climate change*. Cambridge University Press.

Firoz C, Mohammed and Banerji, Haimanti and Sen, J. (2014). “A Methodology To Define The Typology Of Rural Urban Continuum Settlements In Kerala.” *J. Reg. Dev. Plan.*, 3(1), pp. 49–60.

FSI. (2019). “India state of forest report.” *For. Surv. India*.

Gadgil, M., Krishnan, B. J., Ganeshaiah, K. N., Vijayan, V. S., Borges, R., Sukumar, R., Noronha, L., Nayak, V. S., Subramaniam, D. K., and Varna, R. V. (2011). “Report of the Western Ghats ecology expert panel.” *Submitt. to Minist. Environ. For. Gov. India*.

Gao, T., Xie, L., and Liu, B. (2016). “Association of extreme precipitation over the Yangtze River Basin with global air–sea heat fluxes and moisture transport.” *Int. J. Climatol.*, Wiley Online Library, 36(8), pp. 3020–3038.

Gao, Y., Zhang, J., Yan, F., Leung, L. R., Luo, K., Zhang, Y., and Bell, M. L. (2020). “Nonlinear effect of compound extreme weather events on ozone formation over the United States.” *Weather Clim. Extrem.*, Elsevier, 30, pp. 100285.

George, J. (2020). “Long-term changes in climatic variables over the Bharathapuzha river basin, Kerala, India.” *Theor. Appl. Climatol.*, Springer, 142, pp. 269–286.

Ghatak, D., Zaitchik, B., Hain, C., and Anderson, M. (2017). “The role of local heating in the 2015 Indian Heat Wave.” *Sci. Rep.*, Nature Publishing Group, 7(1), pp. 1–8.

Ghosh, S., Luniya, V., and Gupta, A. (2009). “Trend analysis of Indian summer monsoon rainfall at different spatial scales.” *Atmos. Sci. Lett.*, Wiley Online Library, 10(4), pp. 285–290.

Gogoi, P. P., Vinoj, V., Swain, D., Roberts, G., Dash, J., and Tripathy, S. (2019). “Land use and land cover change effect on surface temperature over Eastern India.” *Sci. Rep.*, Nature Publishing Group UK London, 9(1), pp. 8859.

Goldblatt, R., You, W., Hanson, G., and Khandelwal, A. K. (2016). “Detecting the boundaries of urban areas in india: A dataset for pixel-based image classification in google earth engine.” *Remote Sens.*, MDPI, 8(8), pp. 634.

Gomes, V. C. F., Queiroz, G. R., and Ferreira, K. R. (2020). “An overview of platforms for big earth observation data management and analysis.” *Remote Sens.*, MDPI, 12(8), pp. 1253.

Gong, P., Li, X., Wang, J., Bai, Y., Chen, B., Hu, T., Liu, X., Xu, B., Yang, J., and Zhang, W. (2020). “Annual maps of global artificial impervious area (GAIA) between 1985 and 2018.” *Remote Sens. Environ.*, Elsevier, 236, pp. 111510.

Gorelick, N., Hancher, M., Dixon, M., Ilyushchenko, S., Thau, D., and Moore, R. (2017). “Google Earth Engine: Planetary-scale geospatial analysis for everyone.” *Remote Sens. Environ.*, Elsevier, 202, pp. 18–27.

Goswami, B. N., Venugopal, V., Sengupta, D., Madhusoodanan, M. S., and Xavier, P. K. (2006). "Increasing trend of extreme rain events over India in a warming environment." *Science (80-.).*, American Association for the Advancement of Science, 314(5804), pp. 1442–1445.

Govind, N. R., and Ramesh, H. (2019). "The impact of spatiotemporal patterns of land use land cover and land surface temperature on an urban cool island: a case study of Bengaluru." *Environ. Monit. Assess.*, Springer, 191, pp. 1–20.

Gu, X., Zhang, Q., Singh, V. P., Song, C., Sun, P., and Li, J. (2019). "Potential contributions of climate change and urbanization to precipitation trends across China at national, regional and local scales." *Int. J. Climatol.*, Wiley Online Library, 39(6), pp. 2998–3012.

Guhathakurta, P., and Rajeevan, M. (2008). "Trends in the rainfall pattern over India." *Int. J. Climatol. A J. R. Meteorol. Soc.*, Wiley Online Library, 28(11), pp. 1453–1469.

Guhathakurta, P., Rajeevan, M., Sikka, D. R., and Tyagi, A. (2015). "Observed changes in southwest monsoon rainfall over India during 1901–2011." *Int. J. Climatol.*, 35(8), pp. 1881–1898.

Guhathakurta, P., and Saji, E. (2013). "Detecting changes in rainfall pattern and seasonality index vis-à-vis increasing water scarcity in Maharashtra." *J. Earth Syst. Sci.*, Springer, 122(3), pp. 639–649.

Guo, E., Wang, Y., and Bao, Y. (2020). "Assessing spatiotemporal variation of heat waves during 1961–2016 across mainland China." *Int. J. Climatol.*, Wiley Online Library, 40(6), pp. 3036–3051.

Halder, S., Saha, S. K., Dirmeyer, P. A., Chase, T. N., and Goswami, B. N. (2016). "Investigating the impact of land-use land-cover change on Indian summer monsoon daily rainfall and temperature during 1951–2005 using a regional climate model." *Hydrol. Earth Syst. Sci.*, Copernicus GmbH, 20(5), pp. 1765–1784.

Hamed, K. H., & Rao, A. R. (1998). "A modified Mann-Kendall trend test for autocorrelated data." *J. Hydrol.*, 204(1–4), pp. 182- 196.

Han, L., Yu, X., Xu, Y., Deng, X., Yang, L., Li, Z., Lv, D., and Xiao, M. (2021). “Enhanced Summertime Surface Warming Effects of Long-Term Urbanization in a Humid Urban Agglomeration in China.” *J. Geophys. Res. Atmos.*, Wiley Online Library, 126(21), pp. e2021JD035009.

Hao, L., van Westen, C., Rajaneesh, A., Sajinkumar, K. S., Martha, T. R., and Jaiswal, P. (2022). “Evaluating the relation between land use changes and the 2018 landslide disaster in Kerala, India.” *Catena*, Elsevier, 216, pp. 106363.

Hao, Z., Hao, F., Singh, V. P., and Zhang, X. (2018). “Quantifying the relationship between compound dry and hot events and El Niño–southern Oscillation (ENSO) at the global scale.” *J. Hydrol.*, Elsevier, 567, pp. 332–338.

Hingane, L. S., Rupa Kumar, K., and Ramana Murty, B. V. (1985). “Long-term trends of surface air temperature in India.” *J. Climatol.*, Wiley Online Library, 5(5), pp. 521–528.

Huang, H., Chen, Y., Clinton, N., Wang, J., Wang, X., Liu, C., Gong, P., Yang, J., Bai, Y., and Zheng, Y. (2017). “Mapping major land cover dynamics in Beijing using all Landsat images in Google Earth Engine.” *Remote Sens. Environ.*, Elsevier, 202, pp. 166–176.

Huang, J., Fatichi, S., Mascaro, G., Manoli, G., and Peleg, N. (2022). “Intensification of sub-daily rainfall extremes in a low-rise urban area.” *Urban Clim.*, Elsevier, 42, pp. 101124.

Huang, S., Gan, Y., Zhang, X., Chen, N., Wang, C., Gu, X., Ma, J., and Niyogi, D. (2023). “Urbanization amplified asymmetrical changes of rainfall and exacerbated drought: Analysis over five urban agglomerations in the Yangtze River Basin, China.” *Earth’s Futur.*, Wiley Online Library, 11(2), pp. e2022EF003117.

Hunt, K. M. R., and Menon, A. (2020). “The 2018 Kerala floods: a climate change perspective.” *Clim. Dyn.*, Springer, 54(3–4), pp. 2433–2446.

IMD. (2020). *Statement on Climate of India during 2022,INDIA METEOROLOGICAL DEPARTMENT Climate Research and Services (CRS)*.

IMD. (2021). *Statement on Climate of India during 2021*.

IPCC, 2012: Managing the Risks of Extreme Events and Disasters to, The, A. C. C. A. S. R.

of, and Change., I. P. on C. (n.d.). “No Title.” *Cambridge Univ. Press. 582 pp*.

Jain, S. K., and Kumar, V. (2012). “Trend analysis of rainfall and temperature data for India.” *Curr. Sci.*, JSTOR, pp. 37–49.

Jain, S. K., Kumar, V., and Saharia, M. (2013). “Analysis of rainfall and temperature trends in northeast India.” *Int. J. Climatol.*, Wiley Online Library, 33(4), pp. 968–978.

Jaswal, A. K., Rao, P. C. S., and Singh, V. (2015). “Climatology and trends of summer high temperature days in India during 1969–2013.” *J. Earth Syst. Sci.*, Springer, 124(1), pp. 1–15.

Jhajharia, D., and Singh, V. P. (2011). “Trends in temperature, diurnal temperature range and sunshine duration in Northeast India.” *Int. J. Climatol.*, Wiley Online Library, 31(9), pp. 1353–1367.

John, D. A., and Babu, G. R. (2021). “Lessons from the aftermaths of green revolution on food system and health.” *Front. Sustain. food Syst.*, Frontiers Media SA, 5, pp. 644559.

Kalnay, E., and Cai, M. (2003). “Impact of urbanization and land-use change on climate.” *Nature*, 423(6939), pp. 528–531.

Kanellopoulou, E. A. (2002). “Spatial distribution of rainfall seasonality in Greece.” *Weather*, Wiley Online Library, 57(6), pp. 215–219.

Kang, C., Luo, Z., Zong, W., and Hua, J. (2021). “Impacts of Urbanization on Variations of Extreme Precipitation over the Yangtze River Delta.” *Water*, Multidisciplinary Digital Publishing Institute, 13(2), pp. 150.

Kaur, R., and Pandey, P. (2021). “Air pollution, climate change, and human health in Indian cities: a brief review.” *Front. Sustain. Cities*, Frontiers Media SA, 3, pp. 705131.

Kendall, M. G. (1975). “Rank correlation measures, Vol. 202.” *Charles Griffin, London*, pp. 15.

Kennedy, C., Stewart, I., Facchini, A., Cersosimo, I., Mele, R., Chen, B., Uda, M., Kansal, A., Chiu, A., Kim, K.-G., Dubeux, C., La Rovere, E., Cunha, B., Pincetl, S., Keirstead, J.,

Barles, S., Pusaka, S., Gunawan, J., Adegbile, M., and Şahin, A. (2015). “Energy and material flows of megacities.” *Proc. Natl. Acad. Sci. U. S. A.*, 112.

Kishore, P., Basha, G., Venkat Ratnam, M., AghaKouchak, A., Sun, Q., Velicogna, I., and Ouarda, T. (2022). “Anthropogenic influence on the changing risk of heat waves over India.” *Sci. Rep.*, Nature Publishing Group UK London, 12(1), pp. 3337.

Kishtawal, C. M., Niyogi, D., Tewari, M., Pielke Sr, R. A., and Shepherd, J. M. (2010). “Urbanization signature in the observed heavy rainfall climatology over India.” *Int. J. Climatol.*, Wiley Online Library, 30(13), pp. 1908–1916.

Kogo, B. K., Kumar, L., and Koech, R. (2021). “Analysis of spatio-temporal dynamics of land use and cover changes in Western Kenya.” *Geocarto Int.*, Taylor & Francis, 36(4), pp. 376–391.

Kong, Q., Guerreiro, S. B., Blenkinsop, S., Li, X.-F., and Fowler, H. J. (2020). “Increases in summertime concurrent drought and heatwave in Eastern China.” *Weather Clim. Extrem.*, Elsevier, 28, pp. 100242.

Kothawale, D. R., Revadekar, J. V, and Kumar, K. R. (2010). “Recent trends in pre-monsoon daily temperature extremes over India.” *J. earth Syst. Sci.*, Springer, 119(1), pp. 51–65.

Kripalani, R. H., Kulkarni, A., Sabade, S. S., and Khandekar, M. L. (2003). “Indian monsoon variability in a global warming scenario.” *Nat. hazards*, Springer, 29(2), pp. 189–206.

Krishnakumar, K. N., Prasada Rao, G. S. L. H. V, and Gopakumar, C. S. (2009a). “Rainfall trends in twentieth century over Kerala, India.” *Atmos. Environ.*, Elsevier Ltd, 43(11), pp. 1940–1944.

Krishnakumar, K. N., Rao, G. P., and Gopakumar, C. S. (2009b). “Rainfall trends in twentieth century over Kerala, India.” *Atmos. Environ.*, Elsevier, 43(11), pp. 1940–1944.

Krishnamurthy, V., and Shukla, J. (2000). “Intraseasonal and interannual variability of rainfall over India.” *J. Clim.*, 13(24), pp. 4366–4377.

Kruger, A. C., and Shongwe, S. (2004). “Temperature trends in South Africa: 1960–2003.” *Int. J. Climatol.*, 24(15), pp. 1929–1945.

Kulithalai Shiyam Sundar, P., and Deka, P. C. (2022). “Spatio-temporal classification and prediction of land use and land cover change for the Vembanad Lake system, Kerala: a machine learning approach.” *Environ. Sci. Pollut. Res.*, Springer, 29(57), pp. 86220–86236.

Kumar, B. M. (2006). “Land use in Kerala: changing scenarios and shifting paradigms.” *J. Trop. Agric.*, 43, pp. 1–12.

Kumar, B. M., and Nair, P. K. R. (2004). “The enigma of tropical homegardens.” *New Vistas Agrofor. A Compend. 1st World Congr. Agroforestry, 2004*, Springer, 135–152.

Kumar, R., Mishra, V., Buzan, J., Kumar, R., Shindell, D., and Huber, M. (2017). “Dominant control of agriculture and irrigation on urban heat island in India.” *Sci. Rep.*, Nature Publishing Group UK London, 7(1), pp. 14054.

Kumar, S., Chanda, K., and Pasupuleti, S. (2020). “Spatiotemporal analysis of extreme indices derived from daily precipitation and temperature for climate change detection over India.” *Theor. Appl. Climatol.*, Springer, pp. 1–15.

Kumar, V., Jain, S. K., and Singh, Y. (2010). “Analysis of long-term rainfall trends in India.” *Hydrol. Sci. Journal–Journal des Sci. Hydrol.*, Taylor & Francis, 55(4), pp. 484–496.

Lal, P., and Nair, S. B. (2017). “Urbanization in Kerala—what does the census data reveal?” *Indian J. Hum. Dev.*, SAGE Publications Sage India: New Delhi, India, 11(3), pp. 356–386.

Lau, N.-C., and Nath, M. J. (2014). “Model simulation and projection of European heat waves in present-day and future climates.” *J. Clim.*, American Meteorological Society, 27(10), pp. 3713–3730.

Lei, C., Yu, Z., Sun, X., Wang, Y., Yuan, J., Wang, Q., Han, L., and Xu, Y. (2023). “Urbanization effects on intensifying extreme precipitation in the rapidly urbanized Tai Lake Plain in East China.” *Urban Clim.*, Elsevier, 47, pp. 101399.

Li, Y., Fowler, H. J., Argüeso, D., Blenkinsop, S., Evans, J. P., Lenderink, G., Yan, X., Guerreiro, S. B., Lewis, E., and Li, X. (2020). “Strong intensification of hourly rainfall

extremes by urbanization.” *Geophys. Res. Lett.*, Wiley Online Library, 47(14), pp. e2020GL088758.

Li, Z., and Gao, Y. (2022). “Impact of Interaction between Metropolitan Area and Shallow Lake on Daily Extreme Precipitation over Eastern China.” *Atmosphere (Basel).*, MDPI, 13(2), pp. 306.

Liao, W., Li, D., Malyshev, S., Shevliakova, E., Zhang, H., and Liu, X. (2021). “Amplified increases of compound hot extremes over urban land in China.” *Geophys. Res. Lett.*, Wiley Online Library, 48(6), pp. e2020GL091252.

Liao, W., Liu, X., Li, D., Luo, M., Wang, D., Wang, S., Baldwin, J., Lin, L., Li, X., and Feng, K. (2018). “Stronger contributions of urbanization to heat wave trends in wet climates.” *Geophys. Res. Lett.*, Wiley Online Library, 45(20), pp. 11–310.

Liao, W., Wang, D., Liu, X., Wang, G., and Zhang, J. (2016). “Estimated influence of urbanization on surface warming in Eastern China using time-varying land use data.” *Int. J. Climatol.*, 37.

Lin, L., Gao, T., Luo, M., Ge, E., Yang, Y., Liu, Z., Zhao, Y., and Ning, G. (2020). “Contribution of urbanization to the changes in extreme climate events in urban agglomerations across China.” *Sci. Total Environ.*, Elsevier, 744, pp. 140264.

Lin, L., Ge, E., Liu, X., Liao, W., and Luo, M. (2018). “Urbanization effects on heat waves in Fujian Province, Southeast China.” *Atmos. Res.*, Elsevier, 210, pp. 123–132.

Liu, J., and Niyogi, D. (2019). “Meta-analysis of urbanization impact on rainfall modification.” *Sci. Rep.*, Springer, 9(1), pp. 1–14.

Liu, W., Zhan, J., Zhao, F., Yan, H., Zhang, F., and Wei, X. (2019). “Impacts of urbanization-induced land-use changes on ecosystem services: A case study of the Pearl River Delta Metropolitan Region, China.” *Ecol. Indic.*, Elsevier, 98, pp. 228–238.

Liu, X., Hu, G., Chen, Y., Li, X., Xu, X., Li, S., Pei, F., and Wang, S. (2018). “High-resolution multi-temporal mapping of global urban land using Landsat images based on the Google Earth Engine Platform.” *Remote Sens. Environ.*, Elsevier, 209, pp. 227–239.

Liu, X., Huang, Y., Xu, X., Li, X., Li, X., Ciais, P., Lin, P., Gong, K., Ziegler, A. D., and Chen, A. (2020). "High-spatiotemporal-resolution mapping of global urban change from 1985 to 2015." *Nat. Sustain.*, Nature Publishing Group, 3(7), pp. 564–570.

Lu, M., Xu, Y., Shan, N., Wang, Q., Yuan, J., and Wang, J. (2019). "Effect of urbanisation on extreme precipitation based on nonstationary models in the Yangtze River Delta metropolitan region." *Sci. Total Environ.*, Elsevier, 673, pp. 64–73.

Luber, G., and McGeehin, M. (2008). "Climate change and extreme heat events." *Am. J. Prev. Med.*, Elsevier, 35(5), pp. 429–435.

De Luis, M., Gonzalez-Hidalgo, J. C., Brunetti, M., and Longares, L. A. (2011). "Precipitation concentration changes in Spain 1946-2005." *Nat. Hazards Earth Syst. Sci.*, Copernicus GmbH, 11(5), pp. 1259.

De Luis, M., Raventós, J., González-Hidalgo, J. C., Sánchez, J. R., and Cortina, J. (2000). "Spatial analysis of rainfall trends in the region of Valencia (East Spain)." *Int. J. Climatol. A J. R. Meteorol. Soc.*, Wiley Online Library, 20(12), pp. 1451–1469.

Luo, M., and Lau, N.-C. (2017). "Heat waves in southern China: Synoptic behavior, long-term change, and urbanization effects." *J. Clim.*, American Meteorological Society, 30(2), pp. 703–720.

Luo, M., and Lau, N.-C. (2019). "Amplifying effect of ENSO on heat waves in China." *Clim. Dyn.*, Springer, 52(5–6), pp. 3277–3289.

Luo, M., and Lau, N.-C. (2021). "Increasing Human-Perceived Heat Stress Risks Exacerbated by Urbanization in China: A Comparative Study Based on Multiple Metrics." *Earth's Futur.*, 9.

Luo, Z., Liu, J., Zhang, Y., Zhou, J., Yu, Y., and Jia, R. (2021). "Spatiotemporal characteristics of urban dry/wet islands in China following rapid urbanization." *J. Hydrol.*, Elsevier, 601, pp. 126618.

Machiwal, D., Gupta, A., Jha, M. K., and Kamble, T. (2019). "Analysis of trend in temperature and rainfall time series of an Indian arid region: comparative evaluation of salient

techniques.” *Theor. Appl. Climatol.*, Springer, 136(1–2), pp. 301–320.

MacQueen, J. (1967). “Some methods for classification and analysis of multivariate observations.” *Proc. fifth Berkeley Symp. Math. Stat. Probab.*, Oakland, CA, USA, 281–297.

Mahmood, R., Pielke Sr, R. A., Hubbard, K. G., Niyogi, D., Dirmeyer, P. A., McAlpine, C., Carleton, A. M., Hale, R., Gameda, S., and Beltrán-Przekurat, A. (2014). “Land cover changes and their biogeophysical effects on climate.” *Int. J. Climatol.*, Wiley Online Library, 34(4), pp. 929–953.

Malik, N., Bookhagen, B., and Mucha, P. J. (2016). “Spatiotemporal patterns and trends of Indian monsoonal rainfall extremes.” *Geophys. Res. Lett.*, Wiley Online Library, 43(4), pp. 1710–1717.

Manalo, J. A., Matsumoto, J., Takahashi, H. G., Villafuerte, M. Q., Olaguera, L. M. P., Ren, G., and Cinco, T. A. (2022). “The effect of urbanization on temperature indices in the Philippines.” *Int. J. Climatol.*, Wiley Online Library, 42(2), pp. 850–867.

Mann, H. B. (1945). “Nonparametric tests against trend.” *Econom. J. Econom. Soc.*, JSTOR, pp. 245–259.

Marelle, L., Myhre, G., Steensen, B. M., Hodnebrog, Ø., Alterskjær, K., and Sillmann, J. (2020). “Urbanization in megacities increases the frequency of extreme precipitation events far more than their intensity.” *Environ. Res. Lett.*, IOP Publishing, 15(12), pp. 124072.

Martinez, C. J., Maleski, J. J., and Miller, M. F. (2012). “Trends in precipitation and temperature in Florida, USA.” *J. Hydrol.*, Elsevier, 452, pp. 259–281.

McGrane, S. J. (2016). “Impacts of urbanisation on hydrological and water quality dynamics, and urban water management: a review.” *Hydrol. Sci. J.*, Taylor & Francis, 61(13), pp. 2295–2311.

McLennan, M. (2021). “The Global Risks Report 2021 16th Edition.” World Economic Forum Cologny, Switzerland.

Meng, X., Gao, X., Li, S., Li, S., and Lei, J. (2021). “Monitoring desertification in Mongolia based on Landsat images and Google Earth Engine from 1990 to 2020.” *Ecol. Indic.*, Elsevier, 129, pp. 107908.

Miller, J. D., and Hutchins, M. (2017). “The impacts of urbanisation and climate change on urban flooding and urban water quality: A review of the evidence concerning the United Kingdom.” *J. Hydrol. Reg. Stud.*, Elsevier, 12, pp. 345–362.

Miller, J. D., Kim, H., Kjeldsen, T. R., Packman, J., Grebby, S., and Dearden, R. (2014). “Assessing the impact of urbanization on storm runoff in a peri-urban catchment using historical change in impervious cover.” *J. Hydrol.*, Elsevier, 515, pp. 59–70.

Min, R., Gu, X., Guan, Y., and Zhang, X. (2023). “Increasing likelihood of global compound hot-dry extremes from temperature and runoff during the past 120 years.” *J. Hydrol.*, Elsevier, 621, pp. 129553.

Mishra, A. K., and Singh, V. P. (2010). “A review of drought concepts.” *J. Hydrol.*, Elsevier, 391(1–2), pp. 202–216.

Mishra, V., Aaadhar, S., Shah, H., Kumar, R., Pattanaik, D. R., and Tiwari, A. D. (2018). “The Kerala flood of 2018: combined impact of extreme rainfall and reservoir storage.” Copernicus GmbH.

Mishra, V., Mukherjee, S., Kumar, R., and Stone, D. A. (2017). “Heat wave exposure in India in current, 1.5 C, and 2.0 C worlds.” *Environ. Res. Lett.*, IOP Publishing, 12(12), pp. 124012.

Mishra, V., and Shah, H. L. (2018). “Hydroclimatological perspective of the Kerala flood of 2018.” *J. Geol. Soc. India*, Springer, 92, pp. 645–650.

Mishra, V., Thirumalai, K., Singh, D., and Aadhar, S. (2020). “Future exacerbation of hot and dry summer monsoon extremes in India.” *Npj Clim. Atmos. Sci.*, Nature Publishing Group, 3(1), pp. 1–9.

Mohan, M., and Kandya, A. (2015). “Impact of urbanization and land-use/land-cover change on diurnal temperature range: A case study of tropical urban airshed of India using remote

sensing data." *Sci. Total Environ.*, Elsevier, 506, pp. 453–465.

Mohanty, A. (2020). "Preparing India for Extreme Climate Events." Council on Energy, Environment and Water (CEEW).

Mondal, A., Khare, D., and Kundu, S. (2015). "Spatial and temporal analysis of rainfall and temperature trend of India." *Theor. Appl. Climatol.*, Springer, 122(1–2), pp. 143–158.

Mondal, A., and Mujumdar, P. P. (2015). "Modeling non-stationarity in intensity, duration and frequency of extreme rainfall over India." *J. Hydrol.*, Elsevier, 521, pp. 217–231.

Mondal, P. P., and Zhang, Y. (2018). "Research progress on changes in land use and land cover in the western Himalayas (India) and effects on ecosystem services." *Sustainability*, MDPI, 10(12), pp. 4504.

Mora, C., Dousset, B., Caldwell, I. R., Powell, F. E., Geronimo, R. C., Bielecki, C. R., Counsell, C. W. W., Dietrich, B. S., Johnston, E. T., and Louis, L. V. (2017). "Global risk of deadly heat." *Nat. Clim. Chang.*, Nature Publishing Group, 7(7), pp. 501–506.

Mukherjee, S., Aadhar, S., Stone, D., and Mishra, V. (2018). "Increase in extreme precipitation events under anthropogenic warming in India." *Weather Clim. Extrem.*, Elsevier, 20, pp. 45–53.

Mukherjee, S., Ashfaq, M., and Mishra, A. K. (2020). "Compound drought and heatwaves at a global scale: The role of natural climate variability-associated synoptic patterns and land-surface energy budget anomalies." *J. Geophys. Res. Atmos.*, Wiley Online Library, 125(11), pp. e2019JD031943.

Mukherjee, S., and Mishra, A. K. (2021). "Increase in compound drought and heatwaves in a warming world." *Geophys. Res. Lett.*, Wiley Online Library, 48(1), pp. e2020GL090617.

Mukherjee, S., and Mishra, V. (2018). "A sixfold rise in concurrent day and night-time heatwaves in India under 2 C warming." *Sci. Rep.*, Springer, 8(1), pp. 1–9.

Murari, K. K., Sahana, A. S., Daly, E., and Ghosh, S. (2016). "The influence of the El N iño Southern Oscillation on heat waves in India." *Meteorol. Appl.*, Wiley Online Library, 23(4), pp. 705–713.

Myhre, G., Shindell, D., Bréon, F.-M., Collins, W., Fuglestvedt, J.,Huang, J., Koch, D., Lamarque, J.-F., Lee, D., Mendoza, B., Nakajima, T., Robock, A., Stephens, G., Takemura, T. and Zhang, H. (2013). "No Title." *Clim. Chang. 2013 Phys. Sci. basis. Contrib. Work. Gr. I to Fifth Assess. Rep. Intergov. Panel Clim. Chang. Cambridge,* pp. 659–740.

Nair, A., Joseph, K. A., and Nair, K. S. (2014). "Spatio-temporal analysis of rainfall trends over a maritime state (Kerala) of India during the last 100 years." *Atmos. Environ.*, Elsevier, 88, pp. 123–132.

Nations, U. (2019). "Department of economic and social affairs, population division." *World Popul. Prospect.*, United Nations New York, 2019.

Nikhil Raj, P. P., and Azeez, P. A. (2012). "Trend analysis of rainfall in Bharathapuzha River basin, Kerala, India." *Int. J. Climatol.*, Wiley Online Library, 32(4), pp. 533–539.

Nirupama, N., and Simonovic, S. P. (2007). "Increase of flood risk due to urbanisation: A Canadian example." *Nat. Hazards*, Springer, 40(1), pp. 25–41.

Noska, R., and Misra, V. (2016). "Characterizing the onset and demise of the Indian summer monsoon." *Geophys. Res. Lett.*, Wiley Online Library, 43(9), pp. 4547–4554.

Oh, S.-G., Son, S.-W., and Min, S.-K. (2021). "Possible impact of urbanization on extreme precipitation–temperature relationship in East Asian megacities." *Weather Clim. Extrem.*, Elsevier, 34, pp. 100401.

Oliver, J. E. (1980). "Monthly precipitation distribution: a comparative index." *Prof. Geogr.*, Taylor & Francis, 32(3), pp. 300–309.

Pai, D. S., NAIR, S., and Ramanathan, A. N. (2013). "Long term climatology and trends of heat waves over India during the recent 50 years (1961-2010)." *Mausam*, 64(4), pp. 585–604.

Pai, D. S., Sridhar, L., Rajeevan, M., Sreejith, O. P., Satbhai, N. S., and Mukhopadhyay, B. (2014). "Development of a new high spatial resolution (0.25× 0.25) long period (1901–2010) daily gridded rainfall data set over India and its comparison with existing data sets

over the region." *Mausam*, 65(1), pp. 1–18.

Pal, I., and Al-Tabbaa, A. (2009). "Trends in seasonal precipitation extremes–An indicator of 'climate change'in Kerala, India." *J. Hydrol.*, Elsevier, 367(1–2), pp. 62–69.

Pal, I., and Al-Tabbaa, A. (2010). "Long-term changes and variability of monthly extreme temperatures in India." *Theor. Appl. Climatol.*, Springer, 100(1), pp. 45–56.

Pal, L., Ojha, C. S. P., and Dimri, A. P. (2021). "Characterizing rainfall occurrence in India: Natural variability and recent trends." *J. Hydrol.*, Elsevier, 603, pp. 126979.

Pan, X., Wang, Z., Gao, Y., Dang, X., and Han, Y. (2021). "Detailed and automated classification of land use/land cover using machine learning algorithms in Google Earth Engine." *Geocarto Int.*, Taylor & Francis, pp. 1–18.

Parastatidis, D., Mitraka, Z., Chrysoulakis, N., and Abrams, M. (2017). "Online global land surface temperature estimation from Landsat." *Remote Sens.*, Multidisciplinary Digital Publishing Institute, 9(12), pp. 1208.

Parthasarathy, B., and Dhar, O. N. (1974). "Secular variations of regional rainfall over India." *Q. J. R. Meteorol. Soc.*, Wiley Online Library, 100(424), pp. 245–257.

Patel, N. N., Angiuli, E., Gamba, P., Gaughan, A., Lisini, G., Stevens, F. R., Tatem, A. J., and Trianni, G. (2015). "Multitemporal settlement and population mapping from Landsat using Google Earth Engine." *Int. J. Appl. Earth Obs. Geoinf.*, Elsevier, 35, pp. 199–208.

Patra, S., Sahoo, S., Mishra, P., and Mahapatra, S. C. (2018). "Impacts of urbanization on land use/cover changes and its probable implications on local climate and groundwater level." *J. urban Manag.*, Elsevier, 7(2), pp. 70–84.

Perkins, S. E., Alexander, L. V, and Nairn, J. R. (2012). "Increasing frequency, intensity and duration of observed global heatwaves and warm spells." *Geophys. Res. Lett.*, 39(20).

Pimonsree, S., Limsakul, A., Kammuang, A., Kachenchart, B., and Kamlangkla, C. (2021). "Urbanization-induced changes in extreme climate indices in Thailand during 1970–2019." *Atmos. Res.*, Elsevier, pp. 105882.

Pimonsree, S., Limsakul, A., Kammuang, A., Kachenchart, B., and Kamlangkla, C. (2022). "Urbanization-induced changes in extreme climate indices in Thailand during 1970–2019." *Atmos. Res.*, Elsevier, 265, pp. 105882.

Poumadere, M., Mays, C., Le Mer, S., and Blong, R. (2005). "The 2003 heat wave in France: dangerous climate change here and now." *Risk Anal. an Int. J.*, Wiley Online Library, 25(6), pp. 1483–1494.

Raghavan, K. (1966). "A climatological study of severe heat waves in India." *Mausam*, 17(4), pp. 581–586.

Raj, A., and Sharma, L. K. (2022). "Assessment of land-use dynamics of the Aravalli range (India) using integrated geospatial and CART approach." *Earth Sci. Informatics*, Springer, pp. 1–26.

Raj, S., Paul, S. K., Chakraborty, A., and Kuttippurath, J. (2020). "Anthropogenic forcing exacerbating the urban heat islands in India." *J. Environ. Manage.*, Elsevier, 257, pp. 110006.

Rana, M. S., and Sarkar, S. (2021). "Prediction of urban expansion by using land cover change detection approach." *Heliyon*, Elsevier, 7(11), pp. e08437.

Rao, K. K., Kulkarni, A., Patwardhan, S., Kumar, B. V., and Kumar, T. V. L. (2020). "Future changes in precipitation extremes during northeast monsoon over south peninsular India." *Theor. Appl. Climatol.*, Springer, 142(1), pp. 205–217.

Rao, P. G. (1993). "Climatic changes and trends over a major river basin in India." *Clim. Res.*, Inter-Research, 2, pp. 215–223.

Ratnam, J. V, Behera, S. K., Ratna, S. B., Rajeevan, M., and Yamagata, T. (2016). "Anatomy of Indian heatwaves." *Sci. Rep.*, Nature Publishing Group, 6(1), pp. 1–11.

Ray, S., and Ray, I. A. (2011). "Impact of population growth on environmental degradation: Case of India." *J. Econ. Sustain. Dev.*, 2(8), pp. 72–77.

Ren, G., and Yaqing, Z. (2014). "Urbanization Effect on Trends of Extreme Temperature Indices of National Stations over Mainland China, 1961–2008." *J. Clim.*, 27, pp. 2340–

2360.

Ren, G., Zhou, Y., Chu, Z., Zhou, J., Zhang, A., Guo, J., and Liu, X. (2008). “Urbanization effects on observed surface air temperature trends in North China.” *J. Clim.*, 21(6), pp. 1333–1348.

Robine, J.-M., Cheung, S. L. K., Le Roy, S., Van Oyen, H., Griffiths, C., Michel, J.-P., and Herrmann, F. R. (2008). “Death toll exceeded 70,000 in Europe during the summer of 2003.” *C. R. Biol.*, 331(2), pp. 171–178.

Rohini, P., Rajeevan, M., and Mukhopadhay, P. (2019). “Future projections of heat waves over India from CMIP5 models.” *Clim. Dyn.*, Springer, 53(1), pp. 975–988.

Rohini, P., Rajeevan, M., and Srivastava, A. K. (2016). “On the Variability and Increasing Trends of Heat Waves over India.” *Sci. Rep.*, 6(1), pp. 26153.

Roy, P. S., Roy, A., Joshi, P. K., Kale, M. P., Srivastava, V. K., Srivastava, S. K., Dwevidi, R. S., Joshi, C., Behera, M. D., and Meiyappan, P. (2015). “Development of decadal (1985–1995–2005) land use and land cover database for India.” *Remote Sens.*, MDPI, 7(3), pp. 2401–2430.

Roy, S. Sen. (2019). “Spatial patterns of trends in seasonal extreme temperatures in India during 1980–2010.” *Weather Clim. Extrem.*, Elsevier, 24, pp. 100203.

Saboohi, R., Soltani, S., and Khodagholi, M. (2012). “Trend analysis of temperature parameters in Iran.” *Theor. Appl. Climatol.*, Springer, 109(3), pp. 529–547.

Sajjad, S. H., Blond, N., Mohsin, T., Shakrullah, K., and Clappier, A. (2021). “Temperature variability over urban, town, and rural areas: The case of Pakistan.” *Int. J. Climatol.*, Wiley Online Library.

Sang, X., Guo, Q., Wu, X., Fu, Y., Xie, T., He, C., and Zang, J. (2019). “Intensity and stationarity analysis of land use change based on CART algorithm.” *Sci. Rep.*, Nature Publishing Group UK London, 9(1), pp. 12279.

Saranya, J. S., Roxy, M. K., Dasgupta, P., and Anand, A. (2022). “Genesis and trends in marine heatwaves over the tropical Indian Ocean and their interaction with the Indian summer

monsoon." *J. Geophys. Res. Ocean.*, Wiley Online Library, 127(2), pp. e2021JC017427.

Saravanan, S., and Abijith, D. (2022). "Flood susceptibility mapping of Northeast coastal districts of Tamil Nadu India using Multi-source Geospatial data and Machine Learning techniques." *Geocarto Int.*, Taylor & Francis, pp. 1–30.

Schleussner, C.-F., Rogelj, J., Schaeffer, M., Lissner, T., Licker, R., Fischer, E. M., Knutti, R., Levermann, A., Frieler, K., and Hare, W. (2016). "Science and policy characteristics of the Paris Agreement temperature goal." *Nat. Clim. Chang.*, Nature Publishing Group UK London, 6(9), pp. 827–835.

Sen, P. K. (1968). "Estimates of the regression coefficient based on Kendall's tau." *J. Am. Stat. Assoc.*, Taylor & Francis, 63(324), pp. 1379–1389.

Şen, Z. (2012). "Innovative trend analysis methodology." *J. Hydrol. Eng.*, American Society of Civil Engineers, 17(9), pp. 1042–1046.

Şen, Z. (2017). "Innovative trend significance test and applications." *Theor. Appl. Climatol.*, Springer, 127, pp. 939–947.

Seto, K., Güneralp, B., and Hutyra, L. (2012). "Global Forecasts of Urban Expansion to 2030 and Direct Impacts on Biodiversity and Carbon Pools." *Proc. Natl. Acad. Sci.*, 109, pp. 16083–16088.

Shafiq, M. U., Rasool, R., Ahmed, P., and Dimri, A. P. (2019). "Temperature and precipitation trends in Kashmir Valley, north western Himalayas." *Theor. Appl. Climatol.*, Springer, 135(1–2), pp. 293–304.

Sharma, S., and Mujumdar, P. (2017). "Increasing frequency and spatial extent of concurrent meteorological droughts and heatwaves in India. Sci Rep 7, 15582."

Shastri, H., Paul, S., Ghosh, S., and Karmakar, S. (2015). "Impacts of urbanization on Indian summer monsoon rainfall extremes." *J. Geophys. Res. Atmos.*, Wiley Online Library, 120(2), pp. 496–516.

Shelestov, A., Lavreniuk, M., Kussul, N., Novikov, A., and Skakun, S. (2017). "Exploring Google Earth Engine platform for big data processing: Classification of multi-temporal

satellite imagery for crop mapping." *Front. Earth Sci.*, Frontiers Media SA, 5, pp. 17.

Shepherd, J. M. (2006). "Evidence of urban-induced precipitation variability in arid climate regimes." *J. Arid Environ.*, Elsevier, 67(4), pp. 607–628.

Shepherd, J. M., Pierce, H., and Negri, A. J. (2002). "Rainfall modification by major urban areas: Observations from spaceborne rain radar on the TRMM satellite." *J. Appl. Meteorol. Climatol.*, American Meteorological Society, 41(7), pp. 689–701.

Shi, Z., Jia, G., Zhou, Y., Xu, X., and Jiang, Y. (2021). "Amplified intensity and duration of heatwaves by concurrent droughts in China." *Atmos. Res.*, Elsevier, 261, pp. 105743.

Simon, A., and Mohankumar, K. (2004). "Spatial variability and rainfall characteristics of Kerala." *J. Earth Syst. Sci.*, Springer, 113(2), pp. 211–221.

Singh, J., Vittal, H., Karmakar, S., Ghosh, S., and Niyogi, D. (2016). "Urbanization causes nonstationarity in Indian summer monsoon rainfall extremes." *Geophys. Res. Lett.*, Wiley Online Library, 43(21), pp. 11–269.

Singh, N., Kumar, K. K., and Soman, M. K. (1989). "Some features of the periods contributing specified percentages of rainfall to annual total in Kerala, India." *Theor. Appl. Climatol.*, Springer, 39(3), pp. 160–170.

Singh, R. B. (2000). "Environmental consequences of agricultural development: a case study from the Green Revolution state of Haryana, India." *Agric. Ecosyst. Environ.*, Elsevier, 82(1–3), pp. 97–103.

Singh, S., Mall, R. K., and Singh, N. (2021). "Changing spatio-temporal trends of heat wave and severe heat wave events over India: An emerging health hazard." *Int. J. Climatol.*, Wiley Online Library, 41, pp. E1831–E1845.

Skariah, M., and Suriyakala, C. D. (2022). "Land use/land cover changes (1988–2017) in Central Kerala and the effect of urban built-up on Kerala floods 2018." *Arab. J. Geosci.*, Springer, 15(10), pp. 999.

Sneyers, R. (1991). *On the statistical analysis of series of observations.*

Soman, M. K., Kumar Krishna, K., and Singh, N. (1988). “Decreasing trend in the rainfall of Kerala.” *Curr. Sci.*, Current Science Association, 97(1), pp. 7–12.

Srivastava, A. K., Rajeevan, M., and Kshirsagar, S. R. (2009). “Development of a high resolution daily gridded temperature data set (1969–2005) for the Indian region.” *Atmos. Sci. Lett.*, Wiley Online Library, 10(4), pp. 249–254.

Von Storch, H. (1995). “Misuses of statistical analysis in climate research.” *Anal. Clim. Var. Appl. Stat. Tech.*, pp. 11–26.

Subbaramayya, I., and Rao, D. A. S. (1976). “Heat wave and cold wave days in different states of India.” *MAUSAM*, 27(4), pp. 436–440.

Sussman, H. S., Raghavendra, A., and Zhou, L. (2019). “Impacts of increased urbanization on surface temperature, vegetation, and aerosols over Bengaluru, India.” *Remote Sens. Appl. Soc. Environ.*, Elsevier, 16, pp. 100261.

Tabari, H., and Talaee, P. H. (2011). “Analysis of trends in temperature data in arid and semi-arid regions of Iran.” *Glob. Planet. Change*, Elsevier, 79(1–2), pp. 1–10.

Thaickavil, N. N. (2020). “Land use model for rural-urban transition in Kerala.” *Natl. Conf. Semin. Innov. Eng. Technol. https//www. Res. net/publication/339999743_Land_Use_Model_for_Rural-Urban_Transition_in_Kerala [20 July 2022]*.

The government of Kerala. (2012). “State urbanisation report.” *Retrieved march 28, 2017, from Dep. T. Ctry. Plan. http// townplanning.kerala.gov.in/sur/SUR.pdf*,.

Thomas, J., and Prasannakumar, V. (2016). “Temporal analysis of rainfall (1871–2012) and drought characteristics over a tropical monsoon-dominated State (Kerala) of India.” *J. Hydrol.*, Elsevier, 534, pp. 266–280.

Tian, H., Banger, K., Bo, T., and Dadhwal, V. K. (2014). “History of land use in India during 1880–2010: Large-scale land transformations reconstructed from satellite data and historical archives.” *Glob. Planet. Change*, Elsevier, 121, pp. 78–88.

Tolika, K. (2019). “On the analysis of the temporal precipitation distribution over Greece using

the Precipitation Concentration Index (PCI): annual, seasonal, monthly analysis and association with the atmospheric circulation." *Theor. Appl. Climatol.*, Springer, 137(3–4), pp. 2303–2319.

Trenberth, K. E., Dai, A., Van Der Schrier, G., Jones, P. D., Barichivich, J., Briffa, K. R., and Sheffield, J. (2014). "Global warming and changes in drought." *Nat. Clim. Chang.*, Nature Publishing Group UK London, 4(1), pp. 17–22.

Trenberth, K. E., Jones, P. D., Ambenje, P., Bojariu, R., Easterling, D., Tank, A. K., Parker, D., Rahimzadeh, F., Renwick, J. A., and Rusticucci, M. (2007). "Observations: surface and atmospheric climate change." *Clim. Chang. 2007 Phys. Sci. Basis. Contrib. Work. Gr. 1 to 4th Assess. Rep. Intergov. Panel Clim. Chang.*, Cambridge University Press.

UN, D. (2015). "World urbanization prospects: The 2014 revision." *United Nations Dep. Econ. Soc. Aff. Popul. Div. New York, NY, USA*, 41.

Venkatappa, M., Sasaki, N., Han, P., and Abe, I. (2021). "Impacts of droughts and floods on croplands and crop production in Southeast Asia–An application of Google Earth Engine." *Sci. Total Environ.*, Elsevier, 795, pp. 148829.

Vijay, A., Sivan, S. D., Mudbhatkal, A., and Mahesha, A. (2021). "Long-Term Climate Variability and Drought Characteristics in Tropical Region of India." *J. Hydrol. Eng.*, American Society of Civil Engineers, 26(4), pp. 5021003.

Vijay, A., and Varija, K. (2022). "Machine learning–based assessment of long-term climate variability of Kerala." *Environ. Monit. Assess.*, Springer, 194(7), pp. 498.

Voogt, J. A., and Oke, T. R. (2003). "Thermal remote sensing of urban climates." *Remote Sens. Environ.*, Elsevier, 86(3), pp. 370–384.

Wadhawan, S. K., Singh, B., and Ramesh, M. V. (2020). "Causative factors of landslides 2019: case study in Malappuram and Wayanad districts of Kerala, India." *Landslides*, Springer, pp. 1–9.

Wagle, N., Acharya, T. D., Kolluru, V., Huang, H., and Lee, D. H. (2020). "Multi-temporal land cover change mapping using google earth engine and ensemble learning methods."

Appl. Sci., MDPI, 10(22), pp. 8083.

Walsh, R. P. D., and Lawler, D. M. (1981). "Rainfall seasonality: description, spatial patterns and change through time." *Weather*, Wiley Online Library, 36(7), pp. 201–208.

Wang, G., Zhang, Q., Yu, H., Shen, Z., and Sun, P. (2020a). "Double increase in precipitation extremes across China in a 1.5° C/2.0° C warmer climate." *Sci. Total Environ.*, Elsevier, 746, pp. 140807.

Wang, J., Chen, Y., Liao, W., He, G., Tett, S., Yan, Z., Zhai, P., Feng, J., Ma, W., Huang, C., and Hu, Y. (2021a). "Anthropogenic emissions and urbanization increase risk of compound hot extremes in cities." *Nat. Clim. Chang.*, 11.

Wang, J., Chen, Y., Tett, S. F. B., Yan, Z., Zhai, P., Feng, J., and Xia, J. (2020b). "Anthropogenically-driven increases in the risks of summertime compound hot extremes." *Nat. Commun.*, Nature Publishing Group, 11(1), pp. 1–11.

Wang, P., Tong, X., Qiu, J., Chen, Y., Wu, S., Chan, T. O., Zhu, J., Liu, Z., Zhang, H., and Luo, M. (2022). "Amplification effect of urbanization on atmospheric aridity over China under past global warming." *Earth's Futur.*, Wiley Online Library, pp. e2021EF002335.

Wang, Y., Ren, Y., Song, L., and Xiang, Y. (2021b). "Responses of extreme high temperatures to urbanization in the Beijing–Tianjin–Hebei urban agglomeration in the context of a changing climate." *Meteorol. Appl.*, Wiley Online Library, 28(5), pp. e2024.

Wu, M., Luo, Y., Chen, F., and Wong, W. K. (2019). "Observed link of extreme hourly precipitation changes to urbanization over coastal South China." *J. Appl. Meteorol. Climatol.*, American Meteorological Society, 58(8), pp. 1799–1819.

Wu, S., Wang, P., Tong, X., Tian, H., Zhao, Y., and Luo, M. (2021a). "Urbanization-driven increases in summertime compound heat extremes across China." *Sci. Total Environ.*, Elsevier, 799, pp. 149166.

Wu, X., Hao, Z., Zhang, X., Li, C., and Hao, F. (2020a). "Evaluation of severity changes of compound dry and hot events in China based on a multivariate multi-index approach." *J. Hydrol.*, Elsevier, 583, pp. 124580.

Wu, X., Wang, L., Yao, R., Luo, M., and Li, X. (2021b). “Identifying the dominant driving factors of heat waves in the North China Plain.” *Atmos. Res.*, Elsevier, 252, pp. 105458.

Wu, X., Wang, L., Yao, R., Luo, M., Wang, S., and Wang, L. (2020b). “Quantitatively evaluating the effect of urbanization on heat waves in China.” *Sci. Total Environ.*, Elsevier, 731, pp. 138857.

Xiao, S., Fügener, T., Wende, W., Yan, W., Chen, H., Syrbe, R., and Xue, B. (2022). “The dynamics of vegetation and implications for ecosystem services in the context of urbanisation: An example from Huangyan-Taizhou, China.” *Ecol. Eng.*, Elsevier, 179, pp. 106614.

Xiong, Y., Xu, W., Lu, N., Huang, S., Wu, C., Wang, L., Dai, F., and Kou, W. (2021). “Assessment of spatial–temporal changes of ecological environment quality based on RSEI and GEE: A case study in Erhai Lake Basin, Yunnan province, China.” *Ecol. Indic.*, Elsevier, 125, pp. 107518.

Xu, Z., and Zhao, G. (2016). “Impact of urbanization on rainfall-runoff processes: case study in the Liangshui River Basin in Beijing, China.” *Proc. Int. Assoc. Hydrol. Sci.*, Copernicus Publications Göttingen, Germany, 373, pp. 7–12.

Yaduvanshi, A., Nkemelang, T., Bendapudi, R., and New, M. (2021). “Temperature and rainfall extremes change under current and future global warming levels across Indian climate zones.” *Weather Clim. Extrem.*, Elsevier, 31, pp. 100291.

Yan, Z.-W., Wang, J., Xia, J.-J., and Feng, J.-M. (2016). “Review of recent studies of the climatic effects of urbanization in China.” *Adv. Clim. Chang. Res.*, Elsevier, 7(3), pp. 154–168.

Yang, C., Li, Q., Hu, Z., Chen, J., Shi, T., Ding, K., and Wu, G. (2019). “Spatiotemporal evolution of urban agglomerations in four major bay areas of US, China and Japan from 1987 to 2017: Evidence from remote sensing images.” *Sci. Total Environ.*, Elsevier, 671, pp. 232–247.

Yang, J.-L., and Zhang, G.-L. (2011). “Water infiltration in urban soils and its effects on the quantity and quality of runoff.” *J. soils sediments*, Springer, 11(5), pp. 751–761.

Yang, P., Ren, G., and Yan, P. (2017a). “Evidence for a strong association of short-duration intense rainfall with urbanization in the Beijing urban area.” *J. Clim.*, 30(15), pp. 5851–5870.

Yang, P., Xia, J., Zhang, Y., and Hong, S. (2017b). “Temporal and spatial variations of precipitation in Northwest China during 1960–2013.” *Atmos. Res.*, Elsevier, 183, pp. 283–295.

Yang, X., Hou, Y., and Chen, B. (2011). “Observed surface warming induced by urbanization in east China.” *J. Geophys. Res. Atmos.*, 116(D14).

Yang, X., Ruby Leung, L., Zhao, N., Zhao, C., Qian, Y., Hu, K., Liu, X., and Chen, B. (2017c). “Contribution of urbanization to the increase of extreme heat events in an urban agglomeration in east China.” *Geophys. Res. Lett.*, Wiley Online Library, 44(13), pp. 6940–6950.

Yao, R., Cao, J., Wang, L., Zhang, W., and Wu, X. (2019). “Urbanization effects on vegetation cover in major African cities during 2001-2017.” *Int. J. Appl. Earth Obs. Geoinf.*, Elsevier, 75, pp. 44–53.

Yu, X., Gu, X., Kong, D., Zhang, Q., Cao, Q., Slater, L. J., Ren, G., Luo, M., Li, J., and Liu, J. (2022). “Asymmetrical shift toward less light and more heavy precipitation in an urban agglomeration of East China: Intensification by urbanization.” *Geophys. Res. Lett.*, Wiley Online Library, 49(4), pp. e2021GL097046.

Yu, Y., You, Q., Zuo, Z., Zhang, Y., Cai, Z., Li, W., Jiang, Z., Ullah, S., Tang, X., and Zhang, R. (2023). “Compound climate extremes in China: Trends, causes, and projections.” *Atmos. Res.*, Elsevier, pp. 106675.

Yue, S., and Wang, C. (2004). “The Mann-Kendall Test Modified by Effective Sample Size to Detect Trend in Serially Correlated Hydrological Series.” *Water Resour. Manag.*, 18(3), pp. 201–218.

Zamani, R., Mirabbasi, R., Nazeri, M., Meshram, S. G., and Ahmadi, F. (2018). “Spatio-temporal analysis of daily, seasonal and annual precipitation concentration in Jharkhand state, India.” *Stoch. Environ. Res. risk Assess.*, Springer, 32(4), pp. 1085–1097.

Zhang, D.-L. (2020). “Rapid urbanization and more extreme rainfall events.” *Sci. Bull.*, Elsevier, 65(7), pp. 516–518.

Zhang, K., Yao, Y., Qian, X., and Wang, J. (2019). “Various characteristics of precipitation concentration index and its cause analysis in China between 1960 and 2016.” *Int. J. Climatol.*, Wiley Online Library, 39(12), pp. 4648–4658.

Zhang, M., Li, W., Bi, X., Zong, L., Zhang, Y., and Yang, Y. (2021). “Synergistic Modulations of Large-Scale Synoptic Patterns and Local-Scale Urbanization Effects on Summer Rainfall in South China.” *Front. Clim.*, Frontiers Media SA, 3, pp. 771772.

Zhang, Q., Xu, C., Gemmer, M., Chen, Y. D., and Liu, C. (2009). “Changing properties of precipitation concentration in the Pearl River basin, China.” *Stoch. Environ. Res. Risk Assess.*, Springer, 23(3), pp. 377–385.

Zhang, X., and Yang, F. (2004). “RClimDex (1.0) user manual.” *Clim. Res. Branch Environ. Canada*, 22, pp. 13–14.

Zhao, M., Zhou, Y., Li, X., Cheng, W., Zhou, C., Ma, T., Li, M., and Huang, K. (2020). “Mapping urban dynamics (1992–2018) in Southeast Asia using consistent nighttime light data from DMSP and VIIRS.” *Remote Sens. Environ.*, Elsevier, 248, pp. 111980.

Zhao, N., Jiao, Y., Ma, T., Zhao, M., Fan, Z., Yin, X., Liu, Y., and Yue, T. (2019). “Estimating the effect of urbanization on extreme climate events in the Beijing-Tianjin-Hebei region, China.” *Sci. Total Environ.*, Elsevier, 688, pp. 1005–1015.

Zhou, Y., and Wu, Z. (2016). “Possible impacts of mega-El Niño/Southern Oscillation and Atlantic Multidecadal Oscillation on Eurasian heatwave frequency variability.” *Q. J. R. Meteorol. Soc.*, Wiley Online Library, 142(697), pp. 1647–1661.

Zhu, C., and Li, Y. (2014). “Long-term hydrological impacts of land use/land cover change from 1984 to 2010 in the Little River Watershed, Tennessee.” *Int. Soil Water Conserv. Res.*, Elsevier, 2(2), pp. 11–21.

Zscheischler, J., Westra, S., van den Hurk, B. J. J. M., Seneviratne, S. I., Ward, P. J., Pitman, A., AghaKouchak, A., Bresch, D. N., Leonard, M., Wahl, T., and Zhang, X. (2018).

"Future climate risk from compound events." *Nat. Clim. Chang.*, 8(6), pp. 469–477.

PUBLICATIONS

Journals

Anjali Vijay and Varija, K. (2022). "Machine learning–based assessment of long-term climate variability of Kerala.". Environmental Monitoring and Assessment., Springer, 194(7), pp. 498. https://link.springer.com/article/10.1007/s10661-022-10011-0

Anjali Vijay and Varija, K. (2023). "*Spatio-Temporal Classification of Land Use and Land Cover and its Changes in Kerala using Remote Sensing and Machine Learning Approach*". Environmental Monitoring and Assessment **(Under Review)**

Conference

Anjali Vijay and Varija, K. (2019). "Long-term climatic trend analysis of Ernakulam district, Kerala (India).". *24th HYDRO-International Conference*, Osmania University, Hyderabad, India. December 18-20, 2019.

Presented in Conference

Anjali Vijay and Varija, K. (2021). "Changes In The Frequency of Heat Waves and Extreme Climate Events in the Chaliyar And Periyar River Basin, India.". 4th International Conference on the Status and Future of the World's Large Rivers, Organized by hosted by Moscow State University on 3-6 August 2021

Anjali Vijay and Varija, K. (2017). "Trend Analysis of Climatic Parameters and River Discharge of Lakshmana Tirtha.". 3rd International Conference on the Status and Future of the World's Large Rivers, Organized by the National Institute of Hydrology, Roorkee on 18-21 April 2017.

BIODATA

Name	**Anjali Vijay**
Date of Birth	08.04.1991
Address	Anjali (H), Alathiyoor,Tirur, Malappuram, Kerala, India
Educational details	
2016-Present	Ph.D scholar. at the Department of Water Resources and Ocean Engineering, NITK Surathkal
2014 - 2016	M.Tech in Water Resources Engineering and Management, NITK Surathkal.
2008-2012	B.Tech in Civil Engineering from the University of Calicut
Mobile	9995886264
E-mail	anjalivijay21@gmail.com
Publications	Journals:2 Conferences: 5
Soft computing skills	Python, R Statistical software, ArcGIS, GEE